



Daniel Massari de Souza Coelho

**High temperature corrosion of steels in
single and dual conditions using
atmospheres related to the oxyfuel
process**

TESE DE DOUTORADO

Thesis presented to the **Programa de Pós-Graduação em Engenharia de Materiais e Processos Químicos e Metalúrgicos do Departamento de Engenharia de Materiais do Centro Técnico Científico da PUC-Rio**, as partial fulfillment of the requirements for the degree of **Doutor em Engenharia de Materiais e de Processos Químicos e Metalúrgicos**

Advisor: Prof. Fernando Cosme Rizzo Assunção
Co-Advisor: Prof. Axel Kranzmann

Rio de Janeiro
February 2014



Daniel Massari de Souza Coelho

**High temperature corrosion of steels in
single and dual conditions using
atmospheres related to the oxyfuel process**

Thesis presented as partial fulfillment of the requirements for the degree of Doutor to the Programa de Pós-Graduação em Engenharia de Materiais e Processos Químicos e Metalúrgicos do Departamento de Engenharia de Materiais do Centro Técnico Científico da PUC-Rio. Approved by the Examining Committee undersigned.

Prof. Fernando Cosme Rizzo Assunção

Advisor and President

Departamento de Engenharia de Materiais – PUC-Rio

Prof. Axel Kranzmann

BAM

Prof. Roberto Ribeiro de Avillez

Departamento de Engenharia de Materiais – PUC-Rio

Prof^a. Ivani de Souza Bott

Departamento de Engenharia de Materiais – PUC-Rio

Prof. André Luiz Vasconcellos da Costa e Silva

Universidade Federal Fluminense – UFF

Dr. Mauricio de Jesus Monteiro

INT

Prof. José Eugênio Leal

Coordinator of the Centro Técnico Científico da PUC-Rio

Rio de Janeiro, February 24th, 2014

All rights reserved

Daniel Massari de Souza Coelho

The autor graduated in Industrial and Metallurgical Engineering at PUC-Rio (Pontifícia Universidade Católica do Rio de Janeiro) in 2005. He obtained the degree of Mestre em Engenharia Metalúrgica at PUC-Rio (Pontifícia Universidade Católica do Rio de Janeiro) in 2008.

Bibliographic data

Coelho, Daniel Massari de Souza

High temperature corrosion of steels in single and dual conditions using atmospheres related to the oxyfuel process / Daniel Massari de Souza Coelho; advisor: Fernando Cosme Rizzo Assunção; co- advisor: Axel Kranzmann. – 2014. (em inglês)
166 f. : il. (color.) ; 30 cm

Tese (Doutorado em Engenharia de Materiais) – Pontifícia Universidade Católica do Rio de Janeiro, Rio de Janeiro, 2014.
Inclui bibliografia

1. Engenharia de materiais – Teses. 2. Corrosão em alta temperatura. 3. Ligas Fe-Cr. 4. Aços. 5. Oxidcombustão. I. Assunção, Fernando Cosme Rizzo. II. Kranzmann, Axel. III. Pontifícia Universidade Católica do Rio de Janeiro. Departamento de Engenharia de Materiais. IV. Título.

CDD: 620.11

Acknowledgments

I would like to express my gratitude to:

Dr. Fernando Rizzo, my advisor, for his guidance and support to my research.

Dr. Axel Kranzmann, my co-advisor, for his guidance and for the opportunity to work at BAM.

Dr. Pedro Portella for giving me the opportunity to work at BAM.

Dr. Mauricio Monteiro for his invaluable advice.

All the staff of PUC-Rio and BAM for their assistance and support.

My friend María Mosquera Feijoo for her valuable help in my research.

CNPq, CAPES, DAAD and BAM, for their continuous financial support, which made this thesis possible.

Abstract

Coelho, Daniel Massari de Souza; Assunção, Fernando Cosme Rizzo (Advisor); Kranzmann, Axel (Co-Advisor). **High temperature corrosion of steels in single and dual conditions using atmospheres related to the oxyfuel process.** Rio de Janeiro, 2014. 166p. PhD Thesis – Departamento de Engenharia de Materiais, Pontifícia Universidade Católica do Rio de Janeiro.

The world's increasing demand for energy and the need to control carbon dioxide (CO₂) emissions, the main gas responsible for global warming, requires development of new technologies to produce energy with lower CO₂ emission. Use of alternative renewable sources in energy production is increasing, but not enough to meet the demand. Thus, fossil fuel is still necessary. In this context, oxyfuel together with carbon capture and sequestration (CCS) arises as an alternative to conventional coal-fired power plants, because it does not emit CO₂ during energy production. The oxyfuel process differs from the conventional process by burning pure O₂ and recycled fuel gas instead of air. Therefore, a CO₂-H₂O-rich atmosphere is formed in the boiler, increasing the materials corrosion in contact with this atmosphere. The objective of this work was to investigate the high temperature corrosion behavior of iron alloys subjected to single and dual conditions in CO₂-rich atmospheres. Model and commercial iron alloys with different chromium, cobalt and carbon content were exposed to atmospheres containing CO₂, H₂O and SO₂ at 600°C for 1000 hours. The samples were analyzed in single atmosphere condition, when all sample faces were exposed to the same gas, and in dual atmosphere condition where the samples were exposed to water vapor on one side, to a gas on the other, creating an hydrogen gradient in the sample. The samples were characterized using TEM, SEM, EDS and light microscope. Results showed different corrosion rates according to chemical composition and microstructure of the samples and gases. Results showed that corrosion is higher in dual condition than in single condition. Most of the model alloys presented less corrosion than commercial steel VM12 in CO₂-rich atmospheres. However, steel VM12 presented better results when exposed to water vapor.

Keywords

High Temperature Corrosion; Fe-Cr Alloys; Steels; Oxyfuel

Resumo

Coelho, Daniel Massari de Souza; Assunção, Fernando Cosme Rizzo (Orientador); Kranzmann, Axel (Co-Orientador). **Corrosão de aços em alta temperatura em condições simples e duplas utilizando atmosferas relacionadas ao processo de oxidação.** Rio de Janeiro, 2014. 166 p. Tese de Doutorado – Departamento de Engenharia de Materiais, Pontifícia Universidade Católica do Rio de Janeiro.

A crescente demanda mundial por energia e a necessidade do controle de emissão de gás carbônico (CO_2), principal gás responsável pelo aquecimento global, exigem o desenvolvimento de novas tecnologias para a produção de energia com menor emissão de CO_2 . O uso de fontes alternativas na produção energética está aumentando, mas não é suficiente para suprir a demanda, portanto o uso de combustíveis fósseis ainda é necessário. Neste contexto, o uso da oxidação em usinas a carvão em conjunto com a captura e sequestro de carbono (CCS) surge como uma alternativa às usinas convencionais a carvão, pois não emite CO_2 na produção de energia. O processo de oxidação difere basicamente do convencional pela queima de O_2 puro e gás reciclado ao invés de ar. Com isso uma atmosfera rica em CO_2 e H_2O é formada no boiler, podendo aumentar a corrosão dos materiais em contato com o gás. Este trabalho teve como objetivo investigar o comportamento em corrosão em alta temperatura de ligas de ferro submetidas a condições simples e duplas em atmosferas ricas em CO_2 . Ligas experimentais e comerciais de ferro com diferentes teores de cromo, cobalto e carbono foram expostas a atmosferas contendo CO_2 , H_2O e SO_2 a 600°C durante 1000 horas. As amostras foram analisadas em condição simples, onde a amostra é exposta a um mesmo gás em todas as faces e em condição dupla onde a amostra é exposta a vapor d'água de um lado e um gás do outro, criando um gradiente de hidrogênio na amostra. As amostras foram caracterizadas por MEV, MET, EDS e microscópio óptico. Os resultados demonstraram que há maior corrosão em condição dual que em condição simples. A maioria das ligas experimentais apresentaram menor oxidação que o aço comercial VM12 em atmosferas ricas em CO_2 . Entretanto o aço VM12 apresentou melhores resultados quando exposto ao vapor d'água.

Palavras-Chave

Corrosão em Alta Temperatura; Ligas Fe-Cr; Aços; Oxidação

Contents

1	Introduction	27
2	Literature Review	29
2.1	The Oxyfuel Process	29
2.2	High temperature corrosion	33
2.2.1	Scale growth rate	33
2.3	Corrosion in Different Atmospheres.....	34
2.3.1	O ₂ Corrosion	34
2.3.2	Dual Condition	46
2.4	Whiskers Growth.....	51
2.5	Selective Oxidation of Multiphase Alloys	52
2.6	Diffusional Growth of Ferrite.....	55
3	Materials and Methods	57
3.1	Materials and Gases	57
3.2	Methodology	60
3.2.1	Single Atmosphere Condition Experiment	62
3.2.2	Dual Atmosphere Condition Experiment.....	64
4	Results	65
4.1	Alloy P1	65
4.1.1	Single Atmosphere Condition	66
4.1.2	Dual Atmosphere Condition	76
4.2	Alloy P2.....	86
4.2.1	Single Atmosphere Condition	87
4.3	Alloy P3.....	92
4.3.1	Single Atmosphere Condition	92
4.3.2	Dual Atmosphere Condition	96
4.4	Alloy P4.....	102
4.4.1	Single Atmosphere Condition	102
4.4.2	Dual Atmosphere Condition	108
4.5	Alloy P5.....	116
4.5.1	Single Atmosphere Condition	116

4.5.2	Dual Atmosphere Condition	121
4.6	VM12	130
4.6.1	Single Atmosphere Condition	130
4.6.2	Dual Atmosphere Condition	138
4.7	RFe12	145
4.7.1	Single Atmosphere Condition	145
5	Discussion.....	150
5.1	Alloy Composition and Structure	150
5.1.1	Chromium Effect	150
5.1.2	Cobalt Effect	151
5.1.3	Carbon Effect	151
5.1.4	Other Alloying Elements Comparison.....	152
5.2	Gas Composition.....	152
5.3	Dual atmosphere condition.....	153
6	Conclusions	156
7	Bibliography	158

List of Figures

Figure 1: Electricity production by fuel in 2011 [14].	29
Figure 2: Atmospheric CO ₂ Concentration [16].	30
Figure 3: Power plant efficiency and CO ₂ emission of different types of coal-fired power plants [15].	31
Figure 4: The oxyfuel process [26].	32
Figure 5: Fe-O Diagram [34].	35
Figure 6: Iron oxidation mechanism showing diffusion pattern through wustite, magnetite and hematite at temperatures above 570 °C [34].	35
Figure 7: CO ₂ oxidation mechanism.	37
Figure 8: Mass change of a Fe-15Cr steel at 900 °C for different water vapor contents in gas [48].	38
Figure 9: Breakaway oxidation sequence of a chromia-forming steel in an O ₂ /H ₂ O gas [48].	40
Figure 10: Molecular transportation within pores with Fe(OH) ₂ [52].	41
Figure 11: H ₂ O-H ₂ transportation in voids [52].	41
Figure 12: 10%Cr steel with pre-oxidizing time from 0 to 50 hours exposed to steam for 360ks. The result shows decreasing corrosion rate with the increasing pre-oxidation time [57].	42
Figure 13: Oxidation products formed in different Cr contents [61].	44
Figure 14: Weight change vs temperature chart showing a similar corrosion behavior until 600 °C and faster oxidation for lower Cr content alloys above this temperature [63].	44
Figure 15: Specific mass change for 5 different model alloys in different gas compositions at 650 °C for 96h [64].	45
Figure 16: Representation of nodular oxide growth [66].	46
Figure 17: Results of scale thickness in dual and single atmosphere conditions for the three steels used in the [67].	47
Figure 18: Scheme of activity before pore formation in scale [75].	50
Figure 19: Scheme of activity after pores formation in scale [75].	50
Figure 20: Blade growth in iron oxide proposed by Voss et al [80].	51
Figure 21: Left and right (a): nanowire growth mechanism. Right (b): nanoblade growth mechanism [84,81].	52
Figure 22: Classification of classical substitution alloying elements in steel (X). Above: according to their interaction with C. Below: according to their estimated binding energies with the austenite/ferrite interface.	56

Figure 23: Light Microscope pictures. Top left: alloy P1. Top right: alloy P2. Bottom left: alloy P3. Bottom right: alloy P4.	58
Figure 24: Light Microscope pictures. Top left: alloy P5. Top right: VM12. Bottom left: RFe12.	59
Figure 25: Top Left: Single atmosphere condition samples. Top right: Dual atmosphere condition sample (20mm x 3mm) on the gas side. Bottom left: Dual atmosphere condition sample (20mm x 3mm) on the gas water vapor side with the bevel for sealing. Bottom right: Dual atmosphere condition sample (15mm x 3mm) on the gas side. The sample is in the middle pressed by an iron (RFe12) ring. The water vapor side has the same bevel from the water vapor side samples with 22mm x 3mm.	61
Figure 26: Single condition furnace, Oxisim.	63
Figure 27: Sample-holder from the single condition experiment where the samples are glued with cement for high temperature applications.	63
Figure 28: Sample holder. The sample lies between two Al ₂ O ₃ tubes and sealing is done using gold O-Rings. Inlet gas and inlet water vapor are injected by 316 stainless steel tubes.	64
Figure 29: Furnaces used in the dual condition experiments. The experiment was run with the furnaces in the vertical position.	64
Figure 30: Stereomicroscope pictures of alloy P1 exposed to Gas 1 at 600°C for 1000h in a single atmosphere condition. The white part in the bottom of the sample is the cement used to stick the sample to the sample holder. Most part of the sample is homogeneous, but for the top. This may be an effect of the gas flow.	66
Figure 31: SEM secondary electrons (SE) pictures of the surface of alloy P1 exposed to Gas 1 at 600°C for 1000h in a single atmosphere condition. Top left: Iron rich nodules randomly distributed on surface with different sizes. Top right: Iron-rich nodule with hematite whiskers. Bottom Left: Nodules with whiskers and porosity. Bottom right: Nodule growing in a Cr ₂ O ₃ layer.	67
Figure 32: Light microscope pictures of alloy P1 exposed to Gas 1 at 600°C for 1000h in a single atmosphere condition. The sample presented a continuous layer of Cr ₂ O ₃ and some nodules rich in iron. On the right picture using polarized light, the red color of the whiskers on the top of the nodule identifies that phase as hematite.	67
Figure 33: The EDS from alloy P1 scale exposed to Gas 1 at 600°C for 1000h in a single atmosphere condition shows the presence of O, Cr, Fe	

and S. This indicates that the scale is formed by a Fe/Cr spinel, Cr ₂ O ₃ or both of them. Sulfur presence not only in the scale, but also in the metal, clearly shows that the sulfur from the gas penetrates into the sample.....	68
Figure 34: Stereomicroscope pictures of alloy P1 exposed to Gas 2 at 600°C for 1000h in a single atmosphere condition showing iron rich nodules with hematite on the top concentrated in one side of the sample.	69
Figure 35: SEM backscattered electrons (BSE) pictures of the surface of alloy P1 exposed to Gas 2 at 600°C for 1000h in a single atmosphere condition. Nodules are merging themselves and are very porous with blades on the top.	69
Figure 36: Light microscope pictures of alloy P1 exposed to Gas 2 at 600°C for 1000h in a single atmosphere condition. Isolated nodules are extremely porous and the internal oxide layer grows in irregular pattern inside the metal.....	70
Figure 37: SEM (BSE) pictures of alloy P1 exposed to Gas 2 at 600°C for 1000h in a single atmosphere condition. Left side: isolated nodules rich in iron. Right side: Nodule composed of hematite, magnetite and spinel characterized by EDS in Figure 38.....	70
Figure 38: EDS line scan of alloy P1 exposed to Gas 2 at 600°C for 1000h in a single atmosphere condition. The external oxide layer is composed of a thin outer hematite layer followed by a magnetite layer. The internal oxide is formed by a Fe/Cr spinel with higher Cr content closer to the external oxide layer and to the metal.	71
Figure 39: EDS of Alloy P1 exposed to Gas 2 at 600°C for 1000h in a single atmosphere condition. It shows higher chromium content close to the metal and sulfur diffusion from the gas into the metal. A Cr ₂ O ₃ layer is formed in the metal/scale interface.	71
Figure 40: Macro pictures of both sides of alloy P1 sample exposed to Gas 3 at 600°C for 1000h in a single atmosphere condition. The white color at the bottom is the cement used to glue the sample to the sample-holder. Despite the area around the cement, oxidation was homogeneous in the remainder of the sample.	72
Figure 41: SEM (SE) pictures of alloy P1 surface exposed to Gas 3 at 600°C for 1000h in a single atmosphere condition. Nodules are merging themselves and are porous with blades on the top.	72

Figure 42: Light microscope pictures of alloy P1 exposed to Gas 3 at 600°C for 1000h in a single atmosphere condition. Isolated nodules are porous and the internal oxide layer grows in a preferential pattern inside the metal.....	73
Figure 43: EDS of Alloy P1 exposed to Gas 3 at 600°C for 1000h in a single atmosphere condition. It shows a hematite layer in contact with the gas (top right), a spinel layer with less Cr (bottom left) and a spinel layer with more Cr (bottom right).....	73
Figure 44: FIB pictures of Alloy P1 exposed to Gas 3 at 600°C for 1000h in a single atmosphere condition. All the three points are FeCr ₂ O ₄ , as seen in Figure 45 for point 1.....	74
Figure 45: Left: TEM picture of point 1 of Figure 44 showing FeCr ₂ O ₄ nanocrystals. Right: Convergent Beam Electron Diffraction (CBED) of one of the crystals and the simulation below.....	74
Figure 46: TEM picture and CBED of the scale outside the iron rich nodules showing Cr ₂ O ₃ whiskers.....	75
Figure 47: TEM picture, EDS and CBED of the structure beneath the Cr ₂ O ₃ whiskers. This phase is FeCr ₂ O ₄	75
Figure 48: Stereomicroscope pictures of alloy P1 exposed to Gas 1 at 600°C for 1000h in a dual atmosphere condition. The sample has a slight difference between oxidation in the center and the border.	76
Figure 49: SEM (Left: SE. Right: BSE) pictures of alloy P1 surface exposed to Gas 3 at 600°C for 1000h in a dual atmosphere condition. Nodules distributed heterogeneously on the surface and have different morphologies.	76
Figure 50: EDS line scan from Figure 49 picture (right) of alloy P1 exposed to Gas 1 at 600°C for 1000h in a dual atmosphere condition showing three nodules. From the right to the left, a Fe oxide rich nodule is followed by a Cr oxide rich nodule. Right from the Cr oxide-rich there is an oxide with S and Cr.....	77
Figure 51: SEM (SE) pictures of alloy P1 surface exposed to Gas 3 at 600°C for 1000h in a dual atmosphere condition. Left: Iron oxide nodule with some whiskers/blades growing on the surface. Right: Cr oxide nodule with whiskers on the surface.....	77
Figure 52: Light microscope and SEM pictures of alloy P1 exposed to Gas 1 at 600°C for 1000h in a dual atmosphere condition showing low surface oxidation and some small nodules.	78

Figure 53: Stereomicroscope pictures of alloy P1 exposed to Gas 1 at 600°C for 1000h in a dual atmosphere condition. The sample has a slight difference between the oxidation in the center and the border. 78

Figure 54: SEM (BSE) pictures of the surface of alloy P1 exposed to Gas 1 at 600°C for 1000h in a dual atmosphere condition. Blades are observed in the grain boundaries and a porous structure composes the grains. 79

Figure 55: Light microscope pictures of alloy P1 exposed to Gas 1 at 600°C for 1000h in a dual atmosphere condition. A thick porous scale formed on the surface with a high porosity on the external scale. 79

Figure 56: SEM (BSE) pictures of alloy P1 exposed to Gas 1 at 600°C for 1000h in a dual atmosphere condition. Left: On the surface, an area with blades and another without. Right: Internal oxidation and high porosity in the scale/metal interface. 80

Figure 57: EDS line of alloy P1 exposed at 600°C for 1000h in a dual atmosphere condition on the water vapor side. External scale is formed by iron oxides with Fe content increasing towards the internal oxide scale. Internal oxide scale is formed by a Fe/Cr spinel with different Cr content. Near the scale/metal interface, the Cr content increases expressively. 80

Figure 58: EDS of Alloy P1 exposed to Gas 1 at 600°C for 1000h in a dual atmosphere condition on the water vapor side. Point 4 shows a brighter structure of Fe/Cr spinel with a Co. Point 3 shows a darker area with more Cr and no Co. Point 6, shows an area of internal oxidation, where both metal and oxide were scanned by EDS. 81

Figure 59: Stereomicroscope pictures of alloy P1 exposed to Gas 3 at 600°C for 1000h in a dual atmosphere condition. The sample exhibits different colors and morphologies on the surface. 81

Figure 60: SEM (Left: BSE. Right: SE) pictures of alloy P1 exposed to Gas 3 at 600°C for 1000h in a dual atmosphere condition. A porous phase and a mixture of whiskers and blades form the surface of the scale. 82

Figure 61: Light microscope pictures of alloy P1 exposed to Gas 3 at 600°C for 1000h in a dual atmosphere condition. A thick continuous scale formed on the surface of alloy P1 with pores in the external and internal scale. On the top, hematite is present. 82

Figure 62: EDS of Alloy P1 exposed to Gas 3 at 600°C for 1000h in a dual atmosphere condition on the gas side. Point 4 shows a Cr₂O₃ layer in contact with the metal. Points 2 and 3 show sulfur inside the metal. 83

Figure 63: EDS line scan of Alloy P1 exposed to Gas 3 at 600°C for 1000h in a dual atmosphere condition on the gas side. It shows an external scale composed of hematite and magnetite, and an internal scale composed by spinel and Cr ₂ O ₃ . Sulfur is present in the spinel layer.	83
Figure 64: Stereomicroscope pictures of alloy P1 exposed to Gas 3 at 600°C for 1000h in a dual atmosphere condition on the water vapor side.	84
Figure 65: SEM (SE) pictures of alloy P1 exposed to Gas 3 at 600°C for 1000h in a dual atmosphere condition on the gas side. A porous phase and a mixture of whiskers and blades form the surface of the scale.	85
Figure 66: Light microscope pictures of alloy P1 exposed to Gas 3 at 600°C for 1000h in a dual atmosphere condition on the water vapor side. Thick continuous scale formed on the sample with pores in external and internal scale. Hematite is present on top.	85
Figure 67: EDS of Alloy P1 exposed to Gas 3 at 600°C for 1000h in a dual atmosphere condition on the water vapor side. Point 1 shows a bright point where the Co content is higher in scale. Point 6 is closer to the metal interface than point 3 and has more Cr.	86
Figure 68: Stereomicroscope pictures of alloy P2 exposed to Gas 2 at 600°C for 1000h in a single atmosphere condition. The white part at the sample bottom is the cement used to stick the sample to the sample holder.	87
Figure 69: SEM (SE) pictures of the surface of alloy P2 exposed to Gas 1 at 600°C for 1000h in a single atmosphere condition. Both pictures display slight surface oxidation without the evidence of iron oxide rich nodules.	87
Figure 70: SEM (BSE) pictures of alloy P2 exposed to Gas 1 at 600°C for 1000h in a single atmosphere condition. A protective thin scale with whiskers on the top formed at the surface of alloy.	88
Figure 71: EDS from alloy P2 scale exposed to Gas 1 at 600°C for 1000h in a single atmosphere condition. Cr ₂ O ₃ forms the external scale, while Fe/Cr spinel forms isolated nodules in the internal scale.	88
Figure 72: Stereomicroscope pictures of alloy P2 exposed to Gas 2 at 600°C for 1000h in a single atmosphere condition.	89
Figure 73: SEM (BSE) pictures of the surface of alloy P2 exposed to Gas 2 at 600°C for 1000h in a single atmosphere condition.	89
Figure 74: SEM (BSE) pictures of alloy P2 exposed to Gas 2 at 600°C for 1000h in a single atmosphere condition. A protective thin scale with whiskers on top formed on the surface, and some nodules with an internal scale seem to nucleate.	90

Figure 75: Left: Macro picture of alloy P2 exposed to Gas 3 at 600°C for 1000h in a single atmosphere condition. The white part in the bottom of the sample is the cement used to stick the sample to the sample holder. Right: SEM (SE) picture showing randomly-distributed nodules on the surface..... 90

Figure 76: EDS from alloy P2 scale exposed to Gas 3 at 600°C for 1000h in a single atmosphere condition. A continuous thin protective oxide rich in Cr is formed and some iron oxide rich nodules grow on the scale. 91

Figure 77: SEM (BSE) of alloy P2 exposed to Gas 3 at 600°C for 1000h in a single atmosphere condition. A Cr rich oxide covers the surface..... 91

Figure 78: Stereomicroscope pictures of alloy P3 exposed to Gas 1 at 600°C for 1000h in a single atmosphere condition. The white part at the sample bottom is the cement used to glue the sample to the sample holder. There is no evidence of spallation or nodules growing on the surface..... 92

Figure 79: SEM (SE) pictures of the surface of alloy P3 exposed to Gas 1 at 600°C for 1000h in a single atmosphere condition. Both pictures show a small oxidation of the surface with the presence of one nodule..... 93

Figure 80: SEM (BSE) picture of alloy P3 exposed to Gas 1 at 600°C for 1000h in a single atmosphere condition. A protective thin scale with whiskers on top formed at the surface of the alloy. 93

Figure 81: Stereomicroscope and SEM picture of alloy P3 exposed to Gas 2 at 600°C for 1000h in a single atmosphere condition. On the right, some nodules grow on the sample surface..... 94

Figure 82: SEM (BSE) pictures of the surface of alloy P3 exposed to Gas 2 at 600°C for 1000h in a single atmosphere condition. A Cr₂O₃ layer forms the scale with few nodules and porosity. 94

Figure 83: Macro and SEM (SE) pictures of alloy P3 exposed to Gas 3 at 600°C for 1000h in a single atmosphere condition. The white part at the sample bottom is the cement used to glue the sample to the sample holder. In the SEM picture, some nodules have grown on the surface..... 95

Figure 84: EDS from the surface of alloy P3 exposed to Gas 3 at 600°C for 1000h in a single atmosphere condition. Cr₂O₃ forms a continuous thin protective scale and some iron rich nodules grow on the scale..... 95

Figure 85: SEM (BSE) pictures of alloy P3 exposed to Gas 3 at 600°C for 1000h in a single atmosphere condition. A protective thin scale grows on the surface. In the subsurface region there is a microstructural change, 96

Figure 86: Stereomicroscope and SEM (BSE) pictures of alloy P3 exposed to Gas 1 at 600°C for 1000h in a dual atmosphere condition on the gas side. The sample exhibits different colors and morphologies on the surface. 96

Figure 87: Light microscope and microprobe pictures of alloy P3 exposed to Gas 1 at 600°C for 1000h in a dual atmosphere condition in the gas side. Cr₂O₃ layer was formed and a ferrite layer has grown in the metal, and nodules have grown in the metal grain boundaries. 97

Figure 88: Stereomicroscope and SEM (BSE) pictures of alloy P3 exposed to Gas 1 at 600°C for 1000h in a dual atmosphere condition on the gas side. The sample exhibits a thick oxide layer and whiskers on the surface. 97

Figure 89: Light microscope pictures of alloy P3 exposed to Gas 1 at 600°C for 1000h in a dual atmosphere condition on the water vapor side. On external scale, hematite (top layer) and magnetite can be identified. Hematite is also present due to the higher O₂ partial pressure in some spots in the cracks and holes in the magnetite layer. 98

Figure 90: SEM (BSE) pictures of alloy P3 exposed to Gas 1 at 600°C for 1000h in a dual atmosphere condition on the water vapor side. 98

Figure 91: EDS line scan of alloy P3 exposed to Gas 1 at 600°C for 1000h in a dual atmosphere condition on the water vapor side showing a sequence of hematite, magnetite and spinel from the gas side to the metal. 99

Figure 92: Stereomicroscope and SEM (BSE) pictures of alloy P3 exposed to Gas 3 at 600°C for 1000h in a dual atmosphere condition on the gas side. The sample exhibits different colors and morphologies on the surface. In the SEM picture on the left, porous nodules forms on the surface and a cellular structure forms between them. 99

Figure 93: Light microscope pictures of alloy P3 exposed to Gas 3 at 600°C for 1000h in a dual atmosphere condition on the gas side. Ferrite is formed in the metal beneath the scale. 100

Figure 94: Microprobe and SEM (BSE) pictures of alloy P3 exposed to Gas 3 at 600°C for 1000h in a dual atmosphere condition on the gas side. The pictures show ferrite grains growing on the subsurface region. Nodules and pores are also present. 100

Figure 95: Stereomicroscope pictures of alloy P3 exposed to Gas 3 at 600°C for 1000h in a dual atmosphere condition in the water vapor side. A Cr₂O₃ with few nodules are observed. 101

Figure 96: SEM (BSE) pictures of alloy P3 exposed to Gas 3 at 600°C for 1000h in a dual atmosphere condition on the water vapor side. The nodules

are composed of iron oxides and Fe/Cr spinel. Internal oxidation is also present.....	101
Figure 97: EDS line scanning of alloy P3 exposed to Gas 3 at 600°C for 1000h in a dual atmosphere condition on the water vapor side showing a external scale composed of iron oxides, an internal scale composed by Fe/Cr spinel and internal oxidation.....	102
Figure 98: Stereomicroscope pictures of alloy P4 exposed to Gas 1 at 600°C for 1000h in a single atmosphere condition. The white part at sample bottom is the cement used to stick the sample to the sample holder. The dark and bright colors of the rest of the sample may be caused by the gas flow.....	103
Figure 99: SEM (SE) pictures of the surface of alloy P4 exposed to Gas 1 at 600°C for 1000h in a single atmosphere condition. Cr ₂ O ₃ layer with few nodules.....	103
Figure 100: SEM (BSE) pictures of the surface of alloy P4 exposed to Gas 1 at 600°C for 1000h in a single atmosphere condition. Cr ₂ O ₃ layer, but nodules were not found in the cross-section analysis.....	103
Figure 101: Stereomicroscope and SEM (BSE) pictures of alloy P1 exposed to Gas 2 at 600°C for 1000h in a single atmosphere condition showing iron rich nodules with hematite on the top concentrated in one side of the sample.....	104
Figure 102: SEM (BSE) pictures of the surface of alloy P4 exposed to Gas 2 at 600°C for 1000h in a single atmosphere condition. A continuous Cr ₂ O ₃ layer was formed with some cavities in the scale/metal interface.....	104
Figure 103: Macro pictures of both sides of the sample of alloy P4 exposed to Gas 3 at 600°C for 1000h in a single atmosphere condition. The white color on the bottom is the cement used to glue the sample to the sample-holder. The sample exhibits homogenous oxidation.....	105
Figure 104: SEM (SE) pictures of the surface of alloy P4 exposed to Gas 3 at 600°C for 1000h in a single atmosphere condition. Nodules rich in iron and a continuous Cr ₂ O ₃ layer were observed.....	105
Figure 105: EDS of Alloy P4 exposed to Gas 3 at 600°C for 1000h in a single atmosphere condition. (1) Fe oxide-rich nodule and (2) Cr-rich layer.....	106
Figure 106: SEM (BSE) pictures of alloy P4 exposed to Gas 3 at 600°C for 1000h in a single atmosphere condition showing a continuous Cr ₂ O ₃ layer.	106

Figure 107: Light microscope and FIB pictures of alloy P4 exposed to Gas 3 at 600°C for 1000h in a single atmosphere condition showing a decarburized zone in the subscale region.	107
Figure 108: TEM picture and element analysis of alloy P4 exposed to Gas 3 at 600°C for 1000h in a single atmosphere condition showing a Fe depleted region and some Cr carbides beneath it.....	107
Figure 109: Stereomicroscope and SEM (BSE) pictures of alloy P4 exposed to Gas 1 at 600°C for 1000h in a dual atmosphere condition on the gas side. The sample exhibits scale composed of Cr ₂ O ₃ and some nodules....	108
Figure 110: EDS of Alloy P4 exposed to Gas 3 at 600°C for 1000h in a dual atmosphere condition on the gas side. (1) and (3) are iron oxide rich nodules. (2) is Cr ₂ O ₃	109
Figure 111: Light microscope and SEM (BSE) pictures of alloy P4 exposed to Gas 1 at 600°C for 1000h in a dual atmosphere condition on the gas side. Nodules are observed in the light microscope picture on the right. Pores and ferrite growth is observed on the left.	109
Figure 112: EDS map of alloy P4 exposed to Gas 1 at 600°C for 1000h in a dual atmosphere condition on the gas side. Iron oxide concentration is high on external scale and Fe is not present on internal scale. Cr concentration is high on internal scale and in part of external scale. S is present on internal scale near the metal.	110
Figure 113: Stereomicroscope and SEM (BSE) pictures of alloy P4 exposed to Gas 1 at 600°C for 1000h in a dual atmosphere condition on the water vapor side. The sample exhibits different colors and morphologies on the surface (right). The scale is porous and exhibits some nodules (left)	111
Figure 114: Light microscope pictures of alloy P4 exposed to Gas 1 at 600°C for 1000h in a dual atmosphere condition on the water vapor side. Hematite (top layer) and magnetite can be identified on external scale. In the cracks and voids in the magnetite layer hematite is present due to higher O ₂ partial pressure in these places. Internal oxidation is also present. ..	111
Figure 115: EDS of Alloy P4 exposed to Gas 1 at 600°C for 1000h in a dual atmosphere condition. (1) Fe/Cr spinel with a higher Fe and Co concentration than in point (3). (3) Fe/Cr spinel. (4) Metal.	112
Figure 116: SEM (BSE) pictures of alloy P4 exposed to Gas 1 at 600°C for 1000h in a dual atmosphere condition on the water vapor side.	112

Figure 117: Line scan of Figure 116 from alloy P4 exposed to Gas 1 at 600°C for 1000h in a dual atmosphere condition on the water vapor side. Hematite, magnetite and Fe/Cr spinel form from the gas to the metal.	113
Figure 118: Stereomicroscope and SEM (SE) pictures of alloy P4 exposed to Gas 3 at 600°C for 1000h in a dual atmosphere condition. Left: The sample exhibits a reddish surface with some nodules. Right: interface of the severely corroded iron ring with the sample.	113
Figure 119: SEM (BSE) pictures of alloy P4 exposed to Gas 3 at 600°C for 1000h in a dual atmosphere condition on the gas side. A thin layer of Cr ₂ O ₃ formed and ferrite has grown into the metal.	114
Figure 120: Stereomicroscope and SEM (SE) pictures of alloy P4 exposed to Gas 3 at 600°C for 1000h in a dual atmosphere condition on the water vapor side. The sample exhibits a surface with some whiskers.	114
Figure 121: Light microscope pictures of alloy P4 exposed to Gas 3 at 600°C for 1000h in a dual atmosphere condition on the water vapor side. External scale composed of hematite and magnetite and internal scale composed by Fe/Cr spinel.	115
Figure 122: SEM (BSE) pictures of alloy P4 exposed to Gas 3 at 600°C for 1000h in a dual atmosphere condition on the water vapor side. Thick scale with cracks and voids on the left. Internal oxidation is observed on the right. ...	115
Figure 123: EDS line scan of alloy P4 exposed to Gas 4 at 600°C for 1000h in a dual atmosphere condition on the water vapor side. External scale composed of hematite and magnetite and internal scale composed of Fe/Cr spinel.	116
Figure 124: Stereomicroscope and SEM (SE) pictures of alloy P5 exposed to Gas 1 at 600°C for 1000h in a single atmosphere condition. The white part on the sample is the cement used to glue the sample to the sample holder and Cr ₂ O ₃ scale covers the surface with the presence of few nodules.	117
Figure 125: SEM (BSE) pictures of the surface of alloy P5 exposed to Gas 1 at 600°C for 1000h in a single atmosphere condition. Both pictures show slight oxidation of the surface without the evidence of iron-oxide rich nodules.	117
Figure 126: EDS of Alloy P5 exposed to Gas 1 at 600°C for 1000h in a single atmosphere condition. (1) spinel, (2) Cr ₂ O ₃ layer, (3) metal.	118

Figure 127: Stereomicroscope and SEM (BSE) picture of alloy P5 exposed to Gas 2 at 600°C for 1000h in a single atmosphere condition. Formation of few iron-rich oxide nodules on the surface.....	118
Figure 128: EDS of Alloy P5 exposed to Gas 2 at 600°C for 1000h in a single atmosphere condition. It shows a Fe/Cr spinel or Cr ₂ O ₃ (2) and an iron-rich nodule (1).....	119
Figure 129: SEM (BSE) pictures of the surface of alloy P5 exposed to Gas 2 at 600°C for 1000h in a single atmosphere condition. A Cr rich oxide layer forms the scale.	119
Figure 130: Macro and SEM pictures of alloy P5 exposed to Gas 3 at 600°C for 1000h in a single atmosphere condition. The white part in the bottom of the sample is the cement used to glue the sample to the sample holder, and there is a slight difference on the color of the surface due to the gas flow (stereo picture on the left). On the SEM picture on the right, some nodules are present on the surface.....	120
Figure 131: SEM (Left: BSE. Right: SE) picture from the surface of alloy P5 exposed to Gas 3 at 600°C for 1000h in a single atmosphere condition. Cr ₂ O ₃ forms continuous thin protective scale and some iron oxide rich nodules with whiskers grow on the scale.	120
Figure 132: SEM (BSE) pictures of alloy P5 exposed to Gas 3 at 600°C for 1000h in a single atmosphere condition. A protective thin scale grows on the surface and below the surface there is a change in the microstructure in the metal.....	120
Figure 133: Stereomicroscope pictures of alloy P5 exposed to Gas 1 at 600°C for 1000h in a dual atmosphere condition on the gas side. Most of the sample displays a red color hematite on the surface.....	121
Figure 134: SEM (SE) pictures of alloy P5 exposed to Gas 1 at 600°C for 1000h in a dual atmosphere condition on the gas side. A porous phase and a mixture of whiskers and blades form the surface of the scale.	122
Figure 135: EDS of Alloy P5 exposed to Gas 1 at 600°C for 1000h in a dual atmosphere condition on the gas side. (1) Fe oxide nodule. (2) Cr ₂ O ₃ layer. (3) Fe oxide with Co that was also found in other parts of the sample.....	122
Figure 136: SEM (BSE) pictures of alloy P5 exposed to Gas 1 at 600°C for 1000h in a dual atmosphere condition on the gas side. External layer composed of two different magnetite morphologies and internal scale composed of three different spinel morphologies.....	123

Figure 137: EDS line scan of alloy P5 exposed to Gas 1 at 600°C for 1000h in a dual atmosphere condition on the gas side. A magnetite layer composes the external scale, spinel with three different Cr content and S composes the internal layer.	123
Figure 138: Stereomicroscope pictures of alloy P5 exposed to Gas 1 at 600°C for 1000h in a dual atmosphere condition on the water vapor side. The sample exhibits porous gray scale.	124
Figure 139: SEM (SE) pictures of alloy P5 exposed to Gas 1 at 600°C for 1000h in a dual atmosphere condition on the water vapor side. An extremely porous oxide forms the outer scale.	124
Figure 140: Light microscope pictures of alloy P5 exposed to Gas 1 at 600°C for 1000h in a dual atmosphere condition on the water vapor side. Well-defined external and internal scale and internal corrosion.	124
Figure 141: SEM (BSE) pictures of alloy P5 exposed to Gas 1 at 600°C for 1000h in a dual atmosphere condition on the water vapor side. Internal scale shows preferential oxidation of grain boundaries.	125
Figure 142: EDS line scan of alloy P5 exposed to Gas 1 at 600°C for 1000h in a dual atmosphere condition on the water vapor side. Magnetite forms the external scale and Cr/Fe spinel the internal. Close to the metal there is an increase in Cr suggesting that Cr_2O_3 might be the phase present.	125
Figure 143: EDS of Alloy P5 exposed to Gas 1 at 600°C for 1000h in a dual atmosphere condition on the water vapor side. (3) Fe/Cr spinel. (1) and (4), Fe/Cr spinel with Co.	126
Figure 144: Stereomicroscope and SEM pictures of alloy P5 exposed to Gas 3 at 600°C for 1000h on a dual atmosphere condition on the gas side. Iron rich nodules are observed on the surface.	126
Figure 145: Light microscope pictures of alloy P5 exposed to Gas 3 at 600°C for 1000h in a dual atmosphere condition on the gas side. External scale composed of hematite and magnetite and internal scale composed of spinel.	127
Figure 146: SEM (BSE) pictures of alloy P5 exposed to Gas 3 at 600°C for 1000h in a dual atmosphere condition on the gas side. External scale composed of hematite and magnetite and internal scale composed of spinel.	127
Figure 147: EDS line scan of alloy P5 exposed to Gas 3 at 600°C for 1000h in a dual atmosphere condition on the gas side. External scale composed of hematite and magnetite and internal scale composed of spinel.	128

Figure 148: Stereomicroscope and SEM pictures of alloy P5 exposed to Gas 3 at 600°C for 1000h in a dual atmosphere condition on the water vapor side. The sample exhibits different colors and morphologies on the surface.....	128
Figure 149: Light microscope pictures of alloy P5 exposed to Gas 3 at 600°C for 1000h in a dual atmosphere condition on the water vapor side. Hematite (top layer) and magnetite can be identified in the external scale. In the cracks and holes in the magnetite layer hematite is present due to the higher O ₂ partial pressure in these places.....	129
Figure 150: SEM (BSE) pictures of alloy P5 exposed to Gas 3 at 600°C for 1000h in a dual atmosphere condition in the water vapor side. Hematite (top layer) and magnetite can be identified in the external scale. Internal scale composed of Fe/Cr spinel internal oxidation in specific parts.....	129
Figure 151: EDS line scan pictures of alloy P5 exposed to Gas 3 at 600°C for 1000h in a dual atmosphere condition on the water vapor side. Hematite (top layer) and magnetite can be identified on the external scale. Internal scale composed of Fe/Cr spinel.....	129
Figure 152: Stereomicroscope and SEM (SE) pictures of VM12 exposed to Gas 1 at 600°C for 1000h in a single atmosphere. Sample exhibits different colors and morphologies on the surface.....	131
Figure 153: SEM (BSE) pictures of VM12 exposed to Gas 1 at 600°C for 1000h in a single atmosphere condition. Thin scale with the presence of some nodules.....	131
Figure 154: SEM (BSE) pictures of alloy VM12 exposed to Gas 1 at 600°C for 1000h in single atmosphere condition. Large areas with a thin protective oxide layer and some big Fe-rich nodules were observed.....	131
Figure 155: EDS of VM12 exposed to Gas 1 at 600°C for 1000h in a single atmosphere condition. (1) Iron oxide, (5) base metal and (2) amorphous Si oxide.....	132
Figure 156: EDS line scan of VM12 exposed to Gas 1 at 600°C for 1000h in a single atmosphere condition.....	132
Figure 157: Stereomicroscope pictures of VM12 exposed to Gas 2 at 600°C for 1000h in a single condition. The sample exhibits high density of nodules with hematite whiskers on the top of them.....	133
Figure 158: SEM (BSE) pictures of VM12 exposed to Gas 2 at 600°C for 1000h in a single condition. Development and coalescence of nodules producing a porous scale with blade-like whiskers.....	133

Figure 159: EDS of VM12 exposed to Gas 2 at 600°C for 1000h in a single atmosphere condition showing it is composed of iron oxides only.....	134
Figure 160: SEM (BSE) pictures of alloy VM12 exposed to Gas 2 at 600°C for 1000h in a single atmosphere condition showing cavities in the external scale in the magnetite layer and the porosity in the metal/scale interface.	135
Figure 161: EDS line scan of alloy VM12 exposed to Gas 2 at 600°C for 1000h in a single atmosphere condition showing sequence of hematite, magnetite and Fe/Cr spinel from the gas side to the metal.....	135
Figure 162: Stereomicroscope and SEM pictures of VM12 exposed to Gas 3 at 600°C for 1000h in a single atmosphere condition. The sample exhibits nodules on the surface and coalescence of some of them.....	136
Figure 163: EDS of steel VM12 exposed to Gas 3 at 600°C for 1000h in a single atmosphere condition. (4) Iron oxide, (1) and (2) base metal and some oxidation.....	137
Figure 164: EDS of steel VM12 exposed to Gas 3 at 600°C for 1000h in a single atmosphere condition. The nodules are composed of an external scale of iron oxides and an internal scale of Cr oxide.....	137
Figure 165: Stereomicroscope pictures of the surface of steel VM12 exposed to Gas 1 at 600°C for 1000h in a dual atmosphere condition on the gas side. The sample was slightly oxidized and the grinding scratches can still be seen. Small nodules were formed on the surface.....	138
Figure 166: SEM (Left: SE. Right: BSE) pictures of steel VM12 exposed to Gas 1 at 600°C for 1000h in a dual atmosphere condition on the gas side. Thin scale formed by Cr_2O_3 and regions covered by Fe-rich nodules.	138
Figure 167: SEM (BSE) pictures of steel VM12 exposed to Gas 1 at 600°C for 1000h in a dual atmosphere condition on the gas side. Nodules are composed of an internal scale composed of spinel and an outer scale composed of iron oxides. On the right figure, the right structure presents Si nodules on the top, which was also observed in other experiments.	139
Figure 168: EDS of steel VM12 exposed to Gas 1 at 600°C for 1000h in a dual atmosphere condition on the gas side. Sulfur is present in the metal near the scale and the internal scale is composed of spinel. A cobalt-rich region is also observed.	139
Figure 169: Stereomicroscope and SEM (BSE) pictures of the surface of steel VM12 exposed to Gas 1 at 600°C for 1000h in a dual atmosphere condition on the water vapor side. The sample exhibits homogeneous oxidation with the development of a thick porous oxide.....	140

Figure 170: Light microscope and SEM (BSE) pictures of steel VM12 exposed to Gas 1 at 600°C for 1000h in a dual atmosphere condition on the water vapor side. The scale does not have voids in the outer scale and the internal scale is not very porous.....	140
Figure 171: EDS of steel VM12 exposed to Gas 1 at 600°C for 1000h in a dual atmosphere condition on the water vapor side. (1) Spinel. (5) Si oxide. (3) Internal oxidation and a high Si content.	141
Figure 172: Stereomicroscope pictures of surface steel VM12 exposed to Gas 3 at 600°C for 1000h in a dual atmosphere condition on the gas side. Surface composed of hematite layer with whiskers.....	142
Figure 173: Light microscope pictures of steel VM12 exposed to Gas 3 at 600°C for 1000h in a dual atmosphere condition on the gas side. External scale composed of hematite and magnetite and internal scale composed of spinel.	142
Figure 174: SEM (BSE) pictures of steel VM12 exposed to Gas 3 at 600°C for 1000h in a dual atmosphere condition on the gas side. External scale composed of hematite and magnetite (left) and internal scale composed of spinel (right).....	143
Figure 175: EDS of steel VM12 exposed to Gas 3 at 600°C for 1000h in a dual atmosphere condition on the gas side. (2) and (3) iron oxide. (5) Cr/Fe spinel with S and Si.	143
Figure 176: Stereomicroscope and SEM (BSE) pictures of steel VM12 exposed to Gas 3 at 600°C for 1000h in a dual atmosphere condition on the water vapor side. The sample exhibits porous scale with spallation.	144
Figure 177: Light microscope pictures of steel VM12 exposed to Gas 3 at 600°C for 1000h in dual atmosphere condition on the water vapor side. External scale composed of hematite and magnetite and internal scale composed of spinel. The hematite columnar layer can be seen in the right picture as well as the internal oxidation.....	144
Figure 178: SEM (BSE) pictures of steel VM12 exposed to Gas 3 at 600°C for 1000h in dual atmosphere condition on the water vapor side. External scale composed of hematite and magnetite and internal scale composed of spinel.	145
Figure 179: Stereomicroscope and SEM (SE) pictures of the surface of RFe12 exposed to Gas 1 at 600°C for 1000h in a single condition. In the stereo picture (left) it can be seen that the surface of the sample was damaged. On the right, the surface SEM picture of the scale.....	146

Figure 180: Light microscope pictures of RFe12 exposed to Gas 1 at 600°C for 1000h in a single condition. Thick scale was formed with the presence of cracks and few voids.....	146
Figure 181: Stereomicroscope and SEM (BSE) pictures of the surface of RFe12 exposed to Gas 2 at 600°C for 1000h in a single condition. In the stereo picture (left), a large hematite region (red phase) is observed on the bottom of the sample. Porosity and whiskers are observed on the scale surface of the SEM picture on the right.	147
Figure 182: SEM (BSE) pictures of the surface of RFe12 exposed to Gas 2 at 600°C for 1000h in a single condition. Whiskers and pores are observed on the surface of the scale.	147
Figure 183: Light microscope pictures of RFe12 exposed to Gas 2 at 600°C for 1000h in a single condition. There is no evidence of microstructural change in the metal.	147
Figure 184: SEM and light microscope pictures of RFe12 exposed to Gas 2 at 600°C for 1000h in a single condition. Two phases are observed on the scale and hematite whiskers are present on top of the surface.	148
Figure 185: EDS line scanning of RFe12 exposed to Gas 2 at 600°C for 1000h in a single condition. Scale formed by hematite and magnetite.	148
Figure 186: Macro and SEM (BSE) pictures the surface of RFe12 exposed to Gas 3 at 600°C for 1000h in a single condition. Whiskers and a porous iron oxide phase were formed in Gas 3.....	149
Figure 187: Light microscope and SEM pictures of RFe12 exposed to Gas 3 at 600°C for 1000h in a single condition. Thick scale is formed on the surface and there is no evidence of microstructural change in the metal.....	149
Figure 188: EDS line scan of RFe12 exposed to Gas 3 at 600°C for 1000h in a single condition. Scale is composed of hematite and magnetite.	149
Figure 189: Left: Alloy P2 in Gas 1. Right: Alloy P4 in Gas 1.	150
Figure 190: Nodules density on the surface has increased with increase in water vapor concentration.....	152
Figure 191: Carbide consumption in alloy P4 in a single condition in Gas 3.....	153
Figure 192: Decarburization and ferrite growth in alloy P4 in a dual condition in gas 3.....	155

List of Tables

Table 1: Samples Chemical Composition in wt%.	57
Table 2: Gases Compositions at 600°C in vol%.	59
Table 3: Gas fugacity.	60
Table 4: Summary of the experiments. All experiments were done at 600°C for 1000h. X: Experiment done, •: Experiment not done.	62
Table 5: Water vapor side scale thickness in μm . N is the maximum thickness of the nodule.	155

1 Introduction

Carbon dioxide emission (CO_2) is a global concern due to its contribution to the greenhouse effect and, thus, to the temperature increase of the Earth atmosphere. Carbon dioxide emission has different sources, such as industrial processes, use of fossil fuel (largest global emission source) and change in land use, which is the most important source of CO_2 emission in Brazil, having a 75% share in the total CO_2 emission [1-6].

Several alternatives are being developed and used in order to reduce the CO_2 emission by substituting the burning of fossil fuels by biofuel and other renewable energy sources. However, the increase in the use of renewable sources is accompanied by an even larger increase in the use of energy, especially in developing countries like China and India. For this reason, fossil fuel is expected to be the major global source of energy at least until 2030 [7-9].

Carbon capture and storage, CCS, is a technology which is being studied as a way to keep extending the use of fossil fuels, particularly coal, which emits more CO_2 among all fossil fuels. By 2030, it is estimated that there will be more coal-fired power plants using CCS technology than power plants without it [10,11].

Oxyfuel is a new process, under development, to be used in new coal-fired power plants together with CSS producing energy, with zero CO_2 emission. In this process, flue gas at the end of the process bears only water vapor and CO_2 , which is compressed to be sold or stored [12,13].

In this work, a commercial steel (VM12), a high-purity iron and five model alloys with different carbon, chromium and cobalt contents were subjected to typical oxyfuel atmospheres, which display high CO_2 and water vapor content to investigate their high temperature corrosion behavior. In addition to the classic single atmosphere condition, the samples were also exposed to a dual condition atmosphere, in which one side of the sample was exposed to water vapor, and the opposite side to an oxyfuel gas, creating a hydrogen gradient across the sample and a condition similar to the one found in heat exchangers in oxyfuel power plants. The samples were oxidized for 1000h at 600°C and the

microstructures were characterized by microprobe, EDS, optical, transmission and scanning electron microscopy.

The thesis structure is the following:

Chapter 2: Literature Review – In the first part, an overview on energy, CO₂ emission and oxyfuel process is carried out. In the second part, topics related to high temperature corrosion are described.

Chapter 3: Materials and Methods – The alloys, gases and equipment, as well as the methodology of the experiments, are described.

Chapter 4: Results – Experimental results are presented for each alloy, according to the condition (single or dual) and gas composition.

Chapter 5: Discussion – The discussion was divided into three major topics: alloy composition and microstructure; gas composition; and atmosphere condition (single vs dual).

In chapters 6 and 7, Conclusions and Bibliography are described.

2 Literature Review

2.1 The Oxyfuel Process

Since Industrial Revolution, coal has had significant role in supplying energy for society's development and well-being. Currently, around 41% of global electric energy is produced by coal as shown in Figure 1 and coal-fired generation has increased by an estimated 6% from 2010 to 2012 [13-15].

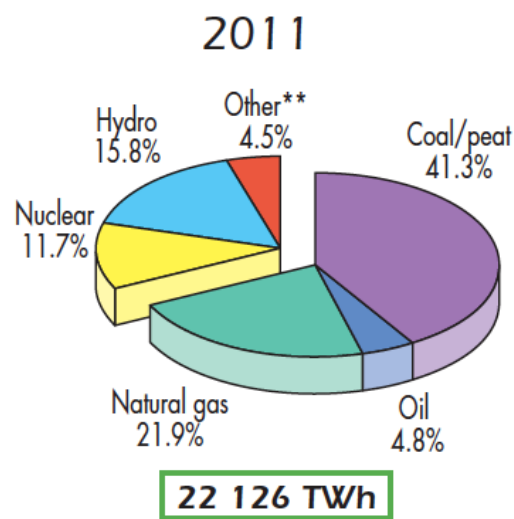


Figure 1: Electricity production by fuel in 2011 [14].

However, use of coal as a fuel has always caused environmental problems to society, even before the Industrial Revolution, and new technologies were developed to make coal utilization cleaner and less hazardous to the environment and society [13].

Today, there is a consensus that main global warming cause is CO₂ anthropogenic emission as reflected in atmospheric CO₂ concentration, which rose from 315.97ppm, in 1959, to 396.48ppm in 2013 (Figure 2) [16-19]. Renewable energy would be an environmental friendly substitution for coal in the energy generation, but its adoption has increased very slowly with its price being still too high [6,7,14,15].

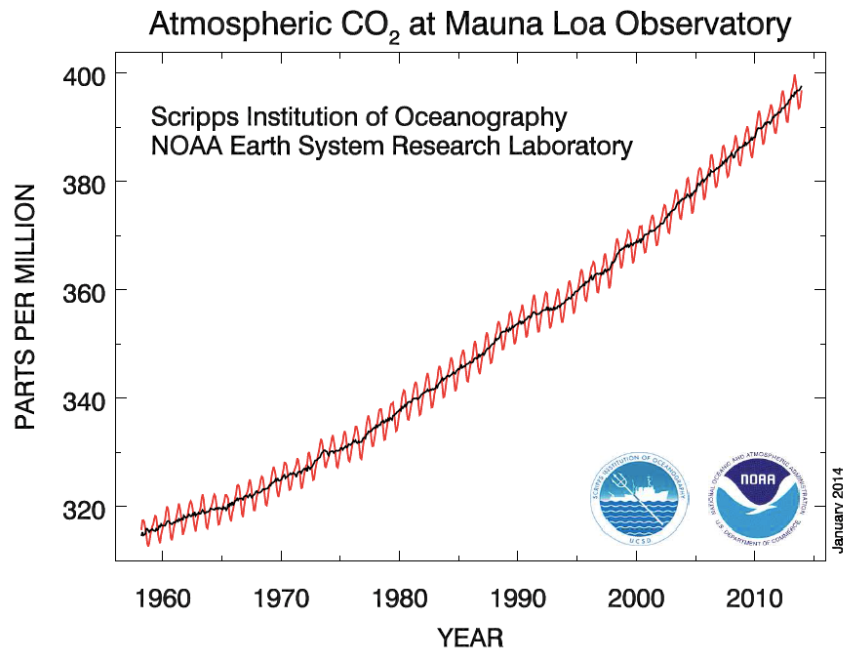


Figure 2: Atmospheric CO₂ Concentration [16].

The use of CCS and the development of (advanced) ultra-supercritical power plants will allow energy production from coal with zero or near zero CO₂ emission. In ultra-supercritical power plants and advanced ultra-supercritical power plants, the temperature used in the process is higher than that currently used, and efficiency can grow from 33% at present, to more than 50% [15,20]. Ultra-supercritical power plants work in higher temperatures and pressures higher than subcritical power plants, increasing efficiency and decreasing CO₂ emission (Figure 3) [15,20]. The introduction of ultra-supercritical power plants is also essential to the development and use of CCS in an economically-viable way, because the energy to separate and compress the CO₂ for CCS consumes further energy, decreasing overall efficiency.



Figure 3: Power plant efficiency and CO₂ emission of different types of coal-fired power plants [15].

Carbon capture in a power plant can be divided into three categories: post-combustion, pre-combustion and oxyfuel. The post-combustion process is used in conventional coal-fired power plants and CO₂ is separated at the end of the process by chemical absorption with monoethanolamine (MEA) or a sterically-hindered amine (KS-1). The process uses low temperatures and can retrofit existing power plants.

In the pre-combustion process, which is used in Integrated Gasification Combined Cycle (IGCC) power plants, a syngas bearing CO, CO₂ and H₂ is produced, and then CO is transformed in CO₂ by water gas shift reaction, and then separated from H₂. The process has good economic and plant efficiency characteristics, but the power plant is costly to construct and the system is more complicated to operate than conventional boilers. [21].

The oxyfuel process works fundamentally by removal of molecular nitrogen prior to gas injection into the boiler. Gas injection in the boiler is a mixture of O₂ and flue gas containing basically CO₂ and H₂O, as shown in Figure 4. Recirculation of flue gas, with prior ash removal, is essential to control burner temperature [21,12]. With high CO₂ concentration, it is easy and cheap to separate SO₂ and H₂O from the flue gas before this is compressed. In the gas compression, a minor quantity of SO_x, NO_x and Hg is also removed in order to obtain the purity necessary to further flue gas use [22-25].

Oxyfuel (O_2/CO_2 recycle) combustion capture

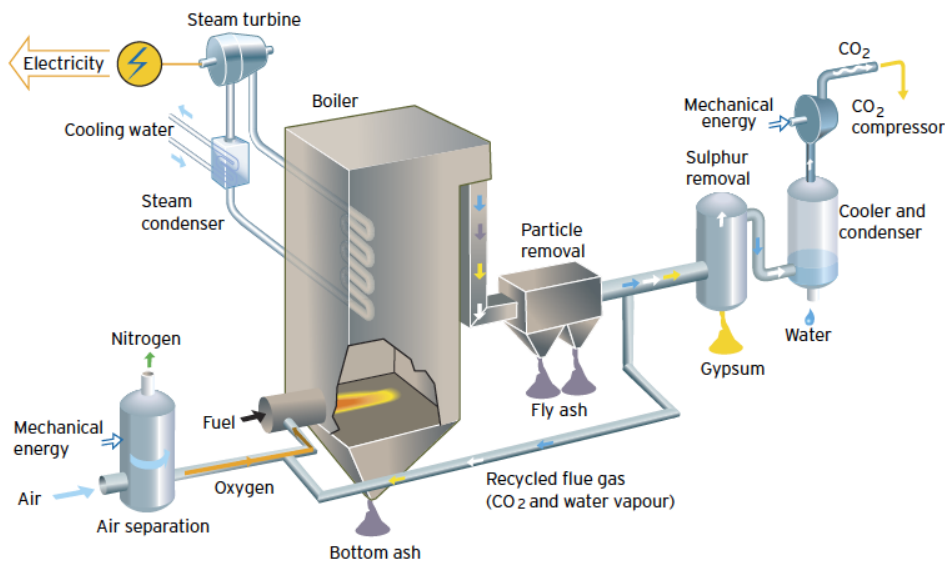


Figure 4: The oxyfuel process [26].

Oxyfuel is more expensive than post-combustion, but it is the most energy- and cost-efficient of all carbon capture technologies, due to its small boiler volume and to flue gas cleaning system [12,21]. The process is being studied and pilot plans, like Schwarze Pumpe from Vattenfall, in Germany, are being tested, but there is no oxyfuel power plant running or being built yet [27,28].

The change in gases and working temperatures of the new power plants has forced new alloys development and viability study of using existing commercial alloys in higher temperatures and in CO_2 -rich gases. All the studies attempted to increase the ferritic and martensitic temperature range of use, instead of employing more expensive nickel alloys. At temperatures above $700^\circ C$, nickel alloys are the main materials studied to be used in power plant applications. Corrosion resistance is a property analyzed in the material selection for high temperatures applications, but the mechanical properties of the materials are more important specially the resistance to creep [29-32].

2.2 High temperature corrosion

2.2.1 Scale growth rate

Scale growth kinetics is governed by the physical phenomena. The two most common kinetic rates are: linear and parabolic. These growth rates are not always isolated, and many times the linear rate precedes the parabolic [33,34].

2.2.1.1 Linear rate

When the corrosion rate is controlled by parameters outside the scale, the linear rate governs the scale growth, being represented by the equations below:

$$\frac{dX}{dt} = k_l$$

Integral form:

$$X = k_l t$$

X = scale thickness (cm)

k_l = linear rate constant (cm/s)

t = time (s)

Linear rate occurs when border reactions control the process, but other mechanisms can lead to the same result. In corrosion in very high temperatures, and with gas mixture containing diluted oxygen, the diffusion in the scale can be fast, but the growth rate is limited by the rate that the oxygen from the gases transfers to the scale. Thus, oxidation rate is controlled by gas properties, such as temperature and O₂ partial pressure. Linear rate is also observed at the beginning of the oxidation process when the scale is very thin and the oxidation is not controlled by diffusion in the scale [33,34].

2.2.1.2 Parabolic rate

The parabolic rate occurs when oxidation is controlled by species diffusion in the scale (oxide layer). This rate is often found in compact scales and defined by the equations below [33,34]:

$$\frac{dX}{dt} = \frac{k_p}{X}$$

$$X^2 = 2k_p t$$

X = scale thickness (cm)

t = time (s)

k_p = parabolic rate constant (cm/s)

k_p is also frequently measured by mass variation of material during the oxidation, because it can be easily measured using thermogravimetric balance. With mass change, Δm , the former equation can be rewritten as:

$$\Delta m^2 = 2k_p t$$

A classical mode to determine k_p experimentally is using the graphic Δm^2 vs t. Nonetheless, after analyzing several experimental data, Monceau and Pieraggi [35] concluded that the equation $\Delta m^2=2k_p t$ was incorrect to determine k_p , because it assumes that the process is always diffusional and that there is no transient regime. The ideal equation would be:

$$t = A + B\Delta m + C\Delta m^2$$

$$C^{-1} = k_p$$

In this case k_p is determined by C in the equation.

2.3 Corrosion in Different Atmospheres

2.3.1 O₂ Corrosion

When iron oxidation takes place in an O₂ atmosphere, oxide formation changes with the O₂ partial pressure forming wustite (Fe_{1-δ}O), magnetite (Fe₃O₄)

and hematite (Fe_2O_3) (Figure 5) [34]. The three phases can be formed during corrosion with the wustite growing on the metal interface, followed by magnetite, and hematite on the gas interface. Wustite is not stoichiometric in all temperatures and in higher oxygen concentrations; wustite is richer in oxygen and can coexist with magnetite forming a thin wustite and magnetite layer separating both phases [33]. Magnetite also deviates from the nominal stoichiometry, but this only happens in higher temperatures [33,34].

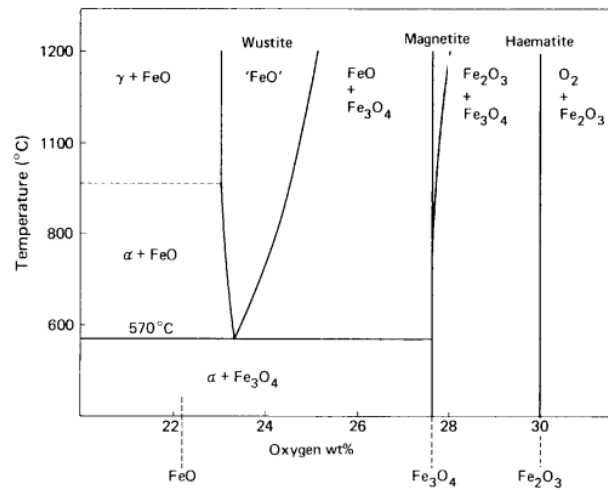


Figure 5: Fe-O Diagram [34].

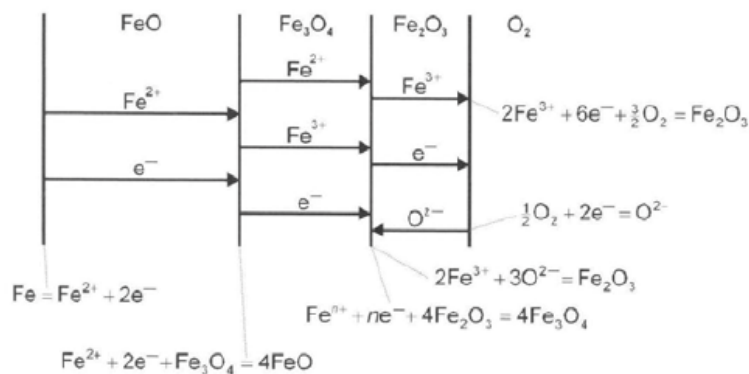


Figure 6: Iron oxidation mechanism showing diffusion pattern through wustite, magnetite and hematite at temperatures above 570°C [34].

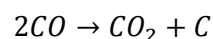
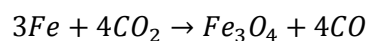
At temperatures above 570°C, a scale composed of a sequence of wüstite, magnetite and hematite layers is formed (Figure 6). In this condition, Fe

cations diffuse from the wustite, which is a p-type semiconductor with cation deficit and high electron and cations mobility, to the magnetite supplying Fe to the wustite layer which forms in the magnetite interface. Magnetite has an inverted spinel structure with Fe^{+2} occupying the octahedral sites and Fe^{+3} the tetrahedral sites. Fe^{2+} , Fe^{+3} and electrons diffuse in the hematite direction forming hematite and magnetite. Hematite is cubic above 400°C and diffusion of Fe^{3+} ions in the gas direction and O_2^- in the metal direction occurs [34].

2.3.1.1 CO_2 Corrosion

An oxyfuel atmosphere is characterized by the high CO_2 concentration due to absence of nitrogen removed prior to coal combustion. However, nitrogen can also be present in the oxyfuel atmosphere due to an incomplete removal of the element from the air. H_2O , O and SO_2 are other components also present in the oxyfuel atmosphere, H_2O being the most important [36].

Considering iron oxidation in pure CO_2 , the CO_2 reaction with Fe produces magnetite and CO. The CO then dissociates into CO_2 and C according to the Boudouard reaction.



Carbon deposition on the metal due to the Boudouard reaction inhibits hematite nuclei coalescence to form a continuous scale. The scale grows by Fe cation outward diffusion, creating vacancies on the metal surface, decreasing the scale adhesion. Insufficient scale adhesion creates microchannels and cracks which allow CO_2 to come inwards and CO to go outwards. This mechanism creates an outer scale, which grows parabolic controlled by Fe diffusion in the scale and an inner scale that grows by individual crystals oxidation created by CO_2 reaction in the voids created by the vacancies formed with the Fe cation diffusion. This mechanism proposed by Gibbs [37] is explained in Figure 7. Oxygen diffusion through magnetite could also be the rate controlling mechanism, but it was shown that it is too slow to control the oxidation rate [38].

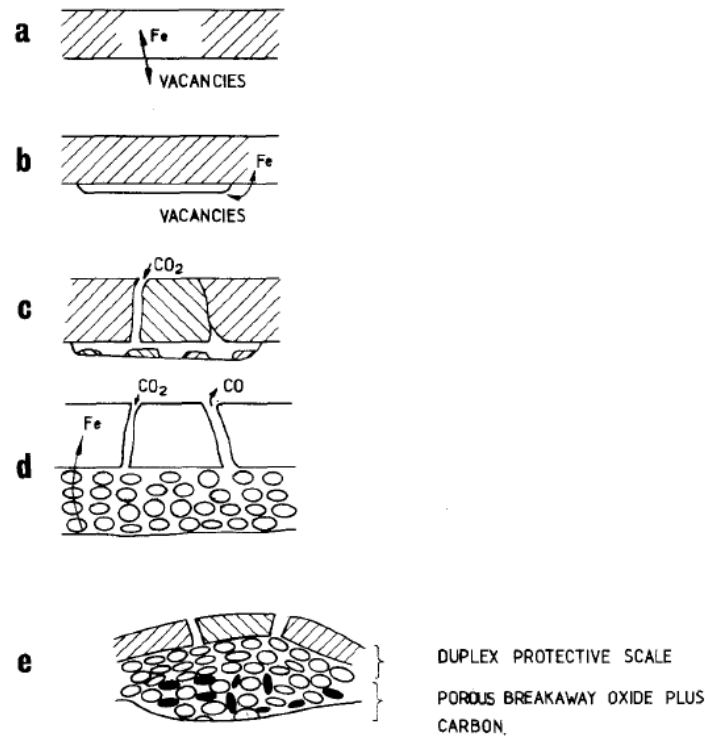
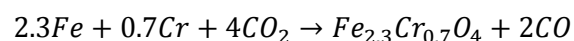


Figure 7: CO₂ oxidation mechanism [38].

Fujii and Messner [39] also worked with pure CO₂, but with Fe-Cr alloys with 20% Cr at temperatures from 700 to 1100°C, and they did not observe the formation of a protective chromia layer. Instead, an outer layer of Fe oxide and an inner layer of wüstite and spinel were formed. In the alloy, chromium-rich carbides precipitated. The oxidation rate is controlled by Fe diffusion through the outer scale.

Rouillard et al. [40-42] studied the T91 steel, with 9%Cr and 1%Mo, in a CO₂ atmosphere. As with the model above, proposed by Gibbs [37], CO₂ reacts with Fe, forming hematite at the gas/oxide interface. At the metal/oxide interface the following reaction takes place.



CO from both reactions produces CO₂ + C due to the Boudouard reaction and carburizes the steel and its deposit in the scale creates nanochannels where CO₂/CO diffusion takes place.

2.3.1.2 H₂O Atmosphere

Water vapor is present in most high temperature applications where metals are used, for instance, in steam engines, in fossil and biofuel combustion and in solid oxide fuel cells (SOFC). The addition of H₂O to a system usually accelerates steel corrosion rate, promoting whisker growth and porosity in scale surface. Volatile species can also be formed by consuming the protective scale and causing a breakaway oxidation [33,36,43].

Chromia forming alloys are particularly affected by gas containing water vapor. The addition of H₂O increases the oxidation rate of the chromia forming alloys, as shown in Figure 8, as observed in several studies [36,44-47]. In many cases, the failure of the protective chromia layer is attributed to the formation of the volatile hydroxides CrO₂(OH)₂.

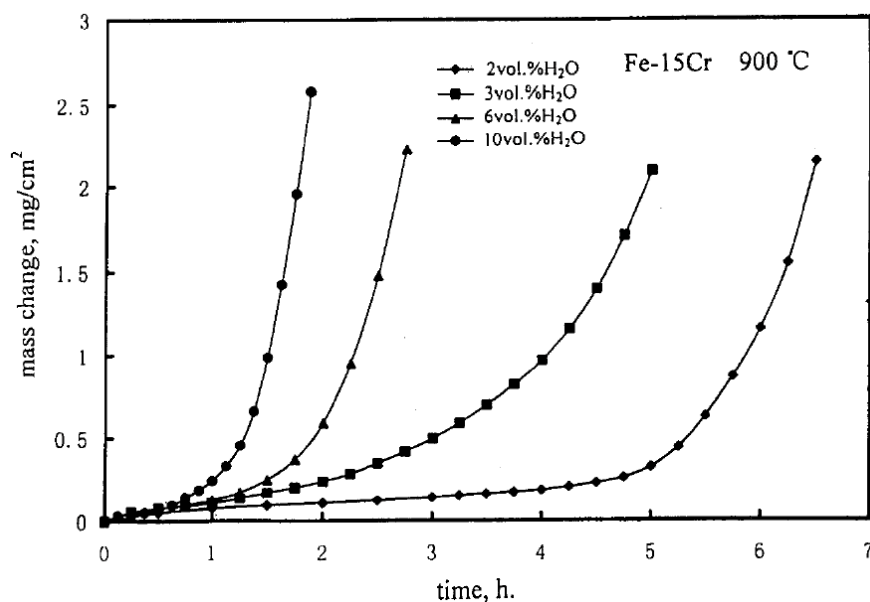
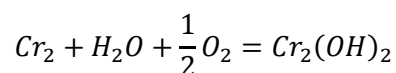
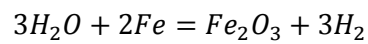


Figure 8: Mass change of a Fe-15Cr steel at 900°C for different water vapor contents in gas [48].

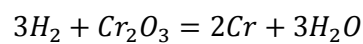
Volatile Cr₂(OH)₂ is a product of the reaction of H₂O with Cr as described in the equation below [48,49]:



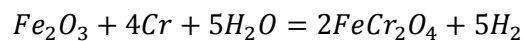
However, this reaction is only possible in high temperatures and high oxygen partial pressures. Jianian et al. [48] proposed a model where the breakaway oxidation accelerated by H₂O is preceded by an incubation period (Figure 9). During the chromia layer growth, pores, microchannels and cracks are formed and H₂O molecules reach the Cr-depleted metal surface through these defects forming hematite Fe₂O₃ and H₂:



H₂ formed with hematite reacts with the chromia layer forming Cr and H₂O.



Cr, hematite and H₂O reacts forming the spinel phase, FeCr₂O₄.



Incubation period is the time necessary for creation of defects in the Cr₂O₃ layer and for spinel phase formation and growth. With the increase in the Cr content of the alloy, incubation period is higher, and the higher the H₂O concentration the shorter the incubation period. With higher temperatures, corrosion rate is usually higher and breakaway oxidation faster, but some alloys have lower oxidation rates at higher temperatures than at lower temperatures. This is caused by higher Cr mobility at metal surface, which increases Cr supply to scale [50].

However, molecular transport in the Cr₂O₃ layer is also possible [33,51]. In this case, the grain size of the Cr₂O₃ layer bears influence in the breakaway oxidation.

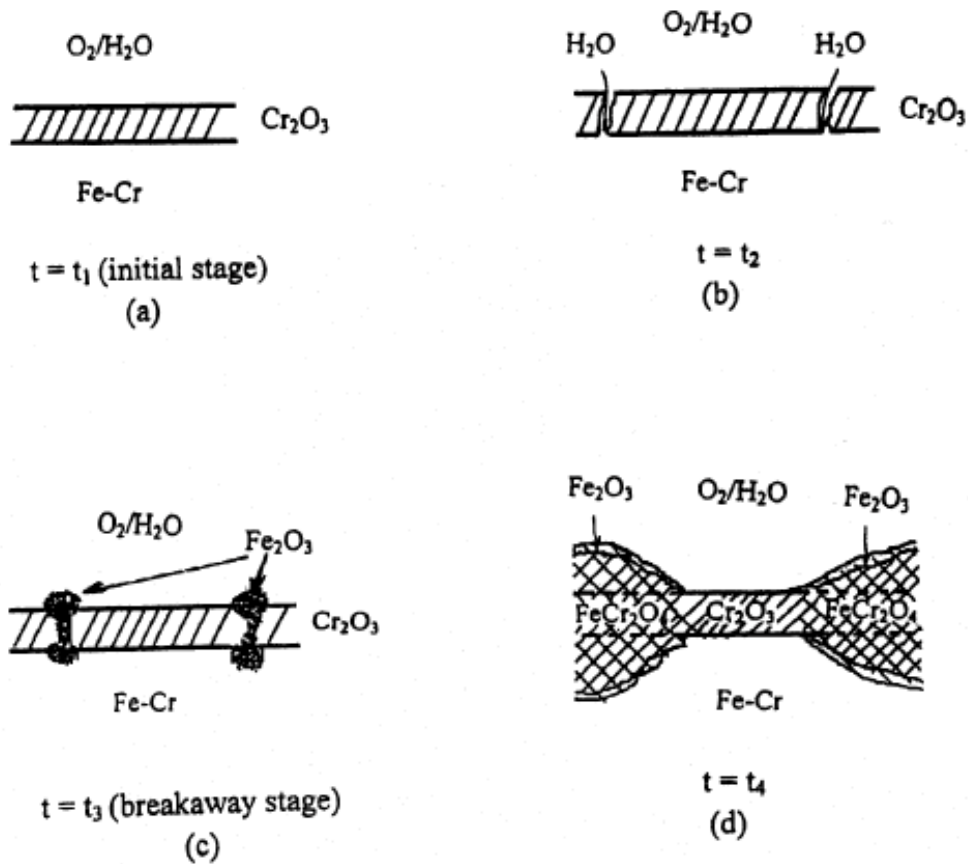


Figure 9: Breakaway oxidation sequence of a chromia-forming steel in an O_2/H_2O gas [48].

Studying P91 steel with 9%Cr, Ehlers et al. [52] suggested that hydroxyls could also accelerate the oxidation rate by performing H_2O transport from the gas to the metal faster. In this model $Fe(OH)_2$ is formed in the inner part of the pore, and diffuses to the outer part of the pore where oxygen partial pressure is higher, forming solid magnetite or hematite. Thus, the Fe ion is transferred faster to the outer scale. Porosity in the magnetite is common, being formed by vacancy condensations produced by the rapid Fe diffusion in the outer magnetite layer. Void formation is the main cause of spallation in steam oxidation [46,53,54].

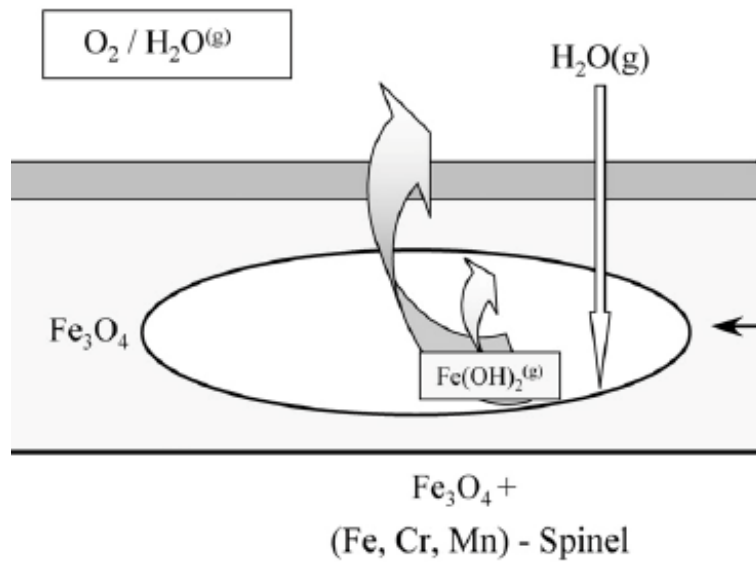


Figure 10: Molecular transportation within pores with $\text{Fe}(\text{OH})_2$ [52].

The influence of voids in oxidation in wet atmospheres was also studied by Rahmel and Tobolski [44], who proposed a mechanism where oxygen can be transported inside scale voids. As shown in Figure 11, H_2O trapped inside the void reacts with Fe from the steel and produces H_2 and an iron oxide. H_2 diffuses to the outer part of the void and reacts with oxide producing H_2O .

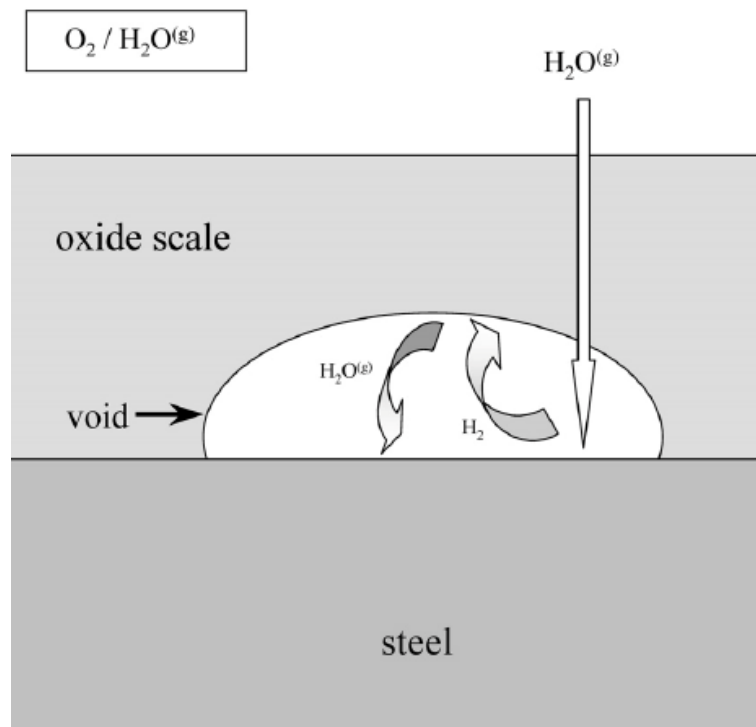


Figure 11: H_2O - H_2 transportation in voids [52].

Water vapor also enhances scale plasticity, which results in better contact with the metal [44,55,56]. A pull adhesion test was done by Monteiro et al. [56] in samples oxidized in dry and wet O_2 at $650^\circ C$ with different steel compositions and water vapor contents. Results showed that the higher the water vapor concentration, the better the adhesion.

Nakai [57] et al. showed that chromia is effective in decreasing hydrogen dissolution in steels when exposed to steam in high temperatures. Chromia layer was produced in 10%Cr steel by oxidizing it in air at $700^\circ C$ for times from 0.5 hour to 50 hours. Then, the samples were exposed to steam at 973K for different times. The result for the 100 hours exposure is depicted in Figure 12, showing that the higher the pre-oxidation time, the lower the corrosion rate due to the chromia layer.

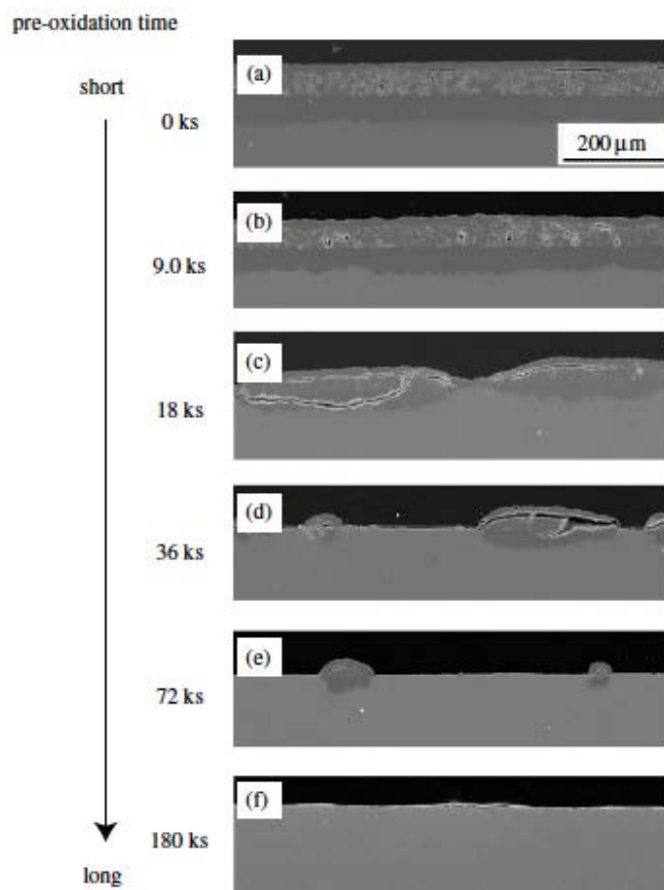


Figure 12: 10%Cr steel with pre-oxidizing time from 0 to 50 hours exposed to steam for 360ks. The result shows decreasing corrosion rate with the increasing pre-oxidation time [57].

In another work, Nakai et al. [58] studied the correlation between steam oxidation and hydrogen dissolution in pure iron and a 10Cr-0.008C steel. It was shown that steam has stronger influence on ternary steel than in the pure iron. In the steel, hydrogen was likely to dissolve in the spinel FeCr_3O_4 , which caused accelerated oxidation in steam when compared to dry air.

Parvathavarthini et al. [59,60] studied the permeability, diffusivity and solubility of hydrogen in steels with different microstructures. It was demonstrated that lattice defects work as traps, increasing hydrogen solubility and decreasing permeability and diffusivity. Martensitic microstructure offered maximum resistance to hydrogen permeability when compared to bainite and ferrite.

2.3.1.3 Oxyfuel Atmosphere

The oxyfuel atmosphere is basically composed of CO_2 and H_2O , but may also include SO_2 , N and O coming from coal or gas. Gas concentrations also change so there is a great range of compositions studied as oxyfuel atmospheres. In addition to the wide range of gas compositions, a great number of steels and new materials are also being studied for temperatures higher than the conventional coal-fired power plants.

The simplest atmosphere is CO_2 - H_2O and the most used composition is 70vol% CO_2 and 30vol% H_2O . Using this gas composition in a temperature range from 500°C to 700°C, Hünert et al. [61,62] investigated steels with 1, 9, 12 and 24%Cr at 80bar for 1000h. Scales formed by these steels had the same oxide sequence in all temperatures as shown in Figure 13. Although scale thickness has increased with temperature increase, scale thickness has decreased in higher temperatures in the alloy with higher Cr. In the 1% Cr, a sequence of FeO and FeO + Fe_3C from gas to metal was observed. In 9 and 12 Cr%, the sequence was Fe_3O_4 , spinel and internal oxidation with Cr rich oxides formation. The sequence in the 24% steel was Fe_2O_3 and Cr_2O_3 .

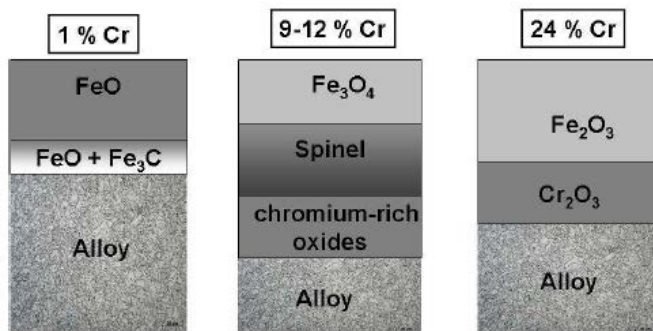


Figure 13: Oxidation products formed in different Cr contents [61].

The same gas composition with the same duration and temperatures from 550 to 700°C was studied by Pirón Abellán et al. [63]. Gas composition was compared with air, 50%Ar–50%H₂O and 50%Ar–50%CO₂. VM12, for example, presented a sequence of Fe₂O₃, Fe₃O₄ + FeCr₃O₄ and internal oxidation layer in 70%CO₂–30%H₂O. In the 50%Ar–50%CO₂ gas, P92 and X20 with 9% and 12% Cr respectively presented intense carburization. In X20 steel, it was stronger where iron rich nodules were present and weaker below the Cr₂O₃ scale. The chart with the sample weight change vs temperature shows that they displayed similar corrosion behavior in temperatures below 600°C, but bore less oxidation at higher temperatures. This characteristic is explained by higher Cr mobility at temperatures above 600°C, allowing the creation of a Cr-rich protective layers.

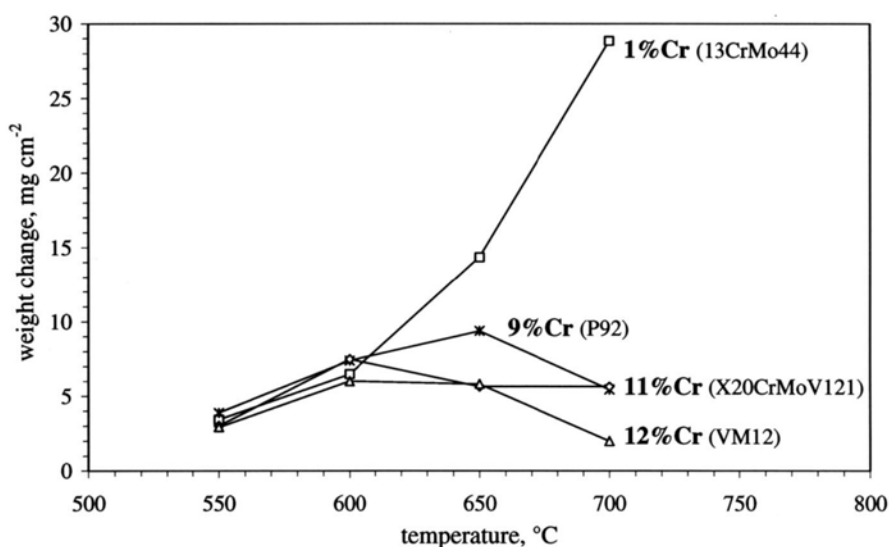


Figure 14: Weight change vs temperature chart showing a similar corrosion behavior until 600°C and faster oxidation for lower Cr content alloys above this temperature [63].

Several steels were also investigated by Mu et al. [64] at 650°C using the 70%CO₂-30%H₂O gas composition and some variations containing Ar and air (Figure 15). All alloys had a higher corrosion in the atmosphere with 70%CO₂-30%H₂O and lower corrosion in air. The authors call attention to the lack of Fe₂O₃ formation, stable at this temperature, but they did not have longer-time experiments. Similar results were reported by Meier et al. [65] who suggested that, in CO₂/H₂O atmospheres, higher chromium content is necessary to form protective scale, because carbide formation reduces Cr flux to the metal/scale interface.

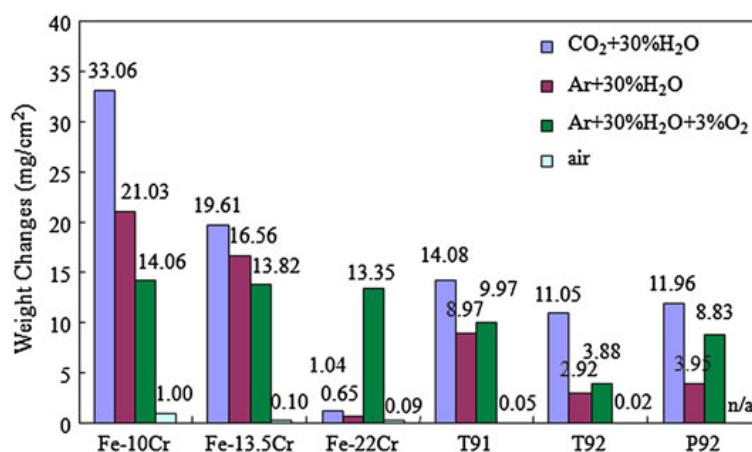


Figure 15: Specific mass change for 5 different model alloys in different gas compositions at 650°C for 96h [64].

Wet and dry CO₂ condition (Ar-20%CO₂, Ar-20%CO₂-5%H₂O and Ar-20%CO₂-20%H₂O mixtures) at 650°C were investigated by Gheno et al. [66] using Fe-Cr and Fe-Ni alloys. Metallographic analysis of the samples shows formation of a protective Cr₂O₃ layer with iron-rich nodules.

The authors propose that the breakaway oxidation of the steels follows this sequence: A protective Cr₂O₃ layer is formed, consuming Cr from the metal beneath it and creating a Cr-depleted zone. A failure in the protective zone, exposes the Cr-depleted zone to the gas and without enough Cr to form Cr₂O₃, Fe/Cr spinel is formed. Fe cations from the newly formed spinel diffuse outwards and Fe₃O₄ is formed. In the spinel, oxygen partial pressure rises locally preventing Cr₂O₃ nucleation. As oxygen diffusion into the alloy is not only inward, but also lateral, internal precipitation and conversion of the Cr₂O₃ layer to spinel oxide spread laterally. Since fast iron and oxygen diffusion across the originally

protective layer is limited to a central region, whereas the inner and outer parts may grow in all directions, the nodule assumes an elliptical shape. The schematic representation of this process is shown in Figure 16.

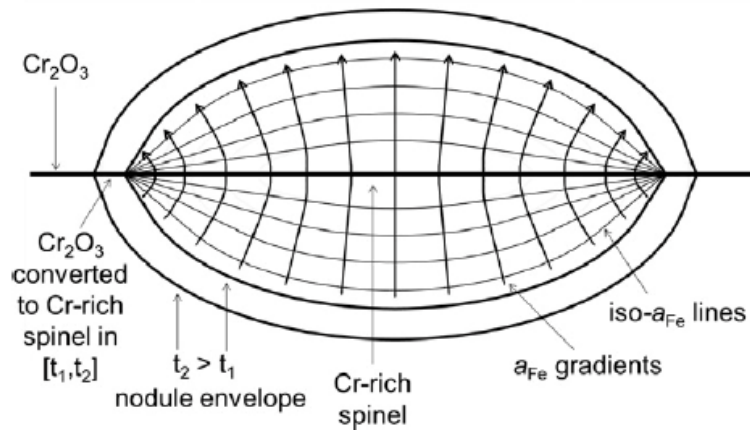


Figure 16: Representation of nodular oxide growth [66].

2.3.2 Dual Condition

The hydrogen diffusion effect between two atmospheres with different H_2 partial pressure separated by a metal is a research topic for steels used in high temperature applications, and most of the published studies are related to the corrosion of steel interconnectors in solid oxide fuel cells (SOFC).

Nakagawa et al. [67] studied 10mm-diameter ferritic steels samples with 2, 9 and 12% Cr at 600°C in a dual condition with air on one side of the sample and a mixture of 50% H_2O and 50% Ar on the other side. The results of the experiment were compared with samples oxidized only in air, and showed a great difference between both conditions in the external and internal scale (Figure 17). The samples oxidized in a single condition, using only air, showed a much slower corrosion rate when compared to the samples exposed to air in a dual condition.

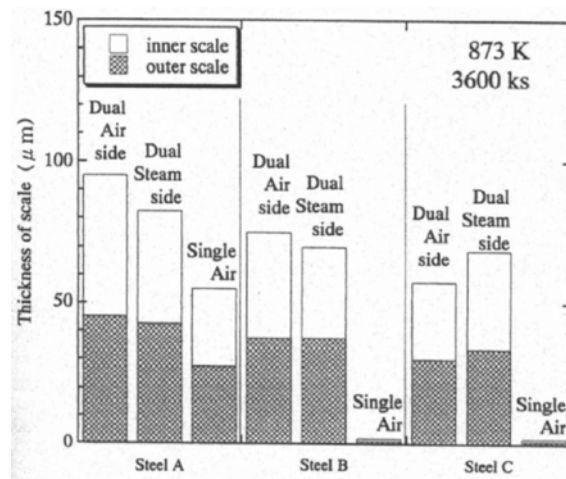


Figure 17: Results of scale thickness in dual and single atmosphere conditions for the three steels used in the [67].

In dual atmosphere condition, the scale in the steam side is formed by an external layer of Fe_3O_4 and an internal spinel. On the air side, an outer layer of Fe_3O_4 and Fe_2O_3 with large pores was observed in the air interface. The inner layer, as on the steam side, was formed by spinel. The Fe_2O_3 layer changed according to the Cr content, forming a thicker outer scale in the 9 and 12% steels.

The difference in the scale thickness of the Fe_2O_3 layer was explained to be controlled by the Fe ions supply. When ions supply is insufficient, oxygen partial pressure in the scale increases and Fe_3O_4 oxidizes, forming Fe_2O_3 . Fe ions diffusion was reduced in 9 and 12% steels, which have an internal scale rich in Cr. Thus, the Fe ions supply to the outer scale was also reduced, promoting the Fe_2O_3 phase.

Hydrogen permeation current measurements showed that, after reaching maximum value, hydrogen permeation in steel decreases parabolically with time when the 50% H_2 and 50% H_2O gas mixture was used. When 100% hydrogen was injected, the hydrogen permeation in steel reached a maximum level, and then a steady state was observed. As the permeation rate decreases parabolically with scale formation on the steam side, hydrogen permeation rate seems to be determined by proton (H^+) diffusion on the steam side.

Microstructure of scale formed on the steam side resembles the microstructure of the air side, except for voids and Fe_2O_3 formation, confirming that the effect of H_2O on the air side is important. The hydrogen effect might be

related to dissociation, that is, hydrogen that has diffused to a void in the scale reacts with oxygen to form H_2O and H_2 .

Yang et al. studied several ferritic stainless steels used in interconnects for solid oxide fuel cell (SOFC) in single and dual atmosphere condition [68-71]. Steel AISI 430, 17% Cr, when exposed to an atmosphere containing H_2 with 3% H_2O in one side and air in the opposite side at $800^\circ C$, presented different scale morphology in the side exposed to air when compared to a single condition. Scale containing Cr_2O_3 and $(Mn, Cr, Fe)_3O_4$ was formed in single condition, whereas Fe_2O_3 was formed in a dual condition [68,69].

In Crofer22, commercial steel with 22% Cr, using air in single condition, external scale containing Mn_3O_4 in contact with air, and Cr_2O_3 beneath it, was observed. On the air side of a dual condition, a fiber-like spinel was also observed in addition to the microstructure seen in the single condition.

In E-brite steel, 27% Cr, Cr_2O_3 was the only phase present in both dual and single condition. In all studies, it was ascertained that the corrosion rate and scale morphology were different in single and dual condition. In Crofer22 and AISI 430, there was greater Fe diffusion in the scale, with this effect more evident in AISI 430, which has smaller chromium content than Crofer22, resulting in a number of hematite nodules. In E-brite, the faster iron and hydrogen diffusion was not ascertained, but the single condition Cr_2O_3 scale was denser than the dual condition scale [68-71].

The iron alloy, SUS 430, with 13% Cr, was studied by Kurokawa et al. [72] in dual condition atmosphere containing air on one side of the sample and gas containing $Ar-H_2-H_2O$ on the opposite side. The samples were oxidized at $800^\circ C$ and scales in both sides of the sample presented the same oxides: $FeCr_2O_4$ in a small quantity and a dense layer of Cr_2O_3 and $MnCr_2O_4$. On the air side, cubic crystals of $MnCr_2O_4$ were observed in grain boundaries, whereas most part of the scale was formed by Cr_2O_3 . On the gas side, Cr_2O_3 whiskers were formed and $MnCr_2O_4$ was observed in grain boundaries. Using thermodynamic data, the authors concluded that the reaction between the iron oxide and Cr_2O_3 resulted in spinel $FeCr_2O_4$. They concluded that the hydrogen gradient due to dual condition did not interfere in the oxidation of the alloy studied.

Tanaka et al. [73] also studied hydrogen permeation in steel SUS 430 at $1000^\circ C$ in an atmosphere containing $Ar-H_2-CO_2$ on one side and $Ar-CO-CO_2$ on

the opposite side, that is, with hydrogen gradient, but without oxygen gradient. In this work, hydrogen permeation was measured after pre-oxidation of the sample, followed by a second step to remove the hydrogen present in the furnace wall.

After pre-oxidation at 1000°C for 60ks in an atmosphere containing Ar-20% H_2 -0.16 H_2O , the surface was covered by a Cr_2O_3 layer with less than 1% $MnCr_2O_4$ randomly distributed on the surface. After that, the sample was also exposed to different atmospheres to remove H_2O and to measure hydrogen permeability.

The hydrogen permeation in the Cr_2O_3 layer was 4 orders of magnitude smaller than in steel, indicating that hydrogen activity gradient in steel is very small and can be ignored. The authors concluded, based on activity dependence, that the hydrogen dissolved in the Cr_2O_3 layer is a neutral atom, located in oxygen sites, at very small concentrations to be considered a minor defect, therefore, not affecting the oxidation behavior of chromia-forming alloys.

Horita et al. [74] used the steel ZMG232-M0 with 22% Cr to study the effect of a dual condition atmosphere in the corrosion behavior of SOFC interconnects. Air was used on one side of the sample, and CH_4 - H_2O diluted in N_2 on the opposite side at 800°C for 1000h. On the CH_4 - H_2O side, Cr_2O_3 was formed in both dual and single condition, but the grain size in dual atmosphere condition was smaller than 1 μm , while the grain size found in single condition was between 1 and 3 μm . As the scale morphologies of both conditions were almost the same, the authors concluded that there was little interference of the dual atmosphere condition for this steel in these corrosion parameters.

Holcomb et al. [75] studied 316L tubes in dual and single condition in atmospheres H_2 -Ar H_2 -air, air and Ar for 100h at 700°C. The results showed that samples exposed to a dual condition presented a thicker and porous scale. The authors propose that the difference between single and dual condition atmospheres is due to the pores formation. Oxygen diffusion occurs in the form of O_2^- ions (Figure 18), when scale is dense, without pores.

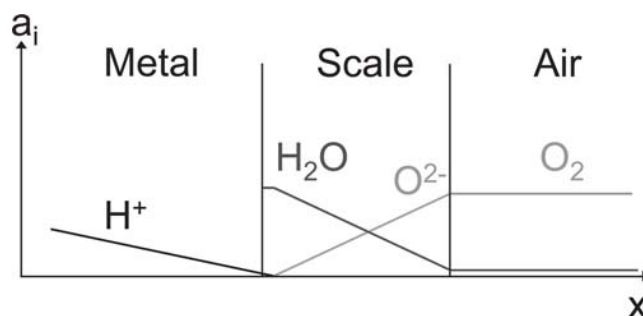


Figure 18: Scheme of activity before pore formation in scale [75].

In the metal/scale interface, reaction between H^+ and O^{2-} produces H_2O with pressure high enough to create pores, and when these pores are formed, oxygen diffuses in the molecular form (Figure 19).

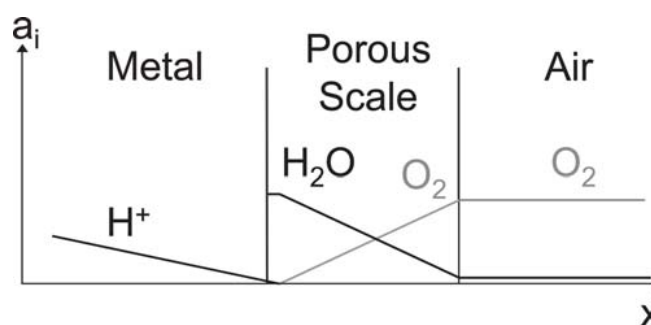


Figure 19: Scheme of activity after pores formation in scale [75].

Sandvik Sanergy HT, a ferritic stainless steel with 22% Cr, was also investigated by Skilbred et al. [76] in single and dual atmosphere conditions, in temperatures between 800 and 900°C for 100, 300 and 500 hours using air on one side and wet or dry H_2+Ar on the opposite side. Using a secondary ion mass spectrometry, SIMS, it was observed that, in a dual condition, there is a greater concentration of hydrogen in oxides formed when compared to single condition. Fe concentration on the surface was also greater in dual condition, especially in nodules formed only in dual atmosphere condition. The authors suggest that hydrogen dissolved as a proton in the oxide increases the vacancy concentration, leading to greater metallic ions diffusion in the oxide.

The difference between single and dual atmosphere conditions was also observed by Rufner et al. [77] studying oxidation behavior of FSSs 430 (17Cr) and 441 (18Cr) at 800°C for up to 300h in single atmosphere (moist air/air) and dual atmosphere (moist air/moist hydrogen) environments. While difference in 430 was subtle, microstructure in the 441 changed from a protective Cr rich oxide to a thick scale with hematite and spinel.

Hünert et al. [78,79] have studied steels in dual condition using pressures up to 8 MPa and concluded that corrosion rate under dual condition is larger than in single condition. The higher the pressure, the higher the carburization and oxidation of the alloys investigated.

2.4 Whiskers Growth

Whiskers growth in oxides displays great dependence on temperature, stress, texture and gas composition, especially H_2O [36,80-84].

Voss et al. [80] discuss blade formation in iron oxides and propose a mechanism summarized in Figure 20. In this mechanism, blades grow in fast Fe diffusion interfaces, which in this case are pores and tunnels at the hematite grain boundaries.

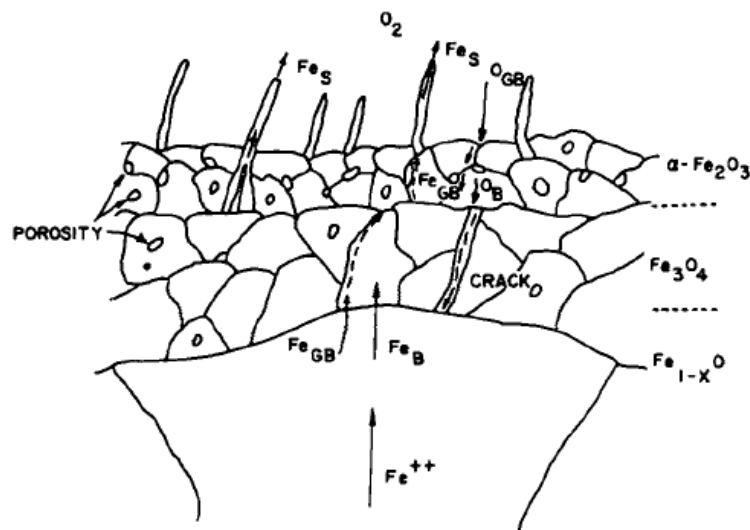


Figure 20: Blade growth in iron oxide proposed by Voss et al [80].

Yuan et al. [81,82,84] studied the nanowires and nanoblades in Fe and Cu oxides and proposed a model explained in Figure 21 where nanowires grow on a polished surface and nanoblades on a sandblasted surface. Nanowires grow in the middle of the hematite grain and the driving force for the growth is relaxation of compressive stress generated from the solid-state transformation at the $\text{Fe}_3\text{O}_4/\text{Fe}_2\text{O}_3$ interface, and Fe diffusion to the surface occurs through grain boundaries. Nanowires grow in grains rather than the grain boundary regions, and formation of twin boundaries is attributed to nanowire initial nucleation and

growth stages on different surface facets of the underlying Fe_2O_3 grain. Fe_2O_3 nanowires grow at their tip, where Fe cations are supplied by substrate-nanowire adatom exchange via surface diffusion. The Fe_2O_3 nanowire growth mechanism was the same found in CuO nanowires.

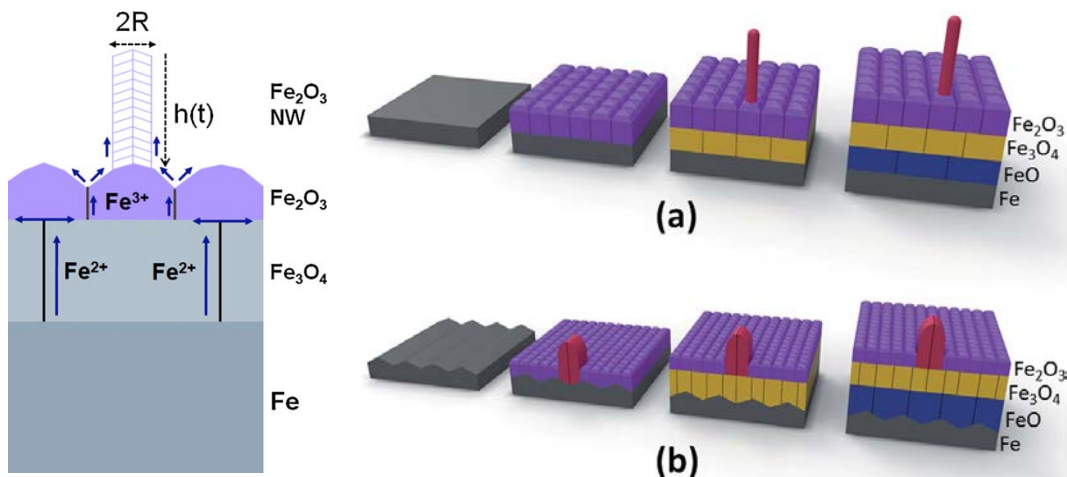


Figure 21: Left and right (a): nanowire growth mechanism. Right (b): nanoblade growth mechanism [81,84].

Nanoblades grow via fast diffusion of Fe atoms through the merged Fe_2O_3 planar grain boundary, which leads to platelet growth with wide and thin blade geometry. Initially, Fe cations supporting nanoblade growth come directly from the underlying Fe substrate through internal grain boundary formed by merging Fe_2O_3 grains. With continued oxidation leading to formation of the thermodynamically more stable phases of Fe_3O_4 and FeO in inner regions, the root region of the nanoblade is thus transformed to Fe_3O_4 to accompany the layered oxide growth (Figure 21). Substrate texture influence in whiskers formation was also investigated by Srivastava et al. [83] with similar results from Yuan et al [81,82,84].

2.5 Selective Oxidation of Multiphase Alloys

Chromium content of an Fe alloy is an important parameter for alloy selection since the higher the chromium content, the more likely the formation of Cr_2O_3 is, which is known as a protective layer due to its slow oxidation rate [33,34]. Chromia, Cr_2O_3 , formation also depends upon the temperature, alloy microstructure, alloying elements and atmosphere composition [33,34].

For the chromia to act as a protective layer it has to be selectively oxidized prior to other non-protective oxides, such as all iron oxides, for example. The faster and the more stable chromia growth, the less probable the growth of non-protective oxide is [33,85]. The minimum solute concentration for the formation of a protective oxide layer is described by the equation below [34,65].

$$N_{Cr}^{(o)} > \left[\left[\frac{\pi g^*}{3} \right] N_O^{(s)} \frac{D_O V_m}{D_{Fe-Cr} V_{CrO_{1.5}}} \right]^{\frac{1}{2}}$$

$N_{Cr}^{(o)}$: Initial solute concentration, Cr

$N_O^{(s)}$: Oxygen solubility in the alloy

g^* : Critical volume fraction of the oxide

D_O : Diffusivity of oxygen in the alloy

V_m : Molar volume of the alloy

$V_{CrO_{1.5}}$: Molar volume of the Cr₂O₃

D_{Fe-Cr} : Alloy interdiffusion coefficient

The equation above is valid for a single-phase alloy, but when second phase is present, the selective oxidation may be different. This is the case of austenitic stainless steels where Cr₂₃C₆ carbides are present. Those carbides are consumed preferentially, and they quickly form a protective chromia layer. Consequently, a carbide-free zone is formed beneath the oxide layer [86-90].

Gesmundo and Gleeson [89] suggested an equation to describe selective oxidation when a second phase is present.

$$[X_m \{X_m + 2f_v(X_p - X_m)\}]^{1/2} \geq \frac{2V_{all}}{V_{ox}} \left(\frac{k_p}{D_B} \right)^{1/2}$$

X_m : Mole fraction of the protective-scale-forming element B in the matrix

X_p : Mole fraction of the protective-scale-forming element B in the precipitate

f_v : Precipitate volume fraction

V_{all} : Molar volume of the alloy

V_{ox} : Molar volume of the oxide

k_p : Parabolic rate constant

D_B : Diffusional coefficient of B

The above equation is better used to preview the corrosion in a multiphase alloy than in the former equation, but does not consider carbide distribution, carbide size, etc. Grain boundary diffusion is much faster than lattice diffusion, as seen in the diffusion coefficients in the equations below, and can play an important role in the corrosion behavior of the alloy.

$$D_{Cr}^{grain} = 2.5 \times 10^{-6} \exp\left(\frac{-44700}{RT}\right)$$

$$D_{Cr}^{latt} = 1.9 \times 10^{-1} \exp\left(\frac{-58800}{RT}\right)$$

Durham et al. [86] and Susanto and Young [88] developed some alloys using computational thermodynamics to investigate how carbide dissolution and the ferrite growth affected the corrosion behavior of the alloys. It was seen that when Si is added to Fe-Cr-C alloys, Cr_2O_3 is formed, ferrite formation is enhanced and a SiO_2 layer is formed at the metal/scale interface. The formation of the protective scale might be due to the faster diffusion of Cr in ferrite than in austenite. Ferrite was formed by a combination of steel decarburization, forming a carbide-free zone and the consumption of Cr by scale.

2.6 Diffusional Growth of Ferrite

The diffusional growth of ferrite can play an important role in corrosion behavior of iron alloys, since Cr can diffuse faster in ferrite than in austenite leading to faster growth of a chromia protective scale [86,88].

Purdy and Kirkaldy [91] used a synthetic austenite/ferrite alloy to investigate the ferrite growth in ferritic steel [92,93]. They used a synthetic ferrite/austenite boundary to avoid stereological problems and to avoid low-energy lattice orientation relationship between austenite and ferrite. The microstructure resembles those found in oxidized alloys where ferrite is formed, except for the oxide layer, which is not present in their investigation. A Fe-0.57C alloy was partially decarburized in wet hydrogen at 920°C and then the H₂ was substituted by argon and slowly cooled to 755°C. As the carbon content at the surface is essentially zero, ferrite nucleates at the surface during the cooling. So a solid polycrystalline layer of ferrite rapidly grows along the decarburized surface toward the interior of the sample. Carbon diffusion away from the ferrite/austenite interface discourages ferrite nucleation of this interface. Once the specified temperature of 755°C was reached, the sample was kept at this temperature for 36h to remove the carbon gradient in both phases. Then the sample was cooled down and reheated many times at 729°C. The results show that ferrite growth and boundary migration occur in an accurate parabolic way and that interfaces likely to be of the disorder type exhibit volume diffusion-controlled growth kinetics.

Other works also investigated the austenite/ferrite interface, albeit adding some alloying elements. C.R Hutchinson et al. [93] studied a Fe-C-Ni and a Fe-C-Mo alloy using an isothermal heat treatment and a decarburization experiment. In Figure 22 they show a classification of the alloying elements and their interaction with steel. In class 1 are the elements with weak interaction with carbon and barely display interaction with the interface. In class 2, there is strong interaction between the elements and the interface, which may cause a solute drag effect. Carbide-forming elements are in class 3, but in some heat treatments, an element from class 2 can move to class 3.

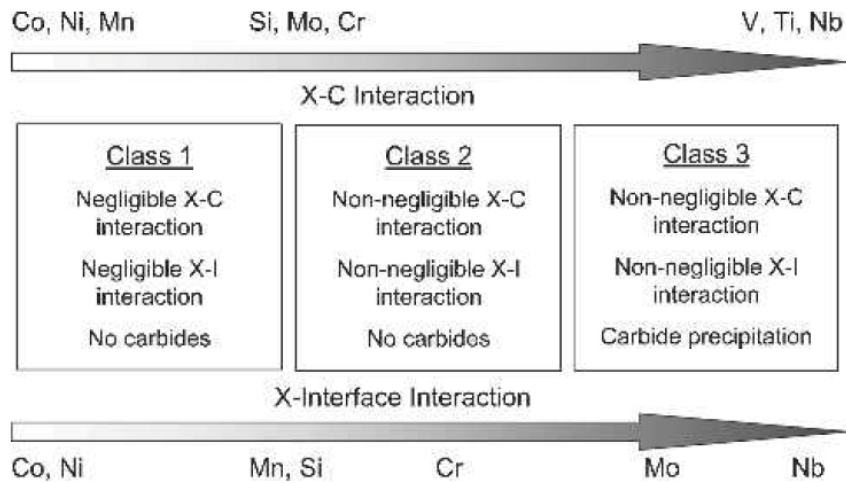


Figure 22: Classification of classical substitution alloying elements in steel (X). Above: according to their interaction with C. Below: according to their estimated binding energies with the austenite/ferrite interface [93].

The results of the Fe-C-Ni alloy confirmed Figure 22 classification showing that Ni has little interaction with C and the interface. On the other hand, the Fe-C-Mo presented additional interaction of Mo with the boundary, which was interpreted as a drag effect.

3 Materials and Methods

3.1 Materials and Gases

In this work, 5 model alloys, 1 commercial steel and pure iron were used. The 5 model alloys (P1, P2, P3, P4 and 5) were produced in the National Institute of Standards and Technology (NIST) using a vacuum electric furnace to produce samples with different Cr, Co and C contents in order to study the influence of the alloying elements on corrosion behavior under single and dual atmosphere conditions. Sample compositions are shown in Table 1.

Before the corrosion experiments, the model samples were heat-treated at 760°C for 1 hour and then cooled in calm air. Samples P1 and P5, which have 0.015% C are ferritic, and samples P2, P3 and P4 with more carbon are martensitic.

The martensitic steel VM 12 was supplied by Vallourec as a plate weighting 10kg. The iron RFe12 was supplied as small coupons.

Table 1: Samples Chemical Composition in wt%.

Samples	Cr	Co	C	W	Mn	Si	V
P1	12,3	1,03	0,01	<0,01	<0,02	0,03	<0,01
P2	12,3	3,09	0,18	0,04	<0,02	0,03	<0,01
P3	14,4	1,06	0,17	0,03	<0,02	0,03	<0,01
P4	14,2	3,1	0,16	0,04	<0,02	0,03	<0,01
P5	14,1	3,04	0,01	<0,01	<0,02	0,03	<0,01
VM 12	11,7	1,51	0,14	1,47	0,28	0,51	0,2
RFe12 (1.1018)	0,01	<0,01	0,01	<0,01	0,03	<0,01	<0,001

From the samples presented on Table 1, P1, P5 and Rfe12 bear a ferritic microstructure, whereas P2, P3, P4 and VM12 have a martensitic microstructure as shown in Figure 23 and Figure 24.

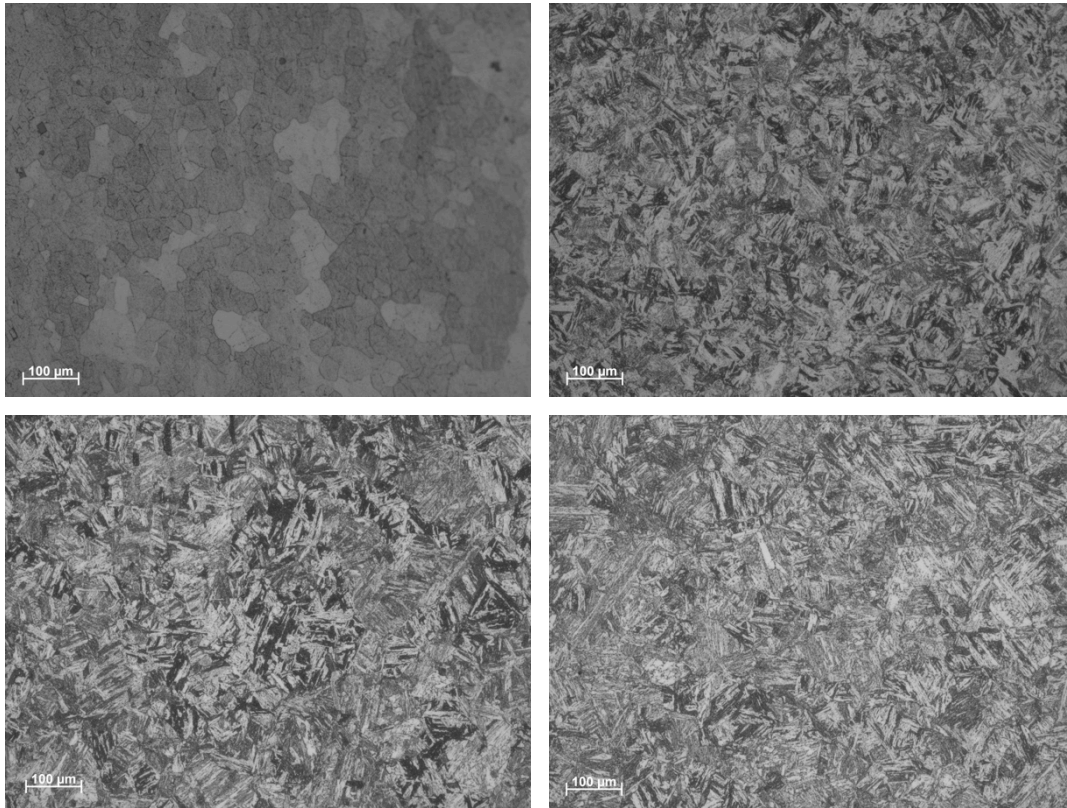


Figure 23: Light Microscope pictures. Top left: alloy P1. Top right: alloy P2. Bottom left: alloy P3. Bottom right: alloy P4.

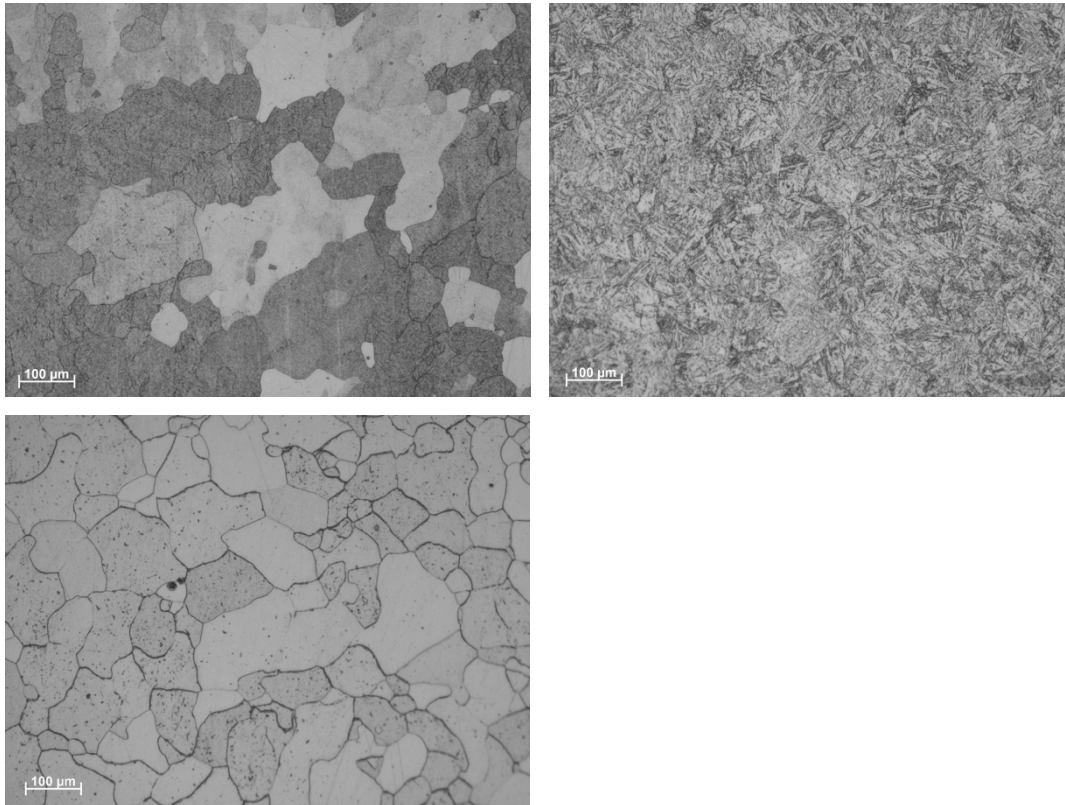


Figure 24: Light Microscope pictures. Top left: alloy P5. Top right: VM12. Bottom left: RFe12.

Three gases with 70vol% CO₂, 1vol% SO₂, and increasing H₂O concentration from Gas 1 to Gas 3 were used. Gas compositions are shown on Table 2.

Table 2: Gases Compositions at 600°C in vol%.

Elements	Gas 1	Gas 2	Gas 3
CO ₂	70	70	70
SO ₂	1	1	1
H ₂ O		1	29
Ar	29	28	

Gases fugacity calculated using Factsage software are shown on Table 3.

Table 3: Gas fugacity.

Fugacity	Gas 1	Gas 2	Gas 3
O ₂ (10 ⁻¹² bar)	29.858	3.1	62.887
CO ₂ (bar)	0.98592	0.97222	0.7
CO (10 ⁻⁷ bar)	24.340	23.556	11.907
H ₂ (10 ⁻⁷ bar)	0	0.0909	13.332

3.2 Methodology

After being heat treated at 760°C for 1 hour and then cooled in still air, the model samples were cut with water to produce samples for the single and dual experiments. VM12 and RFe12 samples were cut in a regular cutting machine with SiC discs.

Samples used in single condition atmosphere were rectangular with 20mm x 10mm x 3mm. In the dual condition experiment, cylindrical samples with two dimensions were used: 20mm x 3mm or 10mm x 3mm. The smaller sample from the dual condition experiment was pressed into an iron (Rfe12) ring to meet the sample-holder dimensions (Figure 25).

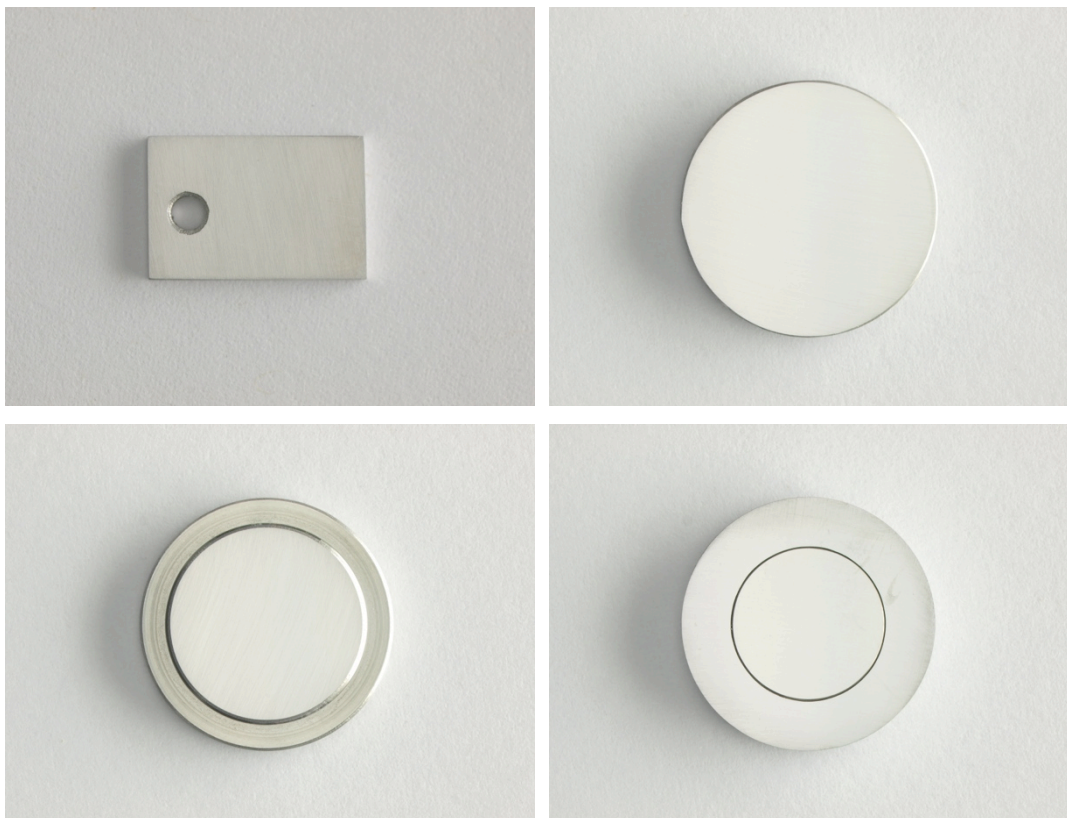


Figure 25: Top Left: Single atmosphere condition samples. Top right: Dual atmosphere condition sample (20mm x 3mm) on the gas side. Bottom left: Dual atmosphere condition sample (20mm x 3mm) on the gas water vapor side with the bevel for sealing. Bottom right: Dual atmosphere condition sample (15mm x 3mm) on the gas side. The sample is in the middle pressed by an iron (RFe12) ring. The water vapor side has the same bevel from the water vapor side samples with 22mm x 3mm.

After being cut, all samples were ground to 1200 grit SiC paper and then they were cleaned in ultrasonic bath with acetone, for ten minutes to remove any contamination, and then rinsed in ethanol. The last sandpaper and the cleaning were always done right before the experiment.

Samples were then exposed to the gases, Gas 1, 2 or 3, for 1000h at 600°C. In a single condition, all samples were exposed to gases 1, 2 and 3 for 1000h at 600°C. In the dual condition experiment, only gases 1 and 2 were used. P2 and RFe12 were not exposed to a dual condition experiment. The summary of the experiments done is shown in Table 4.

Table 4: Summary of the experiments. All experiments were done at 600°C for 1000h. X: Experiment done, •: Experiment not done.

Samples	Single Condition			Dual Condition	
	Gas 1	Gas 2	Gas 3	Gas 1	Gas 3
P1	x	x	x	x	x
P2	x	x	x	•	•
P3	x	x	x	x	x
P4	x	x	x	x	x
P5	x	x	x	x	x
VM12	x	x	x	x	x
RFe (1.1018)	x	x	x	•	•

After the corrosion test, a macro picture of the sample was taken and the surface was analyzed by stereomicroscope, SEM and EDS. After that, samples from the dual condition experiment were mounted in epoxy resin and cut. The single condition samples were only mounted. They were ground and polished with diamond fluid to 1 μ m.

Analysis of the cross-section was performed in all samples by light microscope, SEM and EDS. Some samples were analyzed in TEM, FIB and EPMA.

Microstructure analysis of samples were performed using an stereo microscope (Olympus Model SZX 12), an optical microscope (Olympus Model GX71), a scanning electron microscope (LEO Model 1530 VP) with an EDS (Bruker) attached to it, a transmission electron microscope (JEOL JEM-2200FS and JEOL 4000FX), focused ion beam microscope (FEI Strata FIB200xP TMP) and electron micro probe analysis (JEOL JXA-8900 RL)

3.2.1 Single Atmosphere Condition Experiment

The single condition experiment was done using the **OXIdation-SIMulation-Equipment**, or Oxisim (Figure 26), which is a furnace where the samples are fixed (Figure 27) or hung in an alumina sample holder. The gas flow from each gas is measured by individual gas flow meters, being then mixed together with pre heated H₂O.



Figure 26: Single condition furnace, Oxisim.



Figure 27: Sample-holder from the single condition experiment where the samples are glued with cement for high temperature applications.

3.2.2 Dual Atmosphere Condition Experiment

In the dual condition experiment, each sample was placed in a sample holder consisting of two Al_2O_3 tubes. The sample stays between both tubes and a gold ring is used to seal the system when a pressure is applied (Figure 28).

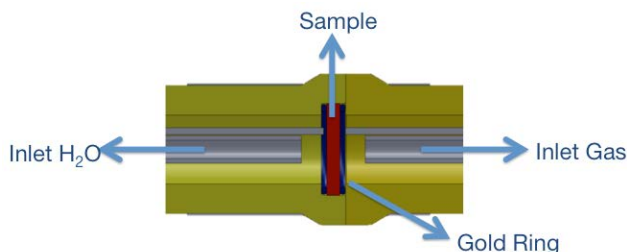


Figure 28: Sample holder. The sample lies between two Al_2O_3 tubes and sealing is done using gold O-Rings. Inlet gas and inlet water vapor are injected by 316 stainless steel tubes.

The sample-holder was then inserted into a tubular furnace (Figure 29) with the water vapor side faced down and the gas side faced up. The gases from the gas side were pre-heated at around 200°C before entering in the furnace and the H_2O entered as a liquid in the furnace. The temperature of the furnace was controlled by three thermocouples in each side. One was positioned less than 5mm from the sample, the second in the middle of the Al_2O_3 tube, and the last one in the outlet gas exit.



Figure 29: Furnaces used in the dual condition experiments. The experiment was run with the furnaces in the vertical position.

4 Results

4.1 Alloy P1

Alloy P1 is a ferritic steel with 12.3% Cr–1.03%Co–0.01%C. It was exposed to gases 1, 2 and 3 in single atmosphere condition, and to gases 1 and 3 in dual atmosphere condition. From all the model alloys and the commercial steel VM12, it was the most severely oxidized alloy in both single and dual condition. This was an expected result considering that from all alloys, but RFe12, P1 and P2 are those with less chromium

In single condition atmosphere in Gas 1, the alloy exhibited randomly distributed nodules on the surface with the coalescence of few of them to form continuous scale. As humidity increases in Gas 2 and 3, nodules density increases and they merge, forming a continuous scale.

Chromia, Cr_2O_3 , is the main oxide of the thin protective scale growing on the samples, but in some parts, spinel FeCr_2O_4 grows underneath this scale. The nodules were always composed of an external scale of hematite, Fe_2O_3 , in contact with air and magnetite, Fe_3O_4 , underneath. Fe/Cr spinel, FeCr_2O_4 , forms the internal scale with different Cr contents in the spinel. Cr concentration increase in the oxide/metal interface, and Cr_2O_3 can form at the interface instead of a Fe/Cr spinel.

Sulfur from the gas is also present in the scale and in the metal, being observed in chromium rich regions.

Nodule surface morphology also changes with water vapor content of the atmospheres. In Gas 1, needle-like whiskers grow on the surface of the nodules and they change to blade-like whiskers in gases 2 and 3.

Porosity is found in all conditions, being characteristic of the nodules rich in iron oxides. Nodules were porous even in the samples oxidized in Gas 1, which did not have water vapor.

In Gas 1 in dual condition, P1 was less oxidized than in single condition on the gas side. This was an unexpected result, since they should have

displayed at least the same corrosion behavior, due to the same gas and alloy composition. Iron oxide nodules were also less porous in a dual condition.

On the other hand, in Gas 3, the dual condition experiment produced a thick porous scale with some whiskers and no Cr_2O_3 in contrast to a single condition, where nodules were found.

The water vapor side of Gas 1 in dual condition produced a porous scale with blades in the grain boundaries of this porous phase. In Gas 3, no blades were found.

4.1.1 Single Atmosphere Condition

4.1.1.1 Gas 1 (70 CO_2 – 1 SO_2 – 29 Ar)

In Gas 1, alloy P1 oxidized almost homogeneously, but from the bottom of the sample in contact with the cement and in the top, where gas flow seems to interfere in sample corrosion as seen in Figure 30.

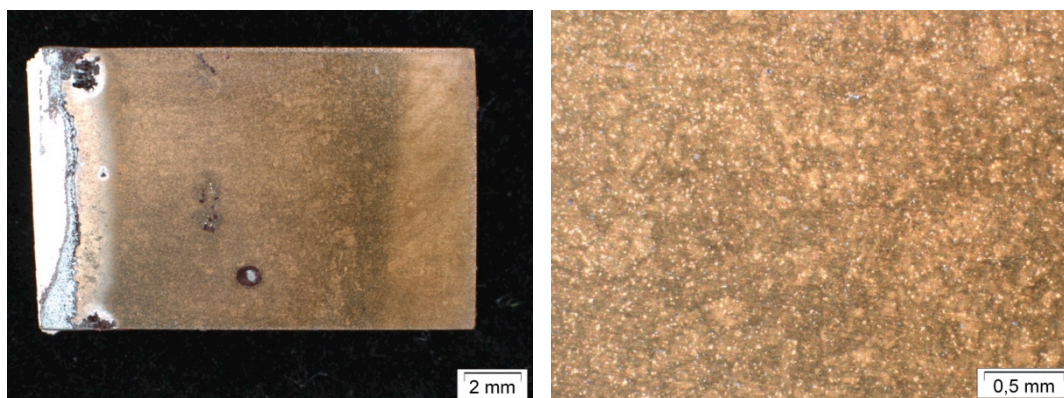


Figure 30: Stereomicroscope pictures of alloy P1 exposed to Gas 1 at 600°C for 1000h in a single atmosphere condition. The white part in the bottom of the sample is the cement used to stick the sample to the sample holder. Most part of the sample is homogeneous, but for the top. This may be an effect of the gas flow.

Several iron-rich nodules have grown randomly on the surface with different sizes, and are randomly distributed. The nodules are highly porous and exhibit hematite whiskers on top. Most part of the surface is covered by a thin layer of Cr_2O_3 (Figure 31).

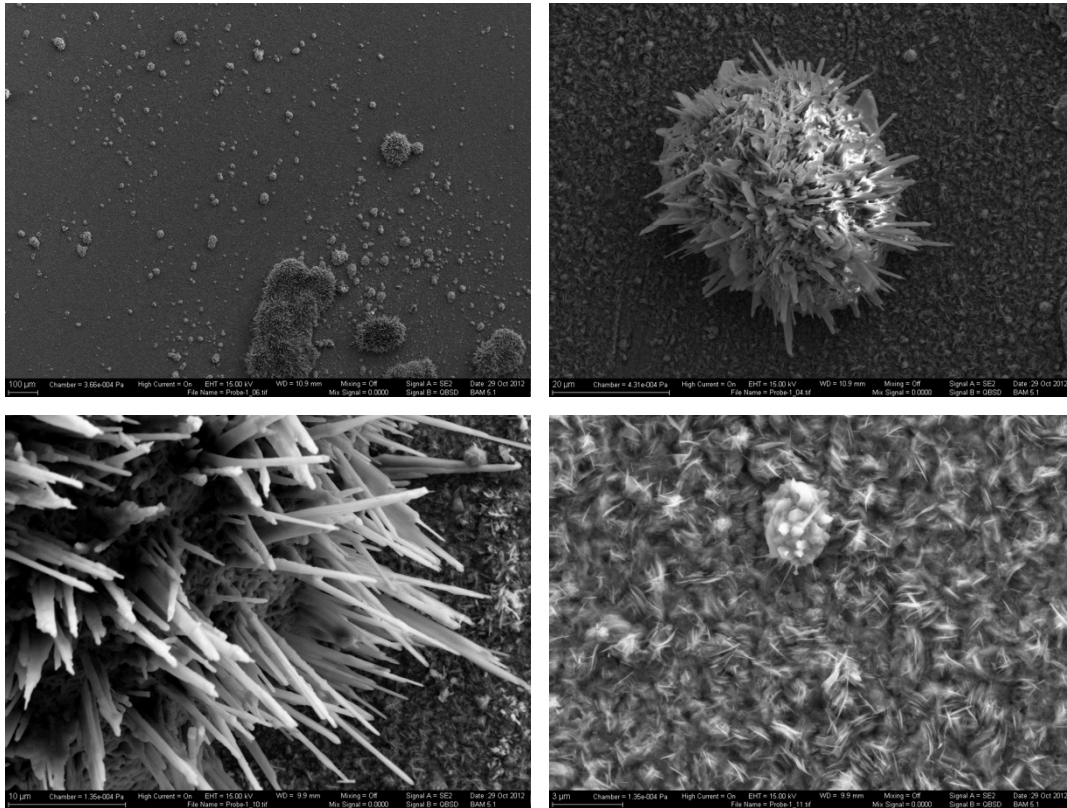


Figure 31: SEM secondary electrons (SE) pictures of the surface of alloy P1 exposed to Gas 1 at 600°C for 1000h in a single atmosphere condition. Top left: Iron rich nodules randomly distributed on surface with different sizes. Top right: Iron-rich nodule with hematite whiskers. Bottom Left: Nodules with whiskers and porosity. Bottom right: Nodule growing in a Cr_2O_3 layer.

The cross-sections of the nodules are shown in Figure 32. The red color of the whiskers in the light microscope using polarized light characterizes the structure as hematite. High porosity seen on the surface is also clear in the picture on the right.

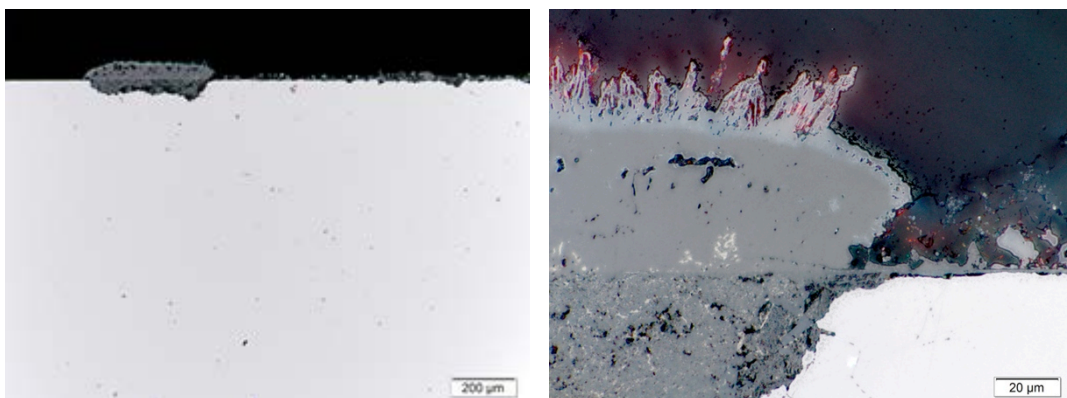


Figure 32: Light microscope pictures of alloy P1 exposed to Gas 1 at 600°C for 1000h in a single atmosphere condition. The sample presented a continuous layer of Cr_2O_3 and some nodules rich in iron. On the right picture using polarized light, the red color of the whiskers on the top of the nodule identifies that phase as hematite.

In Figure 33, the EDS from the scale shows that the thin layer covering the surface is spinel, Cr_2O_3 , or both. Sulfur is also present in both scale and metal, indicating that it permeates from the gas into the sample.

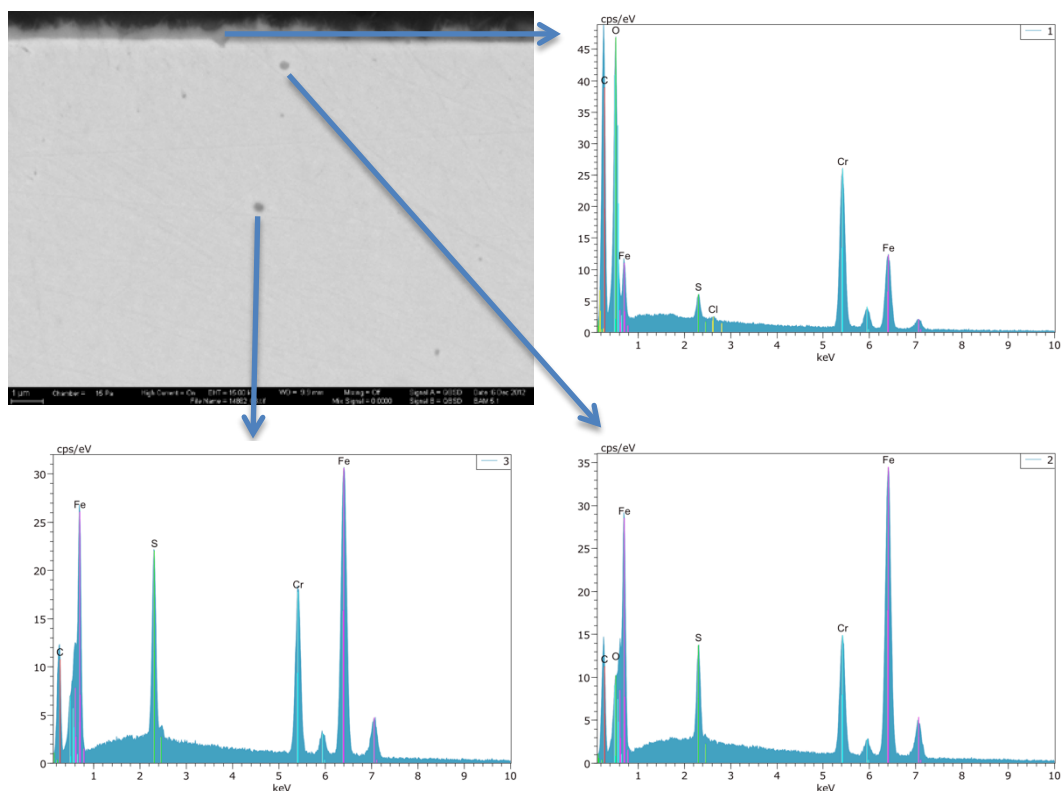


Figure 33: The EDS from alloy P1 scale exposed to Gas 1 at 600°C for 1000h in a single atmosphere condition shows the presence of O, Cr, Fe and S. This indicates that the scale is formed by a Fe/Cr spinel, Cr_2O_3 or both of them. Sulfur presence not only in the scale, but also in the metal, clearly shows that the sulfur from the gas penetrates into the sample.

4.1.1.2 Gas 2 (70 CO_2 – 1 SO_2 – 1 H_2O – 28 Ar)

In Gas 2, alloy P1 was hung to a sample holder (Figure 34) instead of being glued with cement. This sample has more Fe-rich nodules in one region of the surface, indicating that the gas flow also interferes in the corrosion process.

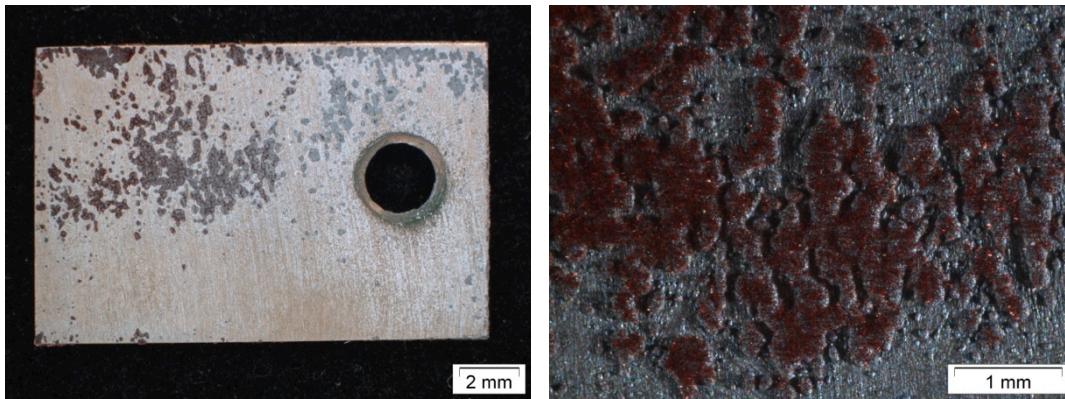


Figure 34: Stereomicroscope pictures of alloy P1 exposed to Gas 2 at 600°C for 1000h in a single atmosphere condition showing iron rich nodules with hematite on the top concentrated in one side of the sample.

Alloy P1 surface exhibited isolates nodules rich in iron and vast areas of merged nodules forming a scale. Nodules are extremely porous and blades grow on their surfaces (Figure 35).

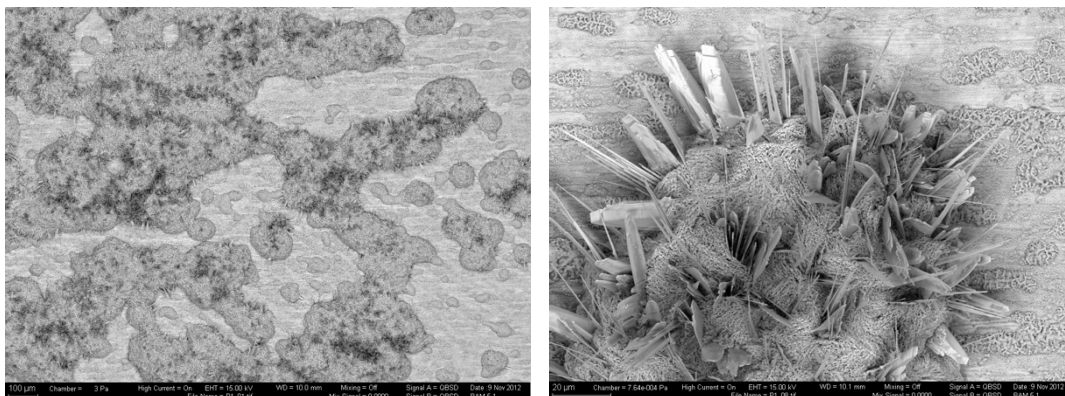


Figure 35: SEM backscattered electrons (BSE) pictures of the surface of alloy P1 exposed to Gas 2 at 600°C for 1000h in a single atmosphere condition. Nodules are merging themselves and are very porous with blades on the top.

In Figure 36, the picture on the left shows isolated nodules with large deep growth inside the metal, showing an irregular pattern of alloy oxidation. The nodule is also extremely porous in both internal and external corrosion layers. The same kind of structure can be seen in SEM in Figure 37.

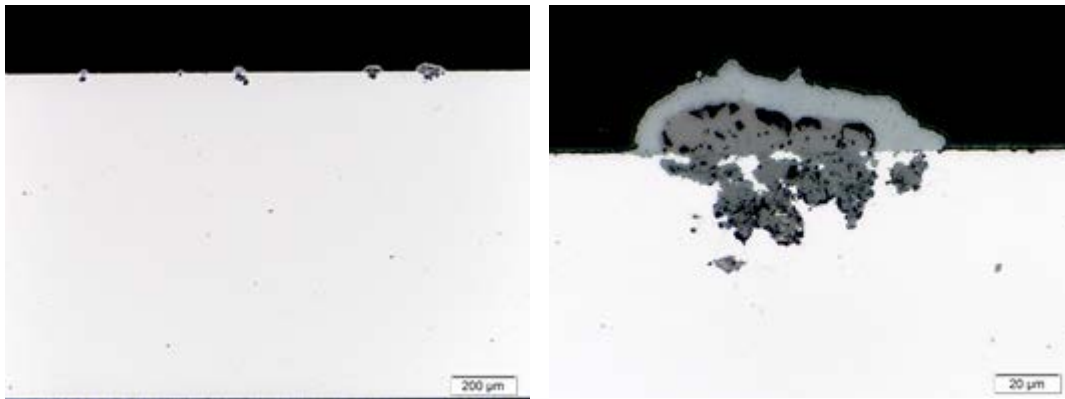


Figure 36: Light microscope pictures of alloy P1 exposed to Gas 2 at 600°C for 1000h in a single atmosphere condition. Isolated nodules are extremely porous and the internal oxide layer grows in irregular pattern inside the metal.

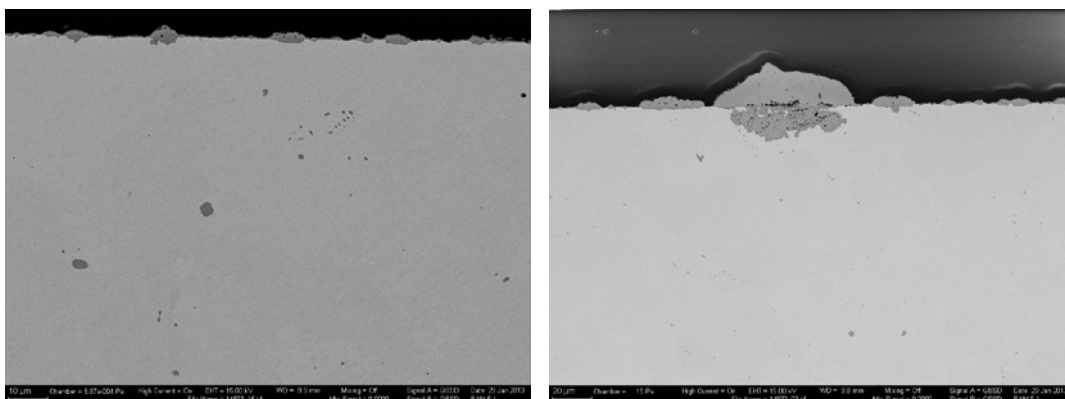


Figure 37: SEM (BSE) pictures of alloy P1 exposed to Gas 2 at 600°C for 1000h in a single atmosphere condition. Left side: isolated nodules rich in iron. Right side: Nodule composed of hematite, magnetite and spinel characterized by EDS in Figure 38.

Nodules found in alloy P1 exposed to Gas 2 always had the same external scale structure, composed of hematite (Fe_2O_3) in the gas interface and of larger magnetite (Fe_3O_4) layer beneath it. The internal layer was composed of Fe/Cr spinel (FeCr_2O_4) with higher Cr content closer to the external scale and to the metal (Figure 38) confirmed by EDS in Figure 39. In Figure 39, a particle with high sulfur is also observed in the metal, indicating that sulfur from the gas diffuses into the metal.

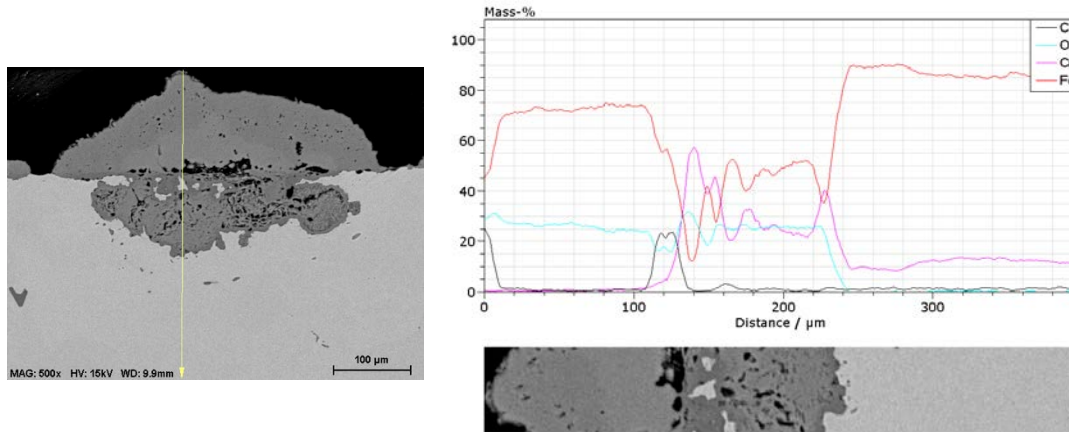


Figure 38: EDS line scan of alloy P1 exposed to Gas 2 at 600°C for 1000h in a single atmosphere condition. The external oxide layer is composed of a thin outer hematite layer followed by a magnetite layer. The internal oxide is formed by a Fe/Cr spinel with higher Cr content closer to the external oxide layer and to the metal.

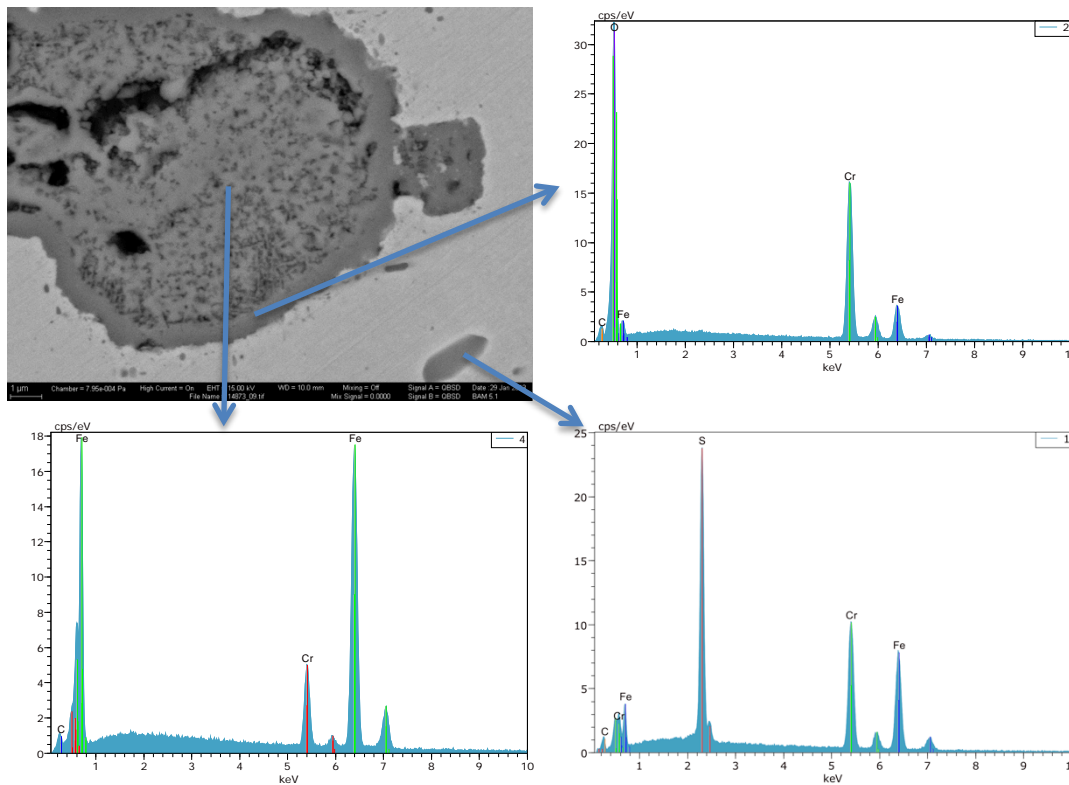


Figure 39: EDS of Alloy P1 exposed to Gas 2 at 600°C for 1000h in a single atmosphere condition. It shows higher chromium content close to the metal and sulfur diffusion from the gas into the metal. A Cr_2O_3 layer is formed in the metal/scale interface.

4.1.1.3 Gas 3 (70 CO₂ – 1 SO₂ – 29 H₂O)

In Gas 3, alloy P1 corrosion was quite homogeneous in the front and at the back of the sample, except for the areas near the cement (Figure 40).

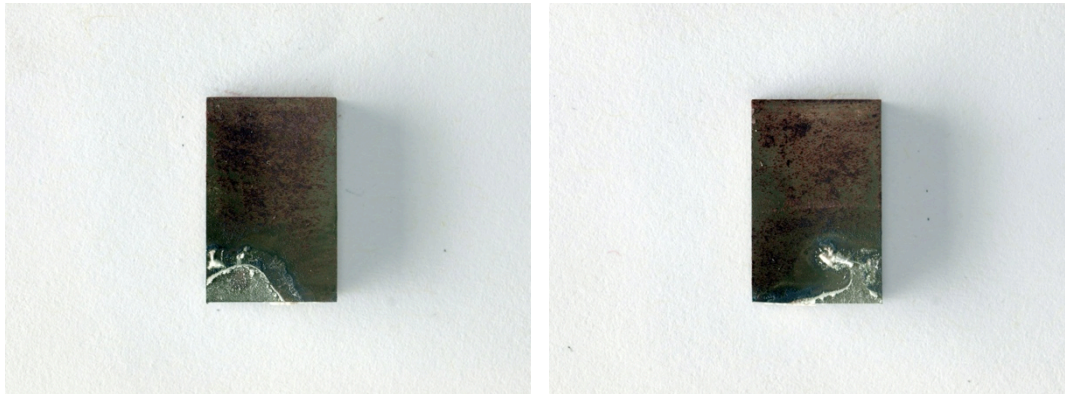


Figure 40: Macro pictures of both sides of alloy P1 sample exposed to Gas 3 at 600°C for 1000h in a single atmosphere condition. The white color at the bottom is the cement used to glue the sample to the sample-holder. Despite the area around the cement, oxidation was homogeneous in the remainder of the sample.

The surface of alloy P1, exhibited isolates nodules rich in iron and merged nodule areas. Nodules are porous and blades grow on their surfaces (Figure 41).

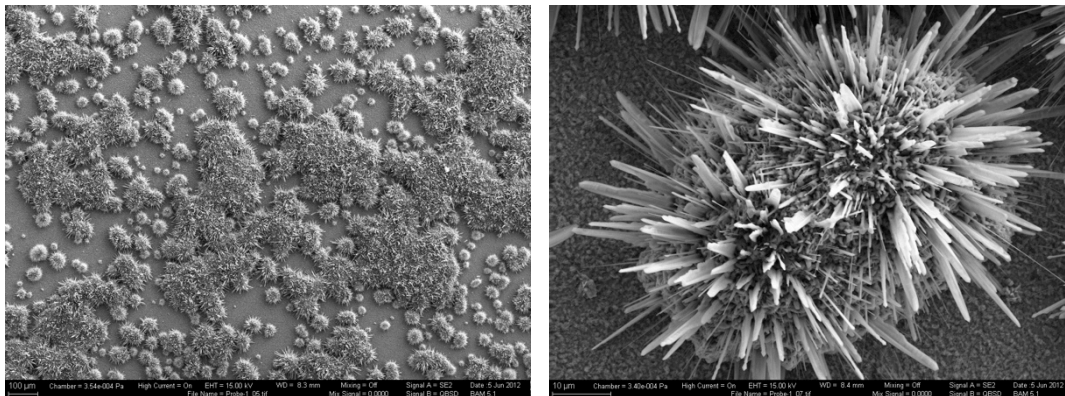


Figure 41: SEM (SE) pictures of alloy P1 surface exposed to Gas 3 at 600°C for 1000h in a single atmosphere condition. Nodules are merging themselves and are porous with blades on the top.

In Figure 42, the picture on the left shows isolated nodules with deep growth inside the metal, showing an irregular pattern of the oxidation in the alloy. Nodules are also porous and exhibit an external red layer of hematite.

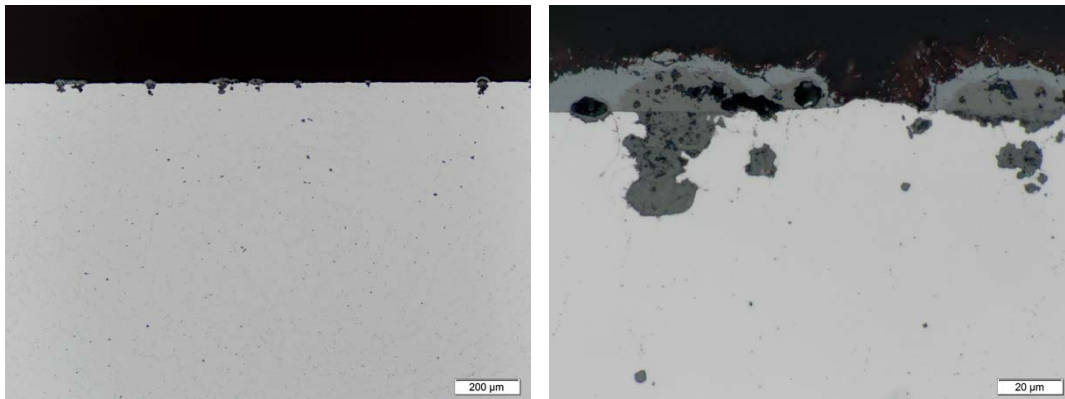


Figure 42: Light microscope pictures of alloy P1 exposed to Gas 3 at 600°C for 1000h in a single atmosphere condition. Isolated nodules are porous and the internal oxide layer grows in a preferential pattern inside the metal.

Iron oxides compose the outer layer of the nodules formed in this condition, as seen in Figure 43. The inner layer is formed by Fe/Cr spinel; two kinds of structures can be observed. Where the spinel is more porous, Cr content is higher and where the layer is more compact, Cr content is lower.

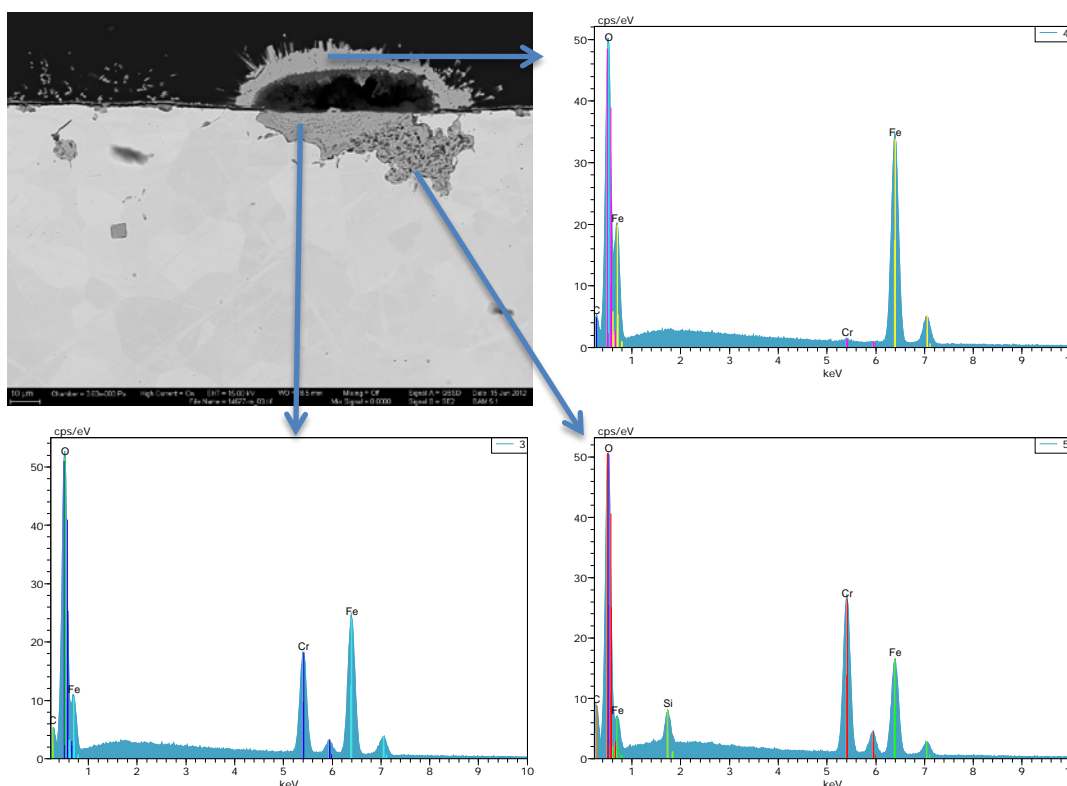


Figure 43: EDS of Alloy P1 exposed to Gas 3 at 600°C for 1000h in a single atmosphere condition. It shows a hematite layer in contact with the gas (top right), a spinel layer with less Cr (bottom left) and a spinel layer with more Cr (bottom right).

The spinel area of another nodule was investigated using FIB (Figure 44) and TEM (Figure 45). In Figure 44, 3 points with different morphologies can be

identified. All of them were studied using TEM and all phases are FeCr_2O_4 , as seen in the analysis of point 1 in Figure 45, for example.

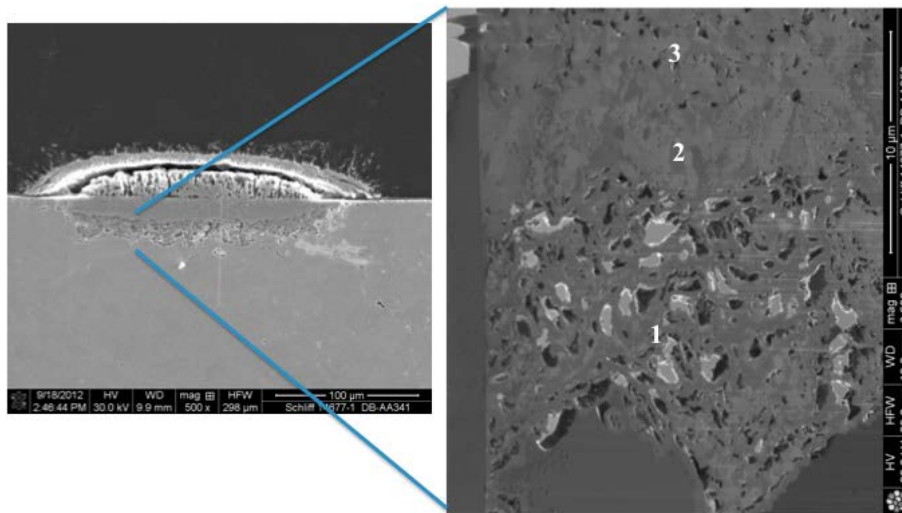


Figure 44: FIB pictures of Alloy P1 exposed to Gas 3 at 600°C for 1000h in a single atmosphere condition. All the three points are FeCr_2O_4 , as seen in Figure 45 for point 1.

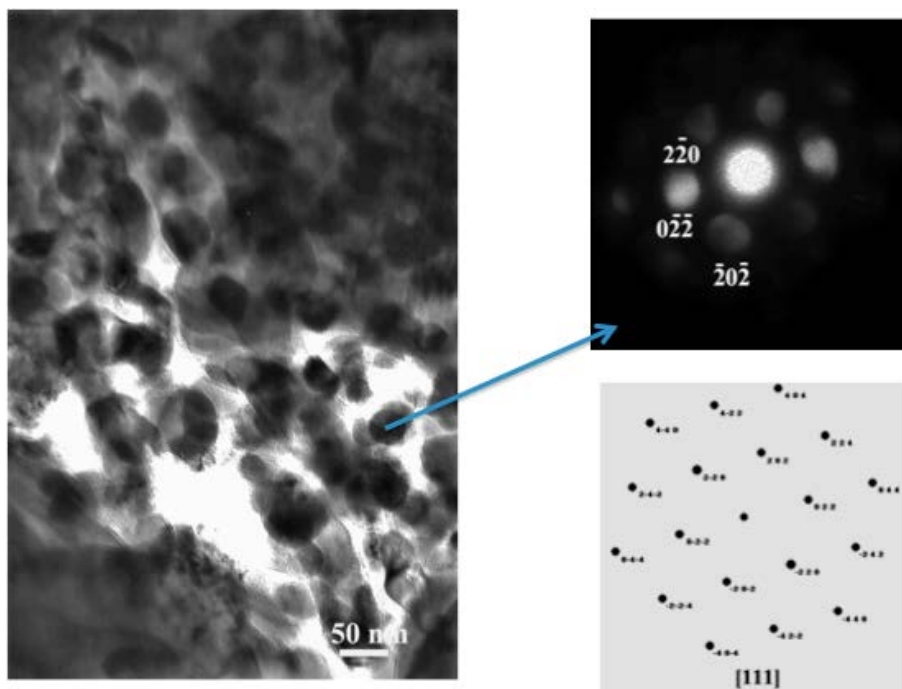


Figure 45: Left: TEM picture of point 1 of Figure 44 showing FeCr_2O_4 nanocrystals. Right: Convergent Beam Electron Diffraction (CBED) of one of the crystals and the simulation below.

Away from the nodules, there are whiskers identified as Cr_2O_3 by CBED, as seen in Figure 46. Underneath the Cr_2O_3 layer, a FeCr_2O_4 layer is also present in some points of the samples as seen in Figure 47.

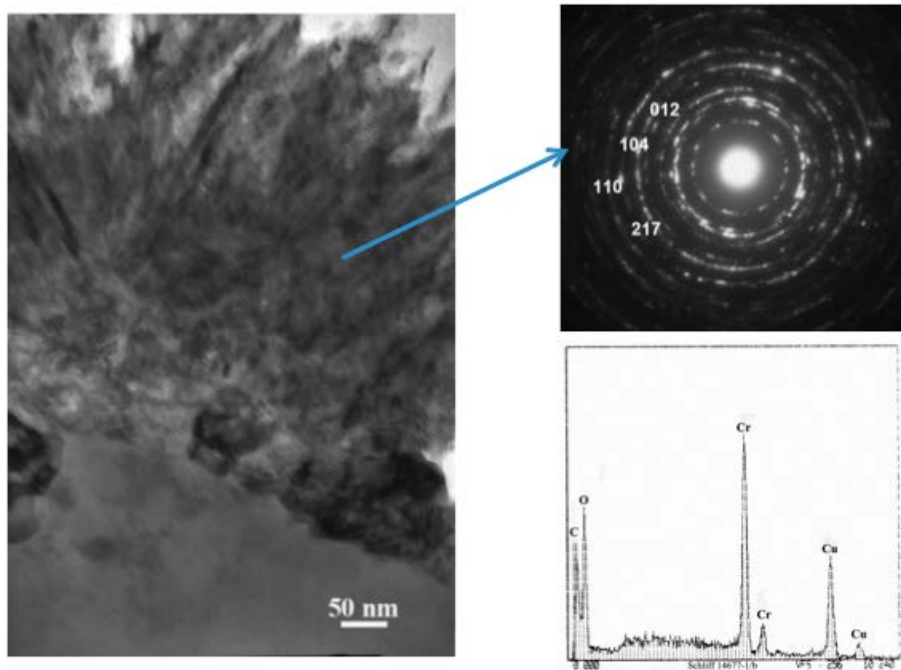


Figure 46: TEM picture and CBED of the scale outside the iron rich nodules showing Cr_2O_3 whiskers.

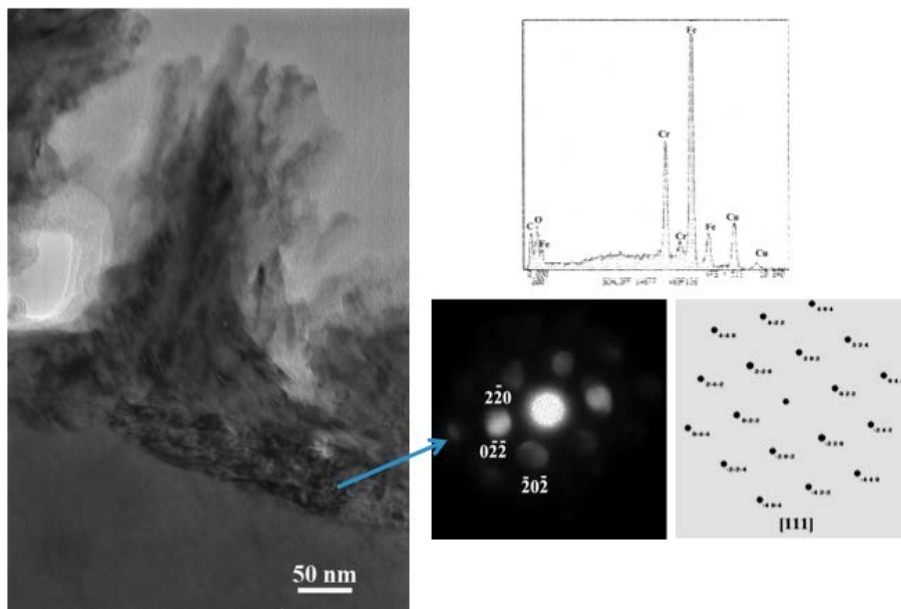


Figure 47: TEM picture, EDS and CBED of the structure beneath the Cr_2O_3 whiskers. This phase is FeCr_2O_4 .

4.1.2 Dual Atmosphere Condition

4.1.2.1 Gas 1 (70 CO₂ – 1 SO₂ – 29 Ar)

4.1.2.1.1 Gas Side

Alloy P1 oxidized almost homogeneously with a slight difference from the center to the border of the sample on the gas side of Gas 1 in the dual condition experiment (Figure 48). Nodules of different morphologies and compositions formed on the surface and are randomly distributed (Figure 49).

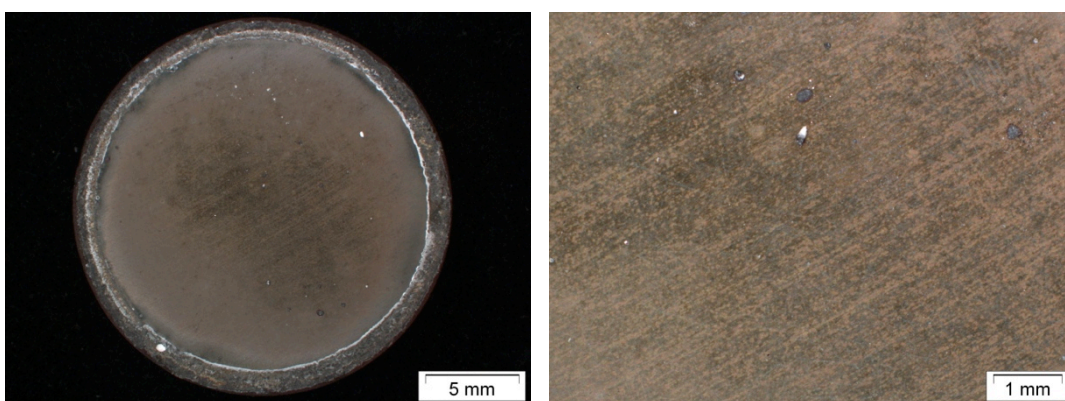


Figure 48: Stereomicroscope pictures of alloy P1 exposed to Gas 1 at 600°C for 1000h in a dual atmosphere condition. The sample has a slight difference between oxidation in the center and the border.

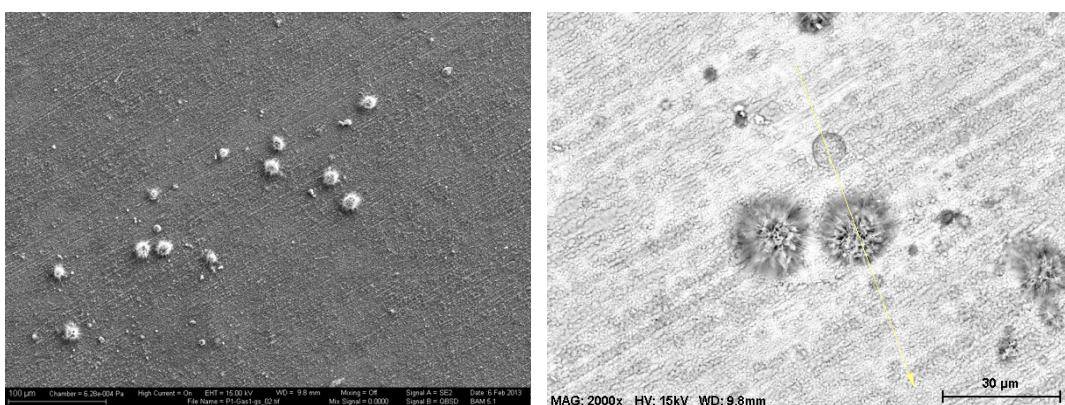


Figure 49: SEM (Left: SE. Right: BSE) pictures of alloy P1 surface exposed to Gas 3 at 600°C for 1000h in a dual atmosphere condition. Nodules distributed heterogeneously on the surface and have different morphologies.

The analysis of those nodules showed that the majority of them are composed of Cr oxide with whisker formation on the surface. Another kind of nodule is composed of iron oxide and does not have the whiskers on the surface,

although there are indications that whiskers are growing on the surface (Figure 50 and Figure 51). A small nodule containing Cr, O and S is also observed.

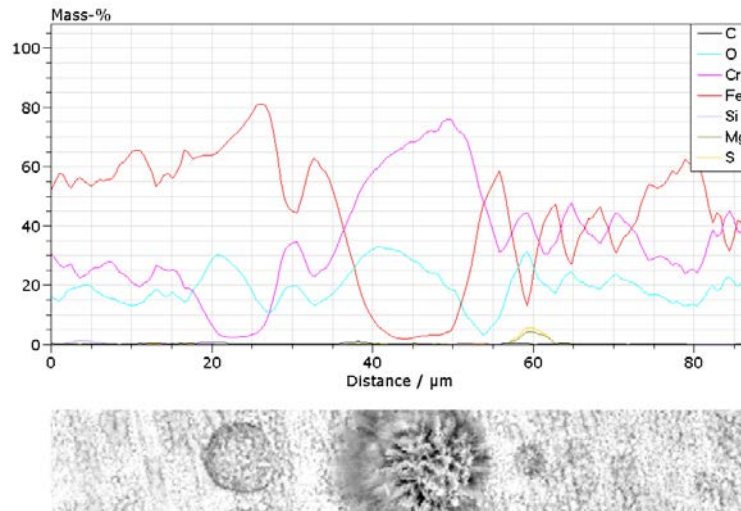


Figure 50: EDS line scan from Figure 49 picture (right) of alloy P1 exposed to Gas 1 at 600°C for 1000h in a dual atmosphere condition showing three nodules. From the right to the left, a Fe oxide rich nodule is followed by a Cr oxide rich nodule. Right from the Cr oxide-rich there is an oxide with S and Cr.

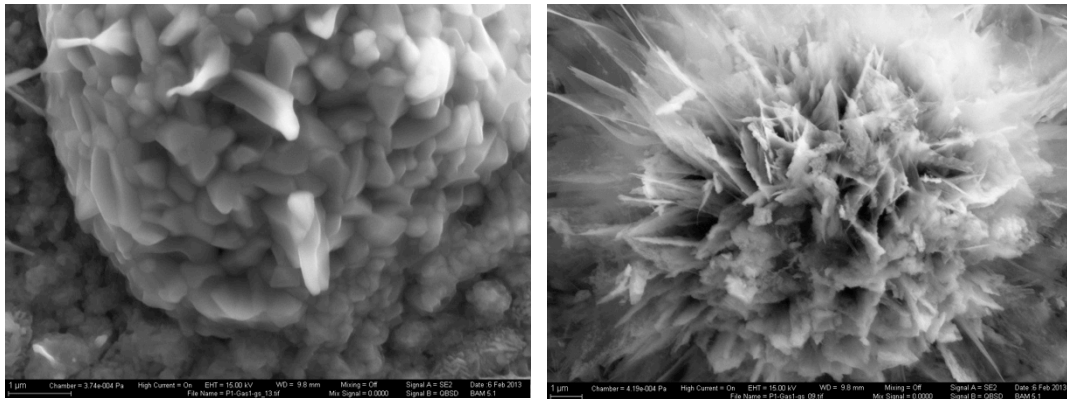


Figure 51: SEM (SE) pictures of alloy P1 surface exposed to Gas 3 at 600°C for 1000h in a dual atmosphere condition. Left: Iron oxide nodule with some whiskers/blades growing on the surface. Right: Cr oxide nodule with whiskers on the surface.

The sample cross-section analysis shows little oxidation and the formation of small porous nodules in the scale (Figure 52).

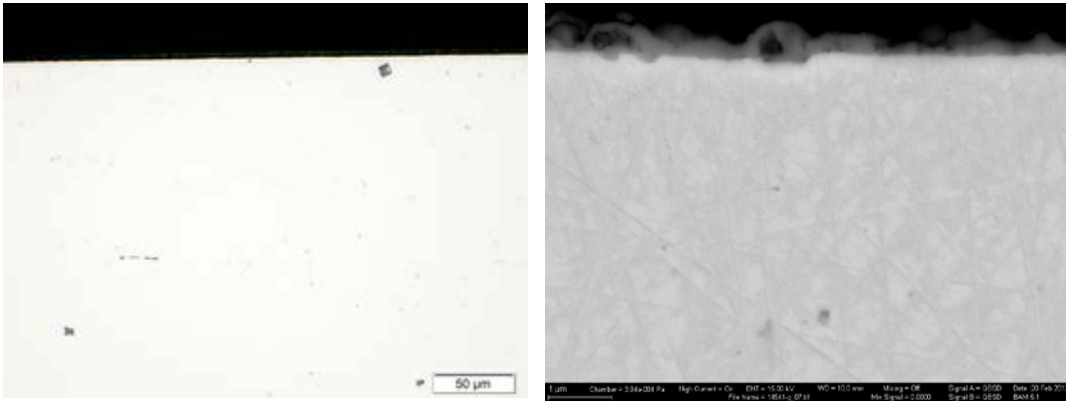


Figure 52: Light microscope and SEM pictures of alloy P1 exposed to Gas 1 at 600°C for 1000h in a dual atmosphere condition showing low surface oxidation and some small nodules.

4.1.2.1.2 Water Vapor Side

Alloy P1 oxidized heterogeneously on the water vapor side of Gas 1 in the dual condition experiment. A grey color is observed in the center of the sample, and a red area is seen on the border. Spallation is also exhibited on the surface (Figure 53).

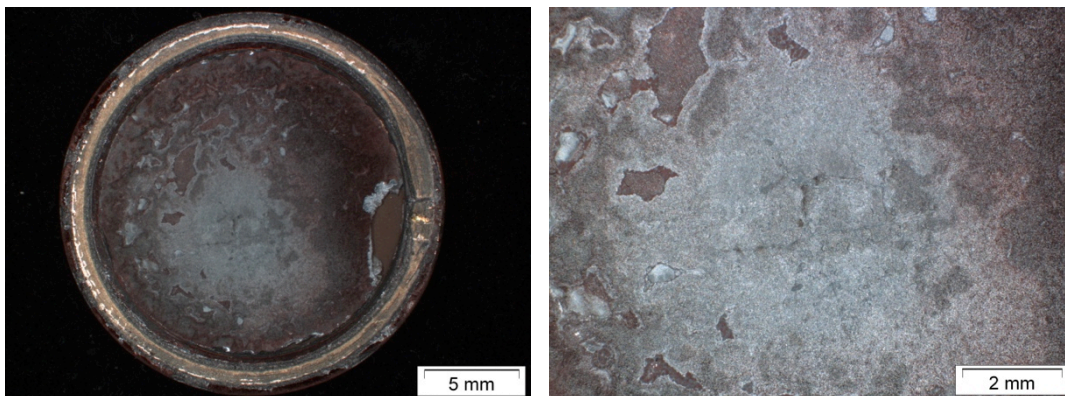


Figure 53: Stereomicroscope pictures of alloy P1 exposed to Gas 1 at 600°C for 1000h in a dual atmosphere condition. The sample has a slight difference between the oxidation in the center and the border.

The surface of the sample analyzed in SEM shows one porous bulk phase and blades, which seem to grow in the bulk phase grain boundaries (Figure 54).

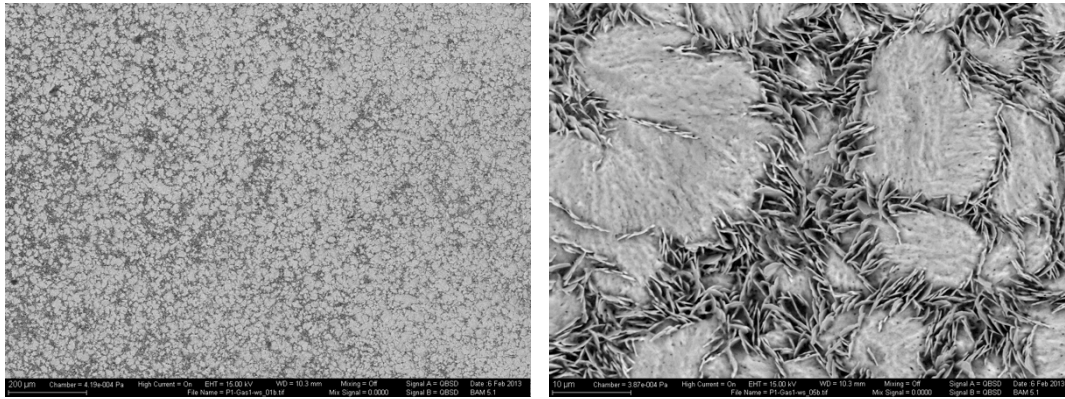


Figure 54: SEM (BSE) pictures of the surface of alloy P1 exposed to Gas 1 at 600°C for 1000h in a dual atmosphere condition. Blades are observed in the grain boundaries and a porous structure composes the grains.

The cross-section of the sample exhibits an external scale composed of two phases and an internal scale with an increasing porosity towards the metal (Figure 55). In Figure 56, the top of the scale presents higher porosity and finer columnar grains where no whiskers are formed. Internal oxidation with higher oxidation in the grain boundaries is observed in the metal.

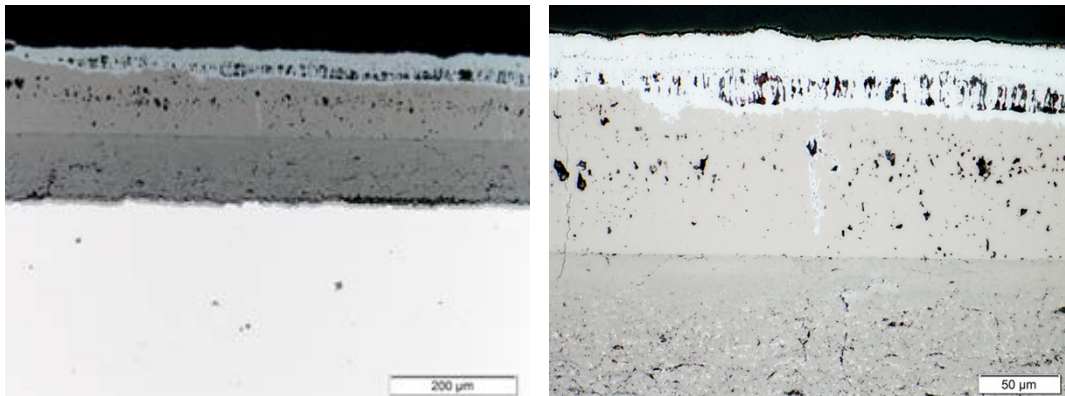


Figure 55: Light microscope pictures of alloy P1 exposed to Gas 1 at 600°C for 1000h in a dual atmosphere condition. A thick porous scale formed on the surface with a high porosity on the external scale.

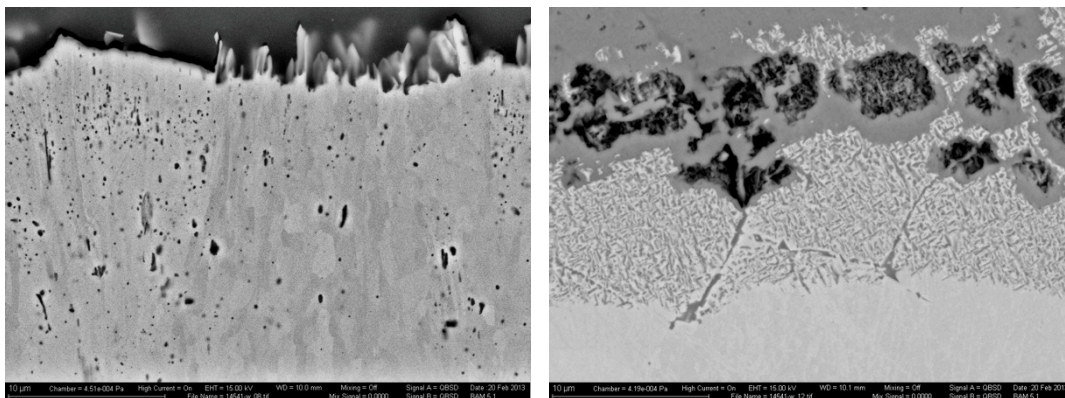


Figure 56: SEM (BSE) pictures of alloy P1 exposed to Gas 1 at 600°C for 1000h in a dual atmosphere condition. Left: On the surface, an area with blades and another without. Right: Internal oxidation and high porosity in the scale/metal interface.

EDS line scanning analysis shows that external scale is composed of hematite and magnetite. Internal scale is composed of spinel with Cr peaks in the middle and in metal/scale interface (Figure 57). EDS analysis in Figure 58 confirms higher chromium concentration closer to metal/scale interface. Cobalt-rich areas are observed in the spinel.

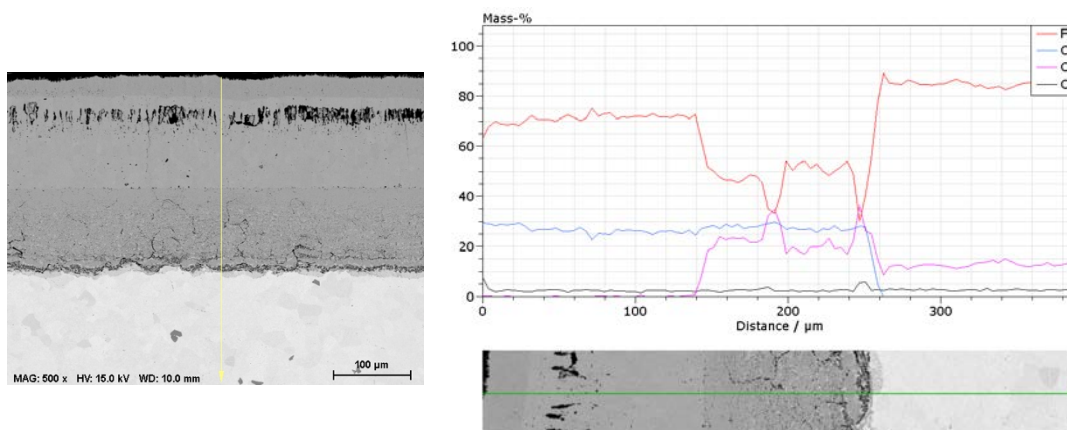


Figure 57: EDS line of alloy P1 exposed at 600°C for 1000h in a dual atmosphere condition on the water vapor side. External scale is formed by iron oxides with Fe content increasing towards the internal oxide scale. Internal oxide scale is formed by a Fe/Cr spinel with different Cr content. Near the scale/metal interface, the Cr content increases expressively.

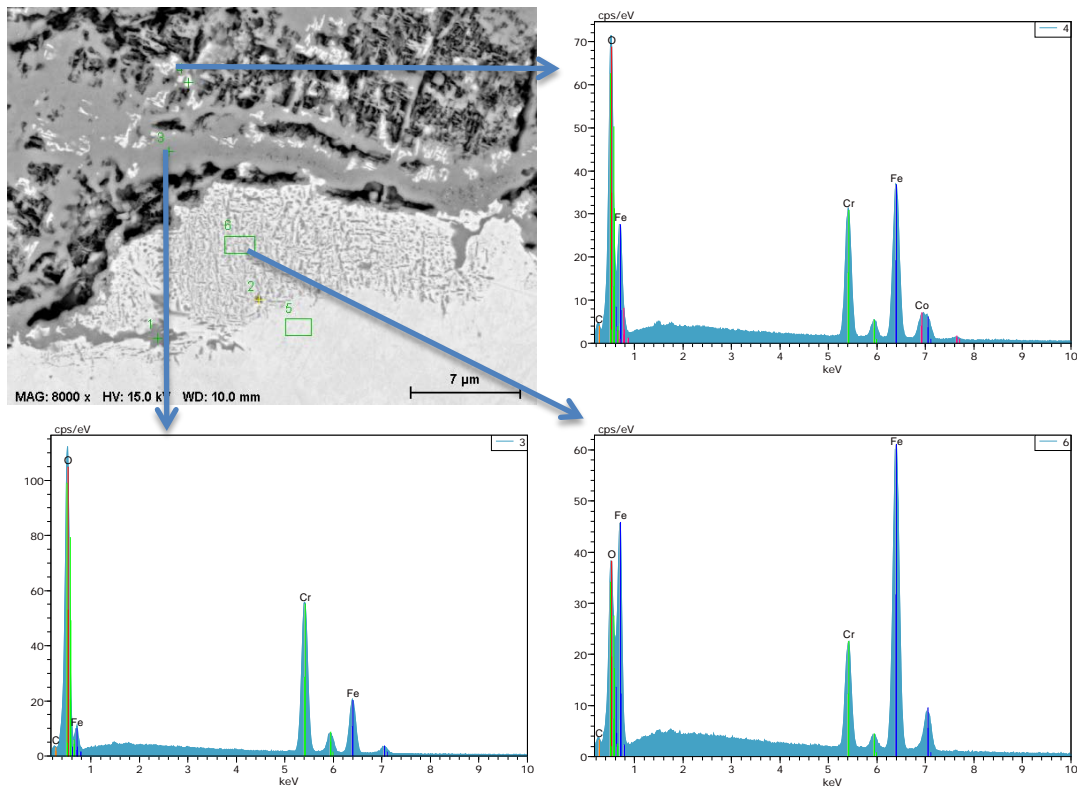


Figure 58: EDS of Alloy P1 exposed to Gas 1 at 600°C for 1000h in a dual atmosphere condition on the water vapor side. Point 4 shows a brighter structure of Fe/Cr spinel with a Co. Point 3 shows a darker area with more Cr and no Co. Point 6, shows an area of internal oxidation, where both metal and oxide were scanned by EDS.

4.1.2.2 Gas 3

4.1.2.2.1 Gas Side

Alloy P1 showed different morphologies and colors on the surface on the gas side of Gas 3 in the dual condition experiment (Figure 59). The surface is composed of a highly porous phase and whiskers/blades (Figure 60).

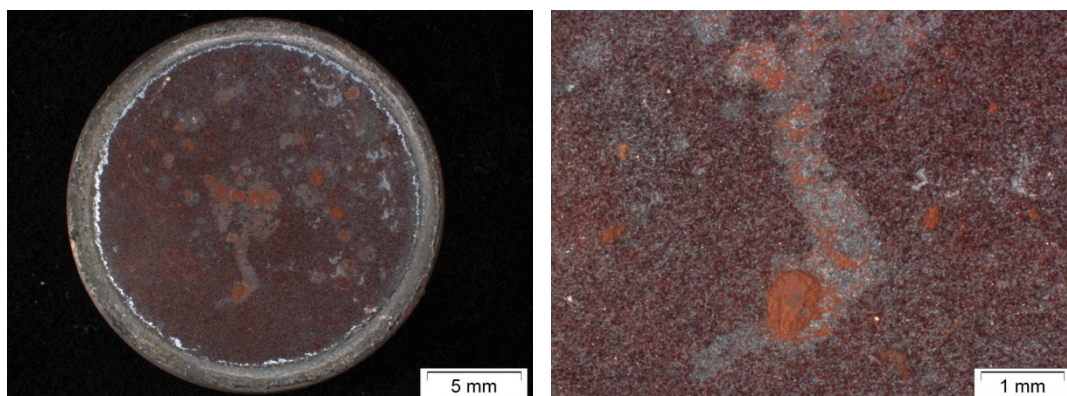


Figure 59: Stereomicroscope pictures of alloy P1 exposed to Gas 3 at 600°C for 1000h in a dual atmosphere condition. The sample exhibits different colors and morphologies on the surface.

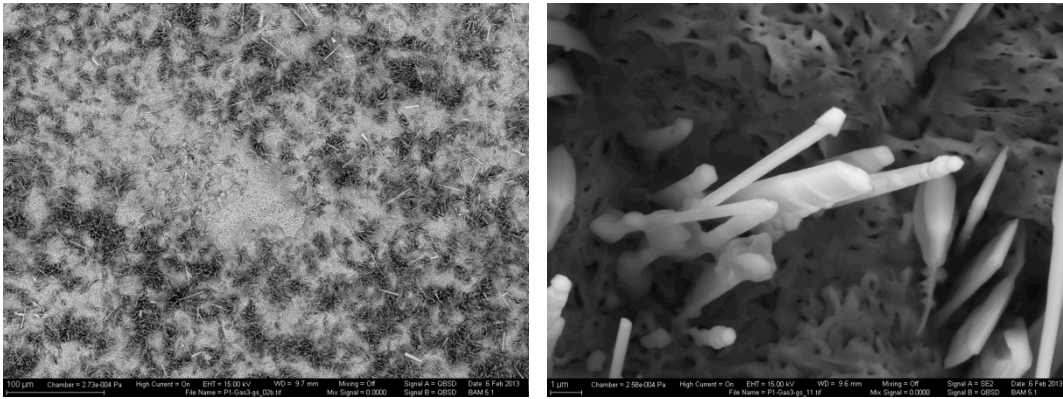


Figure 60: SEM (Left: BSE. Right: SE) pictures of alloy P1 exposed to Gas 3 at 600°C for 1000h in a dual atmosphere condition. A porous phase and a mixture of whiskers and blades form the surface of the scale.

Scale formed in this condition is continuous and very porous (Figure 61). Internal scale is composed of Fe/Cr spinel and Cr_2O_3 closer to metal/scale interface (Figure 62). Sulfur-rich points are also observed in the metal.

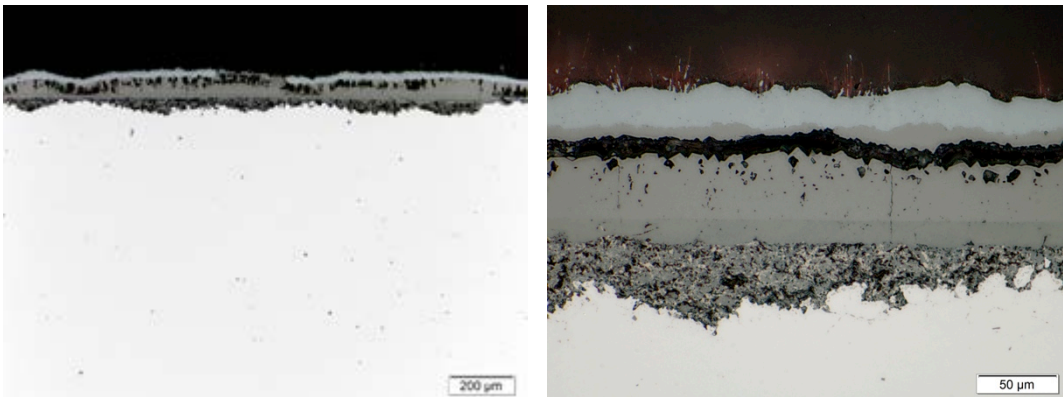


Figure 61: Light microscope pictures of alloy P1 exposed to Gas 3 at 600°C for 1000h in a dual atmosphere condition. A thick continuous scale formed on the surface of alloy P1 with pores in the external and internal scale. On the top, hematite is present.

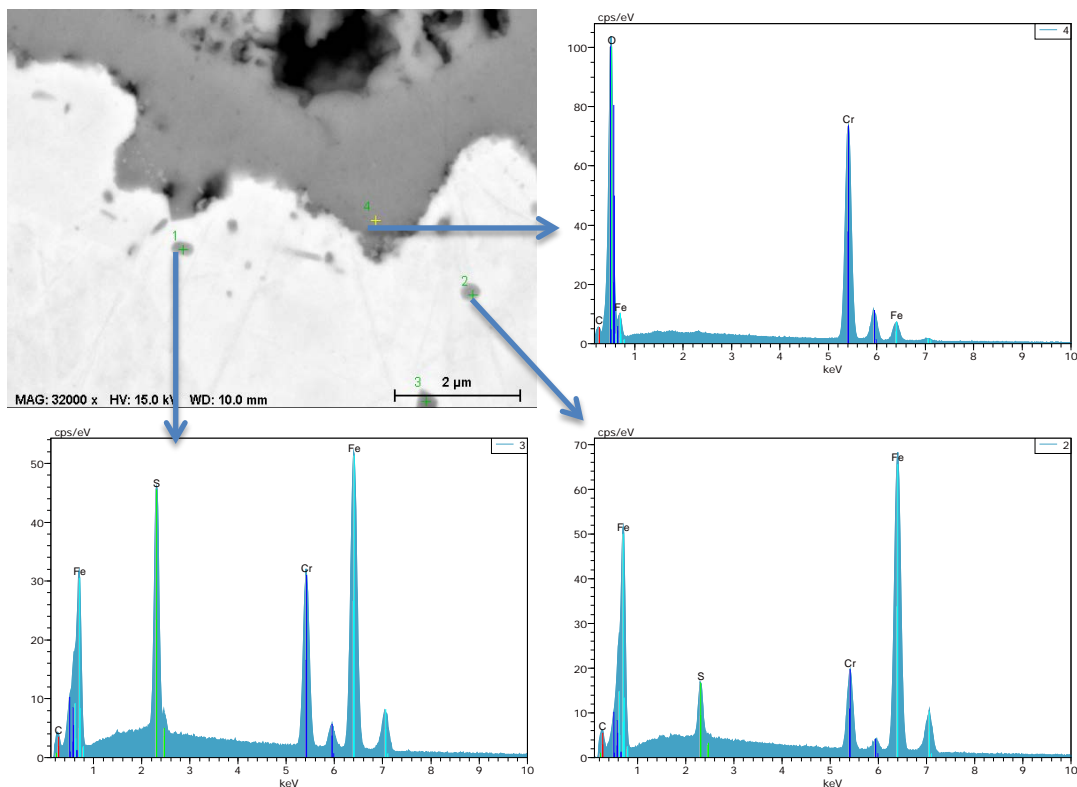


Figure 62: EDS of Alloy P1 exposed to Gas 3 at 600°C for 1000h in a dual atmosphere condition on the gas side. Point 4 shows a Cr_2O_3 layer in contact with the metal. Points 2 and 3 show sulfur inside the metal.

Figure 63 shows EDS line scan of the scale cross section. Scale is composed of hematite in the most external layer following magnetite. Fe/Cr spinel and Cr_2O_3 form the internal layer. Sulfur is present in internal scale and inside metal.

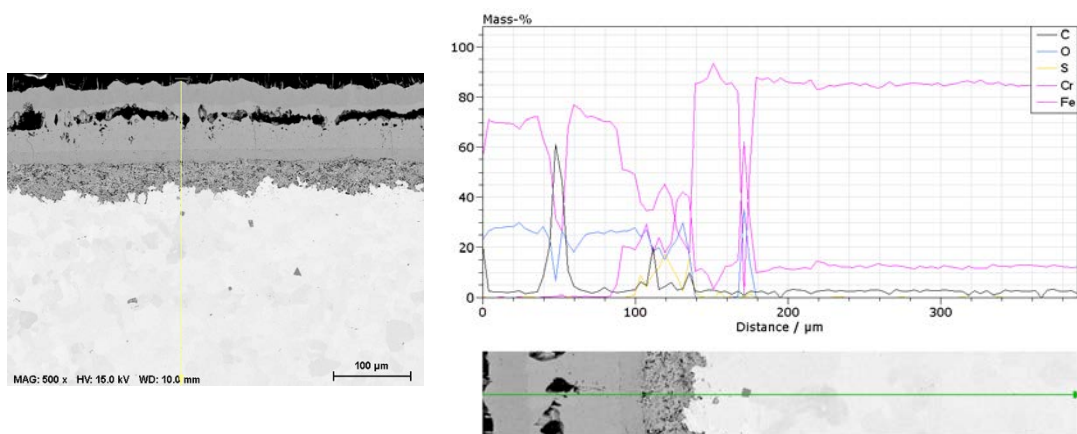


Figure 63: EDS line scan of Alloy P1 exposed to Gas 3 at 600°C for 1000h in a dual atmosphere condition on the gas side. It shows an external scale composed of hematite and magnetite, and an internal scale composed by spinel and Cr_2O_3 . Sulfur is present in the spinel layer.

4.1.2.2.2 Water Vapor Side

Alloy P1 showed spallation in the center of the sample and detachments near the border as a result of the gold O-ring removal on the water vapor side of Gas 3 in the dual condition experiment (Figure 64).

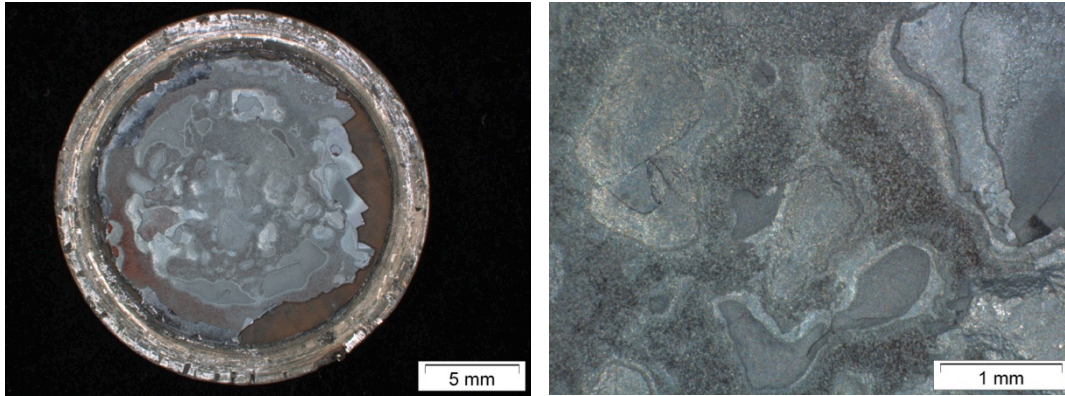


Figure 64: Stereomicroscope pictures of alloy P1 exposed to Gas 3 at 600°C for 1000h in a dual atmosphere condition on the water vapor side.

Buckling is seen on the top left of Figure 65. At the top right, an extremely porous surface due to water vapor corrosion. At the bottom, a sample of the scale underneath the top layer presents a columnar structure.

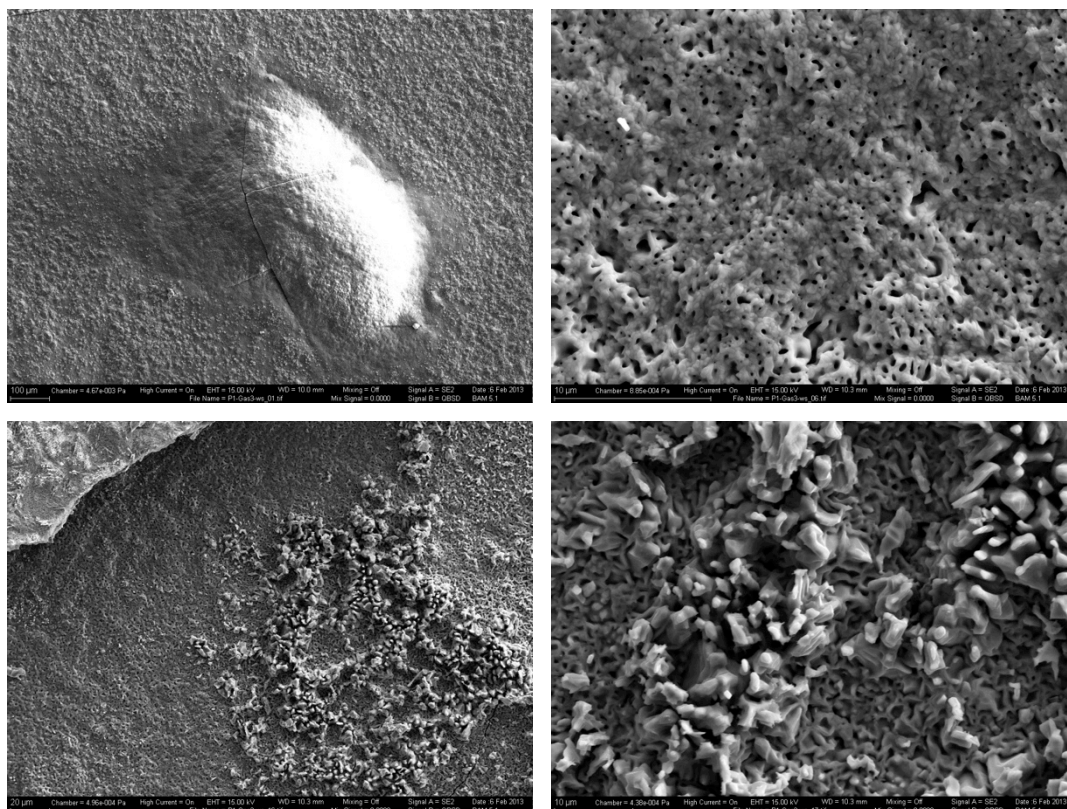


Figure 65: SEM (SE) pictures of alloy P1 exposed to Gas 3 at 600°C for 1000h in a dual atmosphere condition on the gas side. A porous phase and a mixture of whiskers and blades form the surface of the scale.

The scale is composed of internal scale formed by Fe/Cr spinel and an external scale composed of magnetite and hematite (Figure 66).

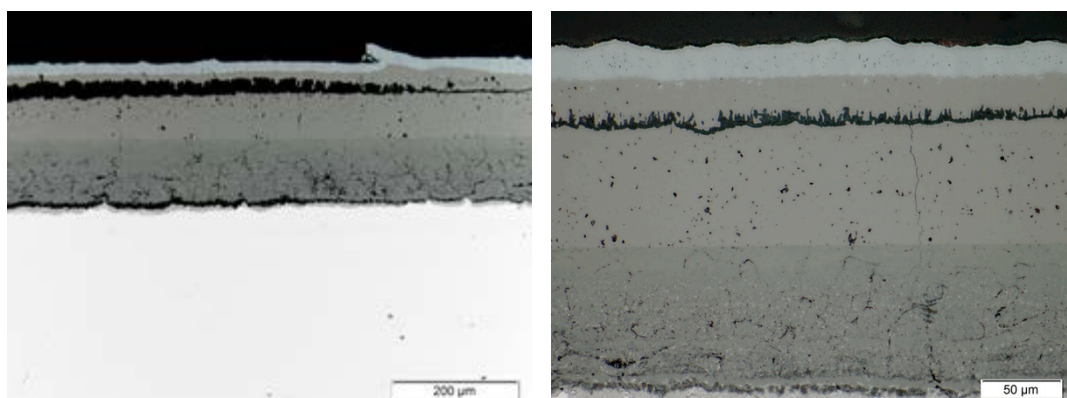


Figure 66: Light microscope pictures of alloy P1 exposed to Gas 3 at 600°C for 1000h in a dual atmosphere condition on the water vapor side. Thick continuous scale formed on the sample with pores in external and internal scale. Hematite is present on top.

EDS analysis (Figure 67) shows that the internal scale is composed of Fe/Cr spinel with different contents of Fe and Cr. Co is present in higher

concentration in some bright areas, as seen in Point 1. The higher Cr concentration near the metal interface is also observed in this sample.

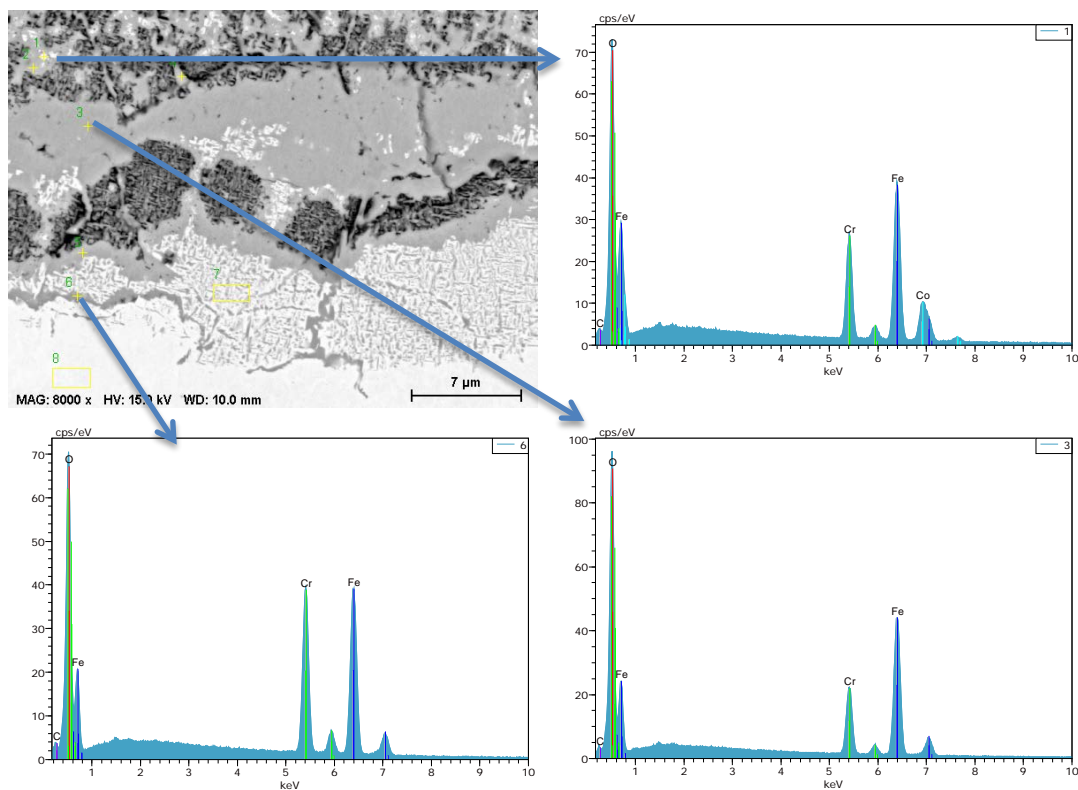


Figure 67: EDS of Alloy P1 exposed to Gas 3 at 600°C for 1000h in a dual atmosphere condition on the water vapor side. Point 1 shows a bright point where the Co content is higher in scale. Point 6 is closer to the metal interface than point 3 and has more Cr.

4.2 Alloy P2

Alloy P2 is a martensitic steel with 12.3%Cr–3.09%Co–0.18%C, exposed to gases 1, 2 and 3 in single atmosphere condition. In all conditions studied, a protective Cr_2O_3 scale was formed with the growth of few nodules rich in iron oxides. Increase in water vapor concentration increased porosity and iron oxide nodule formation, but not significantly

This alloy had closer oxidation behavior to the 14Cr alloys than to 12Cr model alloy P1, and the 12Cr commercial alloy VM12.

4.2.1 Single Atmosphere Condition

4.2.1.1 Gas 1 (70 CO₂ – 1 SO₂ – 29 Ar)

In Gas 1, alloy P2 oxidized almost homogenously, except for sample bottom in contact with the cement. There is no evidence of iron oxide nodules on the surface (Figure 68).

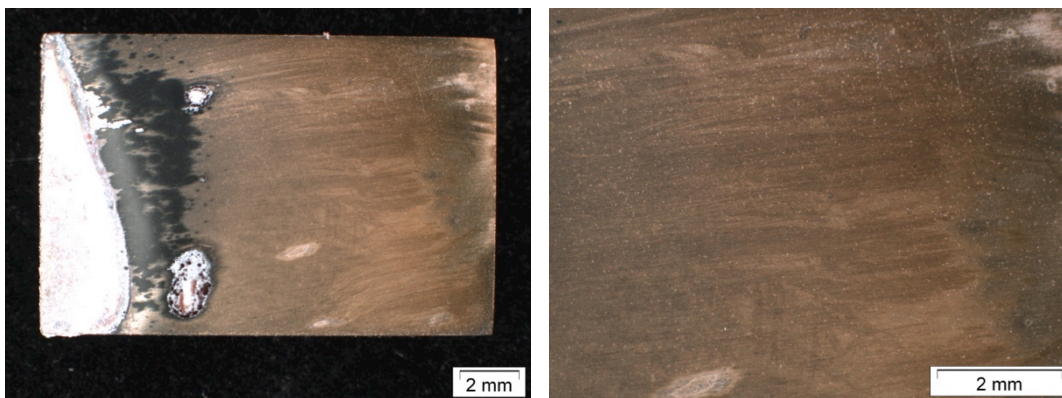


Figure 68: Stereomicroscope pictures of alloy P2 exposed to Gas 2 at 600°C for 1000h in a single atmosphere condition. The white part at the sample bottom is the cement used to stick the sample to the sample holder.

The surface observed in SEM displays slight oxidation and no evidence that the nodules are composed by iron oxides. The nodules are found in higher density in some parts of the sample and present whiskers on the surface. Porosity was not observed (Figure 69 and Figure 70).

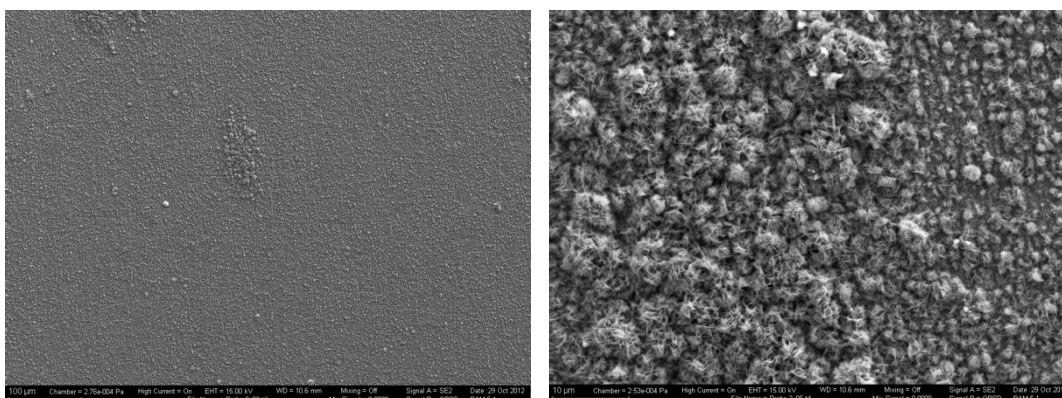


Figure 69: SEM (SE) pictures of the surface of alloy P2 exposed to Gas 1 at 600°C for 1000h in a single atmosphere condition. Both pictures display slight surface oxidation without the evidence of iron oxide rich nodules.

EDS analysis (Figure 71) indicates that Cr₂O₃ composes external scale and in some parts Fe/Cr spinel and porosity is formed in some parts beneath the

Cr_2O_3 scale. Spinel and pores might indicate an initial stage of the breakaway oxidation. The uniform presence of the protective layer of Cr_2O_3 explains the alloy's low oxidation.

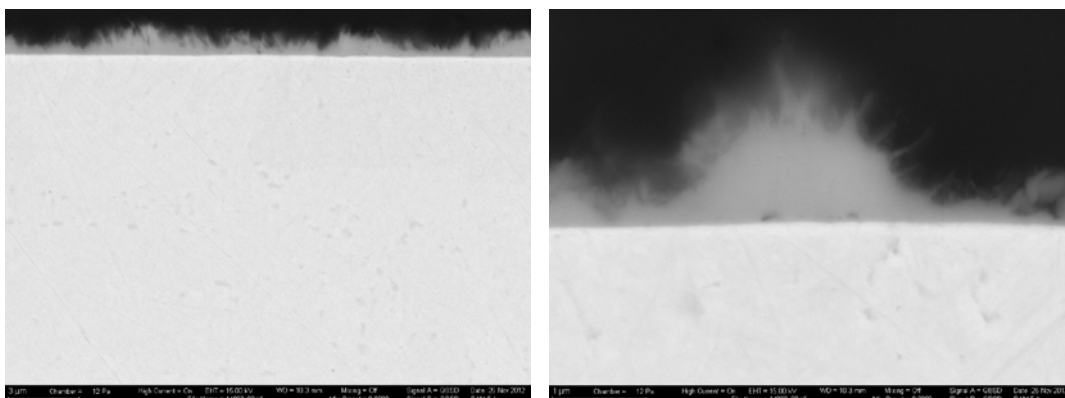


Figure 70: SEM (BSE) pictures of alloy P2 exposed to Gas 1 at 600°C for 1000h in a single atmosphere condition. A protective thin scale with whiskers on the top formed at the surface of alloy.

In Figure 71, EDS from the scale shows that the thin layer covering the surface is spinel, Cr_2O_3 or both of them. Sulfur is also present in both scale and metal indicating that it permeates from the gas into the sample.

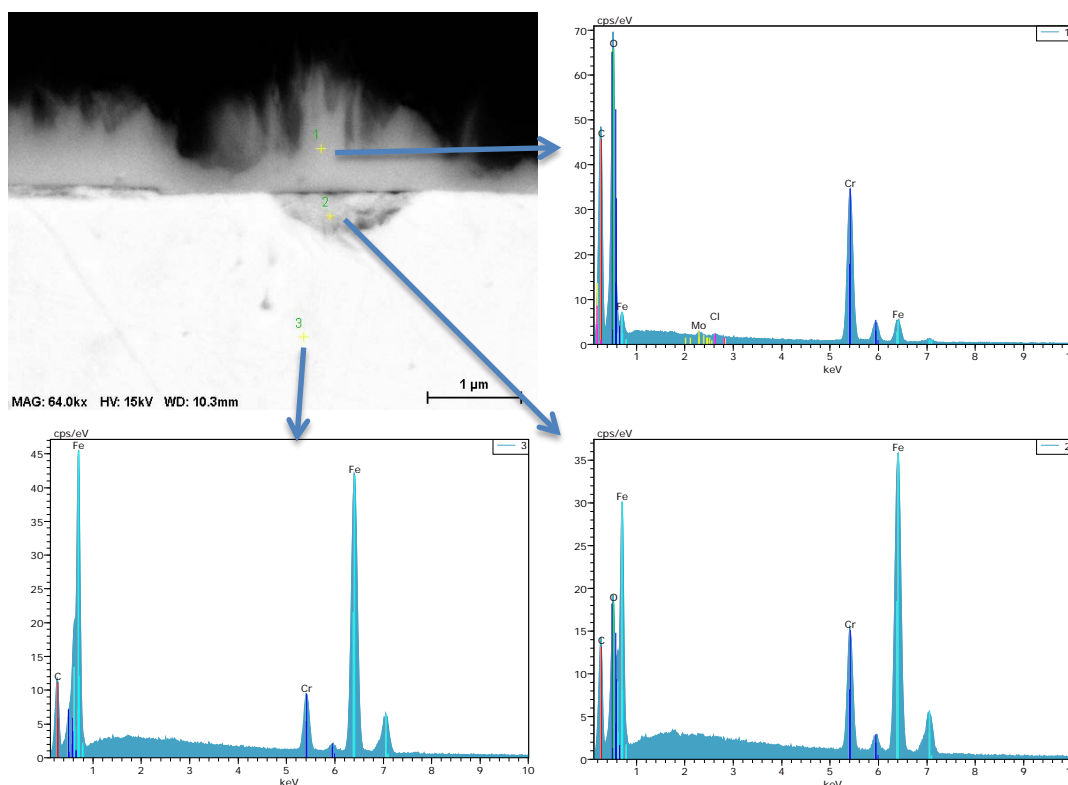


Figure 71: EDS from alloy P2 scale exposed to Gas 1 at 600°C for 1000h in a single atmosphere condition. Cr_2O_3 forms the external scale, while Fe/Cr spinel forms isolated nodules in the internal scale.

4.2.1.2 Gas 2 (70 CO₂ – 1 SO₂ – 1 H₂O – 28 Ar)

In Gas 2, a thin protective scale grows homogeneously on sample surface without any indication of iron oxide nodules (Figure 72).

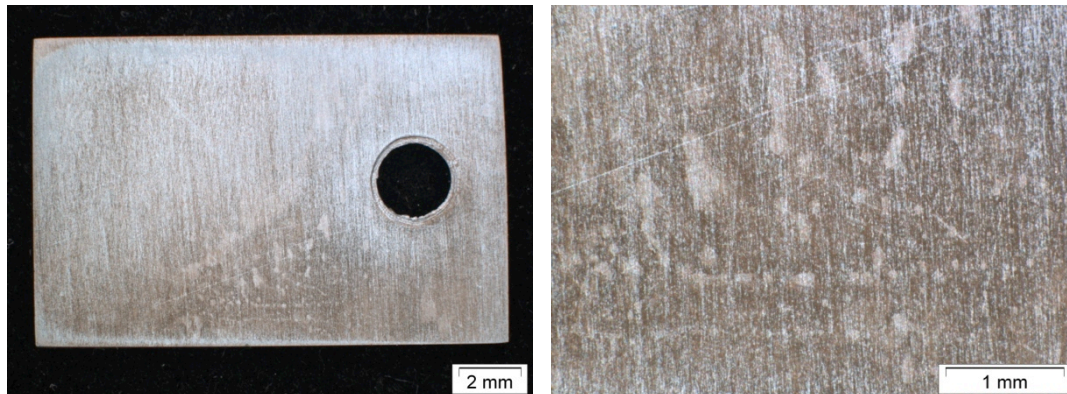


Figure 72: Stereomicroscope pictures of alloy P2 exposed to Gas 2 at 600°C for 1000h in a single atmosphere condition.

The surface observed in SEM, displays slight oxidation, and porosity is observed in some parts of the scale indicating the presence of water in the atmosphere (Figure 73).

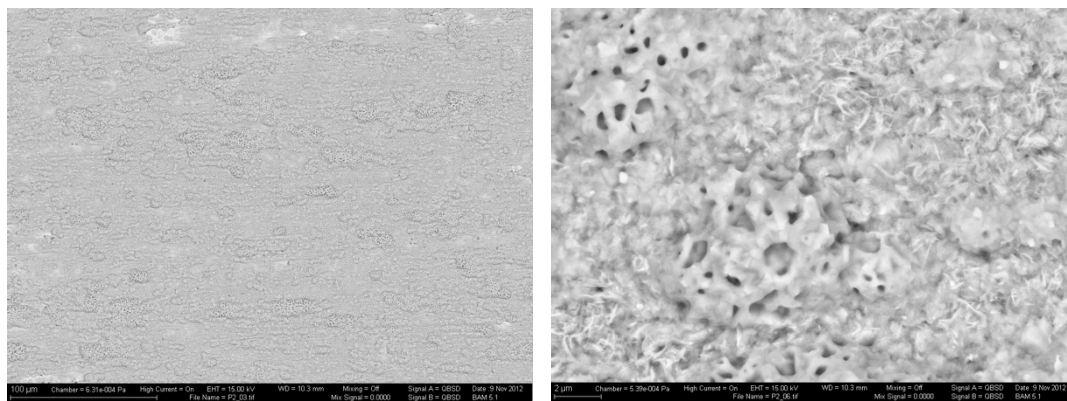


Figure 73: SEM (BSE) pictures of the surface of alloy P2 exposed to Gas 2 at 600°C for 1000h in a single atmosphere condition.

An internal scale forms in some parts of the sample, where nodules without whiskers grow (Figure 74).

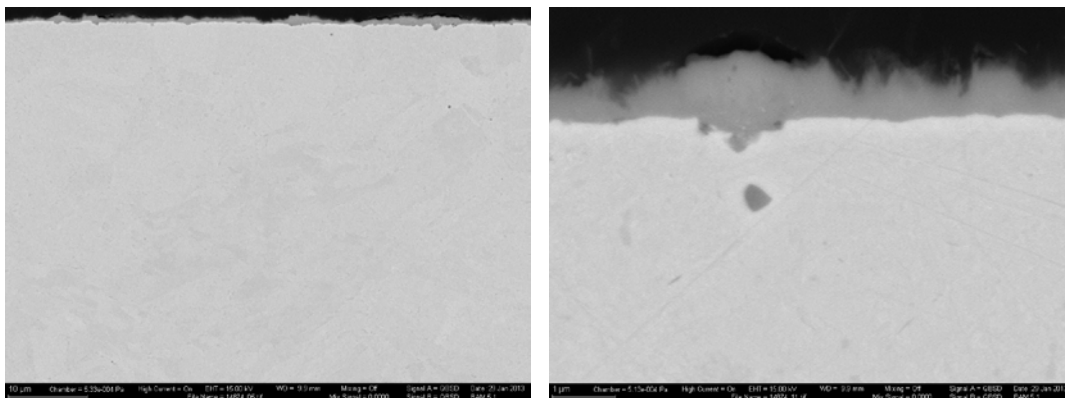


Figure 74: SEM (BSE) pictures of alloy P2 exposed to Gas 2 at 600°C for 1000h in a single atmosphere condition. A protective thin scale with whiskers on top formed on the surface, and some nodules with an internal scale seem to nucleate.

4.2.1.3 Gas 3 (70 CO₂ – 1 SO₂ – 29 H₂O)

In Gas 3, alloy P2 oxidized almost homogeneously, except from the bottom of the sample in contact with the cement. Some randomly-distributed iron rich nodules formed on the surface (Figure 75).

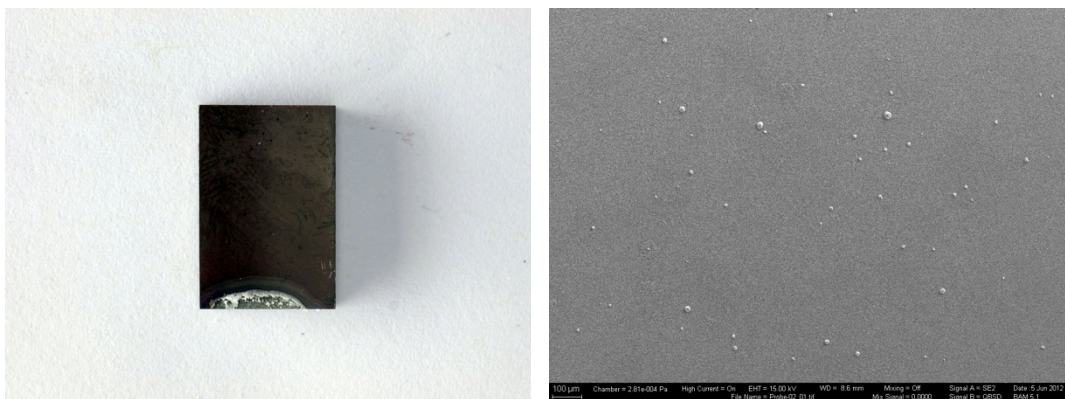


Figure 75: Left: Macro picture of alloy P2 exposed to Gas 3 at 600°C for 1000h in a single atmosphere condition. The white part in the bottom of the sample is the cement used to stick the sample to the sample holder. Right: SEM (SE) picture showing randomly-distributed nodules on the surface.

EDS analysis of a nodule and its surroundings shows that the nodule is richer in Fe, and its surrounding composed of a Cr rich protective phase (Figure 76).

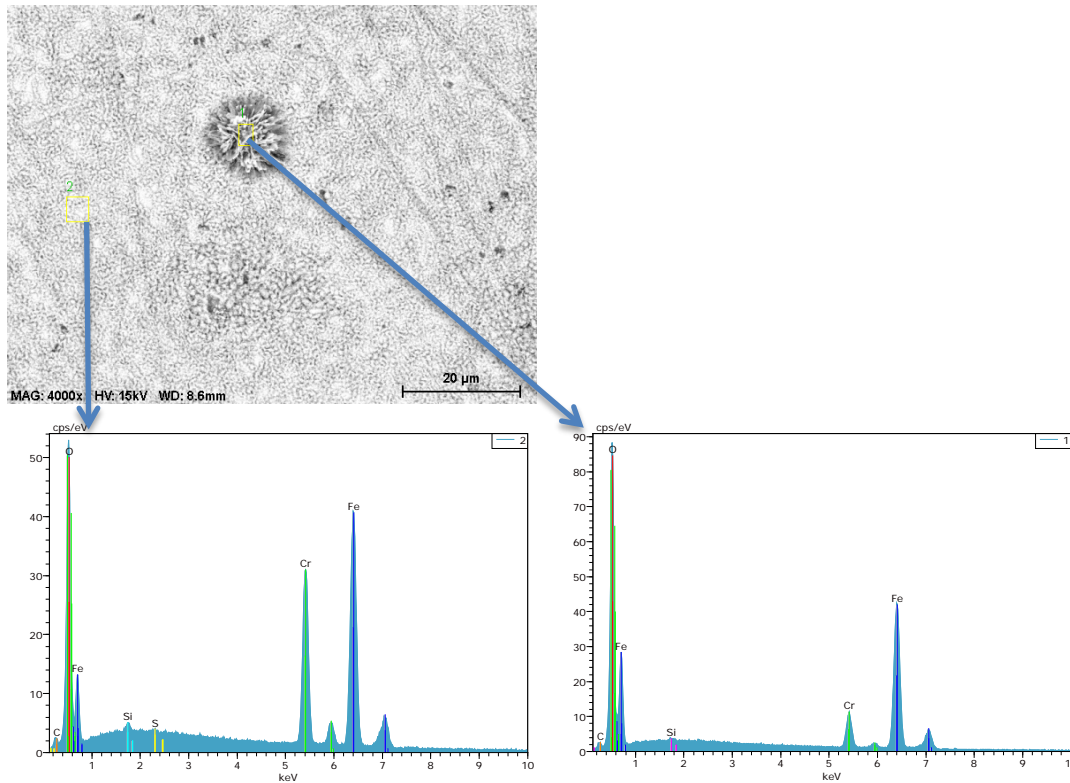


Figure 76: EDS from alloy P2 scale exposed to Gas 3 at 600°C for 1000h in a single atmosphere condition. A continuous thin protective oxide rich in Cr is formed and some iron oxide rich nodules grow on the scale.

Internal scale has also developed in some parts of the sample, as seen in Figure 77. The growth process of different nuclei and surface roughness may have caused the discontinuities in the scale. Change in the microstructure is observed in the subscale region.

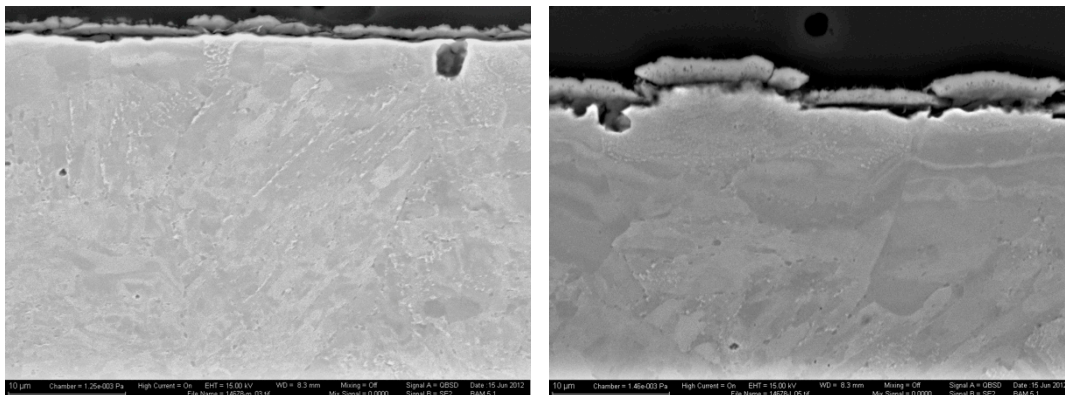


Figure 77: SEM (BSE) of alloy P2 exposed to Gas 3 at 600°C for 1000h in a single atmosphere condition. A Cr rich oxide covers the surface.

4.3 Alloy P3

Alloy P3 is a martensitic steel with 14.4% Cr–1.06%Co–0.17%C, exposed to gases 1, 2 and 3 in single atmosphere condition, and to gases 1 and 3 in dual atmosphere condition.

In single condition, a thin protective Cr_2O_3 layer covers all samples with the growth of few nodules on the surface. Nodule density increases with increase in the water vapor content.

In dual condition, in Gas 1 and 3 a ferritic layer was formed below the interface metal/scale. The oxidation is stronger in the dual condition than in single condition.

4.3.1 Single Atmosphere Condition

4.3.1.1 Gas 1 (70 CO_2 – 1 SO_2 – 29 Ar)

Although gas flow and the cement used to glue the sample have apparently influenced the oxidation rate (Figure 78), a thin continuous protective Cr_2O_3 layer has grown during the corrosion process.

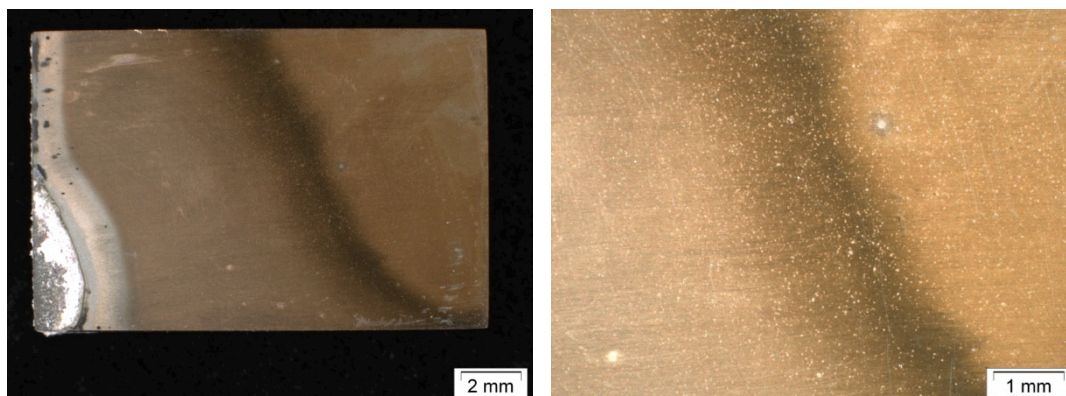


Figure 78: Stereomicroscope pictures of alloy P3 exposed to Gas 1 at 600°C for 1000h in a single atmosphere condition. The white part at the sample bottom is the cement used to glue the sample to the sample holder. There is no evidence of spallation or nodules growing on the surface.

The thin Cr_2O_3 layer was broken in some rare points by nodules such as the one in Figure 79. Cross-section analysis does not reveal any internal scale or nodule rich in iron oxide (Figure 80).

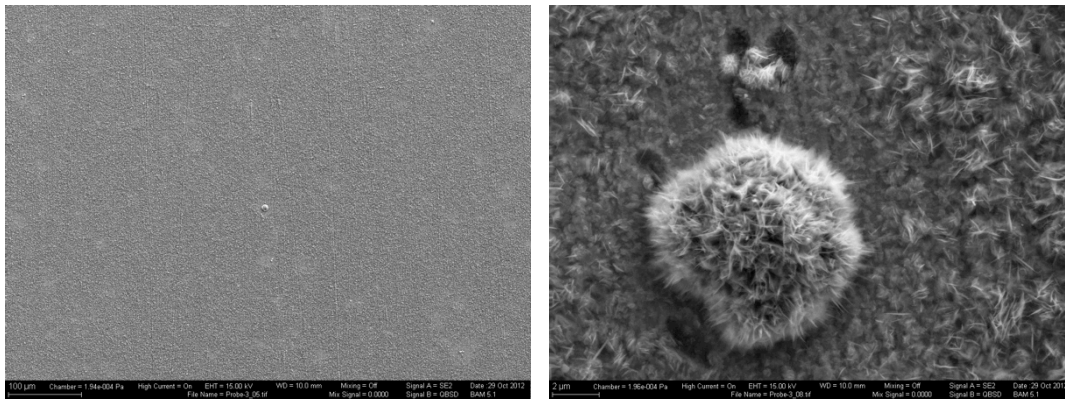


Figure 79: SEM (SE) pictures of the surface of alloy P3 exposed to Gas 1 at 600°C for 1000h in a single atmosphere condition. Both pictures show a small oxidation of the surface with the presence of one nodule.

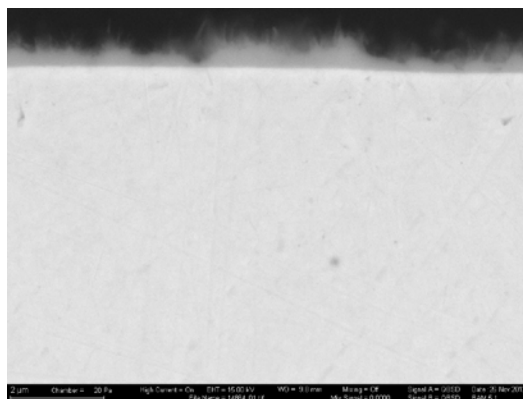


Figure 80: SEM (BSE) picture of alloy P3 exposed to Gas 1 at 600°C for 1000h in a single atmosphere condition. A protective thin scale with whiskers on top formed at the surface of the alloy.

4.3.1.2 Gas 2 (70 CO₂ – 1 SO₂ – 1 H₂O – 28 Ar)

Alloy P3, when exposed to Gas 2, exhibited a Cr₂O₃ layer with some nodules on the surface (Figure 81).

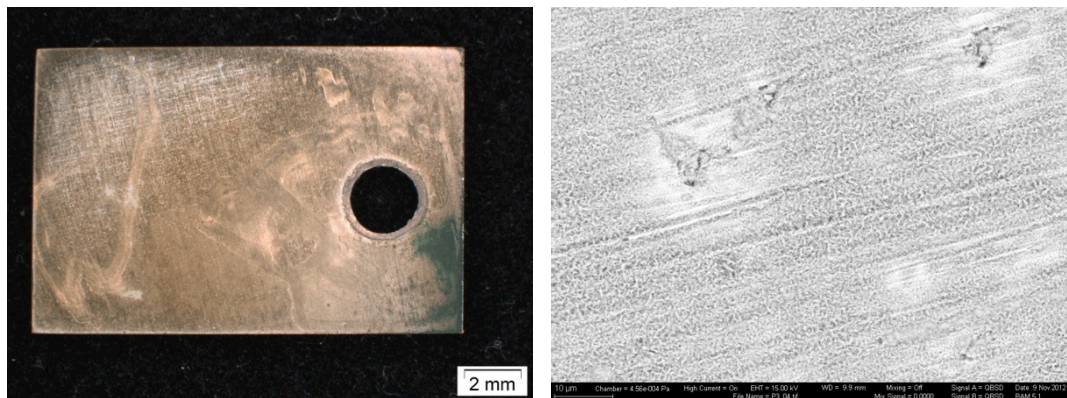


Figure 81: Stereomicroscope and SEM picture of alloy P3 exposed to Gas 2 at 600°C for 1000h in a single atmosphere condition. On the right, some nodules grow on the sample surface.

The sample cross-section shows a Cr_2O_3 layer with some whisker-free nodules growing on the surface (Figure 82).

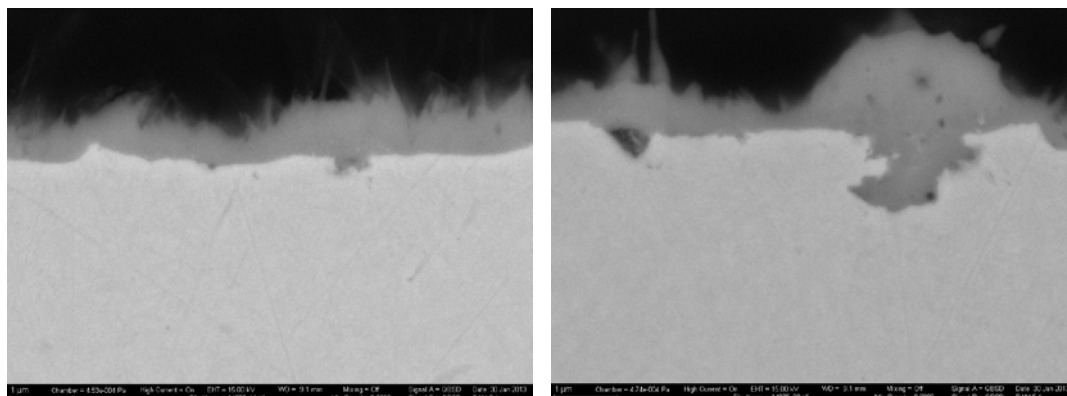


Figure 82: SEM (BSE) pictures of the surface of alloy P3 exposed to Gas 2 at 600°C for 1000h in a single atmosphere condition. A Cr_2O_3 layer forms the scale with few nodules and porosity.

4.3.1.3 Gas 3 (70 CO_2 – 1 SO_2 – 29 H_2O)

In Gas 3, a continuous Cr_2O_3 layer with some nodules has grown in alloy P3 (Figure 83). EDS analysis in Figure 84 shows that the nodules are rich in Fe, and the surface has high carbon concentration

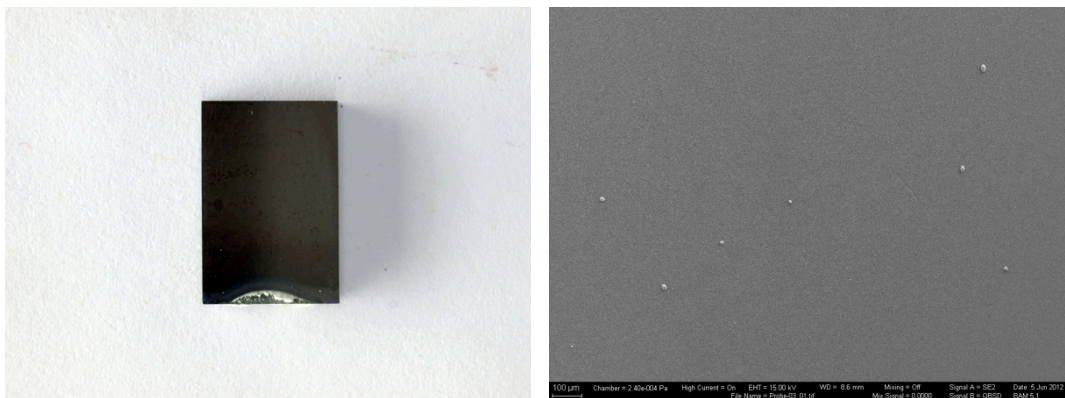


Figure 83: Macro and SEM (SE) pictures of alloy P3 exposed to Gas 3 at 600°C for 1000h in a single atmosphere condition. The white part at the sample bottom is the cement used to glue the sample to the sample holder. In the SEM picture, some nodules have grown on the surface.

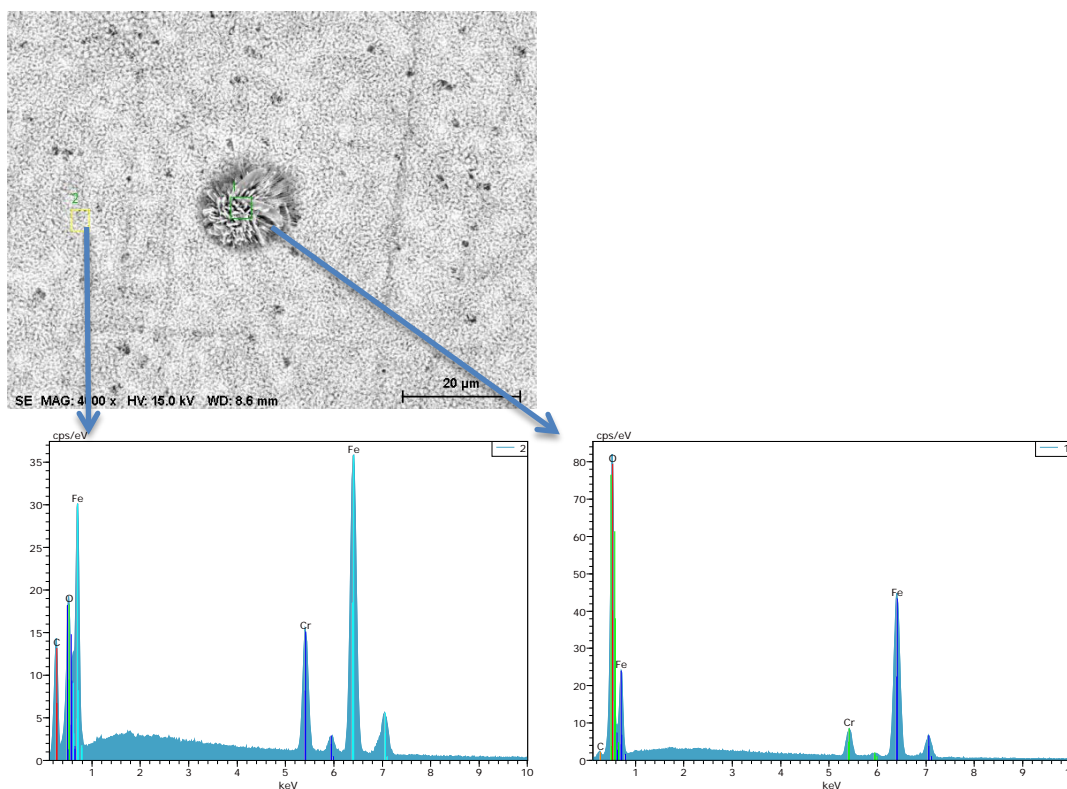


Figure 84: EDS from the surface of alloy P3 exposed to Gas 3 at 600°C for 1000h in a single atmosphere condition. Cr_2O_3 forms a continuous thin protective scale and some iron rich nodules grow on the scale.

The cross section pictures show a thin layer of Cr_2O_3 with a microstructural change in the metal beneath it (Figure 85).

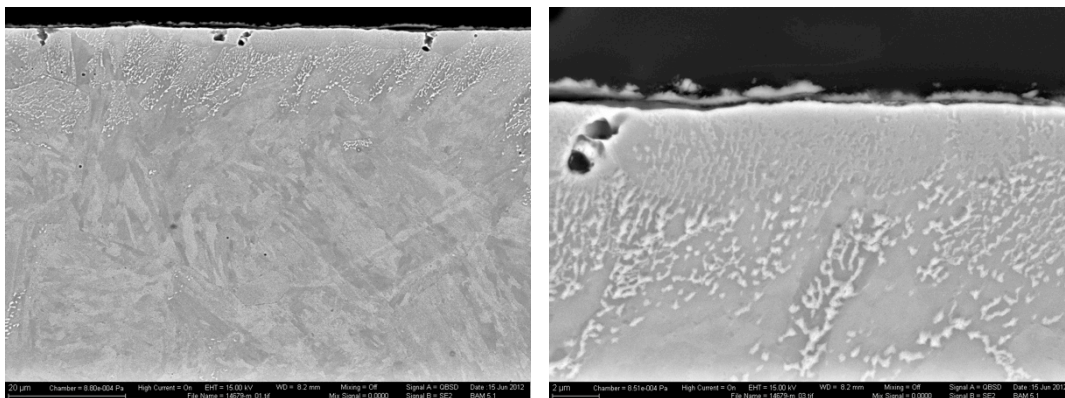


Figure 85: SEM (BSE) pictures of alloy P3 exposed to Gas 3 at 600°C for 1000h in a single atmosphere condition. A protective thin scale grows on the surface. In the subsurface region there is a microstructural change,

4.3.2 Dual Atmosphere Condition

4.3.2.1 Gas 1

4.3.2.1.1 Gas side

Cr_2O_3 layer was formed on the surface of Alloy P3 on the gas side of Gas 1 in the dual condition experiment with a greenish color in the center of the sample. This layer has few nodules on the surface not found in the cross-section analysis (Figure 86 and Figure 87).

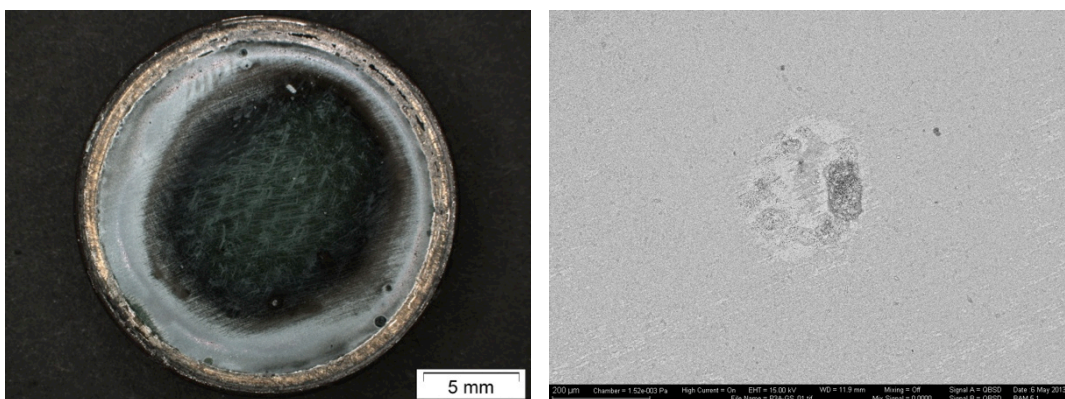


Figure 86: Stereomicroscope and SEM (BSE) pictures of alloy P3 exposed to Gas 1 at 600°C for 1000h in a dual atmosphere condition on the gas side. The sample exhibits different colors and morphologies on the surface.

In the cross section of the sample (Figure 87), a ferrite layer has grown from the surface into the metal. The pictures also show nodules growing on the surface and the microprobe analysis has indicated higher sulfur concentration at the metal/scale interface.

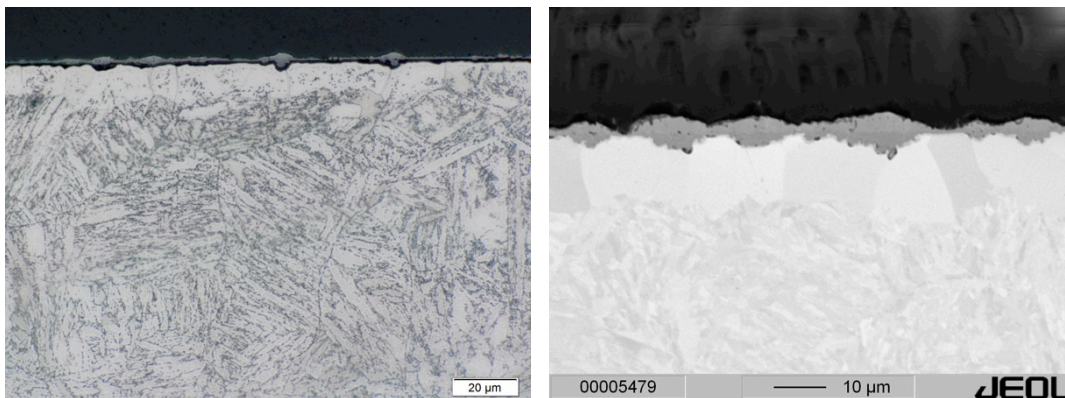


Figure 87: Light microscope and microprobe pictures of alloy P3 exposed to Gas 1 at 600°C for 1000h in a dual atmosphere condition in the gas side. Cr₂O₃ layer was formed and a ferrite layer has grown in the metal, and nodules have grown in the metal grain boundaries.

4.3.2.1.2 Water Vapor Side

A thick scale was formed on the water vapor side of Gas 1 in the dual condition experiment. The scale has a porous phase surrounded by whiskers (Figure 88).

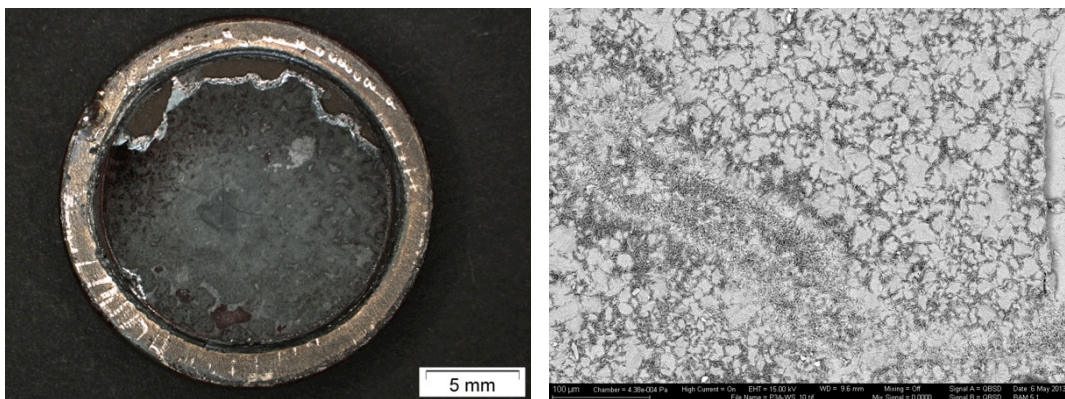


Figure 88: Stereomicroscope and SEM (BSE) pictures of alloy P3 exposed to Gas 1 at 600°C for 1000h in a dual atmosphere condition on the gas side. The sample exhibits a thick oxide layer and whiskers on the surface.

In the cross-section pictures of Figure 89, the internal scale is composed of Fe/Cr Spinel and the external scale of magnetite and hematite (brighter phase on the top). Hematite is also found in cracks and holes in the magnetite layer due to the higher oxygen partial pressure in these places.

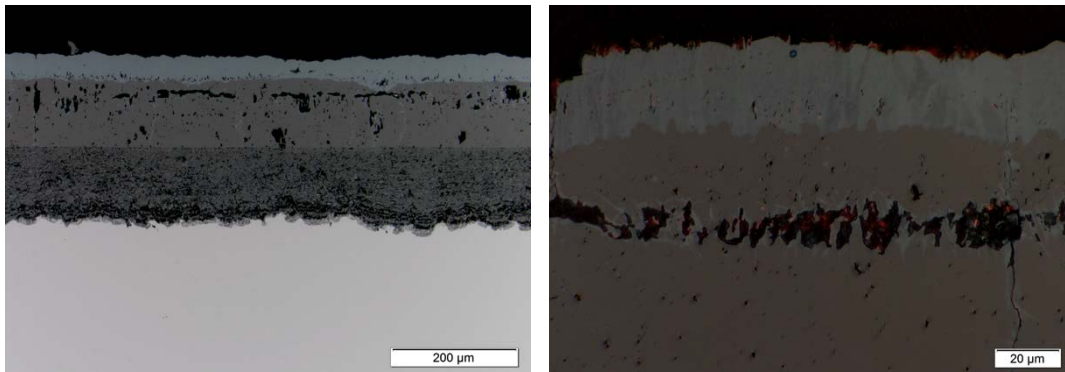


Figure 89: Light microscope pictures of alloy P3 exposed to Gas 1 at 600°C for 1000h in a dual atmosphere condition on the water vapor side. On external scale, hematite (top layer) and magnetite can be identified. Hematite is also present due to the higher O₂ partial pressure in some spots in the cracks and holes in the magnetite layer.

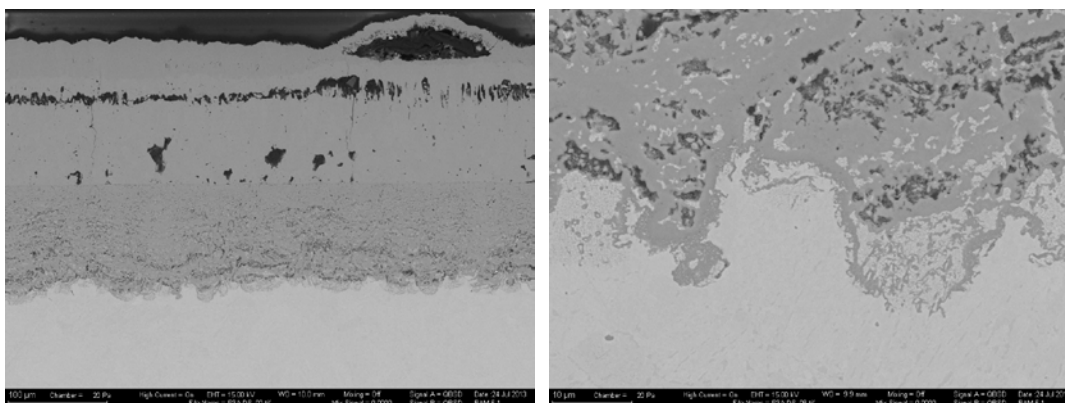


Figure 90: SEM (BSE) pictures of alloy P3 exposed to Gas 1 at 600°C for 1000h in a dual atmosphere condition on the water vapor side.

Figure 90 shows two regions of the sample cross-section, and scale buckling is also observed. Internal oxidation is seen in the right picture. The line scan EDS confirms the sequence of hematite, magnetite and Fe/Cr spinel from the gas to the metal (Figure 91).

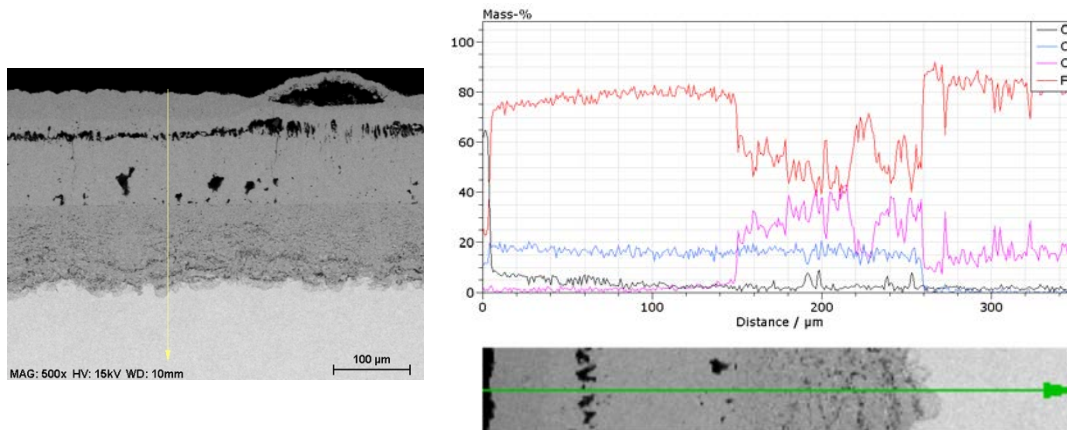


Figure 91: EDS line scan of alloy P3 exposed to Gas 1 at 600°C for 1000h in a dual atmosphere condition on the water vapor side showing a sequence of hematite, magnetite and spinel from the gas side to the metal.

4.3.2.2 Gas 3

4.3.2.2.1 Gas side

Cr_2O_3 layer and nodules were formed on the surface of Alloy P3 on the side of Gas 3 in the dual condition experiment. In the SEM in the right picture of Figure 92, nodules and a cellular structure are observed on the surface.

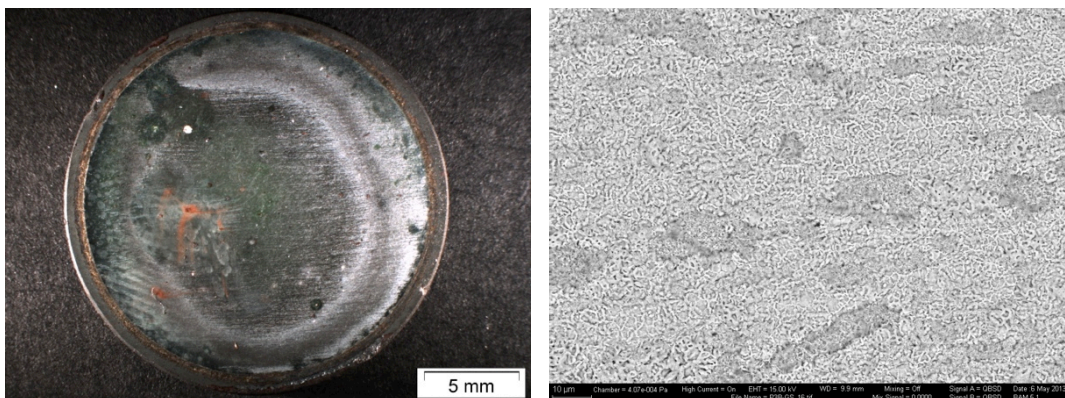


Figure 92: Stereomicroscope and SEM (BSE) pictures of alloy P3 exposed to Gas 3 at 600°C for 1000h in a dual atmosphere condition on the gas side. The sample exhibits different colors and morphologies on the surface. In the SEM picture on the left, porous nodules forms on the surface and a cellular structure forms between them.

A ferrite layer is observed below the scale in the cross-section pictures of Figure 93.

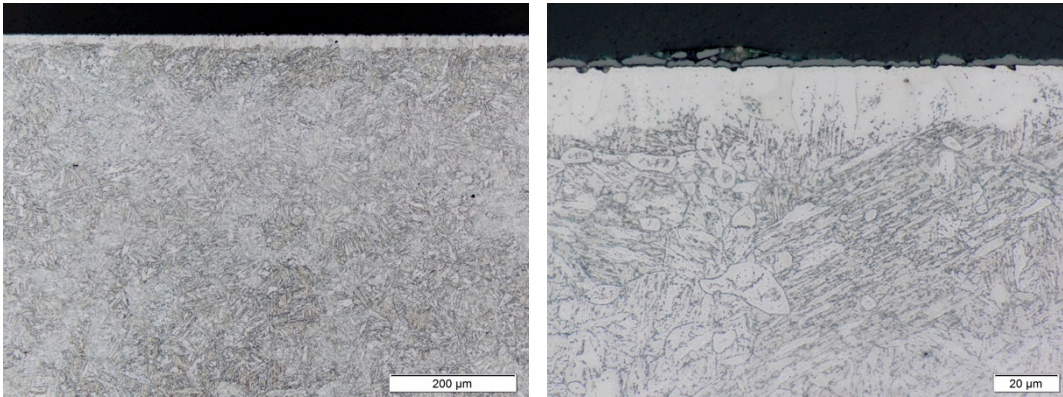


Figure 93: Light microscope pictures of alloy P3 exposed to Gas 3 at 600°C for 1000h in a dual atmosphere condition on the gas side. Ferrite is formed in the metal beneath the scale.

Ferrite growth and nodules formation are observed in the cross-section pictures of Figure 94. Microprobe analysis has shown a higher sulfur concentration at the metal/scale interface.

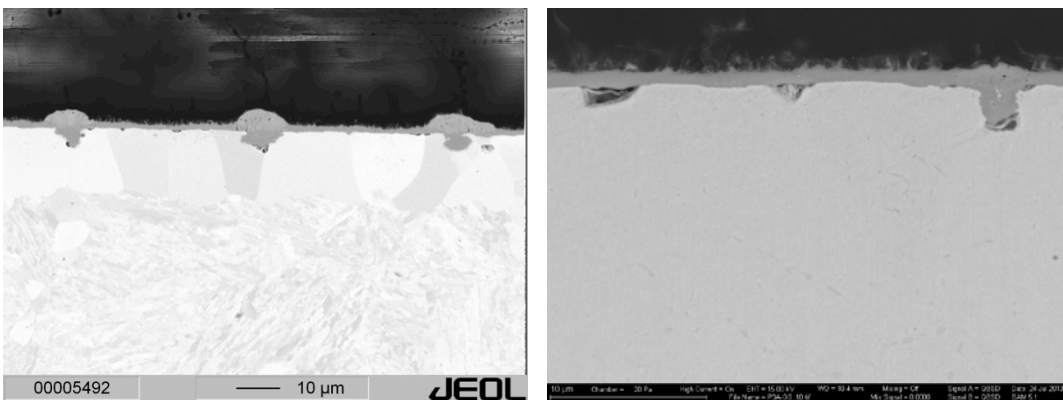


Figure 94: Microprobe and SEM (BSE) pictures of alloy P3 exposed to Gas 3 at 600°C for 1000h in a dual atmosphere condition on the gas side. The pictures show ferrite grains growing on the subsurface region. Nodules and pores are also present.

4.3.2.2.2 Water Vapor Side

An unexpected Cr_2O_3 layer was formed on the surface of Alloy P3 with few nodules rich in Fe on the water vapor side of Gas 3 in the dual condition experiment (Figure 95).

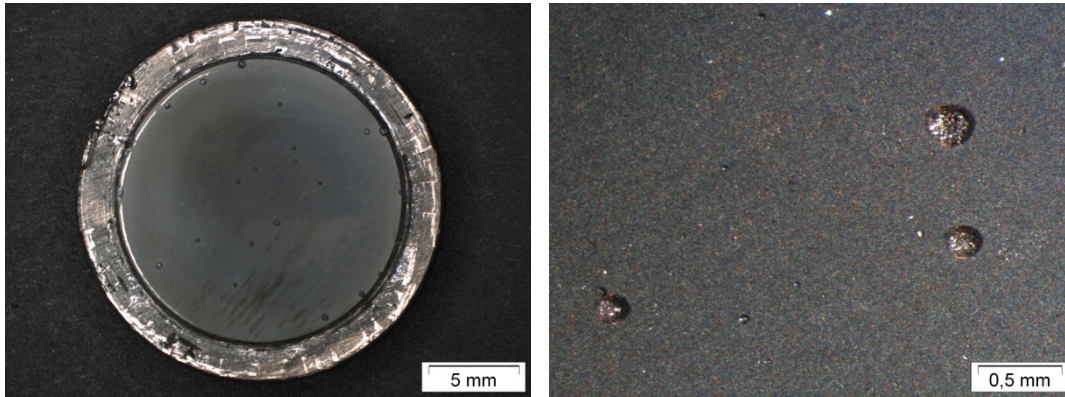


Figure 95: Stereomicroscope pictures of alloy P3 exposed to Gas 3 at 600°C for 1000h in a dual atmosphere condition in the water vapor side. A Cr_2O_3 with few nodules are observed.

The cross-section analysis of the nodule reveals that the selected nodule is composed of external scale of iron oxides and of spinel in the internal scale. Internal oxidation, common in steam oxidation, is also observed (Figure 96 and Figure 97).

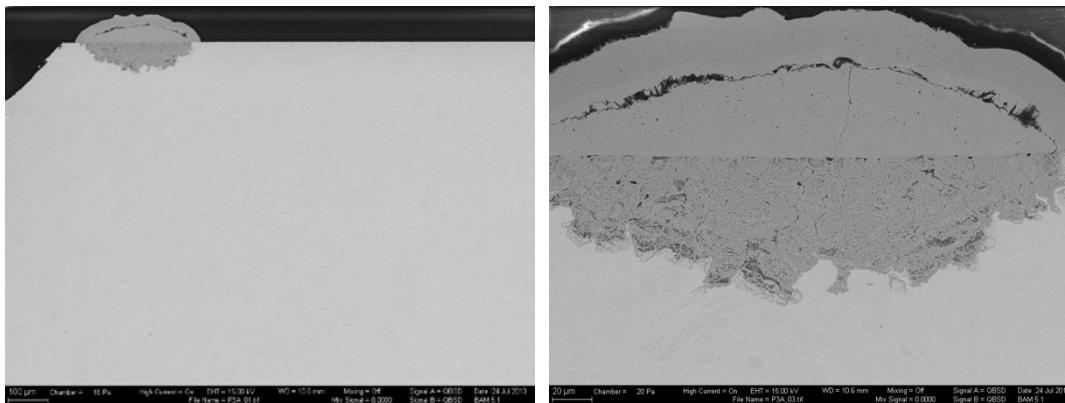


Figure 96: SEM (BSE) pictures of alloy P3 exposed to Gas 3 at 600°C for 1000h in a dual atmosphere condition on the water vapor side. The nodules are composed of iron oxides and Fe/Cr spinel. Internal oxidation is also present.

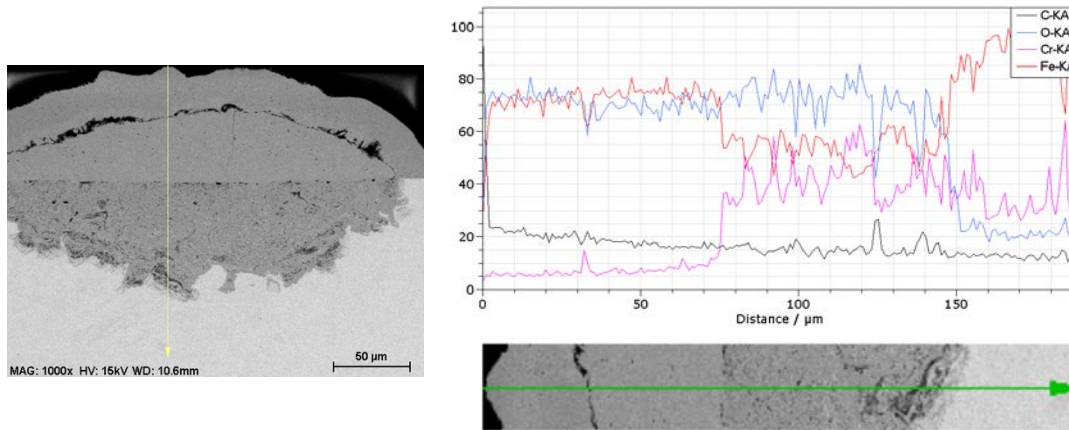


Figure 97: EDS line scanning of alloy P3 exposed to Gas 3 at 600°C for 1000h in a dual atmosphere condition on the water vapor side showing a external scale composed of iron oxides, an internal scale composed by Fe/Cr spinel and internal oxidation

4.4 Alloy P4

Alloy P4 is a martensitic steel with 14.2% Cr–3.1%Co–0.16%C, exposed to gases 1, 2 and 3 in single and to gases 1 and 3 in a dual atmosphere condition.

In a single condition the alloy displayed increase in the nodules density with increase in water vapor concentration from 0% in Gas 1 to 1% in Gas 2 and 29% in Gas 3; not only the density was higher, but also bigger and porous iron oxide rich nodules were present.

In Gas 1 in a dual condition, nodule density was higher in a single condition and a ferrite layer was formed in the metal in the interface with the scale. In Gas 3, nodules were not found in metallographic characterization and in cross-section, but observed in surface analysis. The ferrite layer was also present in this sample, in gases 1 and 3.

4.4.1 Single Atmosphere Condition

4.4.1.1 Gas 1 (70 CO₂ – 1 SO₂ – 29 Ar)

In Gas 1, Alloy P4 oxidized almost homogeneously (Figure 98) although the stereo picture has shown a dark and a light color, which could be a result of the gas flow.

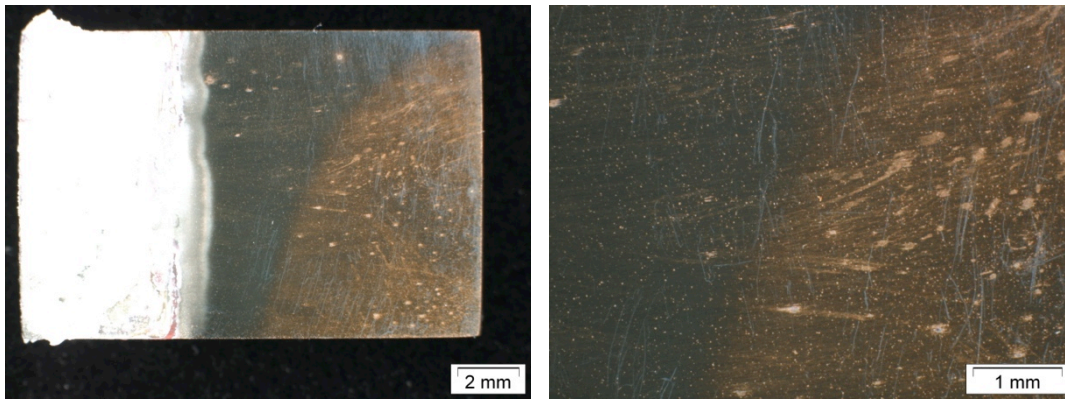


Figure 98: Stereomicroscope pictures of alloy P4 exposed to Gas 1 at 600°C for 1000h in a single atmosphere condition. The white part at sample bottom is the cement used to stick the sample to the sample holder. The dark and bright colors of the rest of the sample may be caused by the gas flow.

Sample surface is composed mainly of Cr_2O_3 and small nodules can be seen in some points (Figure 99 and Figure 100).

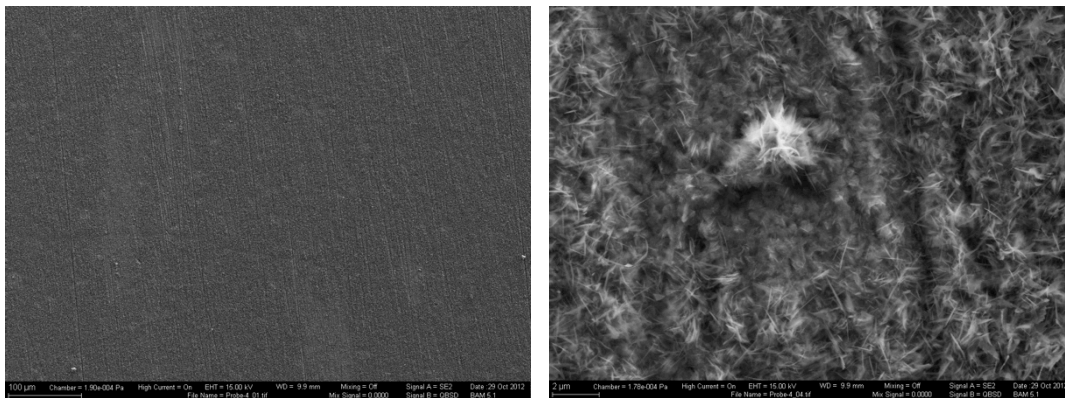


Figure 99: SEM (SE) pictures of the surface of alloy P4 exposed to Gas 1 at 600°C for 1000h in a single atmosphere condition. Cr_2O_3 layer with few nodules.

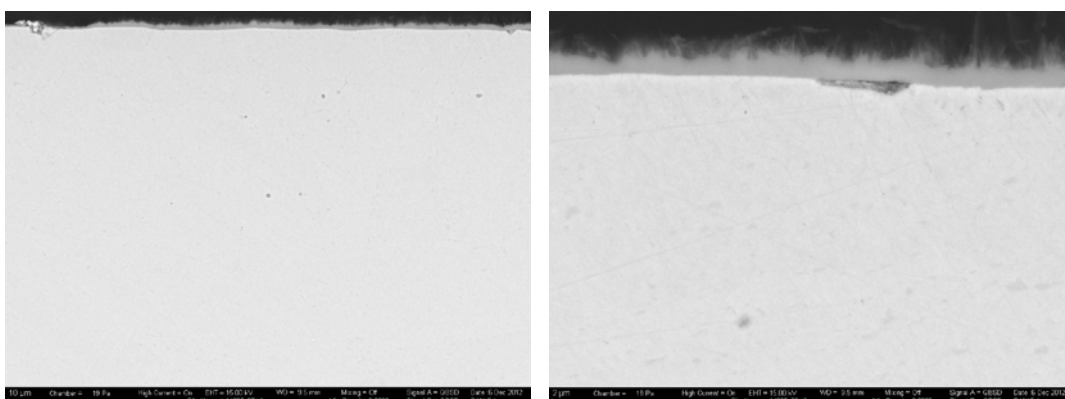


Figure 100: SEM (BSE) pictures of the surface of alloy P4 exposed to Gas 1 at 600°C for 1000h in a single atmosphere condition. Cr_2O_3 layer, but nodules were not found in the cross-section analysis.

4.4.1.2 Gas 2 (70 CO₂ – 1 SO₂ – 1 H₂O – 28 Ar)

In Gas 2, alloy P4 oxidation was homogeneous and few nodules are observed (Figure 101).

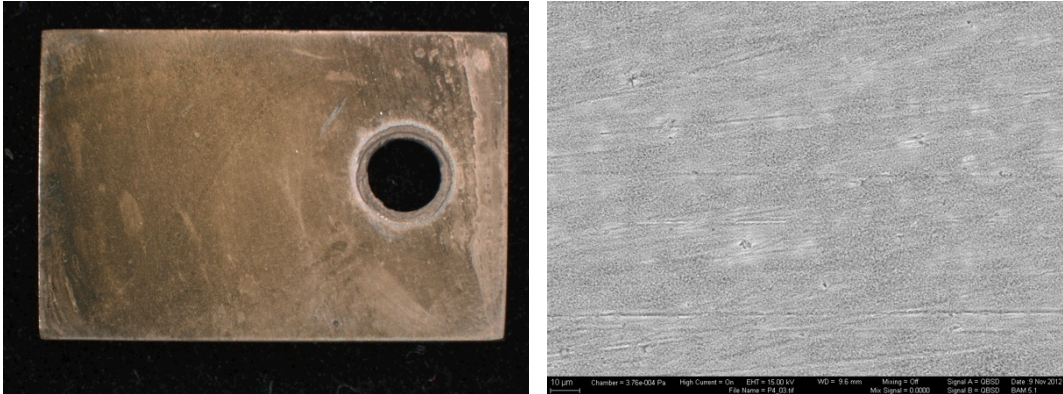


Figure 101: Stereomicroscope and SEM (BSE) pictures of alloy P1 exposed to Gas 2 at 600°C for 1000h in a single atmosphere condition showing iron rich nodules with hematite on the top concentrated in one side of the sample.

In the cross-section pictures (Figure 102), a continuous layer of Cr₂O₃ is seen in a rough surface. Cavities were formed in some regions of the scale/metal interface.

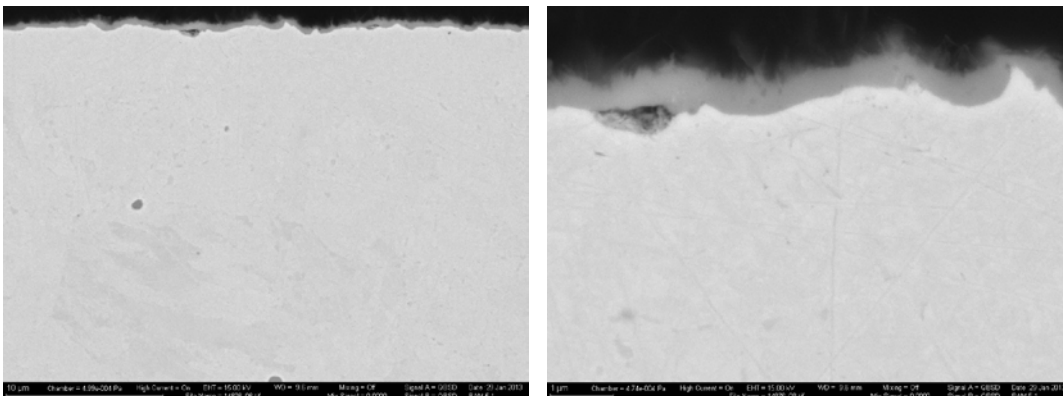


Figure 102: SEM (BSE) pictures of the surface of alloy P4 exposed to Gas 2 at 600°C for 1000h in a single atmosphere condition. A continuous Cr₂O₃ layer was formed with some cavities in the scale/metal interface.

4.4.1.3 Gas 3 (70 CO₂ – 1 SO₂ – 29 H₂O)

In Gas 3, alloy P4 corrosion was almost homogeneous on the sample front and on its back, except for the areas near the cement (Figure 103).

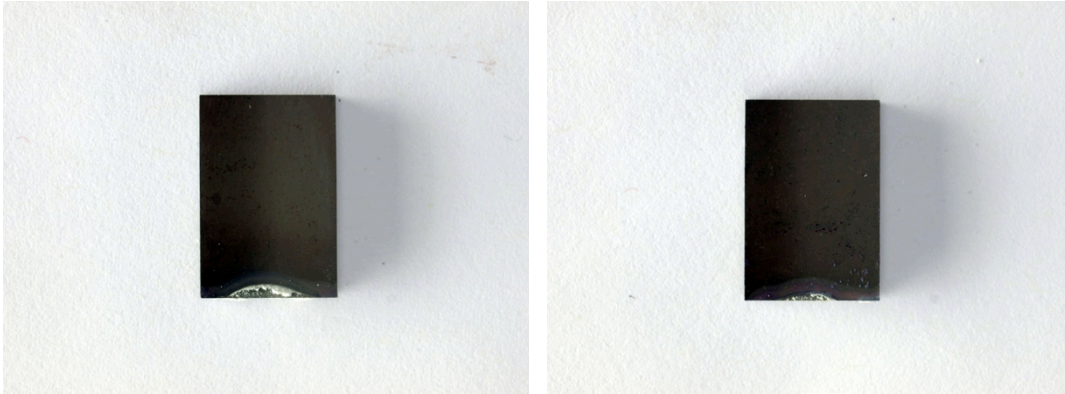


Figure 103: Macro pictures of both sides of the sample of alloy P4 exposed to Gas 3 at 600°C for 1000h in a single atmosphere condition. The white color on the bottom is the cement used to glue the sample to the sample-holder. The sample exhibits homogenous oxidation.

The surface of alloy P4 exhibited isolated nodules rich in iron with whiskers on top (Figure 104).

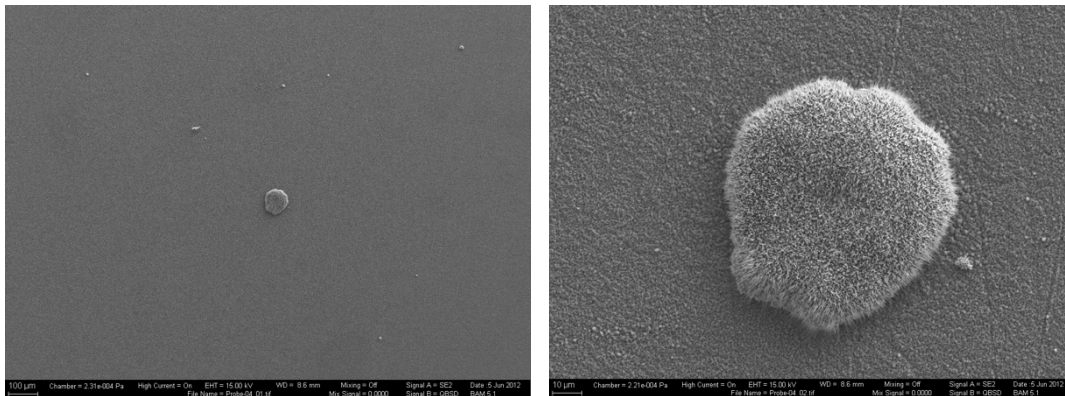


Figure 104: SEM (SE) pictures of the surface of alloy P4 exposed to Gas 3 at 600°C for 1000h in a single atmosphere condition. Nodules rich in iron and a continuous Cr₂O₃ layer were observed.

SEM and EDS in Figure 104 exhibit a porous iron rich nodule and the Cr rich layer near it.

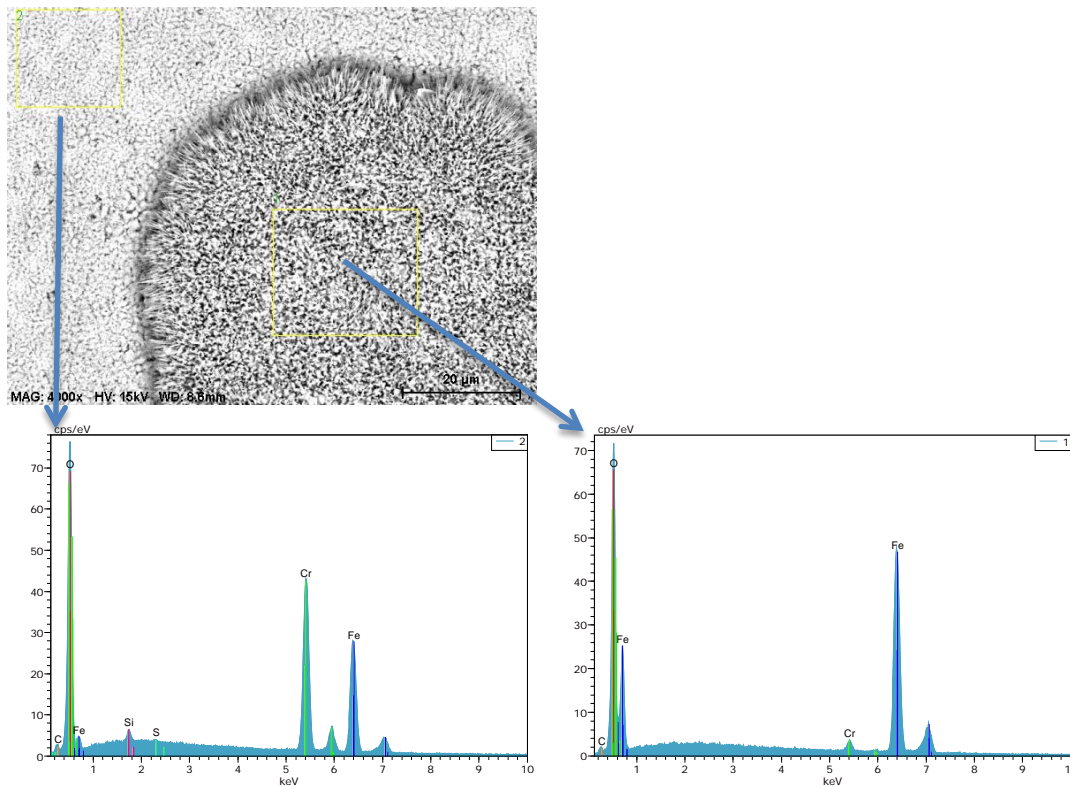


Figure 105: EDS of Alloy P4 exposed to Gas 3 at 600°C for 1000h in a single atmosphere condition. (1) Fe oxide-rich nodule and (2) Cr-rich layer

In the cross section analysis in SEM, only Cr_2O_3 layer was found, without nodules (Figure 106).

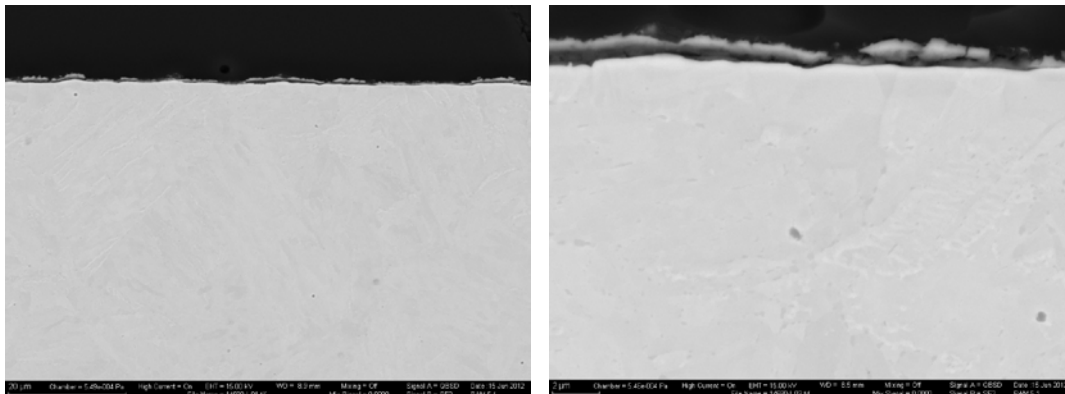


Figure 106: SEM (BSE) pictures of alloy P4 exposed to Gas 3 at 600°C for 1000h in a single atmosphere condition showing a continuous Cr_2O_3 layer.

The etched light microscope picture and the FIB picture in Figure 107 reveal a decarburized zone in the subscale region with ferrite growth. In Figure 108, an analysis of the elements shows a Fe depleted region rich in oxygen under the Cr-rich scale with some defects.

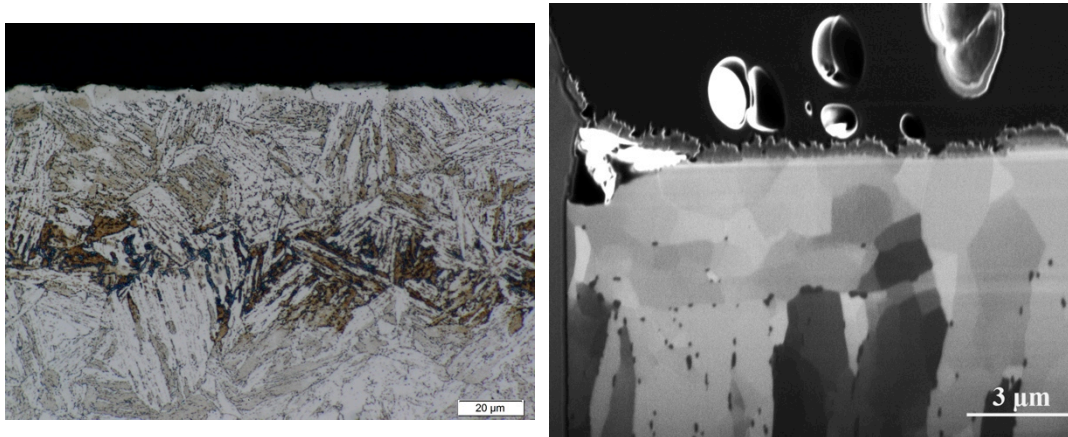


Figure 107: Light microscope and FIB pictures of alloy P4 exposed to Gas 3 at 600°C for 1000h in a single atmosphere condition showing a decarburized zone in the subscale region.

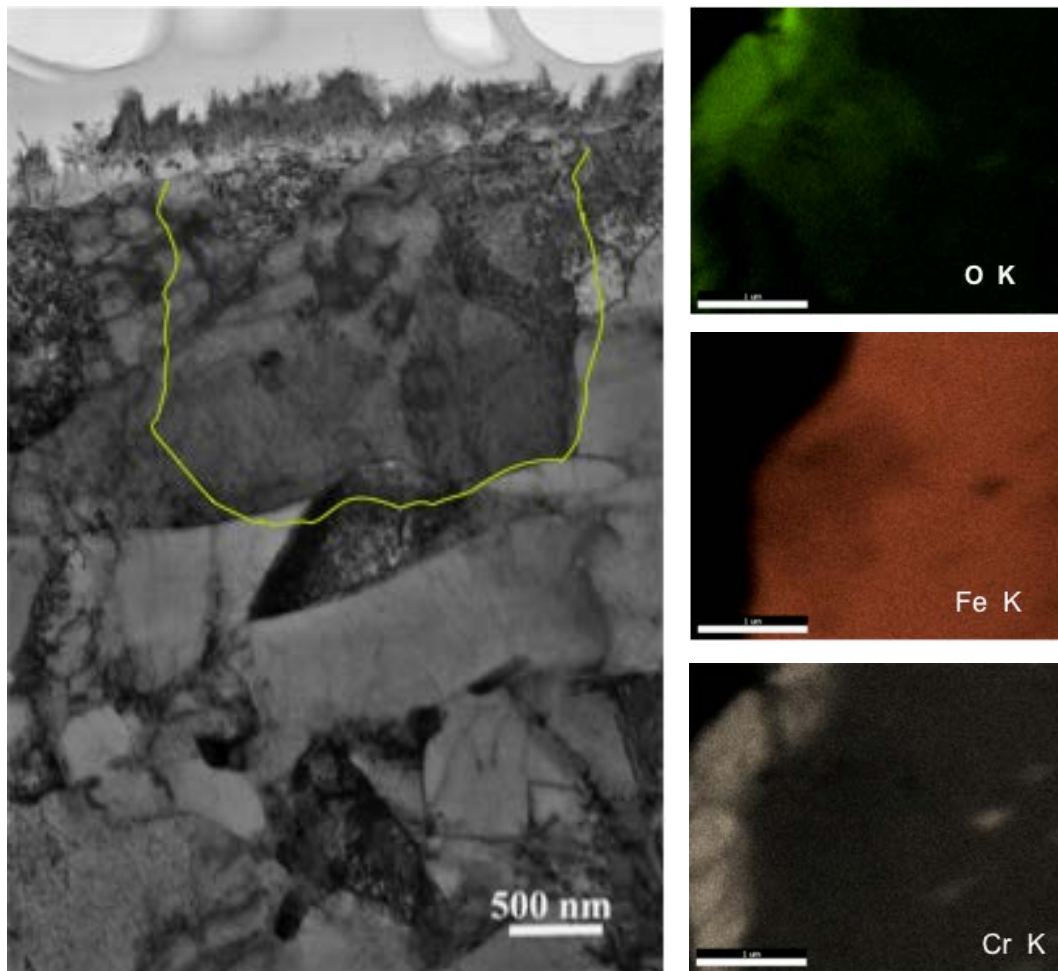


Figure 108: TEM picture and element analysis of alloy P4 exposed to Gas 3 at 600°C for 1000h in a single atmosphere condition showing a Fe depleted region and some Cr carbides beneath it.

4.4.2 Dual Atmosphere Condition

4.4.2.1 Gas 1

4.4.2.1.1 Gas side

A Cr_2O_3 layer and some nodules were observed on the surface on the gas side of Gas 1 in the dual condition experiment (Figure 109).

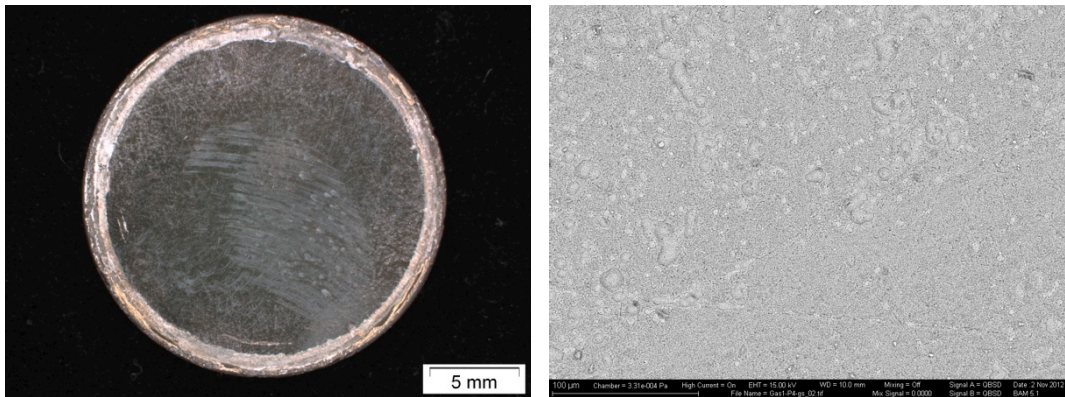


Figure 109: Stereomicroscope and SEM (BSE) pictures of alloy P4 exposed to Gas 1 at 600°C for 1000h in a dual atmosphere condition on the gas side. The sample exhibits scale composed of Cr_2O_3 and some nodules.

The EDS of the nodules shows that they are composed of Fe oxides and that the thin scale is composed of Cr_2O_3 (Figure 110).

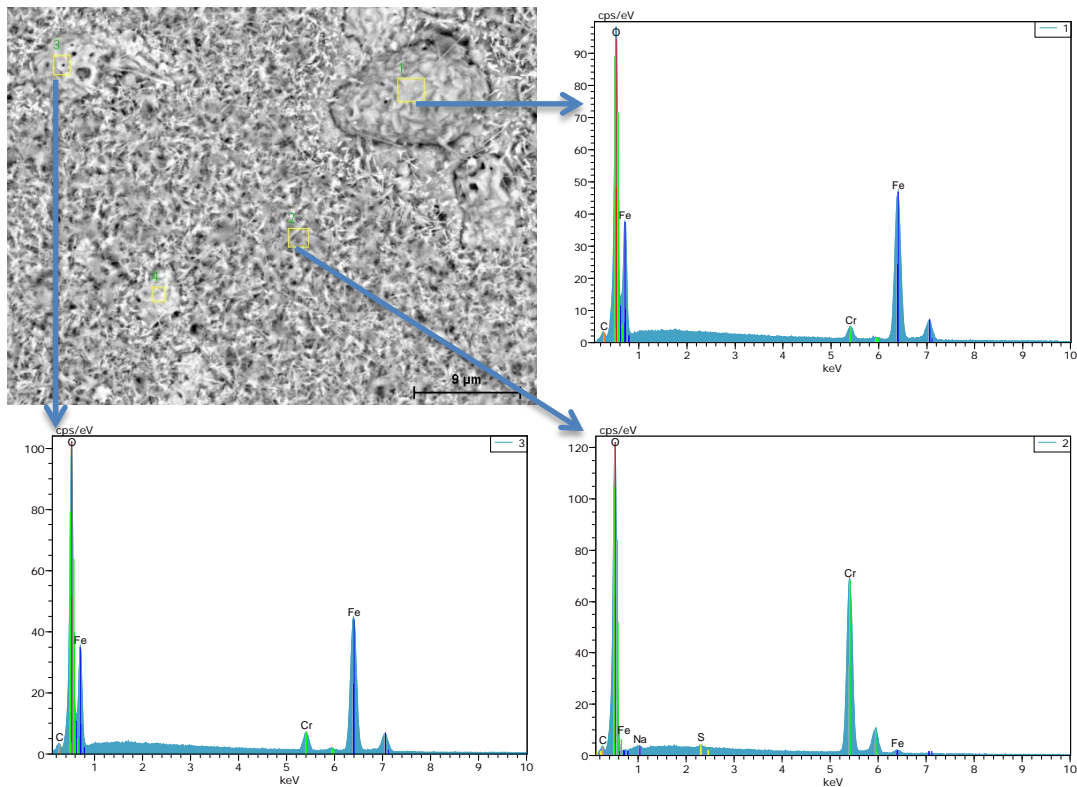


Figure 110: EDS of Alloy P4 exposed to Gas 3 at 600°C for 1000h in a dual atmosphere condition on the gas side. (1) and (3) are iron oxide rich nodules. (2) is Cr_2O_3 .

The sample cross-section shows some nodules and ferrite grows under the scale (Figure 111).

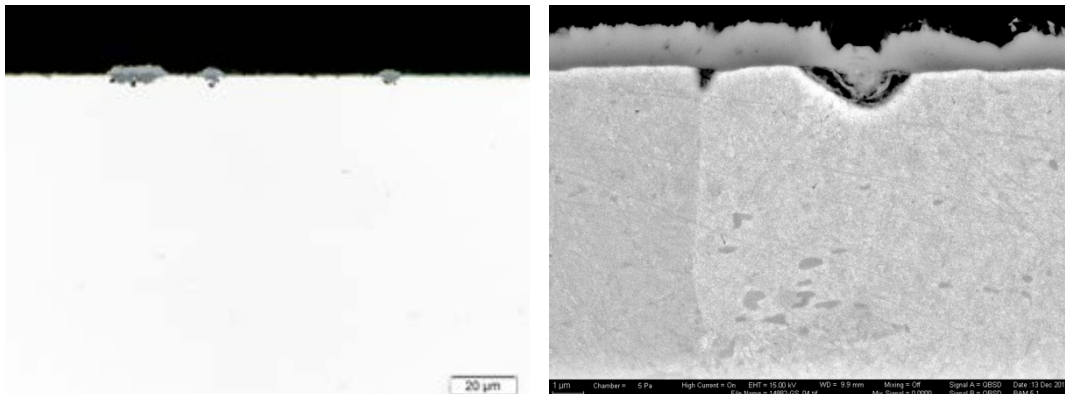


Figure 111: Light microscope and SEM (BSE) pictures of alloy P4 exposed to Gas 1 at 600°C for 1000h in a dual atmosphere condition on the gas side. Nodules are observed in the light microscope picture on the right. Pores and ferrite growth is observed on the left.

The EDS MAP shows external scale rich in Fe and an internal scale rich in Cr. Chromium is also found on the external scale near the internal scale. Sulfur was found close to the metal (Figure 112).

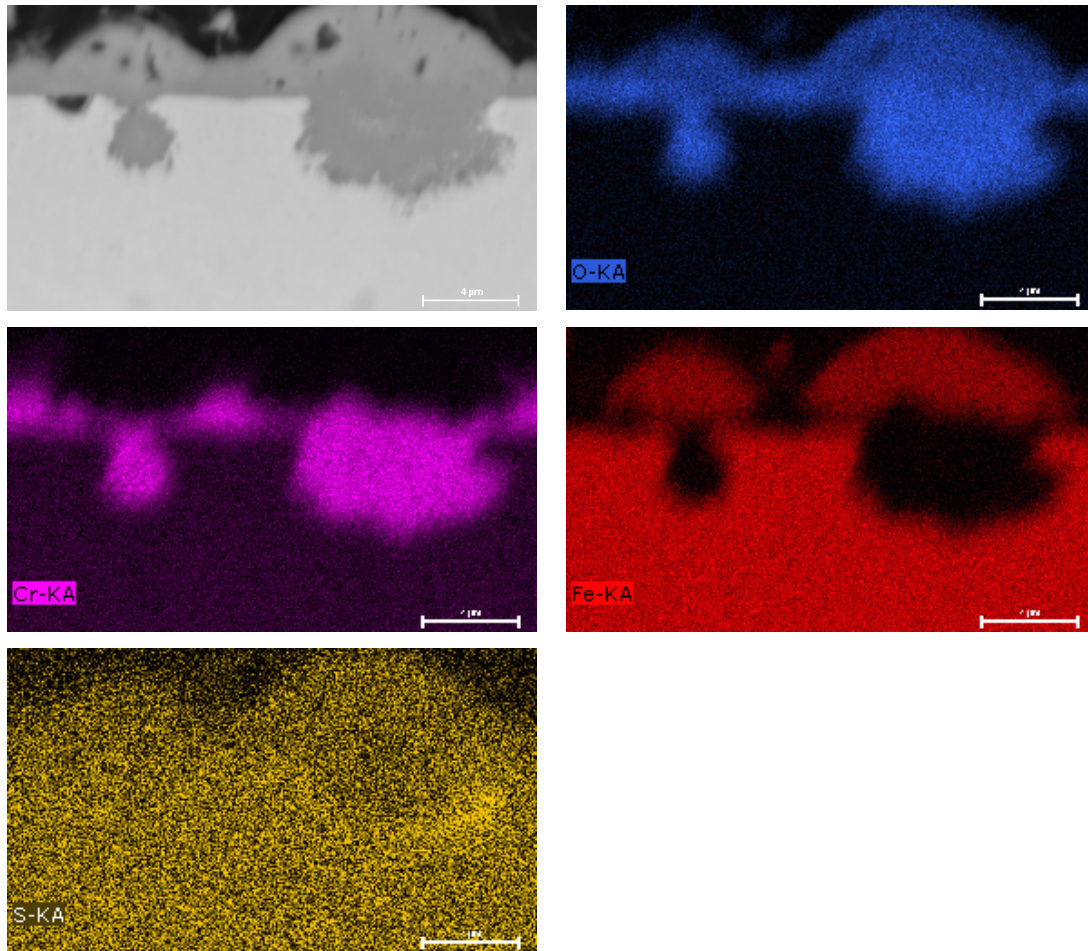


Figure 112: EDS map of alloy P4 exposed to Gas 1 at 600°C for 1000h in a dual atmosphere condition on the gas side. Iron oxide concentration is high on external scale and Fe is not present on internal scale. Cr concentration is high on internal scale and in part of external scale. S is present on internal scale near the metal.

4.4.2.1.2 Water Vapor Side

A porous scale with some iron oxide rich nodules was formed on the water vapor side of Gas 1 in the dual condition experiment (Figure 113).

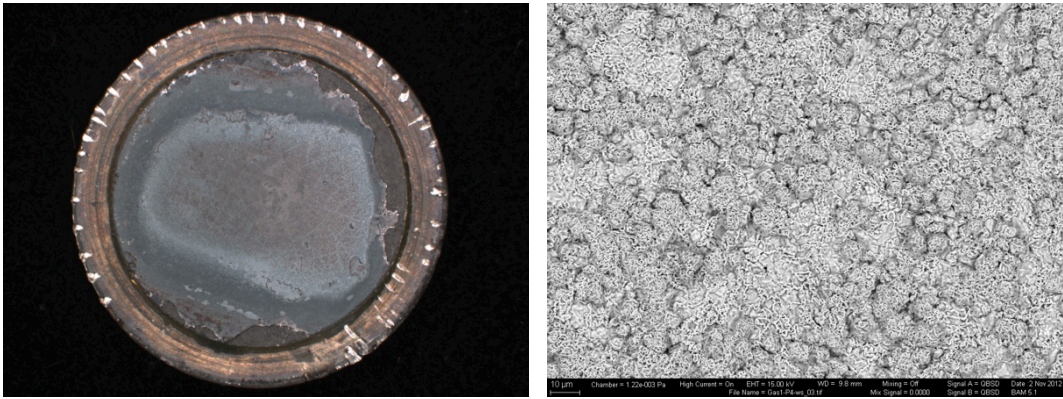


Figure 113: Stereomicroscope and SEM (BSE) pictures of alloy P4 exposed to Gas 1 at 600°C for 1000h in a dual atmosphere condition on the water vapor side. The sample exhibits different colors and morphologies on the surface. The scale is porous and exhibits some nodules (left)

In the cross-section pictures (Figure 114), the internal scale is composed of Fe/Cr spinel and external scale composed of magnetite and hematite (brighter phase on the top). Hematite is also found in cracks and voids in the magnetite layer due to the higher oxygen partial pressure in these places.

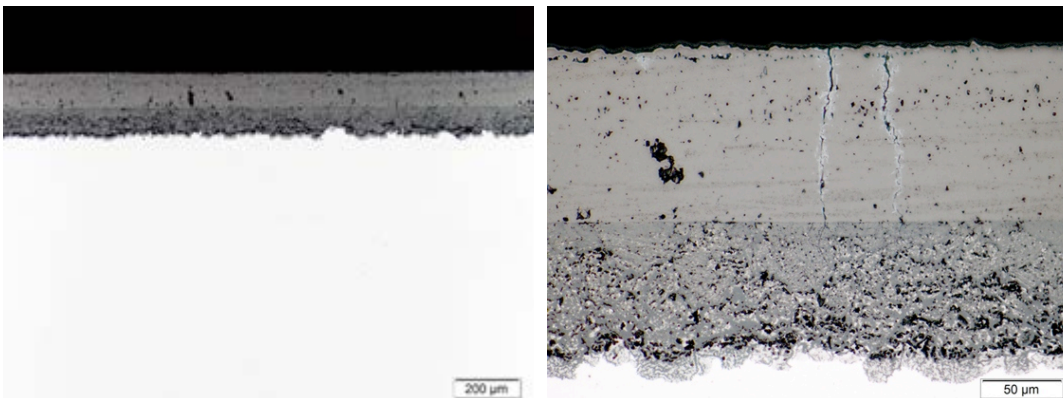


Figure 114: Light microscope pictures of alloy P4 exposed to Gas 1 at 600°C for 1000h in a dual atmosphere condition on the water vapor side. Hematite (top layer) and magnetite can be identified on external scale. In the cracks and voids in the magnetite layer hematite is present due to higher O₂ partial pressure in these places. Internal oxidation is also present.

EDS result in Figure 115 shows the formation of Fe/Cr spinel in the internal scale. Fe content increases when Co is present in the spinel.

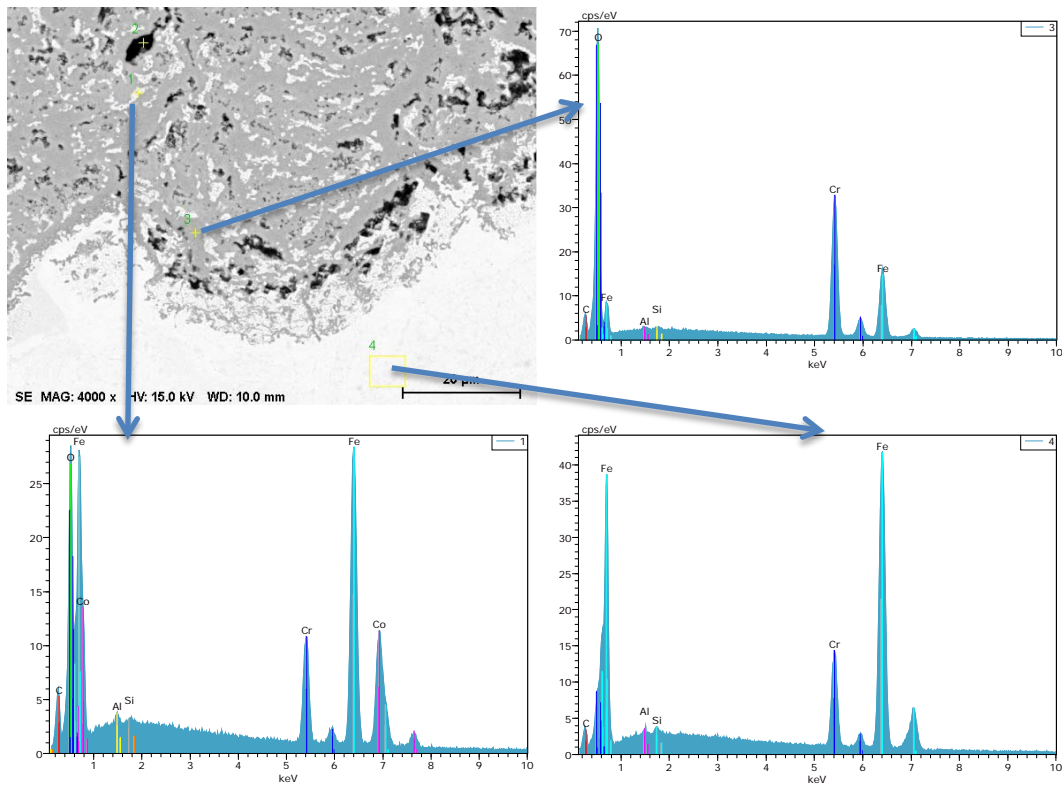


Figure 115: EDS of Alloy P4 exposed to Gas 1 at 600°C for 1000h in a dual atmosphere condition. (1) Fe/Cr spinel with a higher Fe and Co concentration than in point (3). (3) Fe/Cr spinel. (4) Metal.

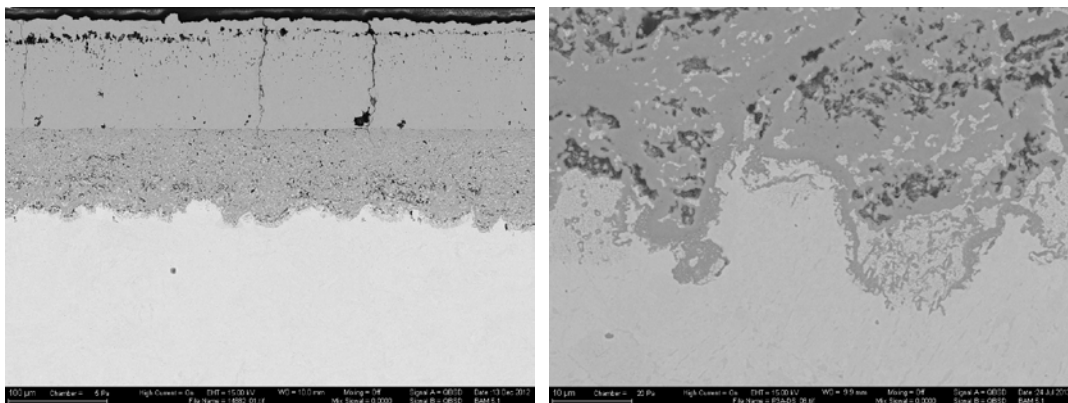


Figure 116: SEM (BSE) pictures of alloy P4 exposed to Gas 1 at 600°C for 1000h in a dual atmosphere condition on the water vapor side.

Figure 116 shows the cross-section with voids, cracks and internal oxidation. Hematite, magnetite and Fe/Cr spinel form from gas to metal. Cr_2O_3 was not found close to the metal (Figure 117).

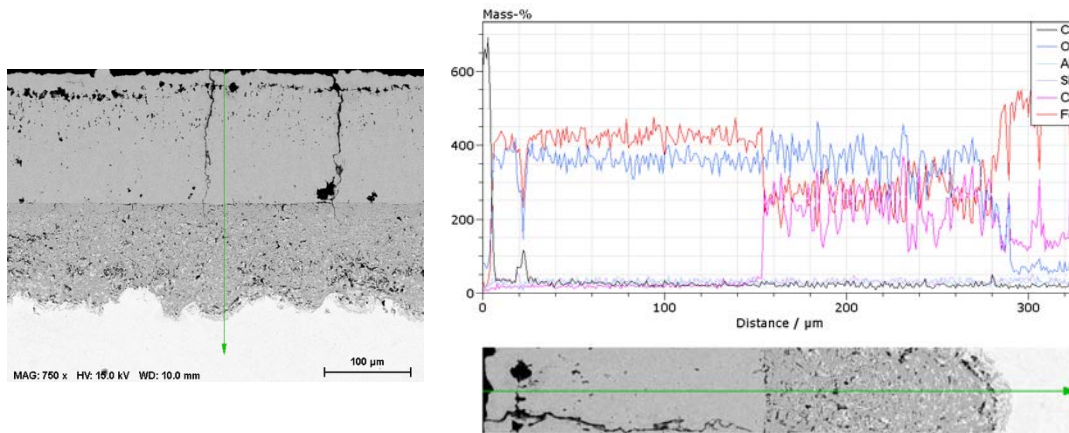


Figure 117: Line scan of Figure 116 from alloy P4 exposed to Gas 1 at 600°C for 1000h in a dual atmosphere condition on the water vapor side. Hematite, magnetite and Fe/Cr spinel form from the gas to the metal.

4.4.2.2 Gas 3

4.4.2.2.1 Gas Side

A Cr_2O_3 layer was formed on the surface of Alloy P4 with some nodules in the side of Gas 3 in the dual condition experiment (Figure 118).

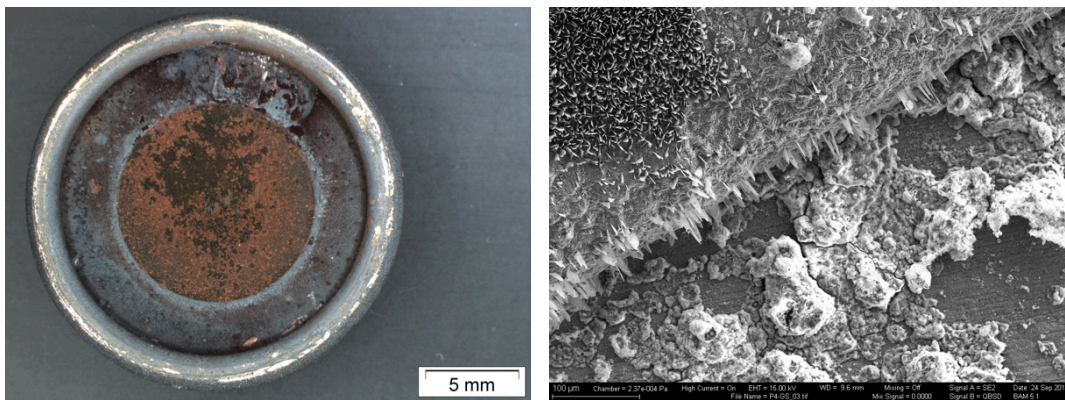


Figure 118: Stereomicroscope and SEM (SE) pictures of alloy P4 exposed to Gas 3 at 600°C for 1000h in a dual atmosphere condition. Left: The sample exhibits a reddish surface with some nodules. Right: interface of the severely corroded iron ring with the sample.

Figure 119 shows sample cross-section with a Cr_2O_3 layer and ferrite growing into the metal. The structures above/behind the scale might be an iron oxide contamination.

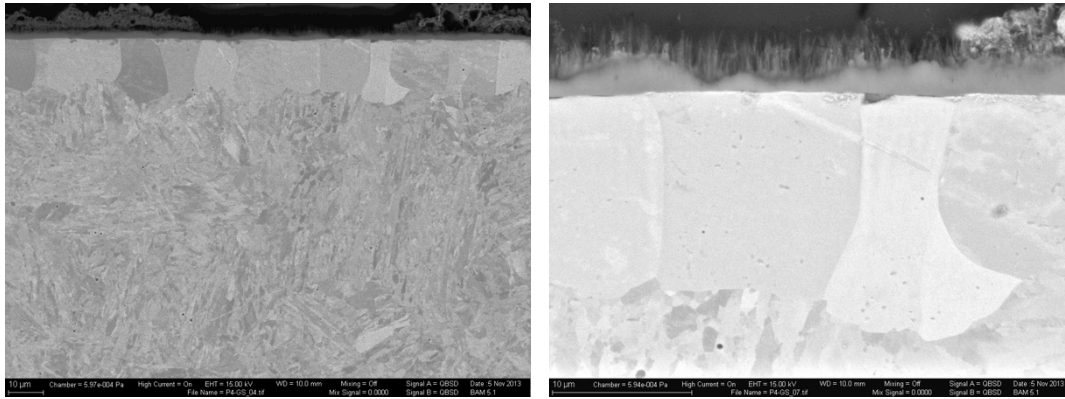


Figure 119: SEM (BSE) pictures of alloy P4 exposed to Gas 3 at 600°C for 1000h in a dual atmosphere condition on the gas side. A thin layer of Cr_2O_3 formed and ferrite has grown into the metal.

4.4.2.2.2 Water Vapor Side

A thick scale with some whiskers was formed on the surface in the side of Gas 3 in the dual condition experiment (Figure 120).

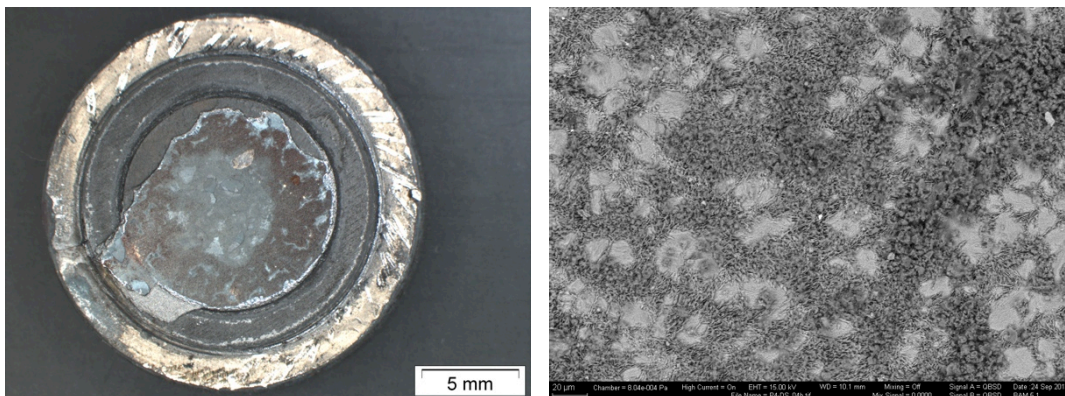


Figure 120: Stereomicroscope and SEM (SE) pictures of alloy P4 exposed to Gas 3 at 600°C for 1000h in a dual atmosphere condition on the water vapor side. The sample exhibits a surface with some whiskers.

In the sample cross-section (Figure 121), external scale presents a brighter color where the oxygen partial pressure is higher (top layer, cracks and voids), that is, hematite and magnetite where the oxygen partial pressure is lower. Internal scale is composed of a denser layer close to external scale and a more porous layer close to metal.

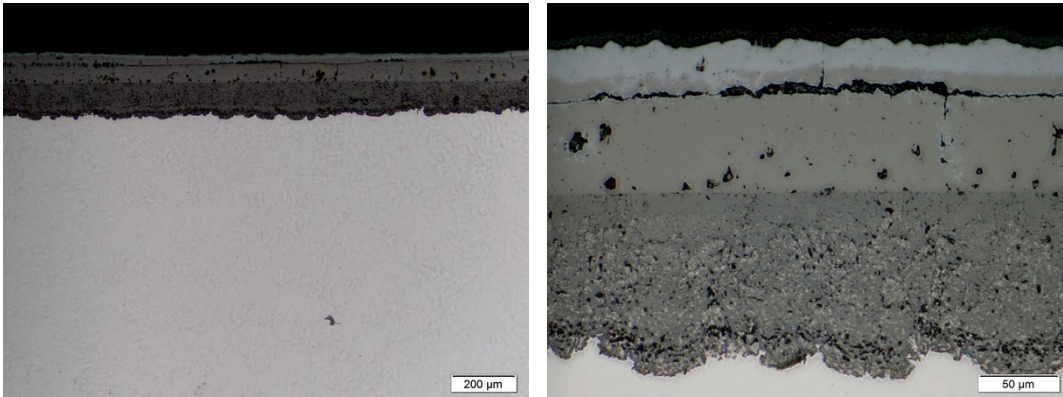


Figure 121: Light microscope pictures of alloy P4 exposed to Gas 3 at 600°C for 1000h in a dual atmosphere condition on the water vapor side. External scale composed of hematite and magnetite and internal scale composed by Fe/Cr spinel.

In Figure 122, thick scale with holes and cracks is observed in external scale, and internal oxidation occurs under internal scale.

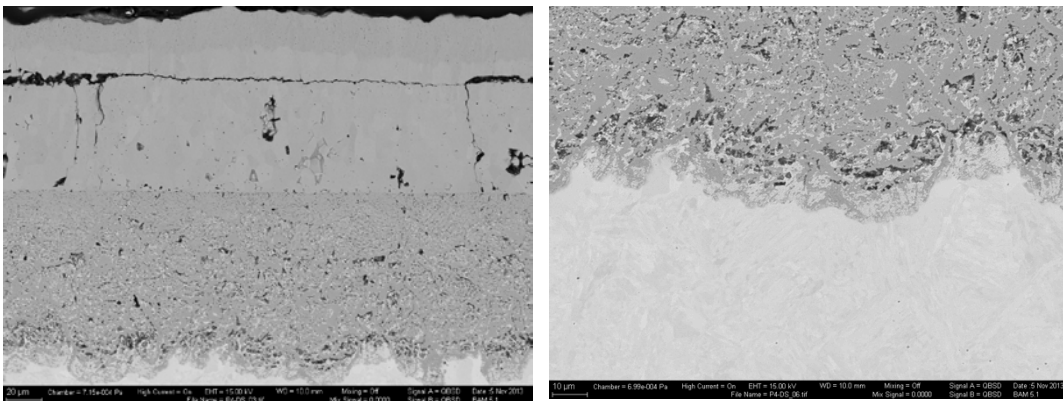


Figure 122: SEM (BSE) pictures of alloy P4 exposed to Gas 3 at 600°C for 1000h in a dual atmosphere condition on the water vapor side. Thick scale with cracks and voids on the left. Internal oxidation is observed on the right.

EDS line scan shows a sequence of hematite and magnetite on external scale. Internal scale is composed of Fe/Cr spinel, and there is a smooth decrease in the metal's oxygen content (Figure 123).

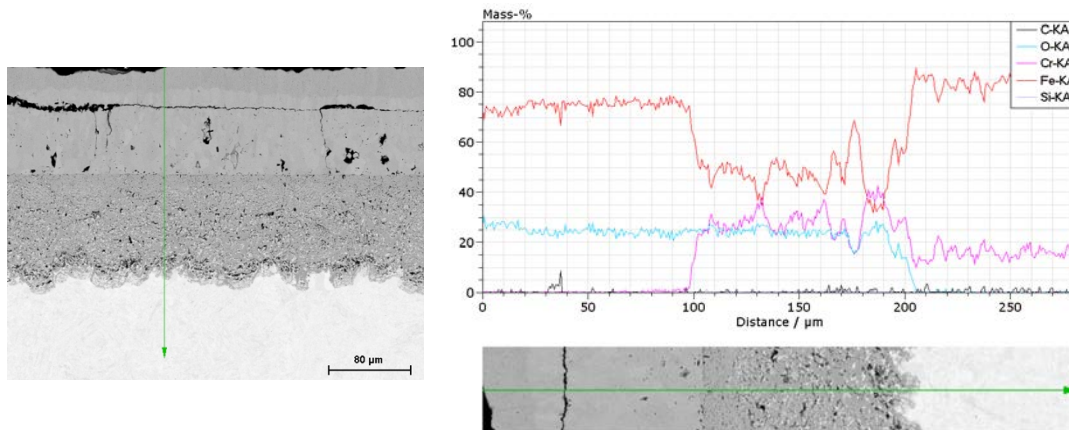


Figure 123: EDS line scan of alloy P4 exposed to Gas 4 at 600°C for 1000h in a dual atmosphere condition on the water vapor side. External scale composed of hematite and magnetite and internal scale composed of Fe/Cr spinel.

4.5 Alloy P5

Alloy P5 is a ferritic steel with 14.1% Cr–3.04%Co–0.01%C, and it was exposed to gases 1, 2 and 3 in single atmosphere condition, and to gases 1 and 3 in dual atmosphere condition.

In single condition, a thin protective Cr_2O_3 layer covers all samples with the growth of few nodules on the surface. The number of nodules increases with the increase in the water vapor content.

In dual condition, alloy oxidation was higher than in a single condition in gases 1 and 3 with the presence of more iron oxide rich nodules covering the surface. In Gas 1, the oxidation was more intense than in Gas 3, and this was not expected due to the higher water vapor content in Gas 3.

4.5.1 Single Atmosphere Condition

4.5.1.1 Gas 1 (70 CO_2 – 1 SO_2 – 29 Ar)

In Gas 1 in a single condition, a Cr_2O_3 scale formed in the surface with few iron oxides rich nodules growing on it. Although the stereo picture shows different colors, the surface on SEM pictures was homogenous (Figure 124).

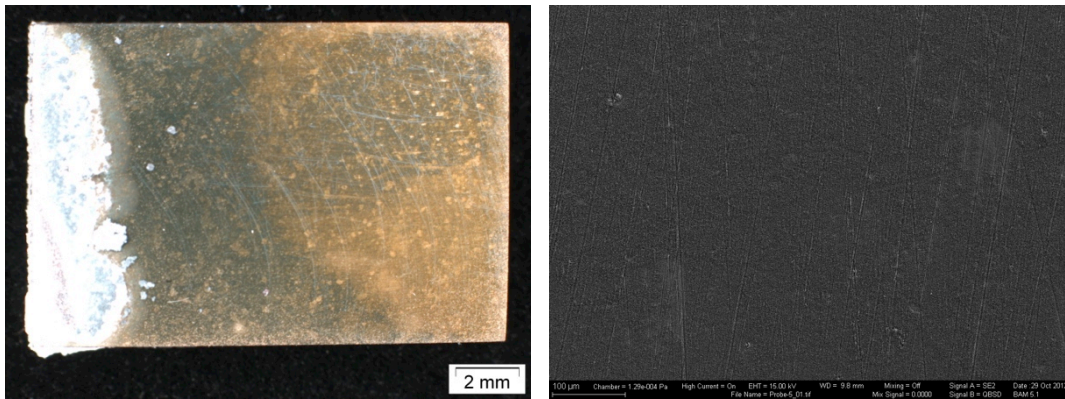


Figure 124: Stereomicroscope and SEM (SE) pictures of alloy P5 exposed to Gas 1 at 600°C for 1000h in a single atmosphere condition. The white part on the sample is the cement used to glue the sample to the sample holder and Cr₂O₃ scale covers the surface with the presence of few nodules.

The thin Cr₂O₃ layer covers most part of the surface. Few regions with formation of pores and spinel were observed (Figure 125 and Figure 126).

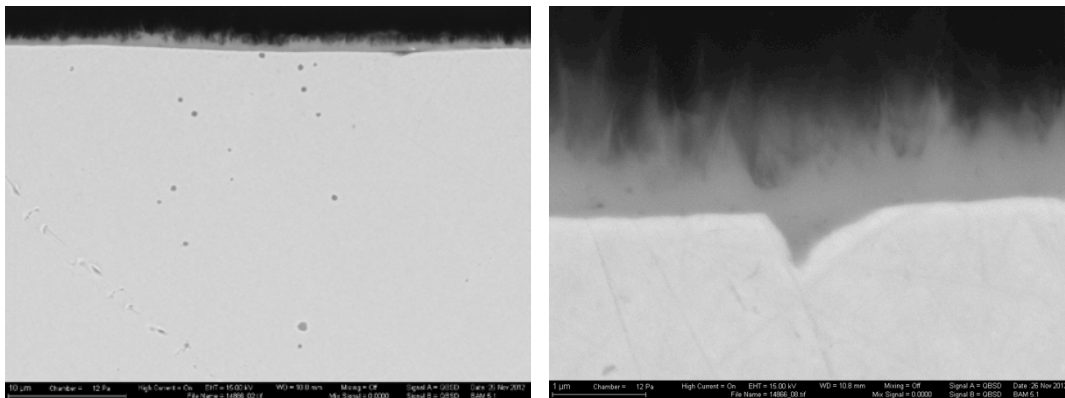


Figure 125: SEM (BSE) pictures of the surface of alloy P5 exposed to Gas 1 at 600°C for 1000h in a single atmosphere condition. Both pictures show slight oxidation of the surface without the evidence of iron-oxide rich nodules.

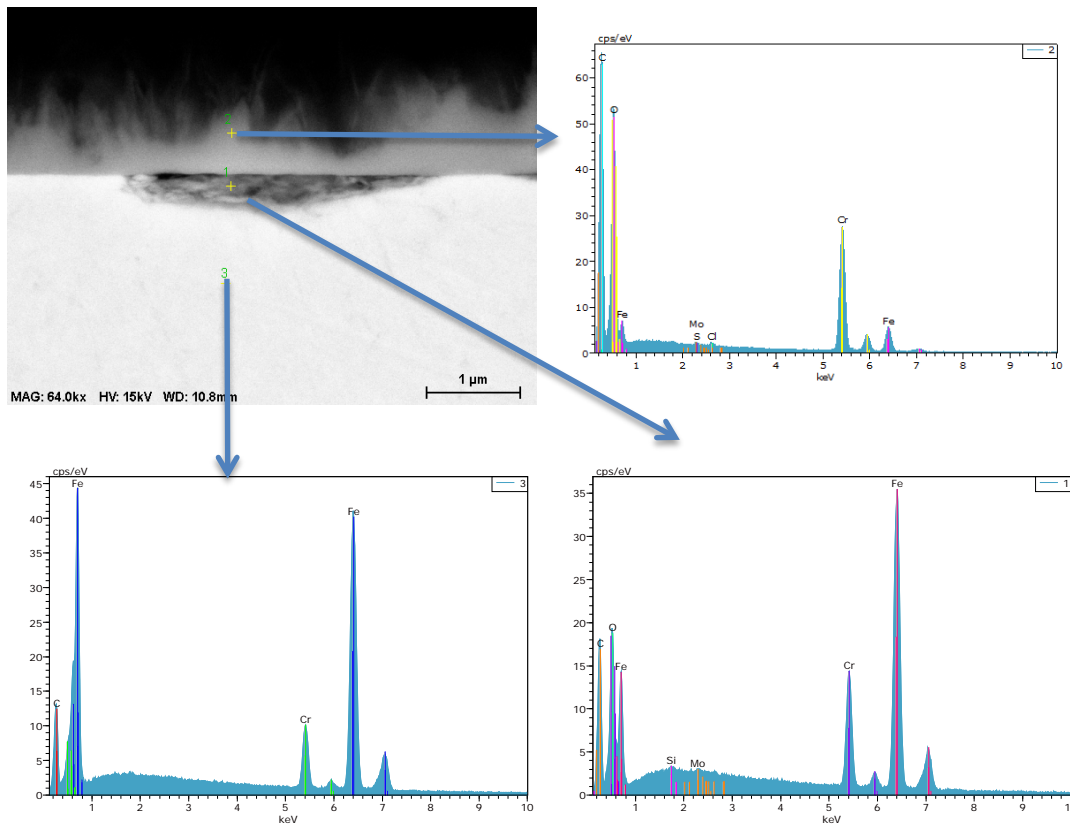


Figure 126: EDS of Alloy P5 exposed to Gas 1 at 600°C for 1000h in a single atmosphere condition. (1) spinel, (2) Cr₂O₃ layer, (3) metal.

4.5.1.2 Gas 2 (70 CO₂ – 1 SO₂ – 1 H₂O – 28 Ar)

Alloy P5, when exposed to Gas 2, exhibited Cr oxide rich layer with some nodules on the surface (Figure 127).

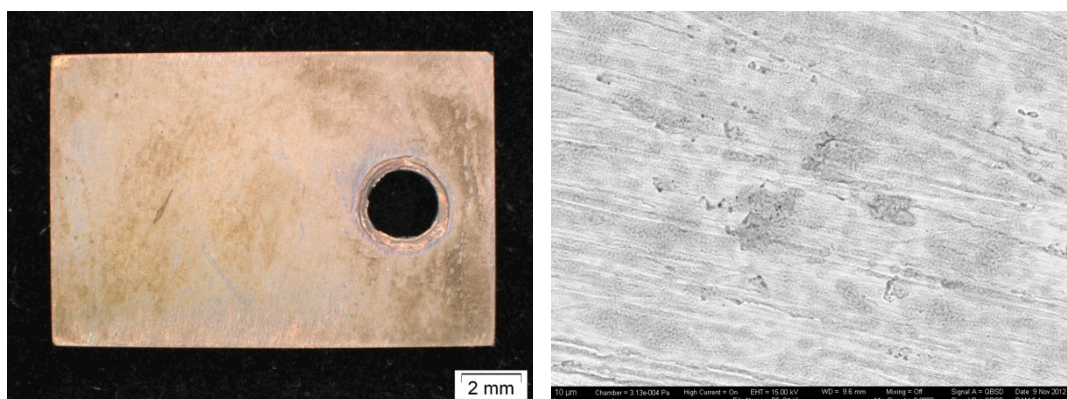


Figure 127: Stereomicroscope and SEM (BSE) picture of alloy P5 exposed to Gas 2 at 600°C for 1000h in a single atmosphere condition. Formation of few iron-rich oxide nodules on the surface.

The surface is composed of a thin layer of Cr-rich oxide (spinel or Cr₂O₃) and few iron-rich nodules (Figure 128 and Figure 129).

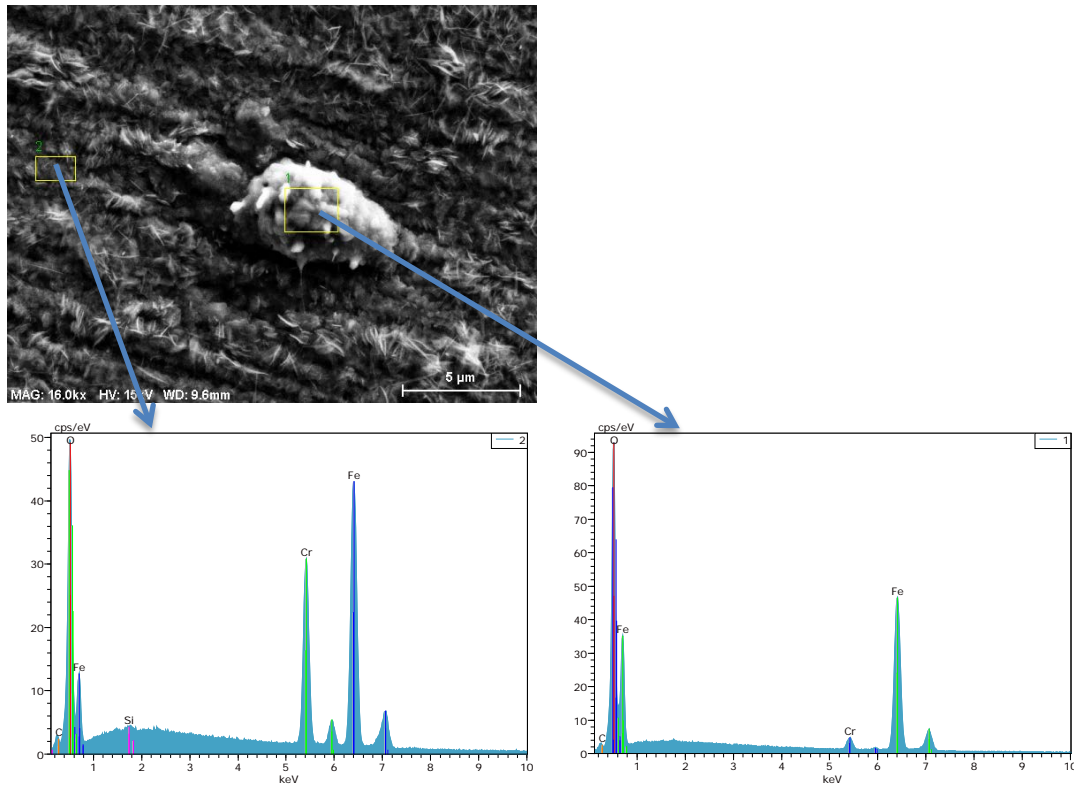


Figure 128: EDS of Alloy P5 exposed to Gas 2 at 600°C for 1000h in a single atmosphere condition. It shows a Fe/Cr spinel or Cr_2O_3 (2) and an iron-rich nodule (1).

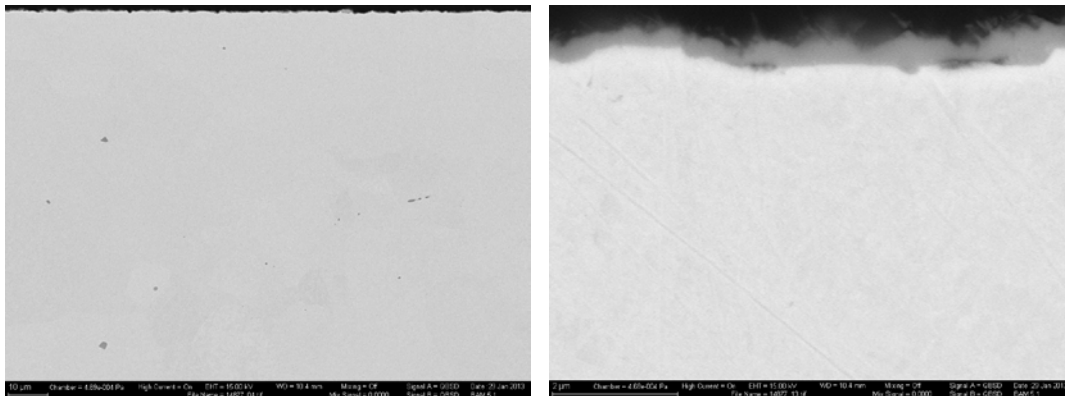


Figure 129: SEM (BSE) pictures of the surface of alloy P5 exposed to Gas 2 at 600°C for 1000h in a single atmosphere condition. A Cr rich oxide layer forms the scale.

4.5.1.3 Gas 3 (70 CO_2 – 1 SO_2 – 29 H_2O)

In Gas 3, few iron rich nodules with whiskers grow on the surface (Figure 130 and Figure 131).

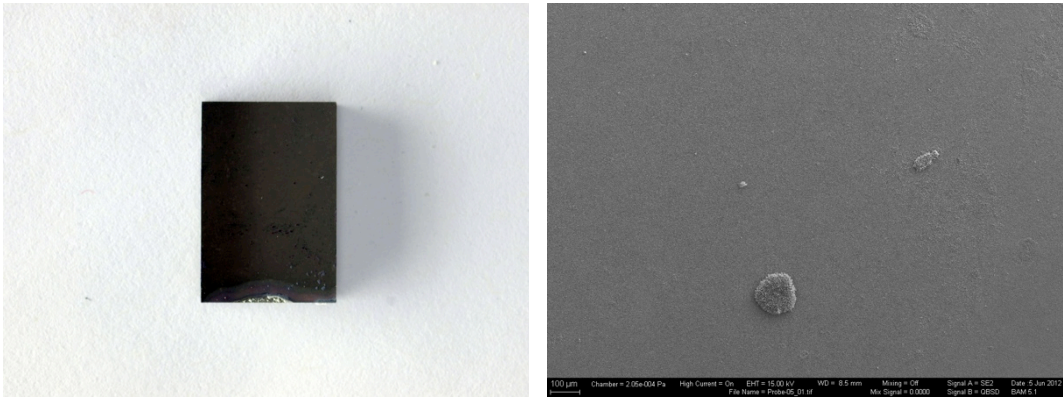


Figure 130: Macro and SEM pictures of alloy P5 exposed to Gas 3 at 600°C for 1000h in a single atmosphere condition. The white part in the bottom of the sample is the cement used to glue the sample to the sample holder, and there is a slight difference on the color of the surface due to the gas flow (stereo picture on the left). On the SEM picture on the right, some nodules are present on the surface.

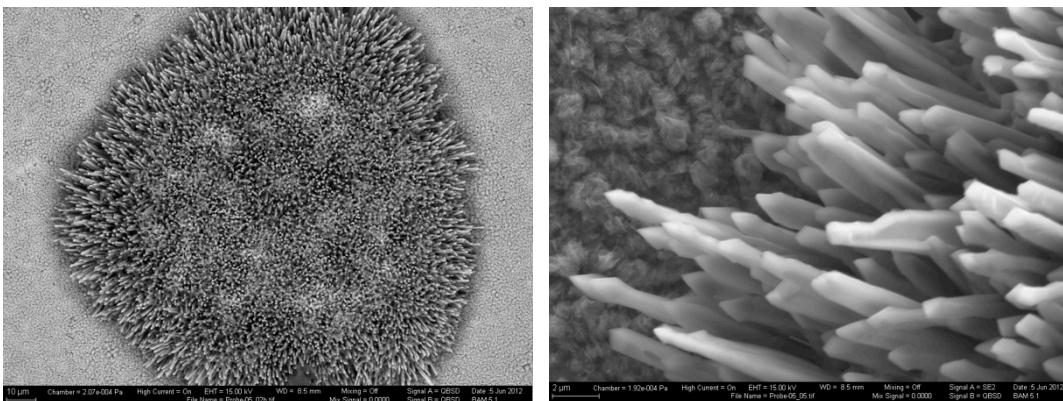


Figure 131: SEM (Left: BSE. Right: SE) picture from the surface of alloy P5 exposed to Gas 3 at 600°C for 1000h in a single atmosphere condition. Cr_2O_3 forms continuous thin protective scale and some iron oxide rich nodules with whiskers grow on the scale.

In the sample cross-section pictures (Figure 132) a microstructural change is observed in the metal near the scale.

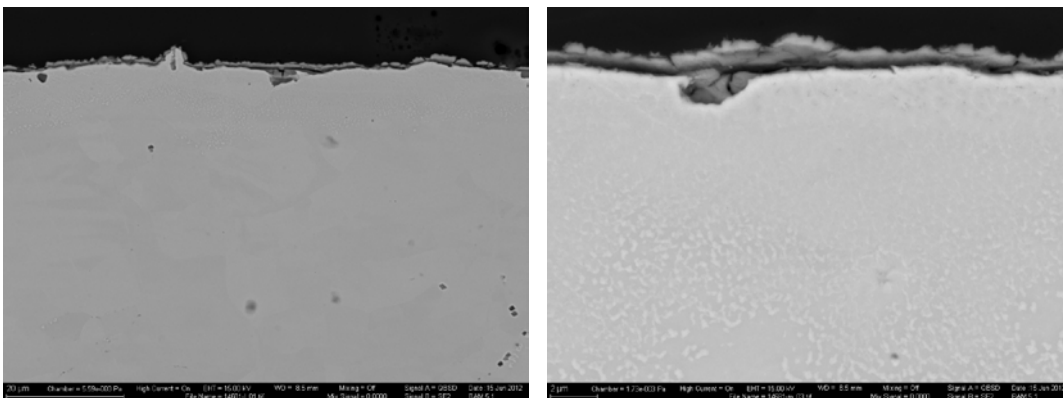


Figure 132: SEM (BSE) pictures of alloy P5 exposed to Gas 3 at 600°C for 1000h in a single atmosphere condition. A protective thin scale grows on the surface and below the surface there is a change in the microstructure in the metal.

4.5.2 Dual Atmosphere Condition

4.5.2.1 Gas 1 (70 CO₂ – 1 SO₂ – 29 Ar)

4.5.2.1.1 Gas side

Thick scale with hematite whiskers was formed on the surface on the gas side of Gas 1 in the single condition experiment. The red color of the stereo pictures confirms the hematite layer (Figure 133). The wavy texture of the surface indicates that merged nodules form this layer.



Figure 133: Stereomicroscope pictures of alloy P5 exposed to Gas 1 at 600°C for 1000h in a dual atmosphere condition on the gas side. Most of the sample displays a red color hematite on the surface.

This sample cross-section shows porous iron oxide rich nodules and hematite whiskers and blades on the surface (Figure 134). EDS confirms that nodules are composed of iron oxides and that the oxide layer between them is Cr₂O₃. Cobalt is also present on the surface, where iron oxide is found. This is an unusual result since Co is normally present in the spinel layer of the internal scale (Figure 135).

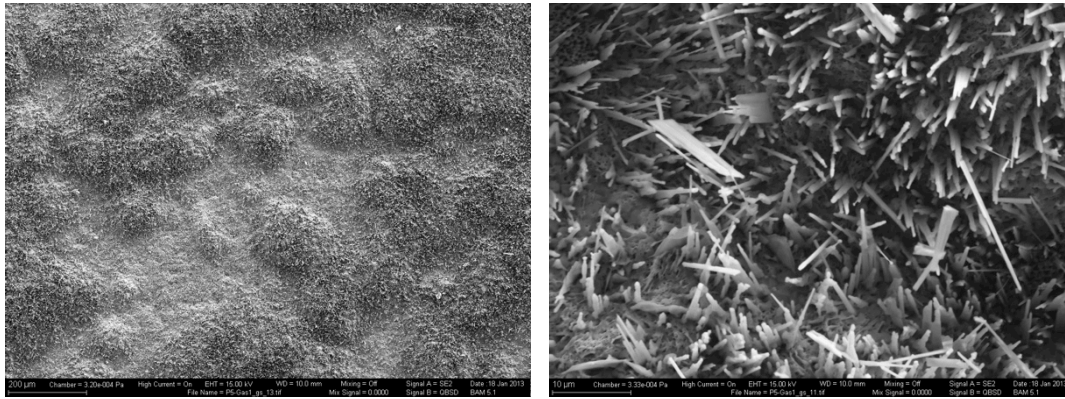


Figure 134: SEM (SE) pictures of alloy P5 exposed to Gas 1 at 600°C for 1000h in a dual atmosphere condition on the gas side. A porous phase and a mixture of whiskers and blades form the surface of the scale.

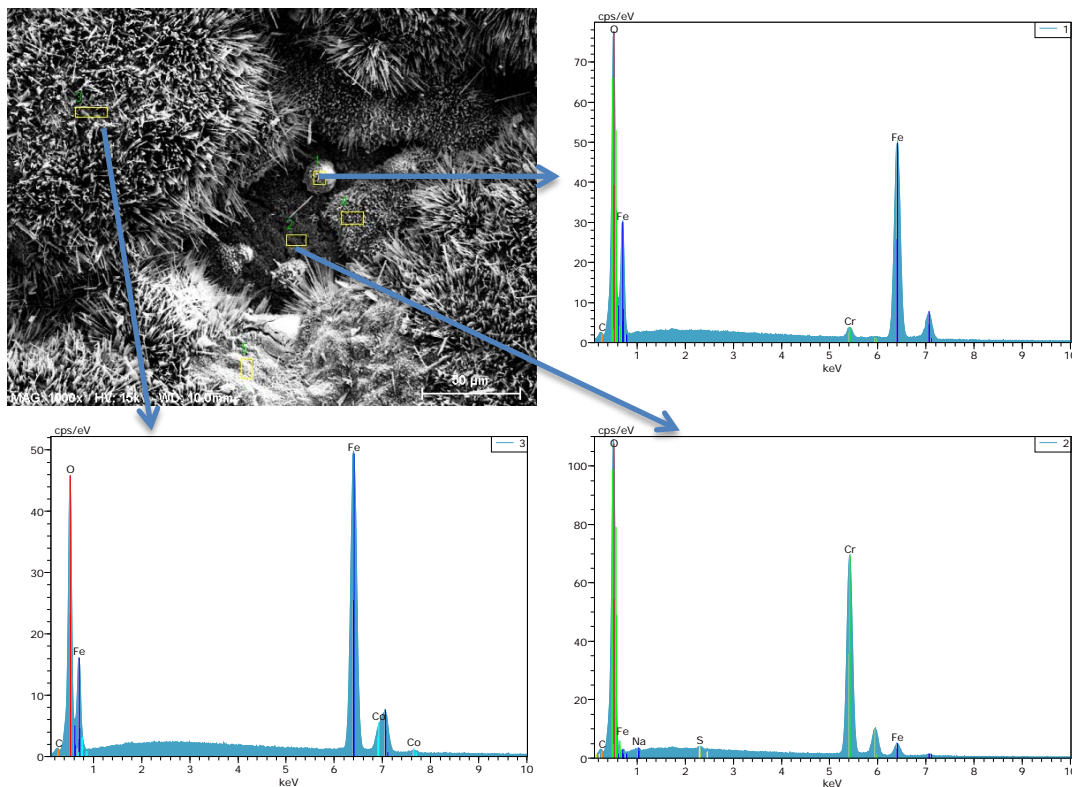


Figure 135: EDS of Alloy P5 exposed to Gas 1 at 600°C for 1000h in a dual atmosphere condition on the gas side. (1) Fe oxide nodule. (2) Cr_2O_3 layer. (3) Fe oxide with Co that was also found in other parts of the sample.

The scale external layer is composed of magnetite and the internal layer of Fe/Cr spinel. The spinel displays three distinct morphologies with increasing Cr content towards the metal. The two internal spinel layers are more porous than the latter and have sulfur, which is not present in the first spinel layer (Figure 136 and Figure 137). Hematite is not present in this EDS line scanning, but the stereomicroscope and SEM pictures confirm its presence.

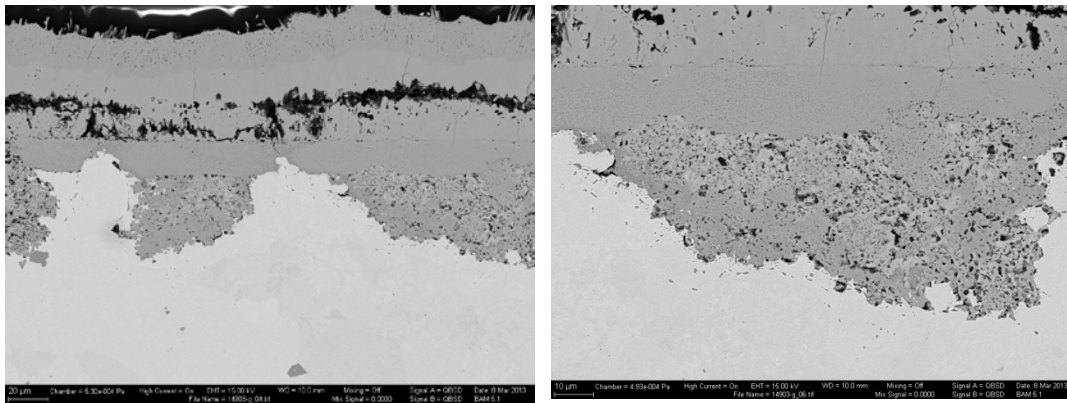


Figure 136: SEM (BSE) pictures of alloy P5 exposed to Gas 1 at 600°C for 1000h in a dual atmosphere condition on the gas side. External layer composed of two different magnetite morphologies and internal scale composed of three different spinel morphologies.

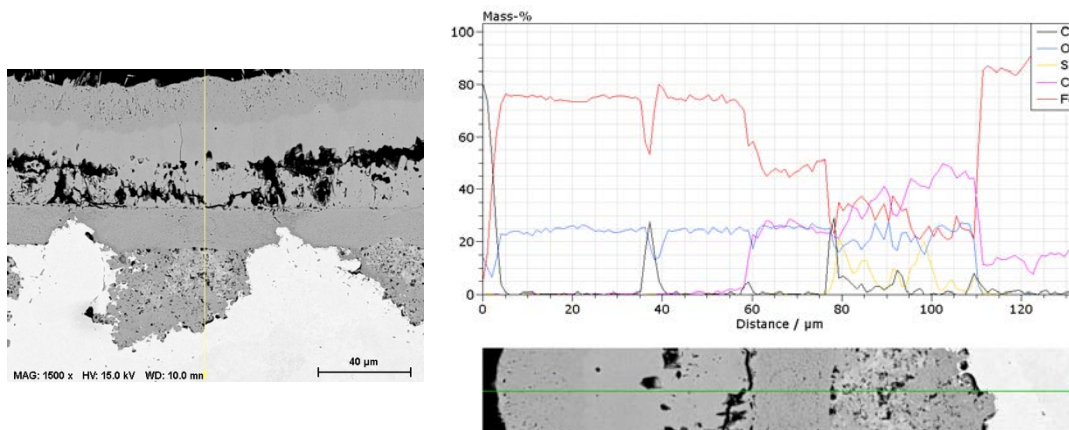


Figure 137: EDS line scan of alloy P5 exposed to Gas 1 at 600°C for 1000h in a dual atmosphere condition on the gas side. A magnetite layer composes the external scale, spinel with three different Cr content and S composes the internal layer.

4.5.2.1.2 Water Vapor Side

On the water vapor side of Gas 1 in the dual condition experiment, a gray porous iron oxide layer was formed on the surface (Figure 138 and Figure 139).

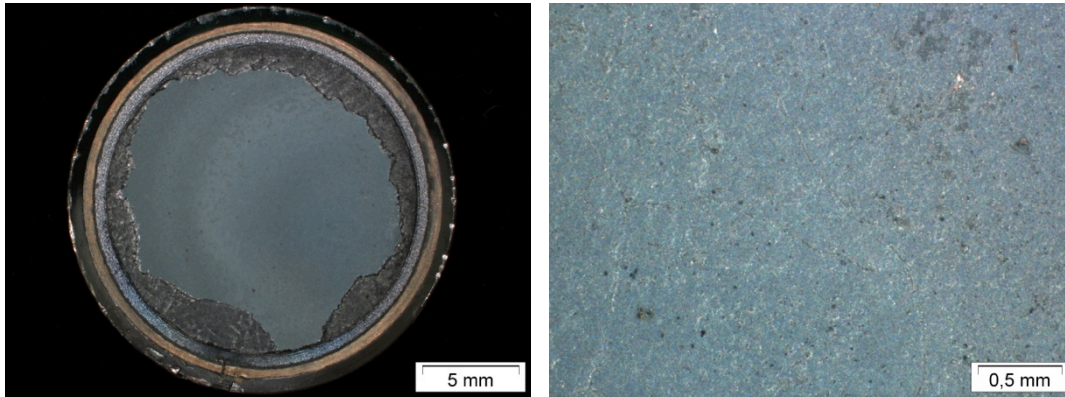


Figure 138: Stereomicroscope pictures of alloy P5 exposed to Gas 1 at 600°C for 1000h in a dual atmosphere condition on the water vapor side. The sample exhibits porous gray scale.

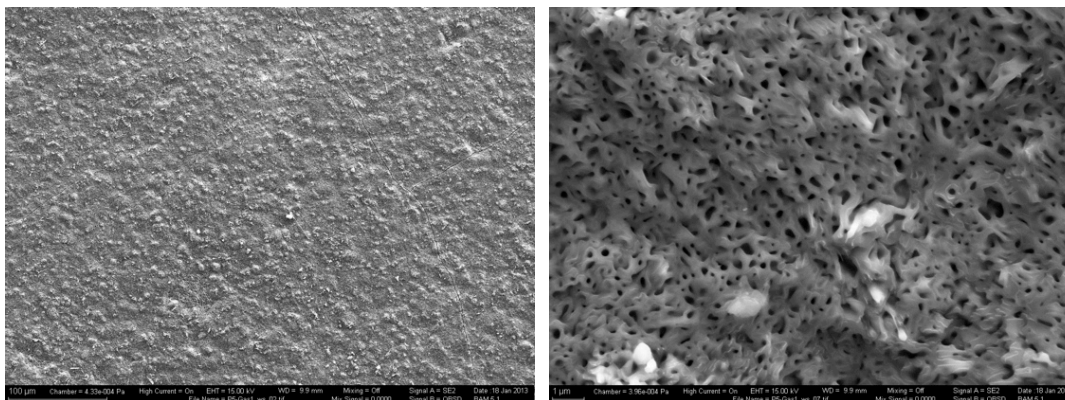


Figure 139: SEM (SE) pictures of alloy P5 exposed to Gas 1 at 600°C for 1000h in a dual atmosphere condition on the water vapor side. An extremely porous oxide forms the outer scale.

Well-defined internal and external scale are seen in the light microscope pictures of this sample. Where porosity and cracks are present, the external layer presents the same bright color as the layer in contact with steam. Internal corrosion is also present (Figure 140).

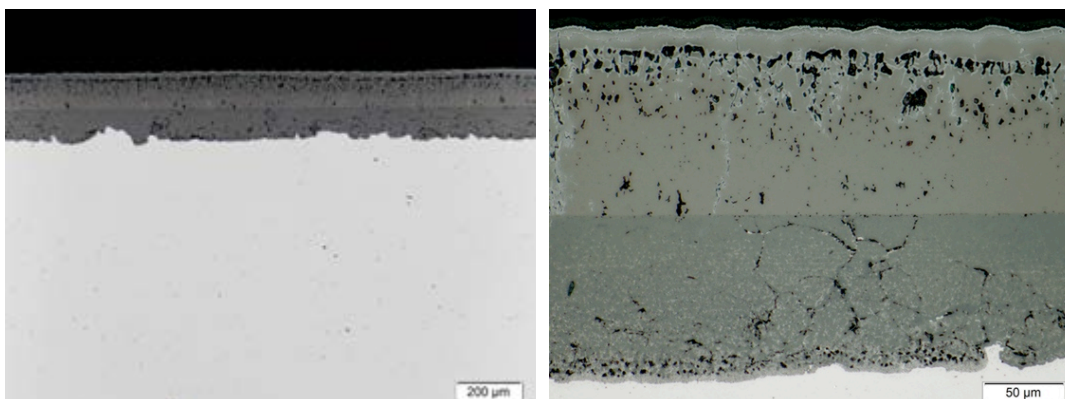


Figure 140: Light microscope pictures of alloy P5 exposed to Gas 1 at 600°C for 1000h in a dual atmosphere condition on the water vapor side. Well-defined external and internal scale and internal corrosion.

The external scale is composed of magnetite and the internal scale of Fe/Cr spinel richer in Cr near the metal. The grain boundaries seem to be the preferential path for oxidation (Figure 141 and Figure 142). In Figure 143 Co is seen on the Fe/Cr spinel layer, where Cr is smaller.

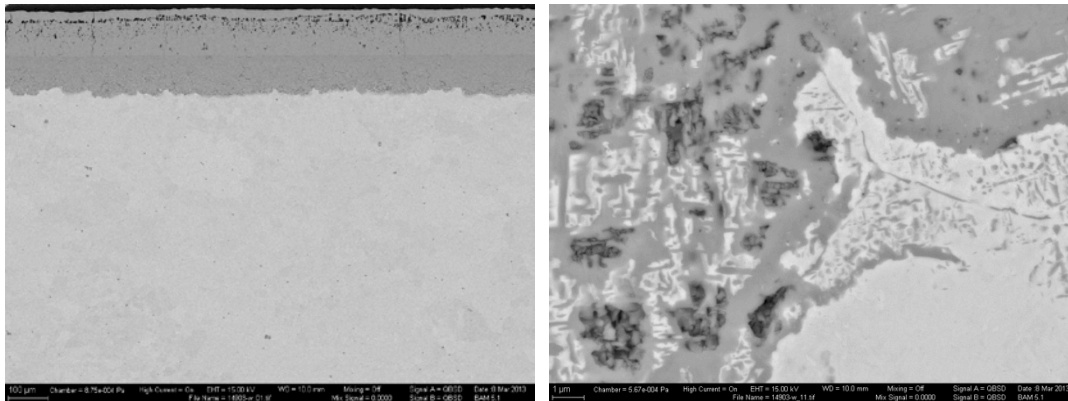


Figure 141: SEM (BSE) pictures of alloy P5 exposed to Gas 1 at 600°C for 1000h in a dual atmosphere condition on the water vapor side. Internal scale shows preferential oxidation of grain boundaries.

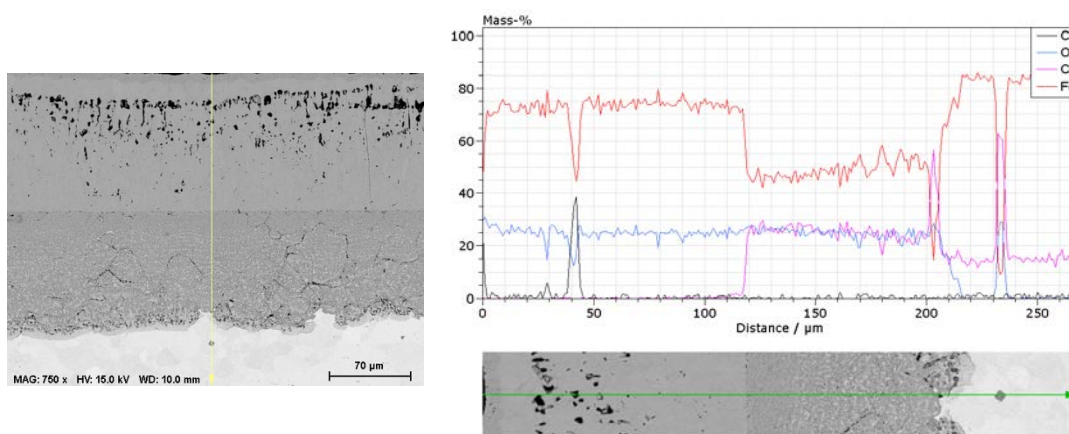


Figure 142: EDS line scan of alloy P5 exposed to Gas 1 at 600°C for 1000h in a dual atmosphere condition on the water vapor side. Magnetite forms the external scale and Cr/Fe spinel the internal. Close to the metal there is an increase in Cr suggesting that Cr_2O_3 might be the phase present.

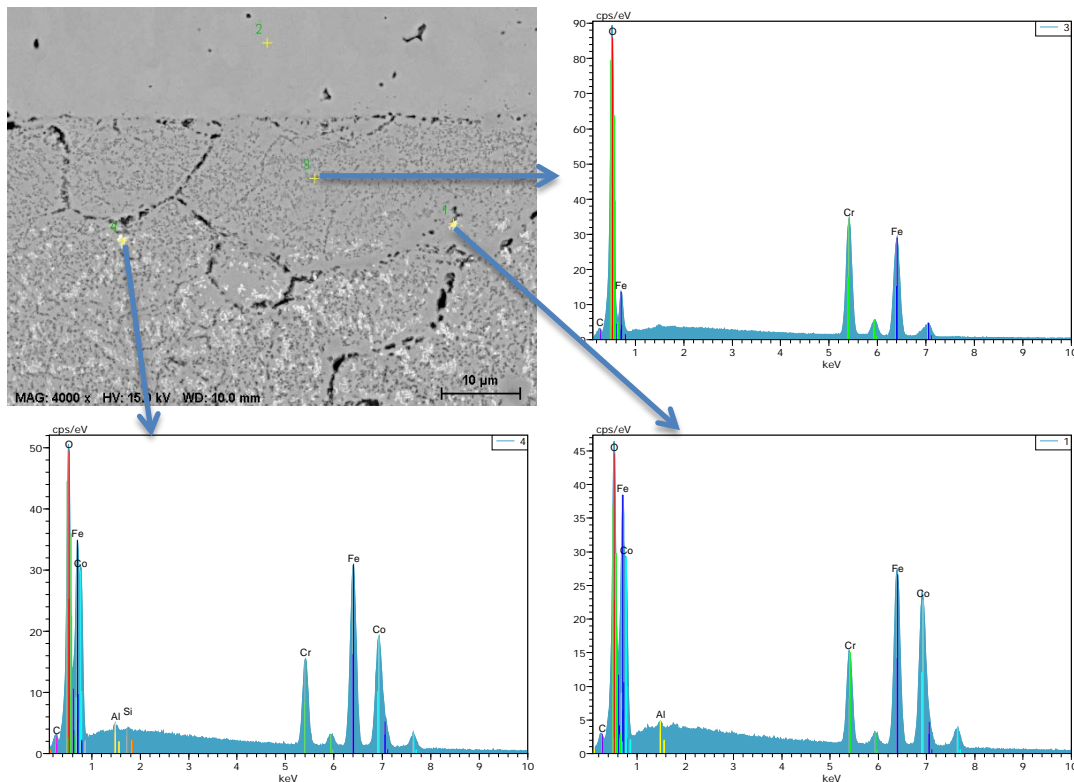


Figure 143: EDS of Alloy P5 exposed to Gas 1 at 600°C for 1000h in a dual atmosphere condition on the water vapor side. (3) Fe/Cr spinel. (1) and (4), Fe/Cr spinel with Co.

4.5.2.2 Gas 3 (70 CO₂ – 1 SO₂ – 29 H₂O)

4.5.2.2.1 Gas side

On the side of Gas 3 in the dual condition experiment, a Cr₂O₃ layer was formed on the surface of Alloy P5 with some iron oxide rich nodules randomly distributed on the surface (Figure 144).



Figure 144: Stereomicroscope and SEM pictures of alloy P5 exposed to Gas 3 at 600°C for 1000h on a dual atmosphere condition on the gas side. Iron rich nodules are observed on the surface.

In Figure 145 and Figure 146 nodules with external scale formed by iron oxides (hematite and magnetite) and internal scale formed by Fe/Cr spinel are shown.

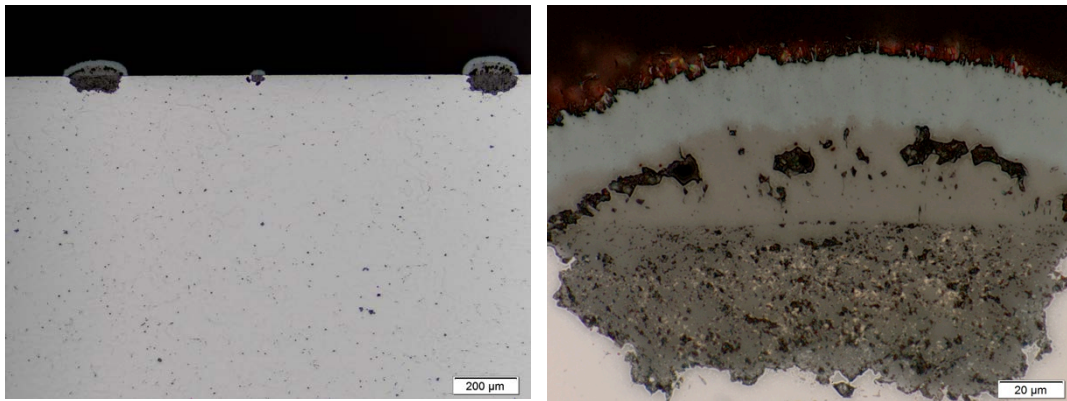


Figure 145: Light microscope pictures of alloy P5 exposed to Gas 3 at 600°C for 1000h in a dual atmosphere condition on the gas side. External scale composed of hematite and magnetite and internal scale composed of spinel.

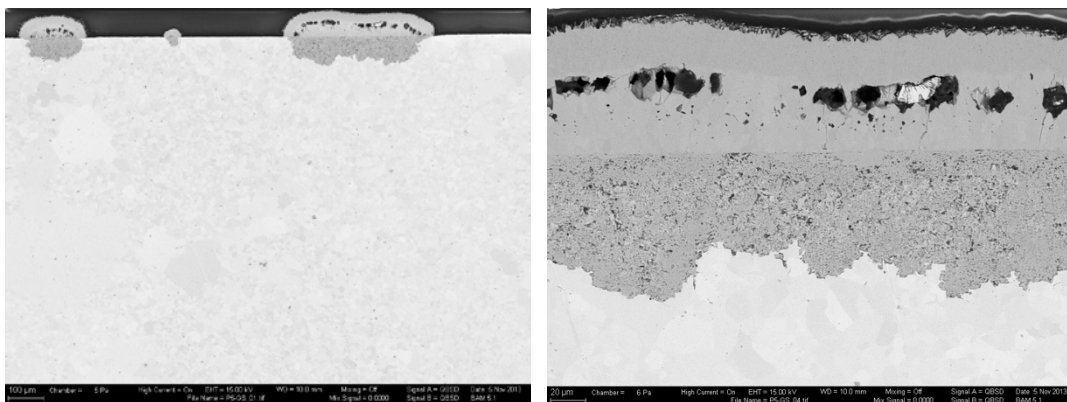


Figure 146: SEM (BSE) pictures of alloy P5 exposed to Gas 3 at 600°C for 1000h in a dual atmosphere condition on the gas side. External scale composed of hematite and magnetite and internal scale composed of spinel.

EDS line scan shows the oxide sequence of hematite, magnetite and spinel. Sulfur was also observed in the spinel layer (Figure 147).

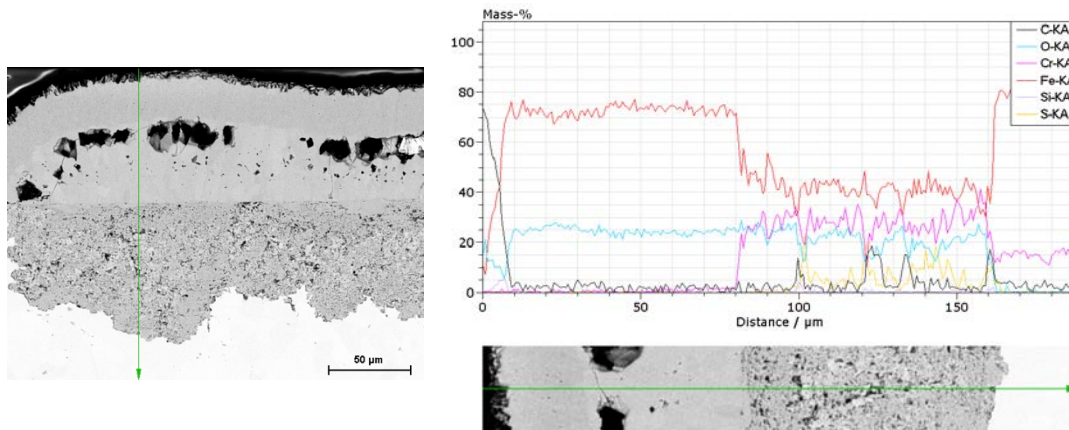


Figure 147: EDS line scan of alloy P5 exposed to Gas 3 at 600°C for 1000h in a dual atmosphere condition on the gas side. External scale composed of hematite and magnetite and internal scale composed of spinel.

4.5.2.2.2 Water Vapor Side

On the water vapor side of Gas 3 in the dual condition experiment, a thick oxide layer was formed on the surface (Figure 148).

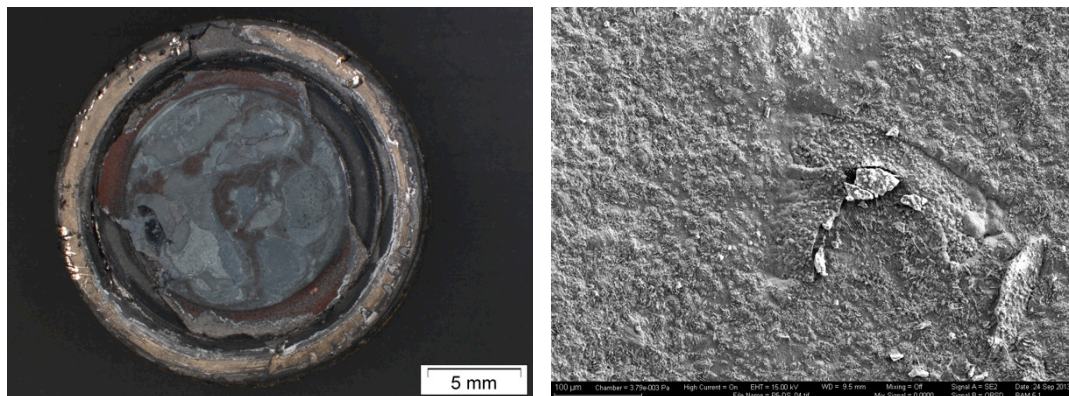


Figure 148: Stereomicroscope and SEM pictures of alloy P5 exposed to Gas 3 at 600°C for 1000h in a dual atmosphere condition on the water vapor side. The sample exhibits different colors and morphologies on the surface.

Scale is formed by an external scale composed of hematite and magnetite and an internal scale composed of spinel and Cr_2O_3 close to the metal surface. Internal oxidation is seen in some parts of the sample (Figure 149, Figure 150 and Figure 151).

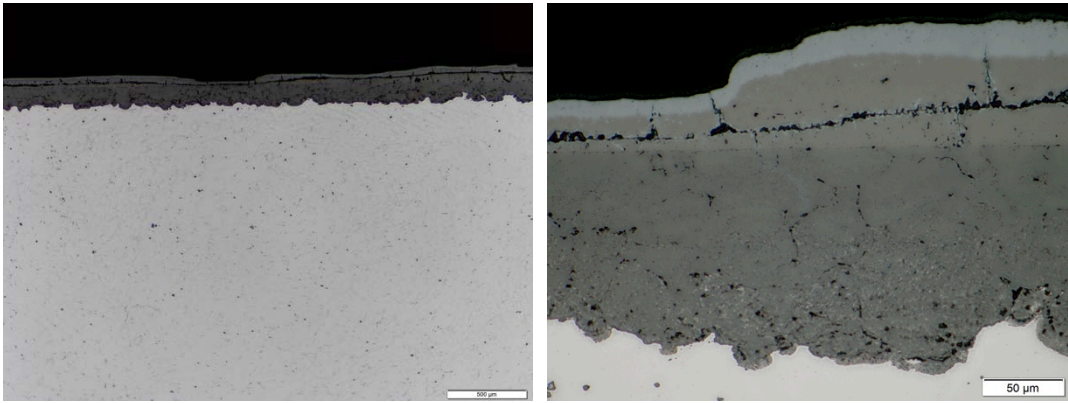


Figure 149: Light microscope pictures of alloy P5 exposed to Gas 3 at 600°C for 1000h in a dual atmosphere condition on the water vapor side. Hematite (top layer) and magnetite can be identified in the external scale. In the cracks and holes in the magnetite layer hematite is present due to the higher O_2 partial pressure in these places.

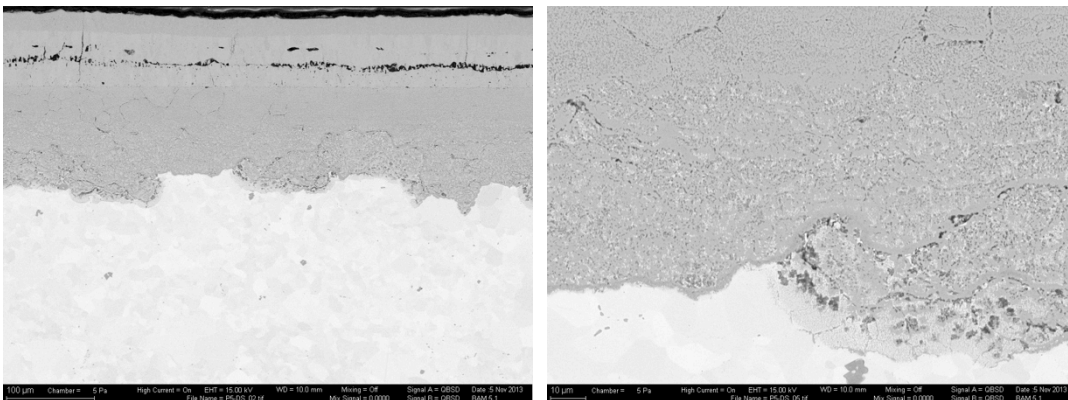


Figure 150: SEM (BSE) pictures of alloy P5 exposed to Gas 3 at 600°C for 1000h in a dual atmosphere condition in the water vapor side. Hematite (top layer) and magnetite can be identified in the external scale. Internal scale composed of Fe/Cr spinel internal oxidation in specific parts.

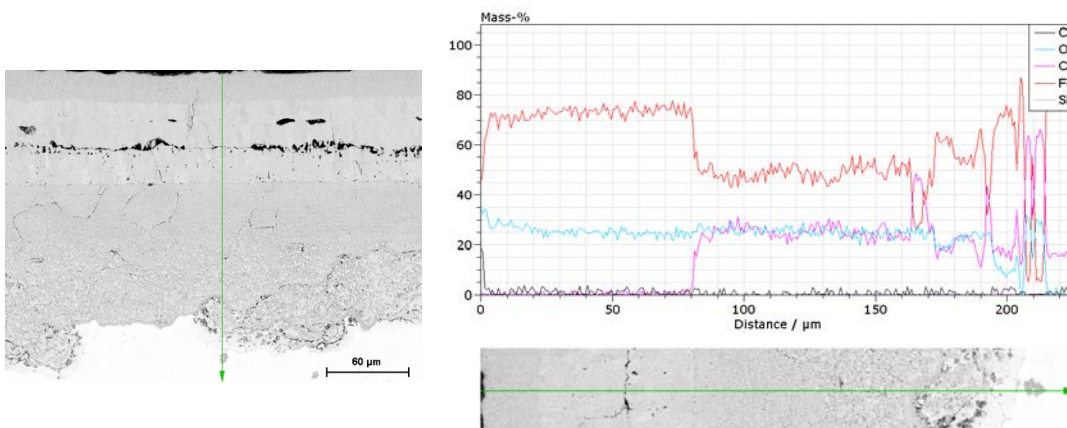


Figure 151: EDS line scan pictures of alloy P5 exposed to Gas 3 at 600°C for 1000h in a dual atmosphere condition on the water vapor side. Hematite (top layer) and magnetite can be identified on the external scale. Internal scale composed of Fe/Cr spinel.

4.6 VM12

Martensitic commercial steel VM12 was exposed to gases 1, 2 and 3 in single atmosphere condition, and to gases 1 and 3 in dual atmosphere condition.

In single condition, a thin protective Cr_2O_3 layer covers all samples with the growth of few nodules of different compositions in Gas 1. In gases 2 and 3, larger and more numerous nodules formed on the surface. These nodules were rich in Fe.

In dual condition, VM12 oxidized more than in single condition, forming a continuous scale rich in Fe on the gas side. In the water vapor side, VM12 exhibited compact scale formed by spinel in the inner part and Fe oxides in the outer part. These alloys had the lowest corrosion rate on the steam side when compared to the other alloys. The water vapor side scale presented less porosity than the gas side scale

4.6.1 Single Atmosphere Condition

4.6.1.1 Gas 1 (70 CO_2 – 1 SO_2 – 29 Ar)

In Gas 1, a thin layer of Cr_2O_3 and some nodules were formed on the surface of VM12. The scratches from sample preparation can be seen on the surface, an evidence of the slight thickness of the scale (Figure 152, Figure 153 and Figure 154).

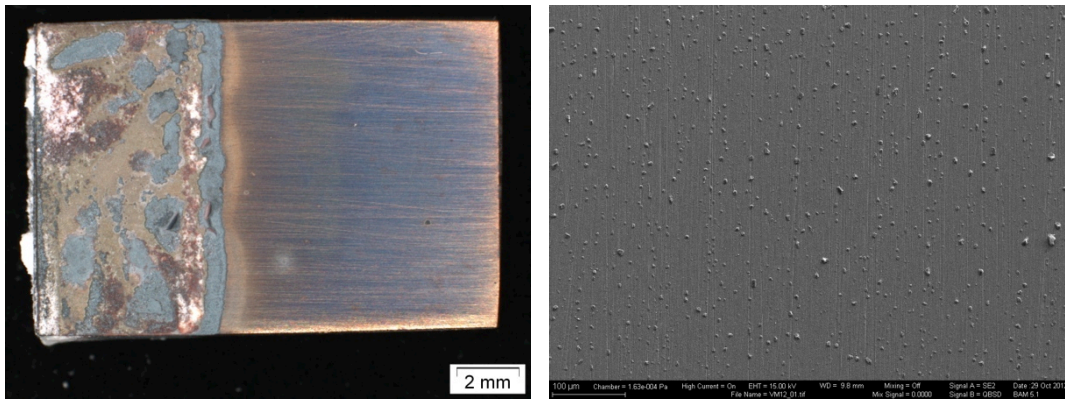


Figure 152: Stereomicroscope and SEM (SE) pictures of VM12 exposed to Gas 1 at 600°C for 1000h in a single atmosphere. Sample exhibits different colors and morphologies on the surface.

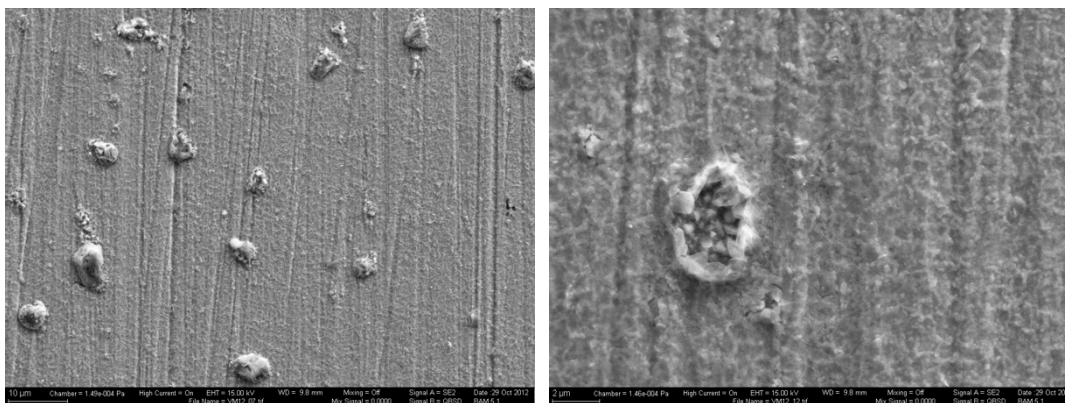


Figure 153: SEM (BSE) pictures of VM12 exposed to Gas 1 at 600°C for 1000h in a single atmosphere condition. Thin scale with the presence of some nodules.

Analysis of an iron oxide-rich nodule shows that a thin layer of partially crystallized amorphous Si oxide is formed between the internal and external scale as shown in Figure 154 and Figure 155.

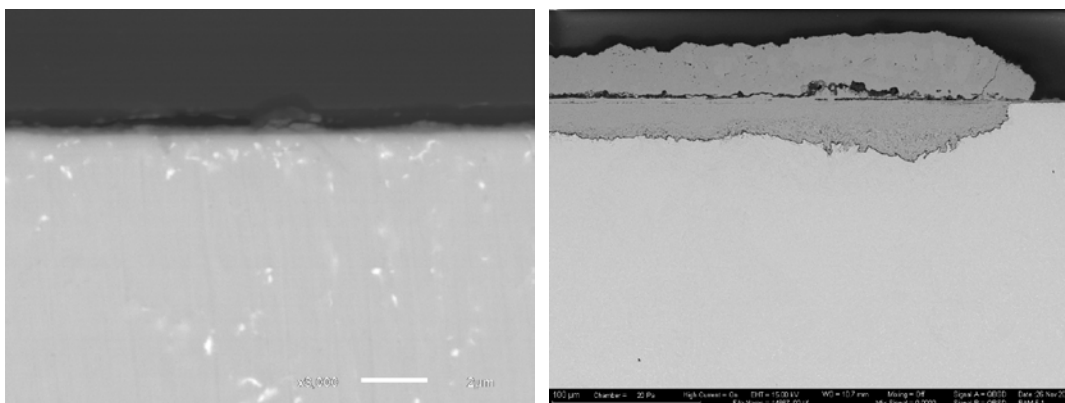


Figure 154: SEM (BSE) pictures of alloy VM12 exposed to Gas 1 at 600°C for 1000h in single atmosphere condition. Large areas with a thin protective oxide layer and some big Fe-rich nodules were observed.

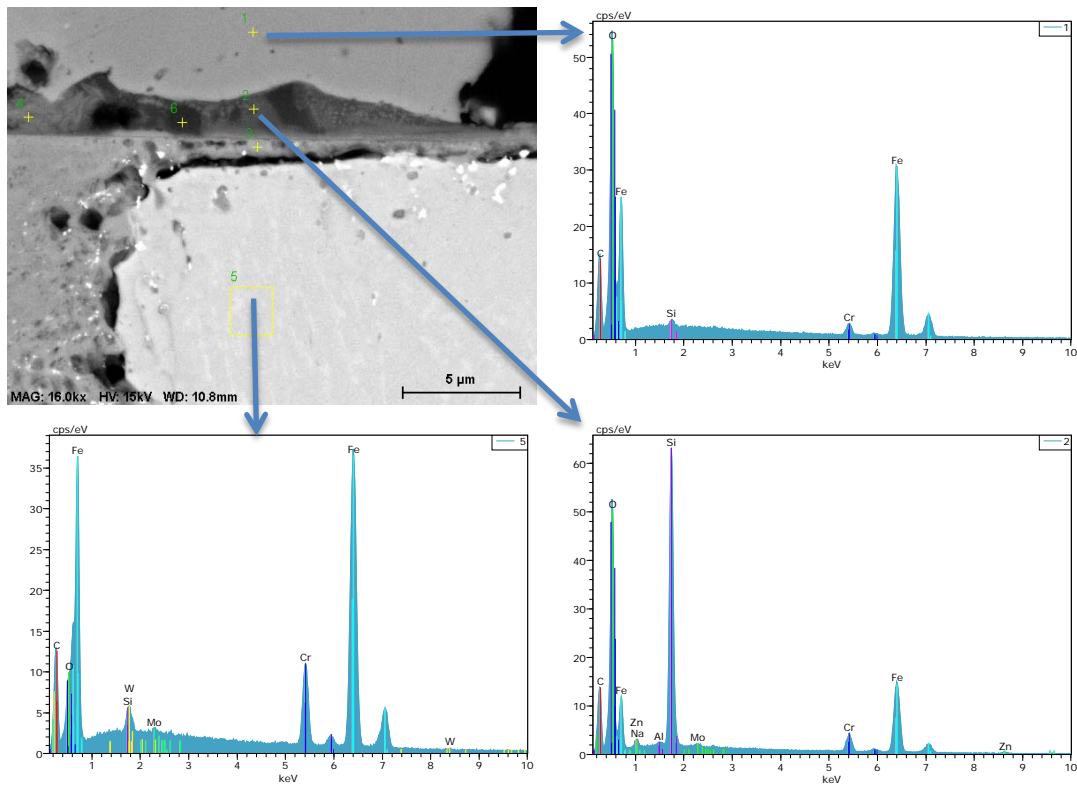


Figure 155: EDS of VM12 exposed to Gas 1 at 600°C for 1000h in a single atmosphere condition. (1) Iron oxide, (5) base metal and (2) amorphous Si oxide.

External scale is composed of hematite and magnetite. Internal scale is composed of spinel with higher chromium concentration close to the metal (Figure 156).

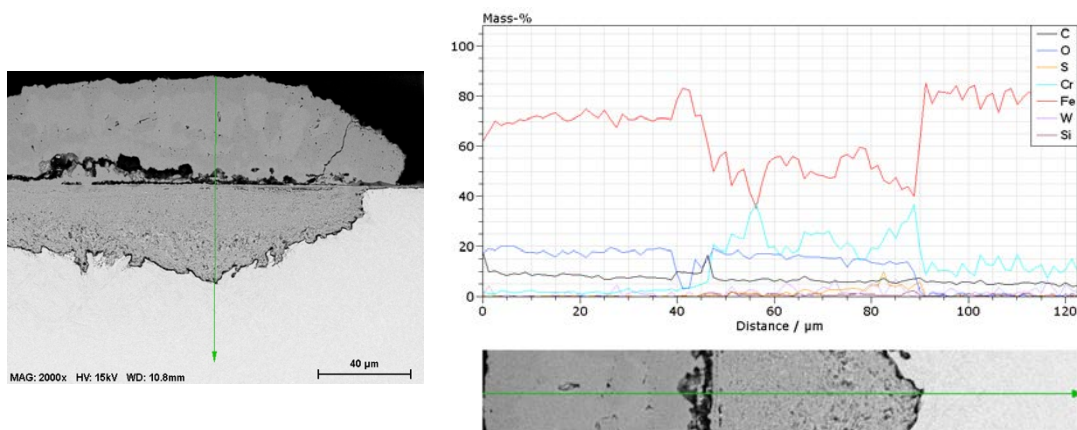


Figure 156: EDS line scan of VM12 exposed to Gas 1 at 600°C for 1000h in a single atmosphere condition.

4.6.1.2 Gas 2 (70 CO₂ – 1 SO₂ – 29 Ar)

In Gas 2, iron oxide-rich nodules were formed on VM12 surface and in a significant part of the sample, nodule coalescence developed a thick scale. Hematite whiskers were formed on the top the nodules (Figure 157).

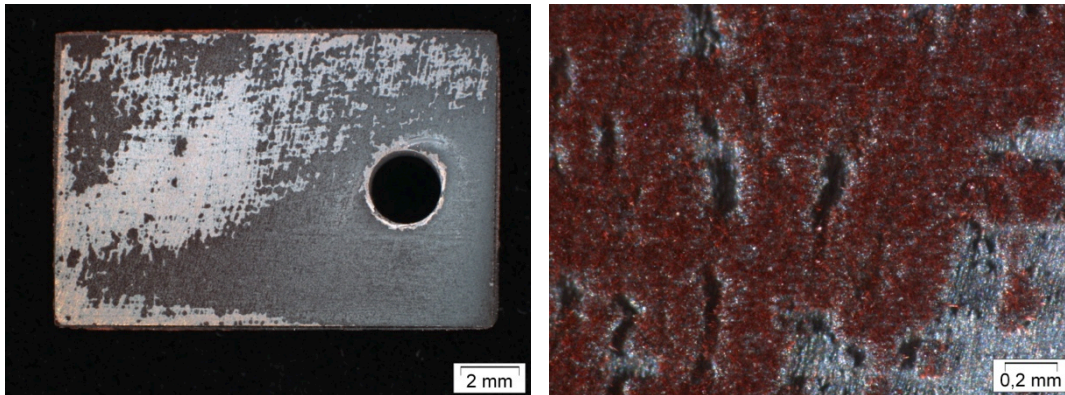


Figure 157: Stereomicroscope pictures of VM12 exposed to Gas 2 at 600°C for 1000h in a single condition. The sample exhibits high density of nodules with hematite whiskers on the top of them.

Blade-like whiskers formed on the surface of the nodules. A continuous scale was formed due to the coalescence of the nodules. The scale is very porous as seen in Figure 158.

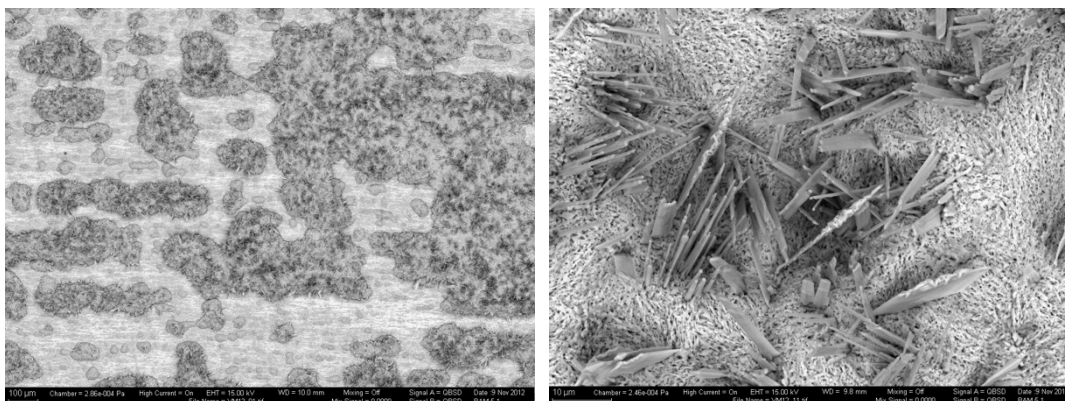


Figure 158: SEM (BSE) pictures of VM12 exposed to Gas 2 at 600°C for 1000h in a single condition. Development and coalescence of nodules producing a porous scale with blade-like whiskers.

EDS analysis of the surface of the porous scale and whiskers shows they are composed of iron oxide only (Figure 159).

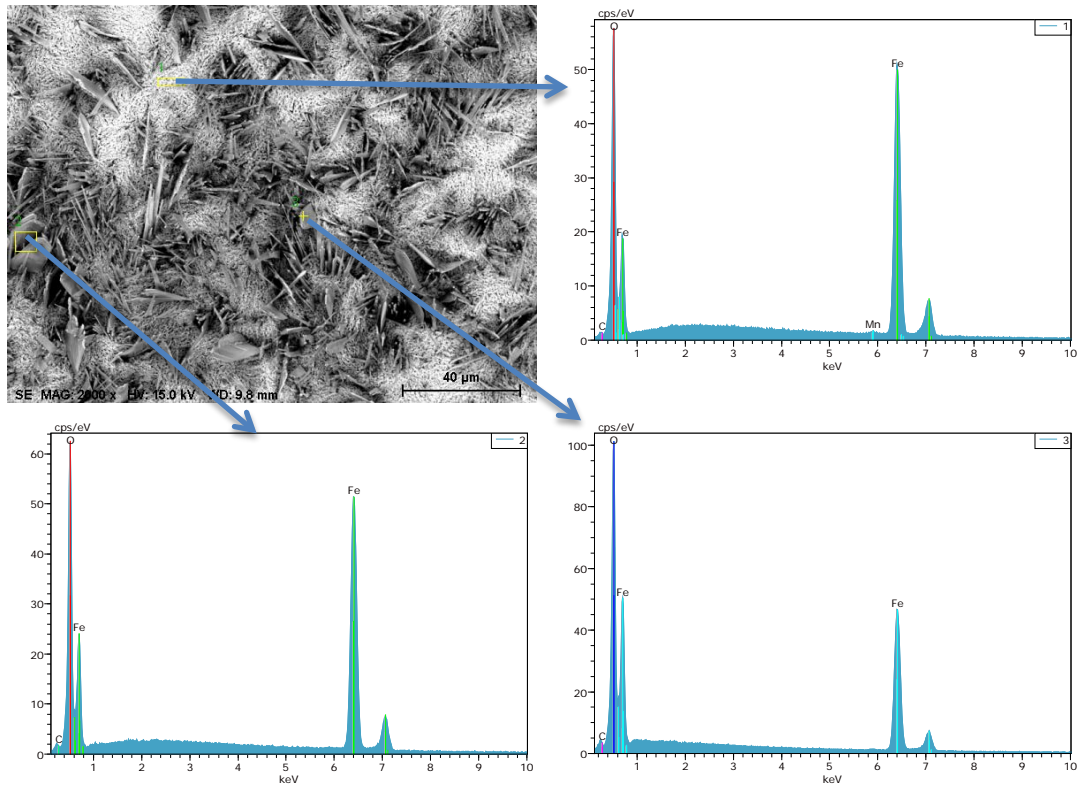


Figure 159: EDS of VM12 exposed to Gas 2 at 600°C for 1000h in a single atmosphere condition showing it is composed of iron oxides only.

Figure 160 shows the formation of a thick scale with large cavities in magnetite layer. The subscale region shows no ferrite growth and it is slightly enriched in C as shown in EDS (Figure 161).

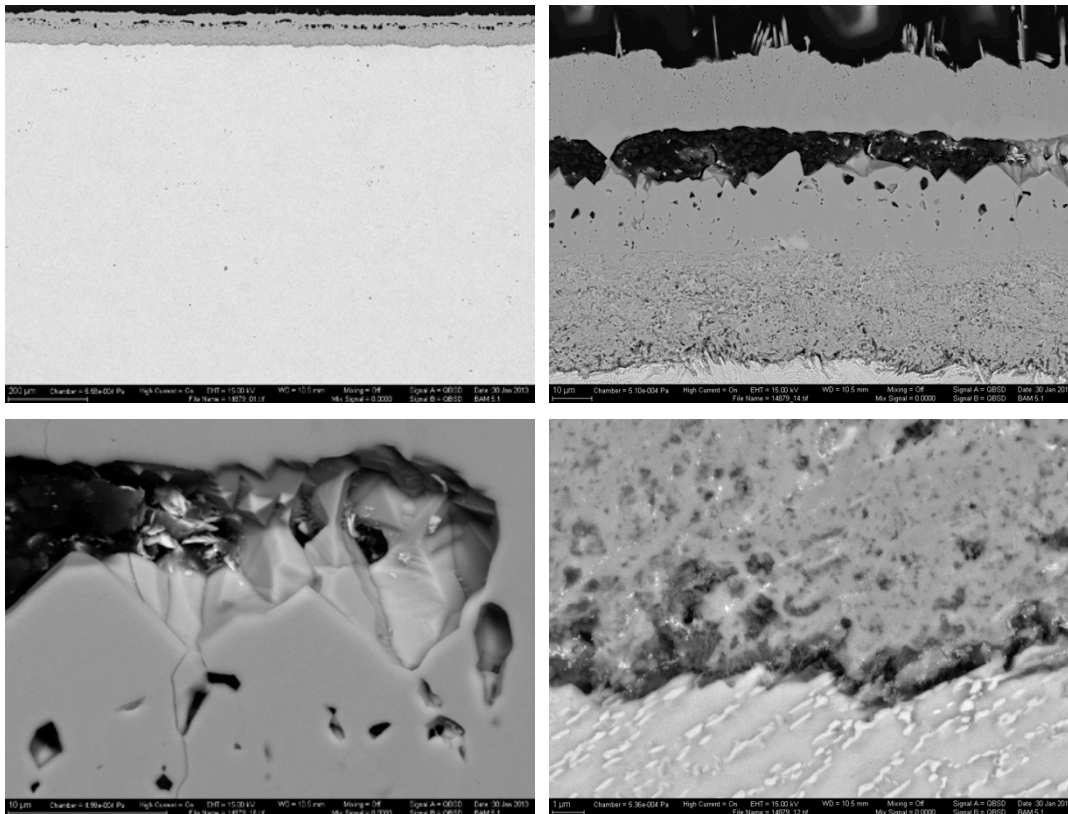


Figure 160: SEM (BSE) pictures of alloy VM12 exposed to Gas 2 at 600°C for 1000h in a single atmosphere condition showing cavities in the external scale in the magnetite layer and the porosity in the metal/scale interface.

EDS line scan shows that the scale is composed of hematite, magnetite and Fe/Cr spinel. S is present only in the spinel layer (Figure 161).

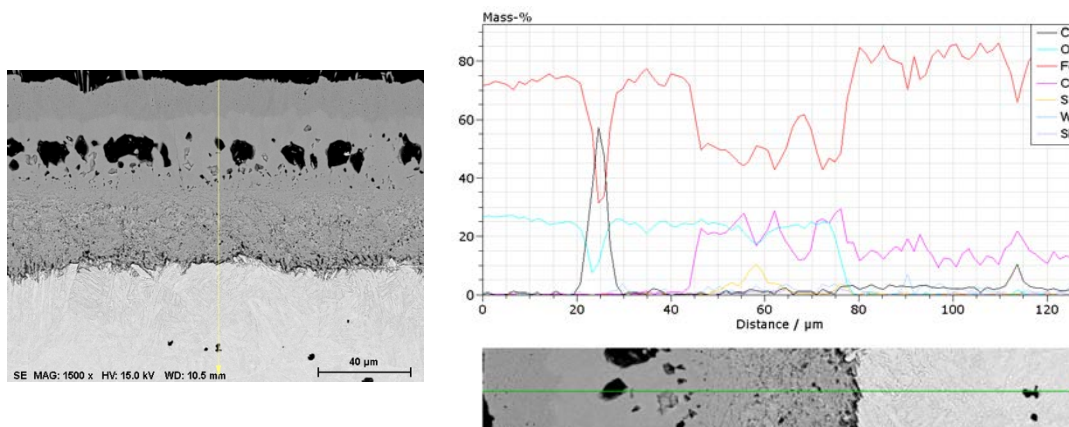


Figure 161: EDS line scan of alloy VM12 exposed to Gas 2 at 600°C for 1000h in a single atmosphere condition showing sequence of hematite, magnetite and Fe/Cr spinel from the gas side to the metal.

4.6.1.3 Gas 3 (70 CO₂ – 1 SO₂ – 29 H₂O)

In Gas 3, iron oxide rich nodules were formed on the surface of VM12 in some parts of the sample, but at a lower density than Gas 2. Hematite whiskers were formed on the top the nodules (Figure 162).

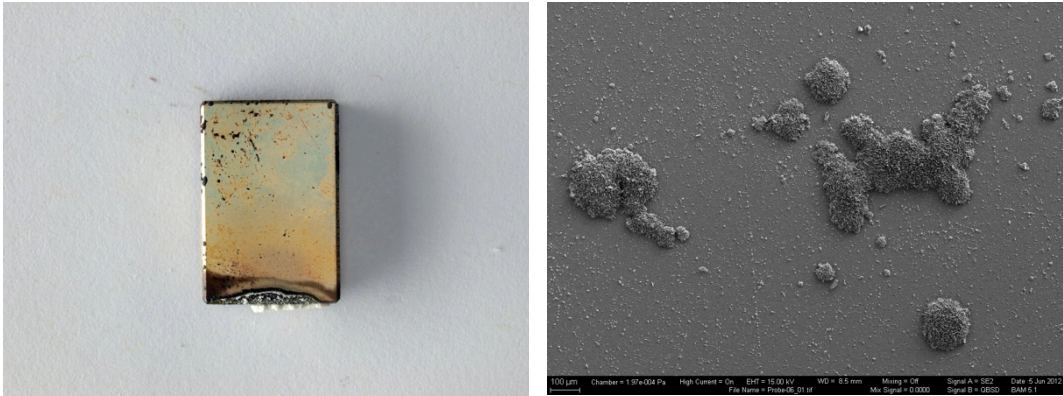


Figure 162: Stereomicroscope and SEM pictures of VM12 exposed to Gas 3 at 600°C for 1000h in a single atmosphere condition. The sample exhibits nodules on the surface and coalescence of some of them.

EDS analysis of a nodule shows that it is composed of iron oxides and surrounded by small iron oxide nodules (Figure 163). The nodules are composed of an external scale of iron oxides and an internal scale of Cr oxide (Figure 164).

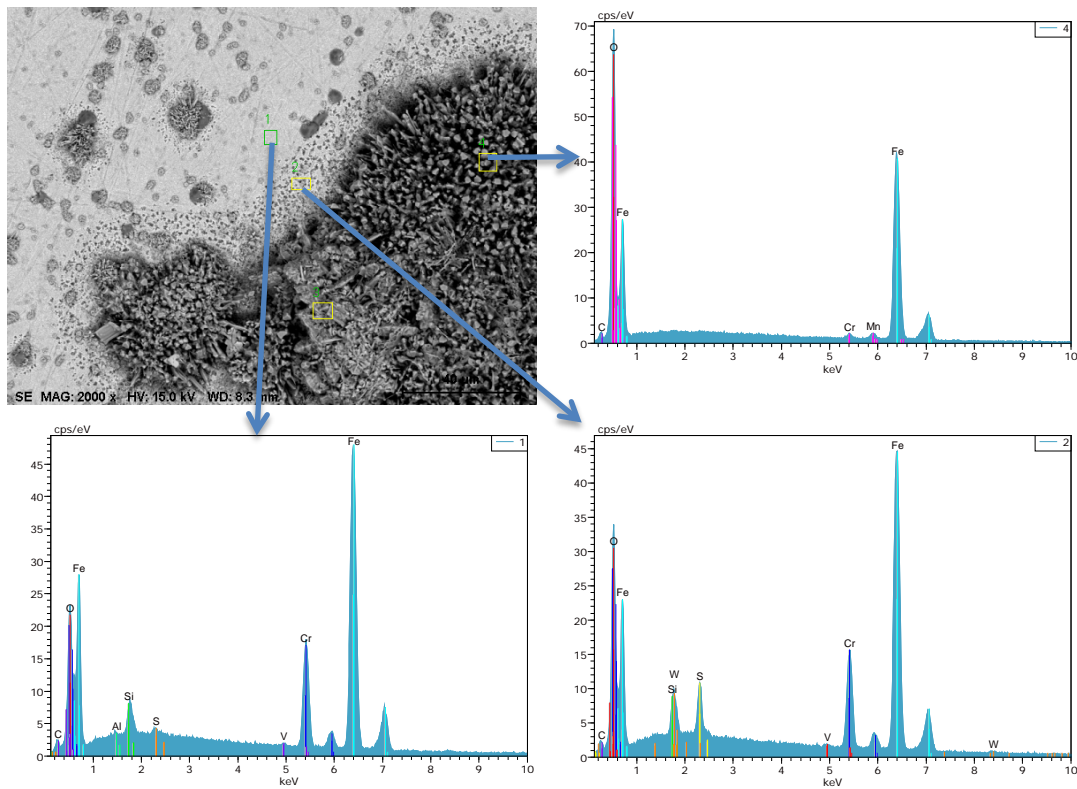


Figure 163: EDS of steel VM12 exposed to Gas 3 at 600°C for 1000h in a single atmosphere condition. (4) Iron oxide, (1) and (2) base metal and some oxidation.

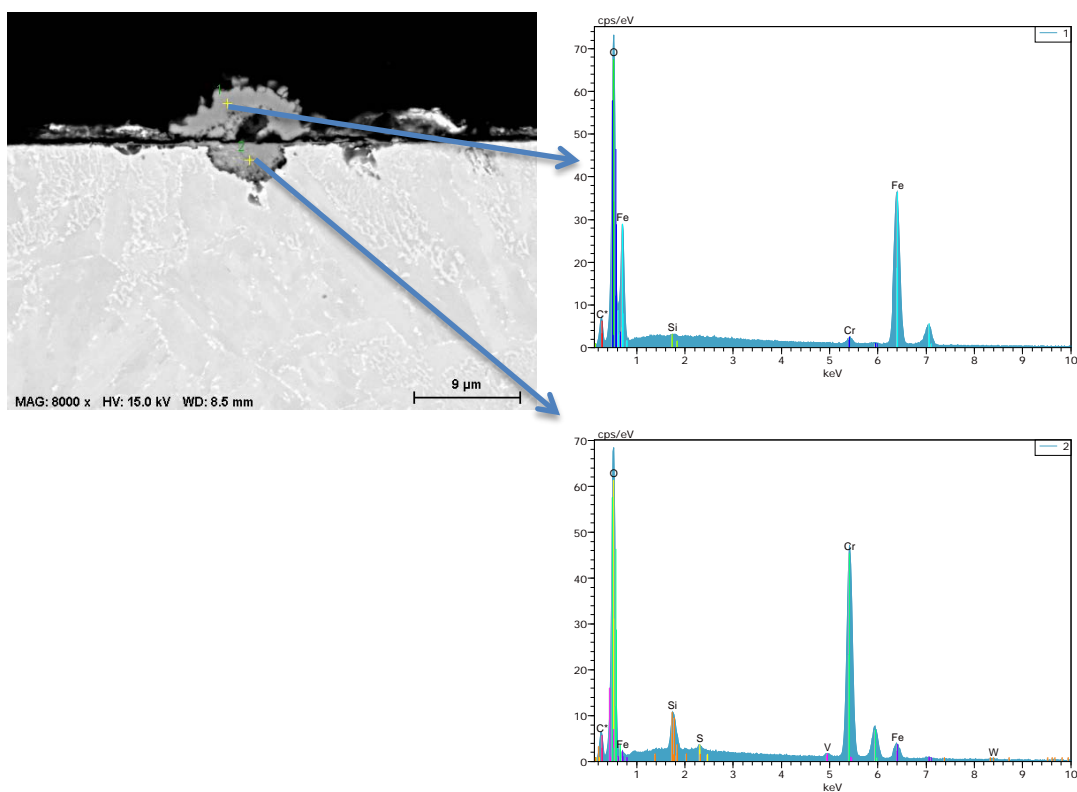


Figure 164: EDS of steel VM12 exposed to Gas 3 at 600°C for 1000h in a single atmosphere condition. The nodules are composed of an external scale of iron oxides and an internal scale of Cr oxide.

4.6.2 Dual Atmosphere Condition

4.6.2.1 Gas 1

4.6.2.1.1 Gas side

VM12 exhibited, on the gas side of steel in dual condition, a Cr_2O_3 layer with nodules rich in Fe. The other part of the sample is composed of a porous layer with whiskers on top. This structure displays the same phase composition as the nodules (Figure 165 and Figure 166).

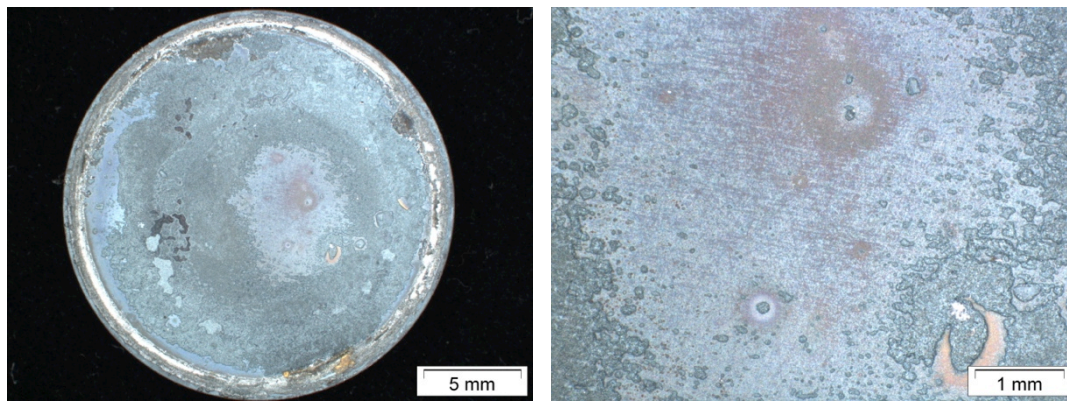


Figure 165: Stereomicroscope pictures of the surface of steel VM12 exposed to Gas 1 at 600°C for 1000h in a dual atmosphere condition on the gas side. The sample was slightly oxidized and the grinding scratches can still be seen. Small nodules were formed on the surface.

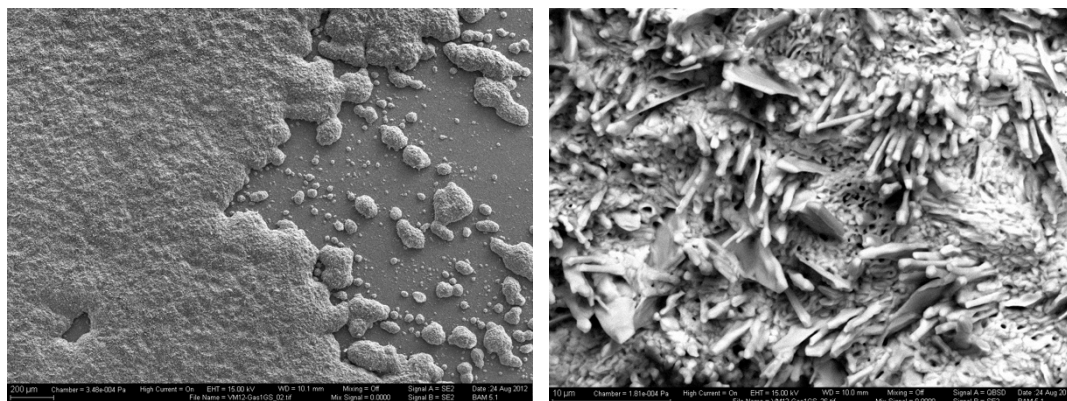


Figure 166: SEM (Left: SE, Right: BSE) pictures of steel VM12 exposed to Gas 1 at 600°C for 1000h in a dual atmosphere condition on the gas side. Thin scale formed by Cr_2O_3 and regions covered by Fe-rich nodules.

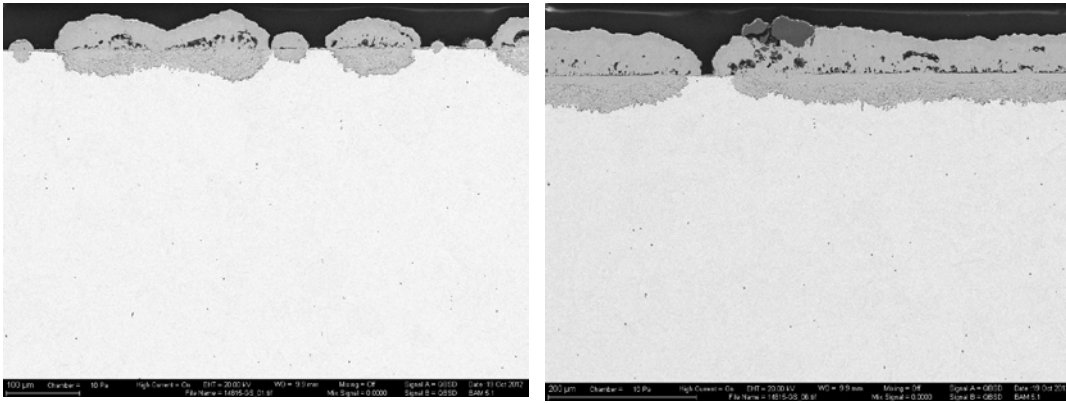


Figure 167: SEM (BSE) pictures of steel VM12 exposed to Gas 1 at 600°C for 1000h in a dual atmosphere condition on the gas side. Nodules are composed of an internal scale composed of spinel and an outer scale composed of iron oxides. On the right figure, the right structure presents Si nodules on the top, which was also observed in other experiments.

EDS analysis shows that sulfur is present in great quantity in the metal close to the scale, indicating that it might have a role in alloy oxidation.

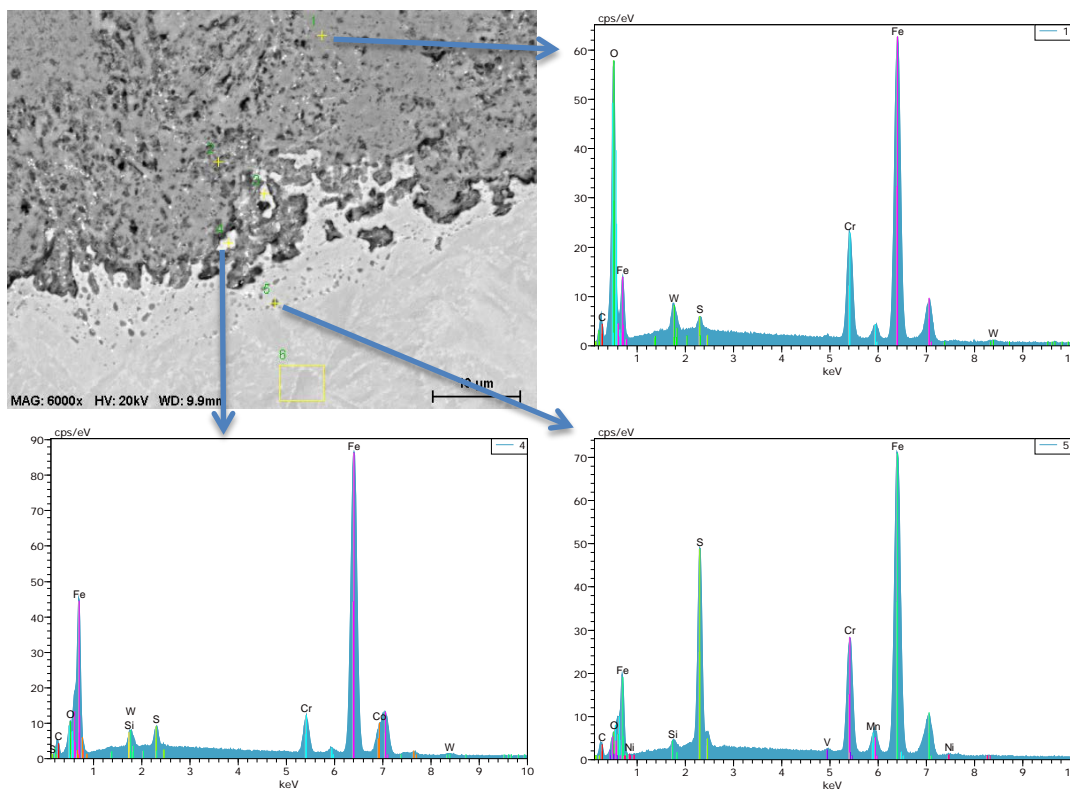


Figure 168: EDS of steel VM12 exposed to Gas 1 at 600°C for 1000h in a dual atmosphere condition on the gas side. Sulfur is present in the metal near the scale and the internal scale is composed of spinel. A cobalt-rich region is also observed.

4.6.2.1.2 Water Vapor Side

On the water vapor side, steel VM12 exposed to a dual condition in Gas 1 exhibited homogeneous corrosion with the development of a thick scale (Figure 169).

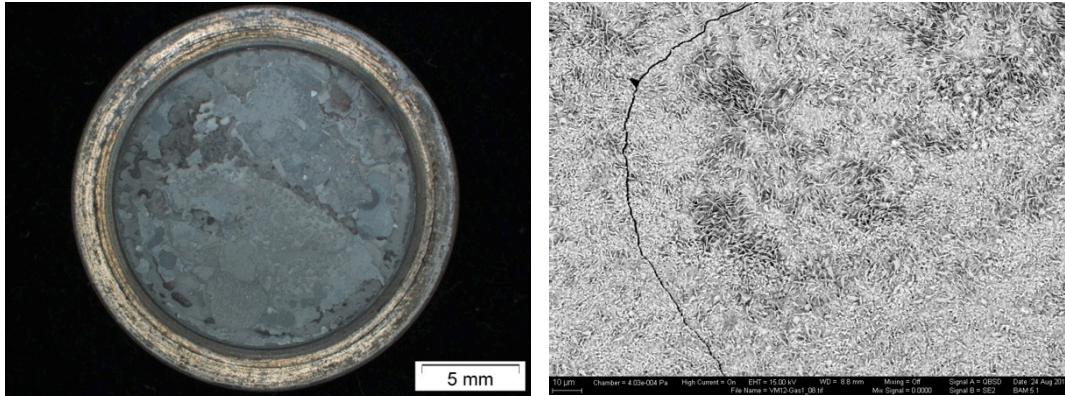


Figure 169: Stereomicroscope and SEM (BSE) pictures of the surface of steel VM12 exposed to Gas 1 at 600°C for 1000h in a dual atmosphere condition on the water vapor side. The sample exhibits homogeneous oxidation with the development of a thick porous oxide.

The external scale formed was thick and with few voids, which is usual in a H₂O oxidation. The internal scale contains a high concentration of Si (Figure 170 and Figure 171).

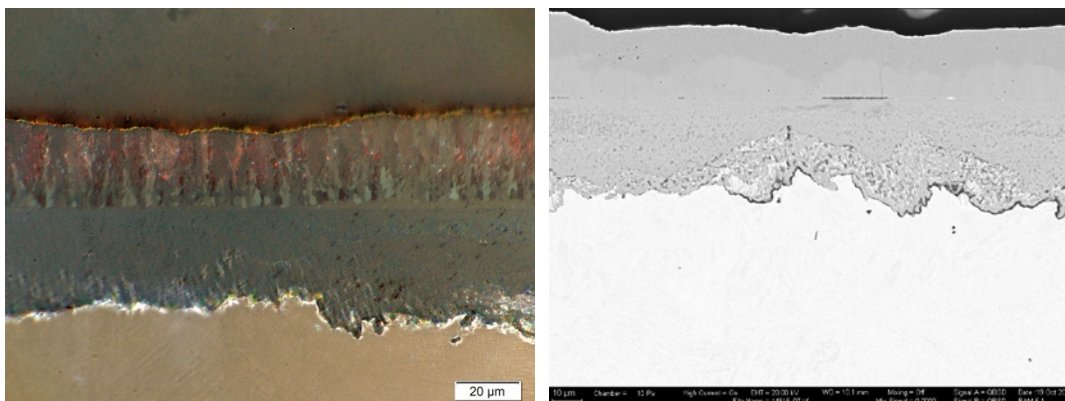


Figure 170: Light microscope and SEM (BSE) pictures of steel VM12 exposed to Gas 1 at 600°C for 1000h in a dual atmosphere condition on the water vapor side. The scale does not have voids in the outer scale and the internal scale is not very porous.

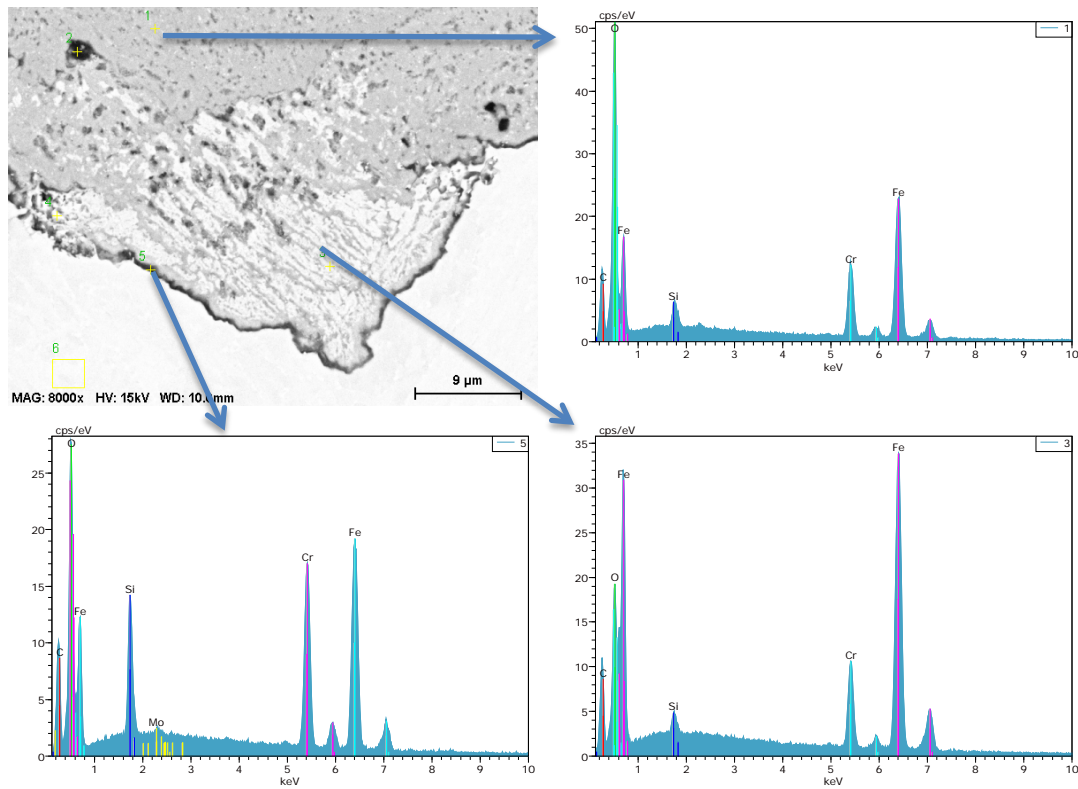


Figure 171: EDS of steel VM12 exposed to Gas 1 at 600°C for 1000h in a dual atmosphere condition on the water vapor side. (1) Spinel. (5) Si oxide. (3) Internal oxidation and a high Si content.

4.6.2.2 Gas 3 (70 CO₂ – 1 SO₂ – 29 H₂O)

4.6.2.2.1 Gas side

On the side of Gas 3, in dual condition experiment, a continuous hematite layer with whiskers covered the entire sample surface as shown in the stereo pictures in Figure 172.

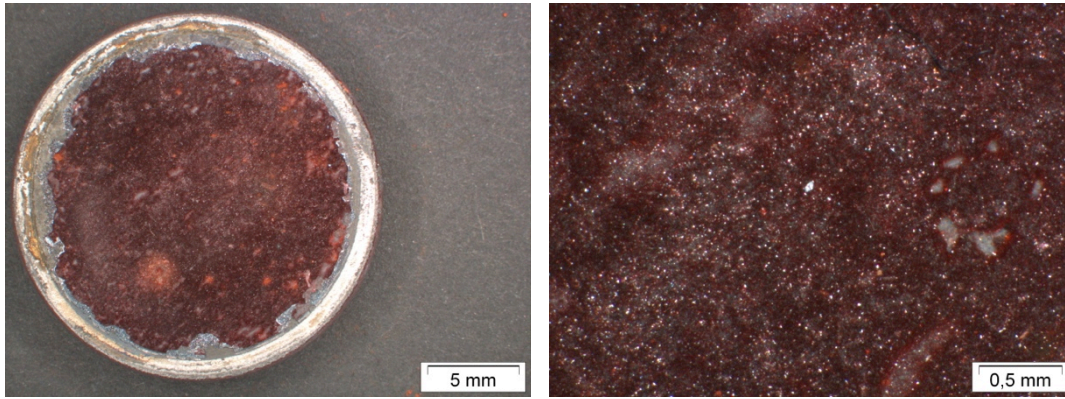


Figure 172: Stereomicroscope pictures of surface steel VM12 exposed to Gas 3 at 600°C for 1000h in a dual atmosphere condition on the gas side. Surface composed of hematite layer with whiskers.

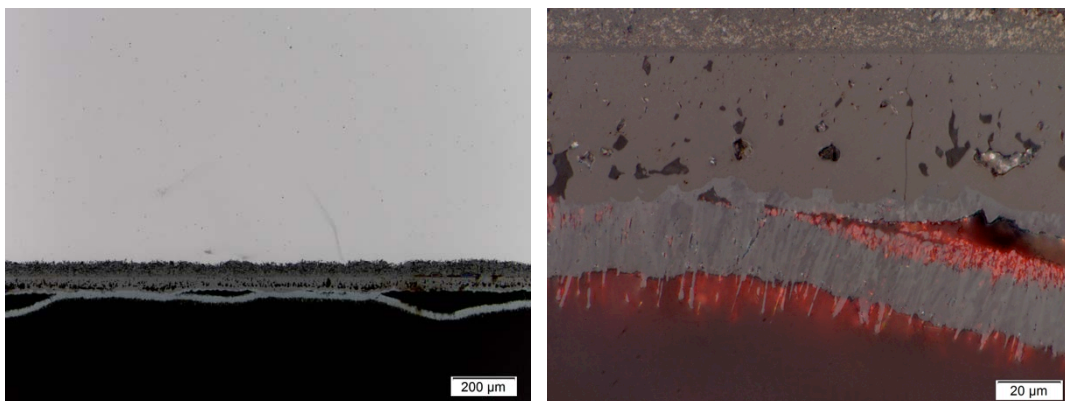


Figure 173: Light microscope pictures of steel VM12 exposed to Gas 3 at 600°C for 1000h in a dual atmosphere condition on the gas side. External scale composed of hematite and magnetite and internal scale composed of spinel.

Figure 173 on the right shows a broken layer made of columnar grains and whiskers on the top. The red color on the top and inside the columnar indicates that it is hematite. Figure 174 shows the columnar hematite layer with whiskers and the internal scale composed of spinel.

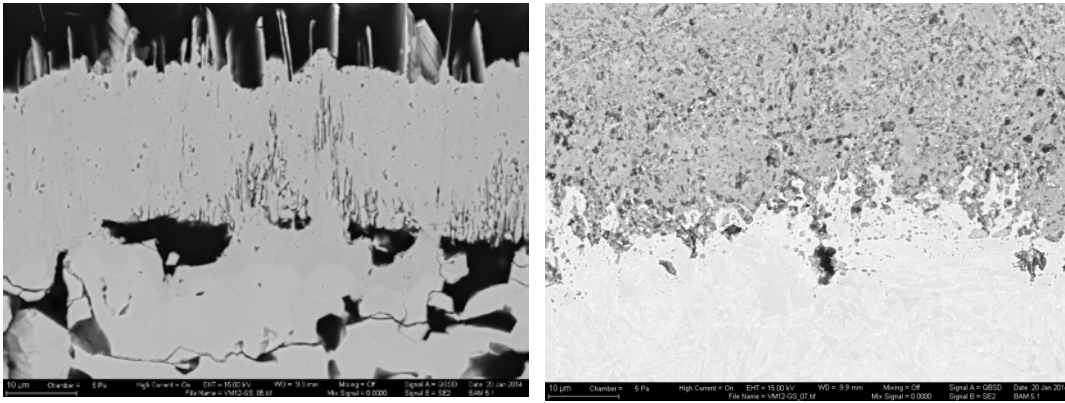


Figure 174: SEM (BSE) pictures of steel VM12 exposed to Gas 3 at 600°C for 1000h in a dual atmosphere condition on the gas side. External scale composed of hematite and magnetite (left) and internal scale composed of spinel (right).

EDS analysis (Figure 175) of the sample confirms that the external layers are composed of iron oxides and the internal layer of Fe/Cr spinel. S and Si are present in the spinel layer.

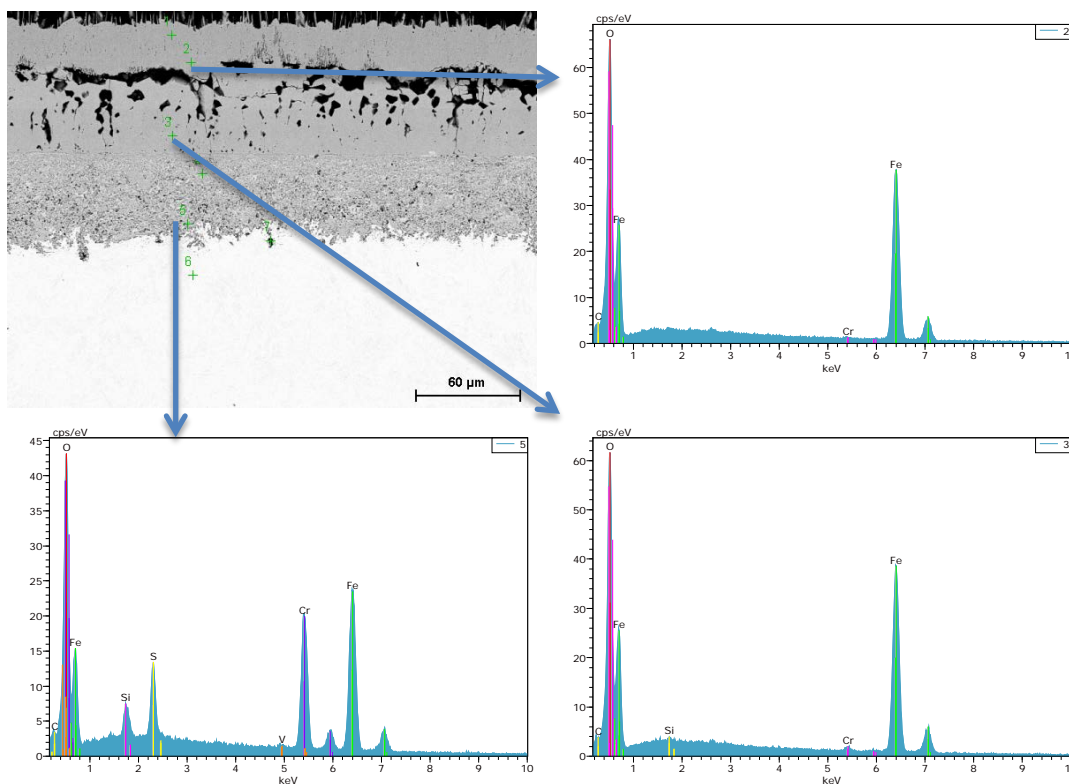


Figure 175: EDS of steel VM12 exposed to Gas 3 at 600°C for 1000h in a dual atmosphere condition on the gas side. (2) and (3) iron oxide. (5) Cr/Fe spinel with S and Si.

4.6.2.2.2 Water Vapor Side

On the water vapor side of Gas 3 in the dual condition experiment, a thick layer with few pores was formed (Figure 176).

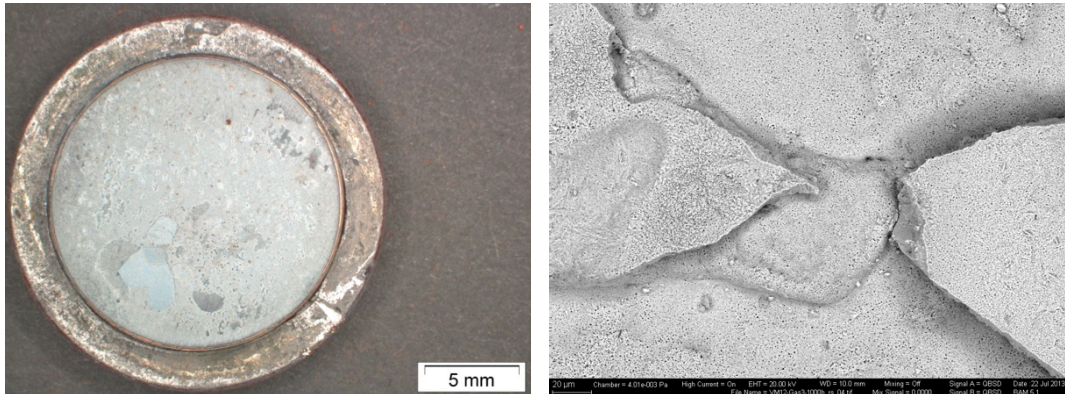


Figure 176: Stereomicroscope and SEM (BSE) pictures of steel VM12 exposed to Gas 3 at 600°C for 1000h in a dual atmosphere condition on the water vapor side. The sample exhibits porous scale with spallation.

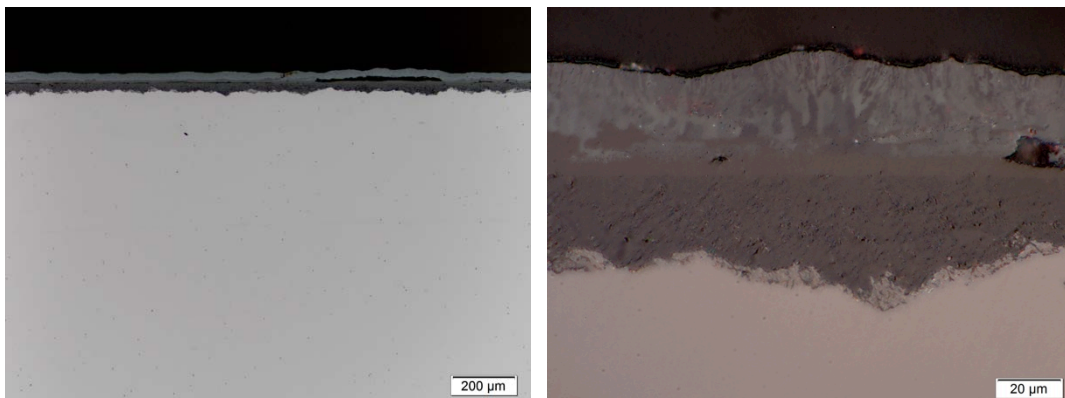


Figure 177: Light microscope pictures of steel VM12 exposed to Gas 3 at 600°C for 1000h in dual atmosphere condition on the water vapor side. External scale composed of hematite and magnetite and internal scale composed of spinel. The hematite columnar layer can be seen in the right picture as well as the internal oxidation.

The columnar structure of the most external layer and internal oxidation of the alloy are observed in Figure 177 and Figure 178.

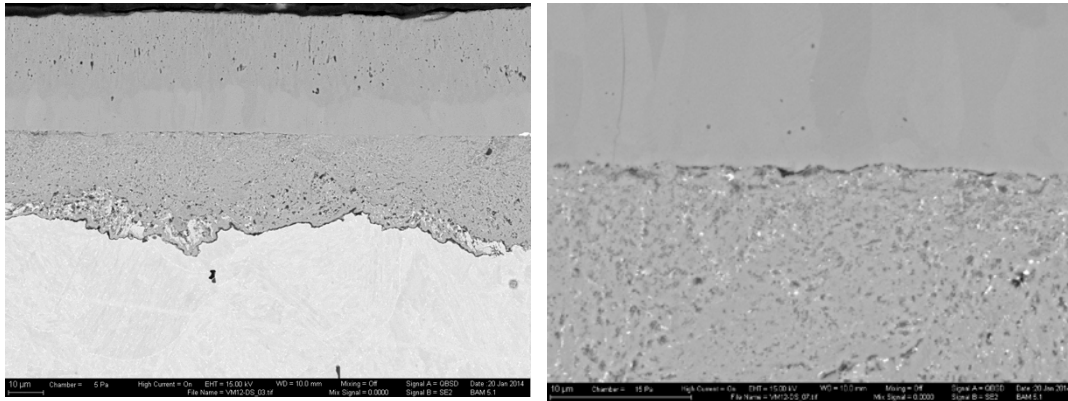


Figure 178: SEM (BSE) pictures of steel VM12 exposed to Gas 3 at 600°C for 1000h in dual atmosphere condition on the water vapor side. External scale composed of hematite and magnetite and internal scale composed of spinel.

4.7 RFe12

RFe12 is iron with at least 98% purity, and exposed to gases 1, 2 and 3 in a single atmosphere condition. In all conditions, scale is composed of hematite and magnetite.

Increase in the water content increases porosity and whisker density on the surface as expected, and no carburization was found.

4.7.1 Single Atmosphere Condition

4.7.1.1 Gas 1

In Gas 1, RFe12 has shown dense scale composed of iron oxides. Spallation was found in the scale, but it was also damaged by removal from the furnace (Figure 179).

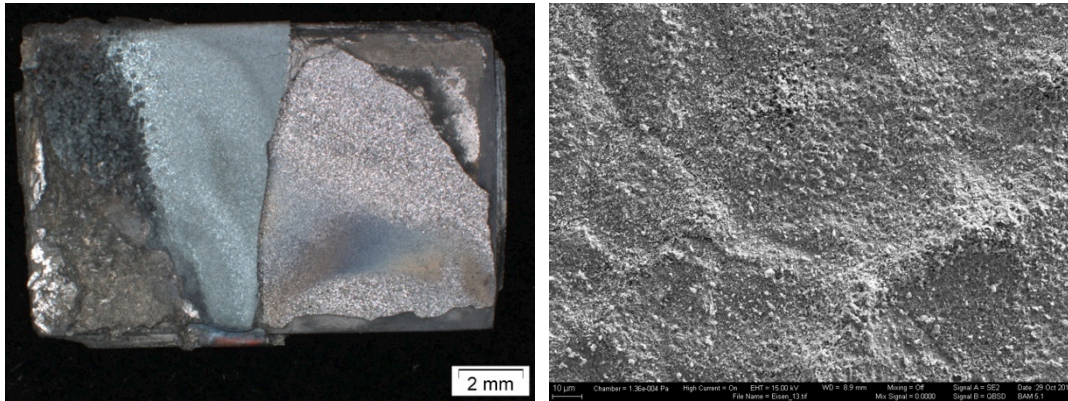


Figure 179: Stereomicroscope and SEM (SE) pictures of the surface of RFe12 exposed to Gas 1 at 600°C for 1000h in a single condition. In the stereo picture (left) it can be seen that the surface of the sample was damaged. On the right, the surface SEM picture of the scale.

A thick scale was formed and the cross section of a part without spallation or damage is shown in Figure 180. No whiskers were observed on the surface.

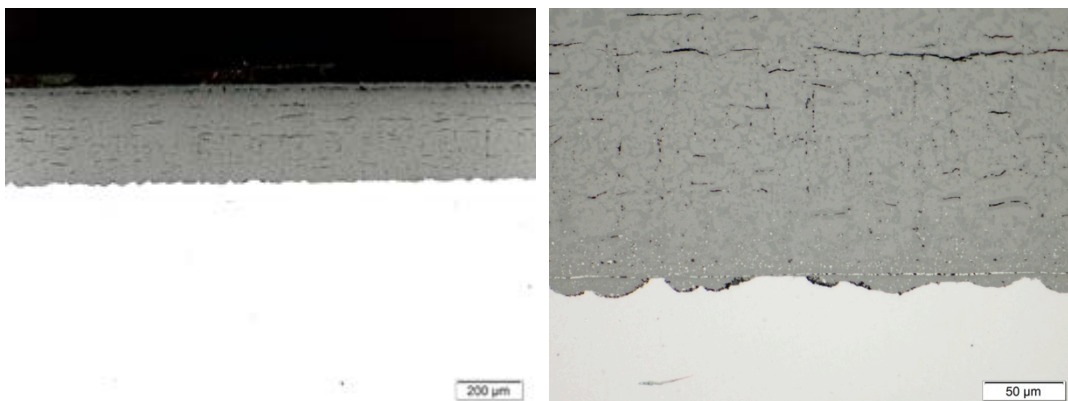


Figure 180: Light microscope pictures of RFe12 exposed to Gas 1 at 600°C for 1000h in a single condition. Thick scale was formed with the presence of cracks and few voids

4.7.1.2 Gas 2 (70 CO₂ – 1 SO₂ – 29 Ar)

The sample oxidized in Gas 2 displays higher concentration of hematite (red color on the left picture of Figure 181) at the bottom than close to the hanging hole probably due to the gas flow influence. Scale surface is also very porous and displays whiskers (Figure 182).

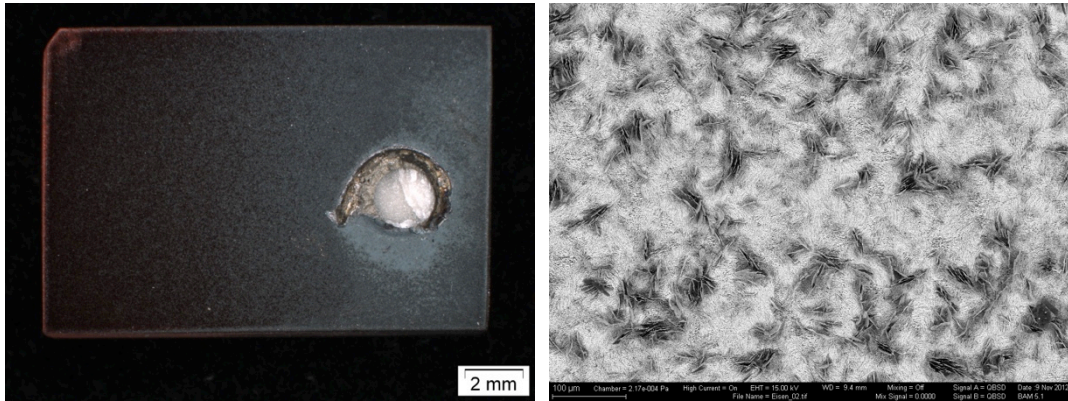


Figure 181: Stereomicroscope and SEM (BSE) pictures of the surface of RFe12 exposed to Gas 2 at 600°C for 1000h in a single condition. In the stereo picture (left), a large hematite region (red phase) is observed on the bottom of the sample. Porosity and whiskers are observed on the scale surface of the SEM picture on the right.

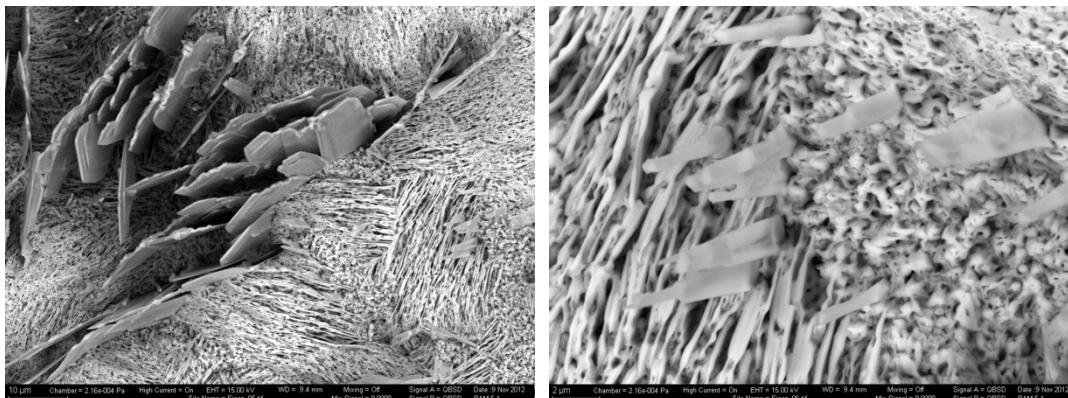


Figure 182: SEM (BSE) pictures of the surface of RFe12 exposed to Gas 2 at 600°C for 1000h in a single condition. Whiskers and pores are observed on the surface of the scale.

There is no evidence of carburization or any other microstructural change in the metal in etched samples of Figure 183.

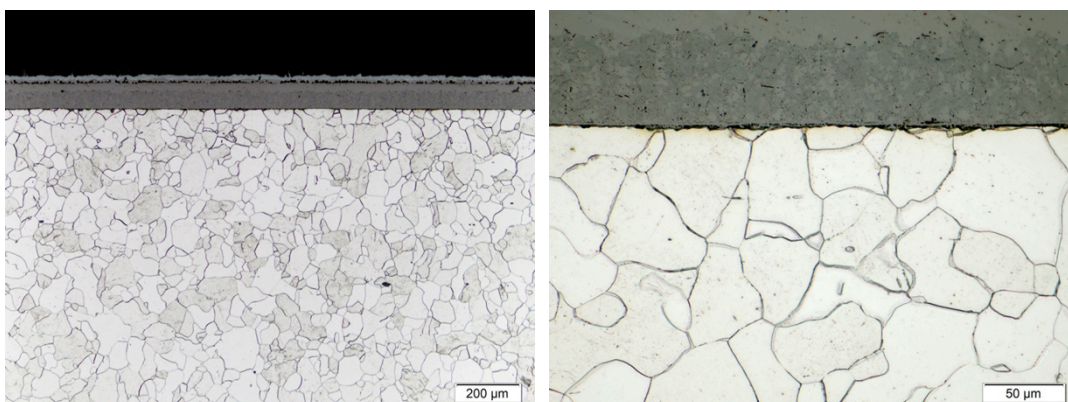


Figure 183: Light microscope pictures of RFe12 exposed to Gas 2 at 600°C for 1000h in a single condition. There is no evidence of microstructural change in the metal.

Scale is composed of a thick layer of magnetite and a thin layer of hematite (Figure 184 and Figure 185).

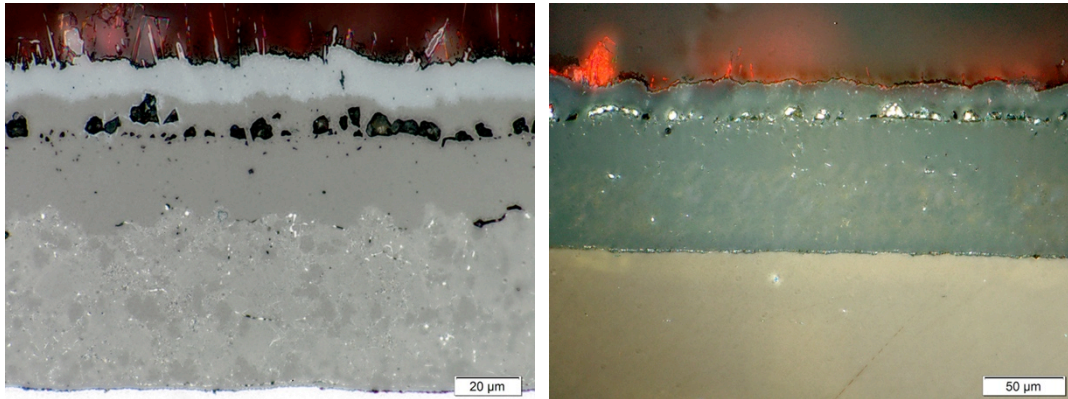


Figure 184: SEM and light microscope pictures of RFe12 exposed to Gas 2 at 600°C for 1000h in a single condition. Two phases are observed on the scale and hematite whiskers are present on top of the surface.

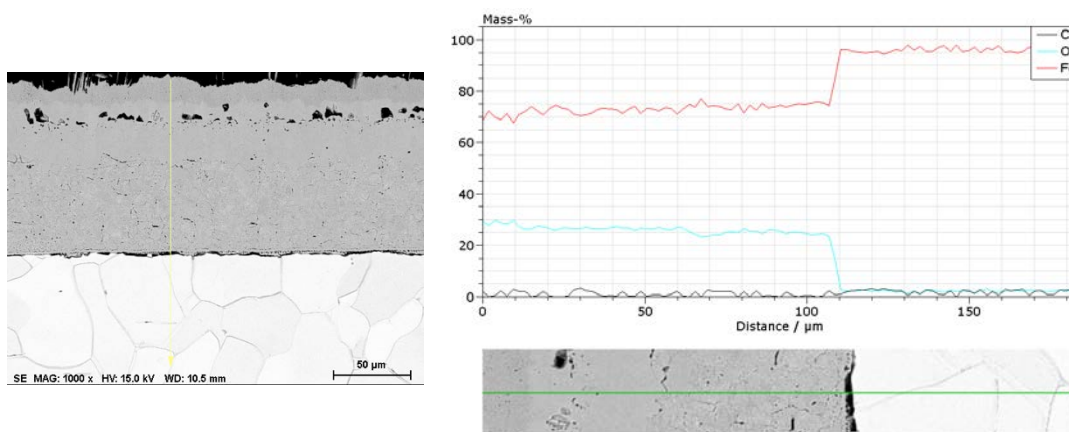


Figure 185: EDS line scanning of RFe12 exposed to Gas 2 at 600°C for 1000h in a single condition. Scale formed by hematite and magnetite.

4.7.1.3 Gas 3 (70 CO₂ – 1 SO₂ – 29 H₂O)

In Gas 3, thick scale was formed on the surface. The scale surface is formed by a porous phase and whiskers (Figure 186 and Figure 187).

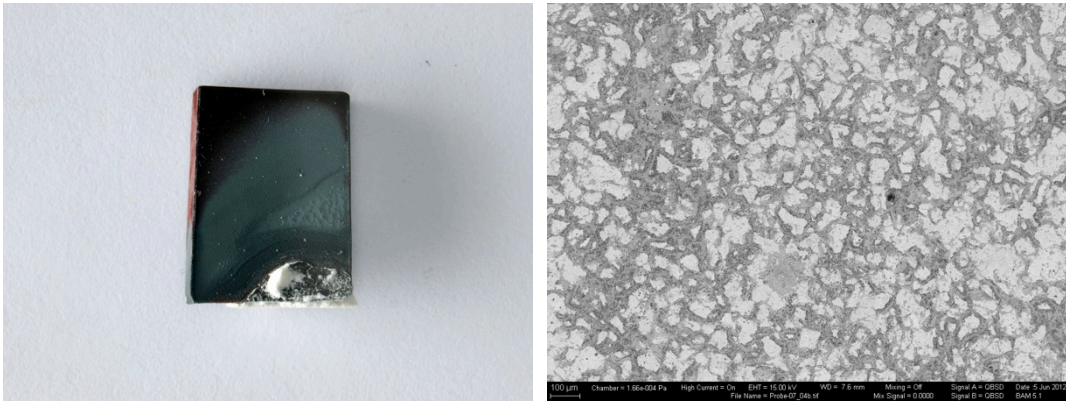


Figure 186: Macro and SEM (BSE) pictures the surface of RFe12 exposed to Gas 3 at 600°C for 1000h in a single condition. Whiskers and a porous iron oxide phase were formed in Gas 3.

EDS line scanning of the cross section in Figure 188 shows that scale is composed of hematite close to the gas surface and magnetite underneath it. There is no evidence of carburization of the metal.

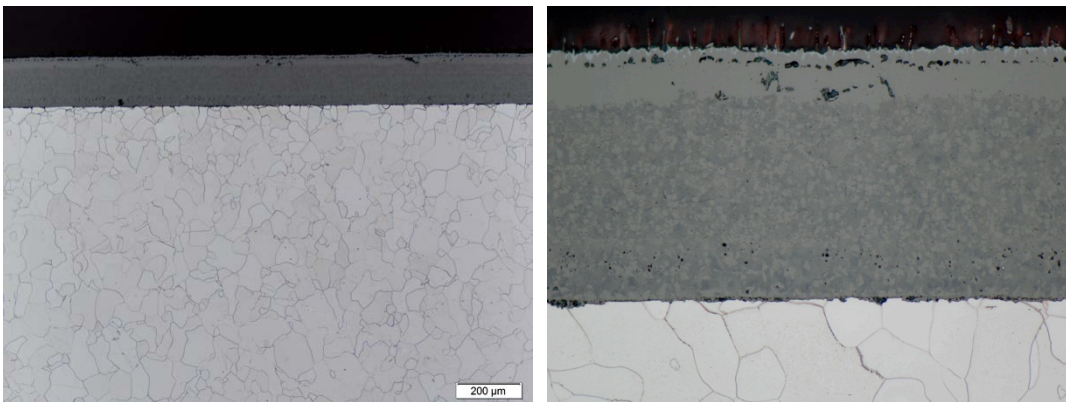


Figure 187: Light microscope and SEM pictures of RFe12 exposed to Gas 3 at 600°C for 1000h in a single condition. Thick scale is formed on the surface and there is no evidence of microstructural change in the metal.

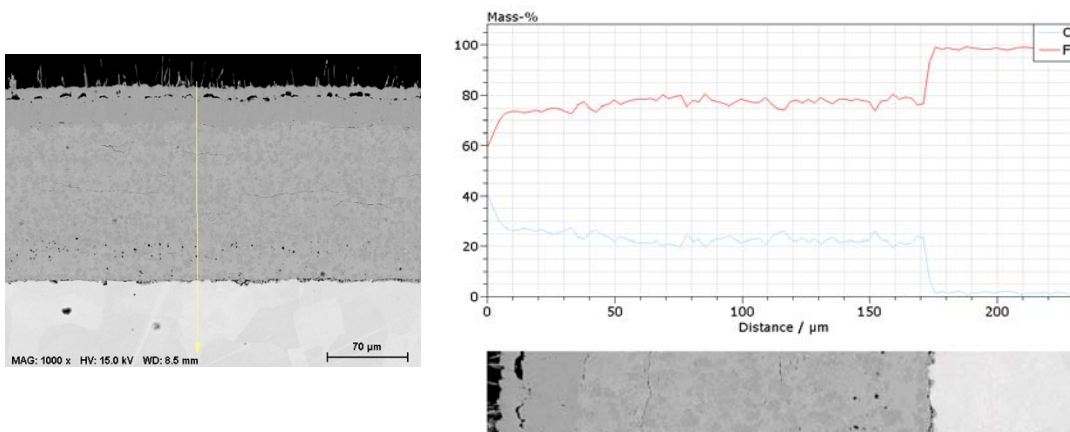


Figure 188: EDS line scan of RFe12 exposed to Gas 3 at 600°C for 1000h in a single condition. Scale is composed of hematite and magnetite.

5 Discussion

The discussion of the results will focus the three parameters which most affected the alloys corrosion behavior: (1) alloy composition and structure; (2) gas composition; (3) dual atmosphere condition.

5.1 Alloy Composition and Structure

5.1.1 Chromium Effect

Alloys P4 and P2 were designed to have the same cobalt (3wt%) and carbon (0.2wt%) content, but different chromium content (14wt% for P4 and 12wt% for P2). Both alloys are martensitic and were exposed in a single condition atmosphere condition to gases 1, 2 and 3.

Both alloys formed a continuous Cr_2O_3 layer with small number of nodules which increased in size and quantity with increase in water vapor concentration (Figure 189).

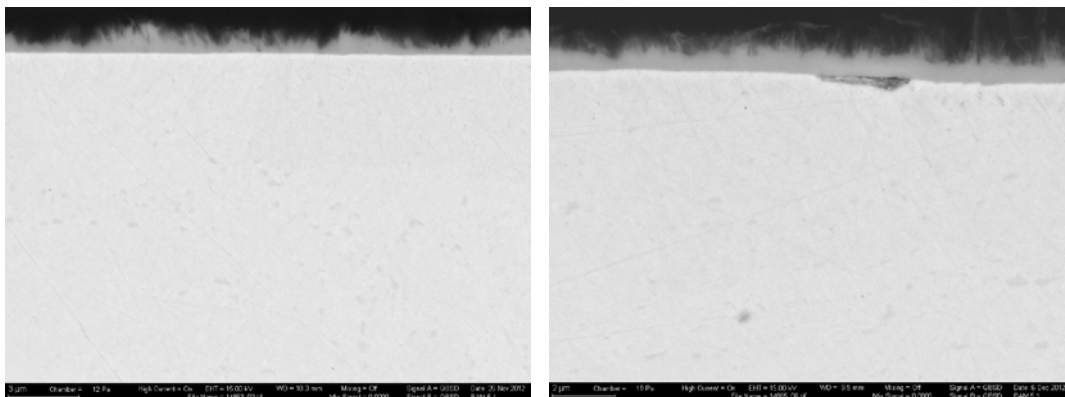


Figure 189: Left: Alloy P2 in Gas 1. Right: Alloy P4 in Gas 1.

No other work has investigated the same compositions, but Meier et al. [65] have worked with several Fe-Cr alloys with Cr concentration from 9 to 35% in the same gas composition. For higher temperatures, up to 600°C, most of the alloys had the same behavior and with temperature increase, the alloys with

more Cr displayed a lower corrosion rate than in lower temperatures. The alloys with 9% Cr had an increase in corrosion rate with increase in temperature. This behavior is due to the capacity of alloys with high Cr content to maintain Cr supply to the scale in higher temperatures. This might be the case in both alloys. They displayed sufficient Cr and mobility to create and maintain the Cr_2O_3 scale.

5.1.2 Cobalt Effect

Alloys P3 and P4 were designed to have the same chromium (14 wt%) and carbon (0.2 wt%) content, but different cobalt content (1 wt% for P3 and 3 wt% for P4). Both alloys are martensitic and were exposed in single atmosphere condition to gases 1, 2 and 3. In dual condition, both alloys were exposed to gases 1 and 3. Both alloys had an increase in nodule formation with increase in water content. Carbide consumption and ferrite growth are also seen in Gas 3 in single condition. In dual condition the ferrite layer is bigger in both alloys and also seen in Gas 1. In dual condition, P3 has shown more nodule formation, but also an unexpected protective layer on the water vapor side in Gas 1 experiment, suggesting that additional experiments should be done to reveal the effect of Co on the corrosion behavior of these alloys. The increase in the ferrite layer in a dual condition might be related to greater Cr consumption and decarburization of the steels [33,88].

5.1.3 Carbon Effect

Alloys P4 (ferritic) and P5 (martensitic) were designed to have the same chrome (14 wt%) and cobalt (3 wt%) content, but different carbon content (0.2 wt% for P4 and 0 wt% for P5). Both alloys were exposed to single atmosphere condition in gases 1, 2 and 3. In dual condition, both were exposed to gases 1 and 3. Both alloys had an increase in nodule formation with increase in water content. P5 was considerably more affected by the dual condition in Gas 1 than P4. It has formed several nodules creating a continuous scale composed of spinel and iron-rich oxides. The faster corrosion of P5 might have been caused by faster permeation of hydrogen in ferritic steels than in martensitic steels [59,60]. In Gas 3, both alloys presented more nodules than in single condition.

5.1.4 Other Alloying Elements Comparison

P1 has lower chromium, cobalt and carbon than P4 and it is ferritic instead of martensitic as P4. In all conditions, P1 had faster oxidation than P4 as expected, because of the lower chromium content. However, P2 has also 12%Cr and had an oxidation behavior closer to P4 than P5. This indicates that the martensitic microstructure may be responsible for better corrosion resistance when compared to the ferritic microstructure, since cobalt and carbon had little interference in the oxidation behavior of 14%Cr samples.

5.2 Gas Composition

Gases 1, 2 and 3 have 0, 1 and 30% H₂O respectively with the same content of CO₂ (30%) and SO₂ (1%). In all alloys, increase in the water vapor concentration has accelerated corrosion of all alloys. This effect was more pronounced in alloy P1, with an increase in the number and size of iron rich nodules (Figure 190). The increase porosity and amount of whisker morphology is also clear in P1 and RFe12.

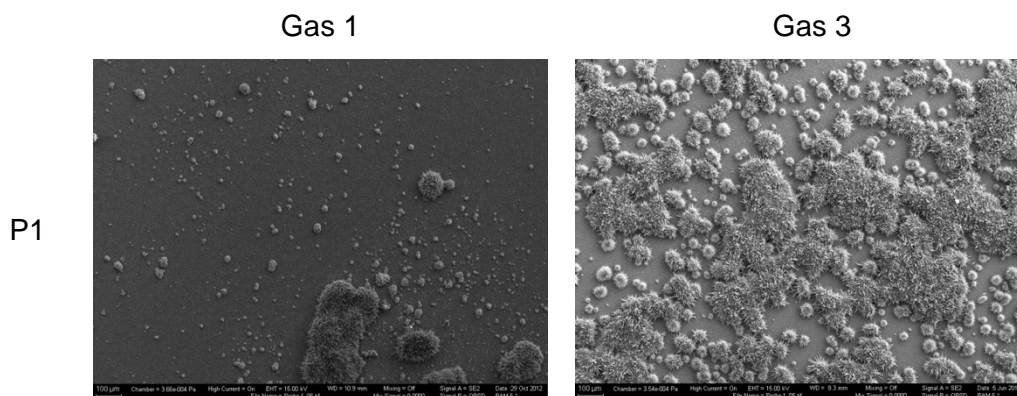


Figure 190: Nodules density on the surface has increased with increase in water vapor concentration.

Water vapor is well known to increase the oxidation rate in steels [33], because of molecular transport of oxygen in the scale caused by it. This explains the faster growth of iron-rich nodules in the presence of water vapor. The increase in nodule number might be caused by Cr hydroxides formation, but in the temperature used there is no evidence of Cr hydroxides formation [36]. The hydrogen diffusion through Cr-rich oxides is slow [73,57], but defects in the scale can enhance hydrogen diffusion. Once hydrogen dissolves in metals, it creates

vacancies [57], which accelerate Fe diffusion. This can lead to faster Fe/Cr spinel formation when CO_2 reacts with Fe [37,40-42].

In Gas 3, ferrite growth was also observed in some alloys in the subscale region and Cr-rich oxides were present. The ferrite region was not found in the water vapor side of the dual experiments, for example. Ferrite growth is related to decarburization of the steels, and where Cr_2O_3 or spinel was present, the corrosion sequence proposed by Gibbs [37] does not take place. Ferrite growth in this case is different from growth proposed by Purdy and Kirkaldy [91] in austenitic steels, where the steels are decarburized and ferrite nucleates at the steel/gas surface.

In this case, consumption of Cr carbides, especially M_{23}C_6 , near the surface would end the drag effect created by precipitates which are first consumed near the surface by the scale. Ferrite grain growth towards the inner part of the sample is controlled by the Cr carbide dissolution. Carbide dissolution and ferrite growth can be clearly seen in alloy P4 in single condition using Gas 3 (Figure 191).

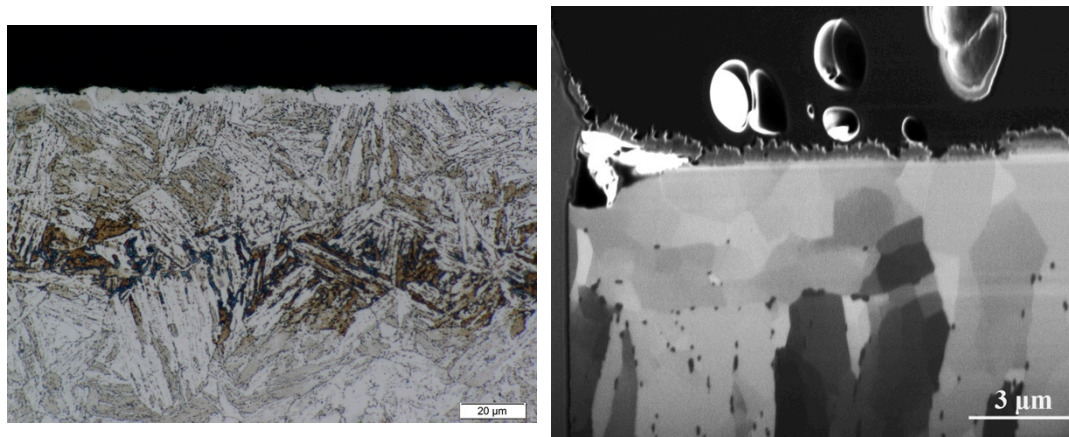


Figure 191: Carbide consumption in alloy P4 in a single condition in Gas 3.

5.3 Dual atmosphere condition

In most samples investigated, corrosion in dual atmosphere condition was greater in dual atmosphere than in single atmosphere on the gas side. This was more pronounced in Gas 3, except for alloy P5. Several studies have investigated the dual effect on steel at different temperatures, compositions, atmospheres and methods, with very diverse results. It is clear that the chromia layer plays an important role in inhibiting hydrogen diffusion from the gas to steel and

decreasing the hydrogen gradient in steel [57,73]. In some studies [67,71,76,77], iron rich nodules are formed in a dual condition even when a protective scale is formed in a single condition experiment.

Studies where the dual atmosphere condition has little or no interference in the corrosion behavior of the alloys are those which used alloys with higher chromium and temperature than with studies where the influence of the dual atmosphere condition was reported. The work of Horita et al. [74] is an example of little influence of dual condition, but the authors used 22%Cr steel and 800°C in the work.

The higher corrosion reported in this thesis would be a result of the higher porosity caused by atmospheres with high hydrogen partial pressure in agreement to the model proposed by Holcomb et al. [75] to explain the dual atmosphere effect. Porosity would increase the scale diffusion by changing the oxygen diffusion mechanism from a point defect O^{2-} diffusion to a molecular O_2 diffusion through pores.

Another evidence of the hydrogen effect in the corrosion of the steels studied can be seen in ferrite growth in martensitic alloys P3, P4 and VM12. In a single condition, ferrite was not found in the subscale region of Gas 1, but a ferrite layer has grown in a dual condition in the same gas. This result shows that oxidation in Gas 1 using a dual condition is similar to a single condition if water vapor is present.

In Gas 3, ferrite layers in alloy P4 and P3 were thicker in a dual condition than in a single condition. An example is the ferrite layer in dual and single condition for alloy P4 in Gas 3 (Figure 191 and Figure 192). In a single condition, the mean scale thickness was 5 μ m and in a dual condition, the mean thickness was 14 μ m.

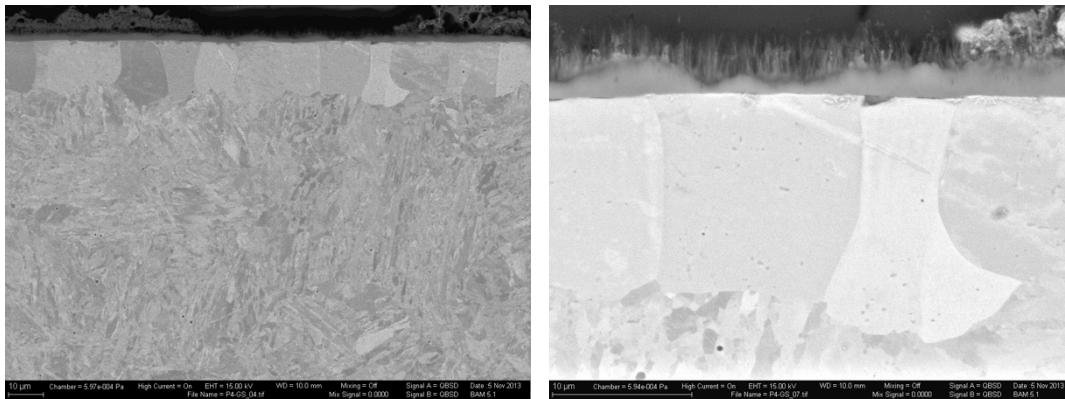


Figure 192: Decarburization and ferrite growth in alloy P4 in a dual condition in gas 3.

In the water vapor side, VM12-SHC showed better corrosion resistance than the model alloys. In gas 1, for example, VM12-SHC presented a mean scale thickness of 58µm, much smaller than the best model alloy, P4, which displayed a mean thickness of 199µm (Table 5).

This results show that the alloying elements of VM12-SHC, not present in the model alloys (W, Si, Mn and V), are important to enhance steam corrosion resistance.

Table 5: Water vapor side scale thickness in µm. N is the maximum thickness of the nodule.

	Gas 1	Gas 3
P1	246	220
P3	255	140 N
P4	199	198
P5	215	200
VM12-SHC	56	61

6 Conclusions

Seven alloys with different chromium, cobalt and carbon content were investigated under atmospheres related to the oxyfuel process. The samples were exposed to single and dual atmospheres conditions at 600°C for 1000h. In the dual atmosphere condition, the samples were exposed to water vapor on one side and gases with CO₂, SO₂ and different H₂O content on the other side, creating a hydrogen gradient in the sample.

Samples exposed to a single atmosphere condition at 600°C for 1000h had a higher oxidation rate with the increase in H₂O content in the gases used (Gas 1: 30CO₂-1SO₂-29Ar, Gas 2: 30CO₂-1SO₂-28Ar-1H₂O and Gas 3: 30CO₂-1SO₂-29H₂O). Not only the composition, but also the microstructure had a determining effect in the corrosion behavior of the alloys studied. Alloys with 14%Cr exhibited higher corrosion resistance than 12%Cr ferritic alloys. The martensitic 12%Cr alloy had similar corrosion behavior as the samples with 14%Cr. This result is probably related to chromium carbide consumption in martensitic alloys to form a protective scale rich in chromium.

In a dual atmosphere condition, most of the samples exhibited a higher corrosion rate than in a single condition. The ferritic microstructure is believed to be more prone to the dual atmosphere effect, because hydrogen diffuses faster in ferrite than in martensite. The other reason for such behavior is that chromium carbide dissolution in martensitic steels supplies chromium fast enough to maintain the protective oxide layer. Carbide consumption is also evidence that the dual atmosphere condition affects the gas, increasing the corrosion rate. In dual condition, carbide dissolution and ferritic growth was observed in Gas 1, which does not contain H₂O. This behavior was only seen in single condition in Gas 3 with 30% H₂O.

Pores formation and molecular diffusion is believed to be the mechanism, which boosts the corrosion rate in a dual condition. Carbide dissolution and ferrite growth seems to help the development of a protective chromium rich oxide layer. However, further investigation has to be performed to confirm both hypotheses.

From all alloys investigated in this work, 14%Cr steel P4 with 3%Co and 0.2C exhibited the best overall corrosion resistance in CO₂-rich atmospheres in single and dual condition. From all 12%Cr steels studied, P2 with 3%Co and 0.2%C had the best corrosion resistance in single atmosphere.

Considering the water vapor side, commercial steel VM12 exhibited the best behavior, producing the thinnest and most compact oxide layers among all the compositions tested.

7 Bibliography

1. IBGE. **Indicadores de Desenvolvimento Sustentável: Brasil 2010**. Rio de Janeiro. 2012. (ISBN: 978-85-240-4133-4).
2. IPCC. **Climate Change 2007: Synthesis Report**. [S.l.]. 2007. (http://www.ipcc.ch/pdf/assessment-report/ar4/syr/ar4_syr.pdf).
3. AGENCY, U. S. E. P. **Inventory of U.S. Greenhouse Gas Emissions and Sinks: 1990 - 2009**. Washington. 2011. (http://www.epa.gov/climatechange/emissions/downloads11/US-GHG-Inventory-2011-Complete_Report.pdf).
4. IEA. **World Energy Outlook 2013 Factsheet**. IEA. [S.l.]. 2013.
5. U.S. ENVIRONMENTAL PROTECTION AGENCY. **INVENTORY OF U.S. GREENHOUSE GAS EMISSIONS AND SINKS: 1990 – 2009**. U.S. Environmental Protection Agency. Pennsylvania. 2011.
6. IEA. **Clean Energy: Progress Report**. [S.l.]. 2011. (http://www.iea.org/papers/2011/CEM_Progress_Report.pdf).
7. IEA. **World Outlook: Executive Summary 2011**. [S.l.]. 2011. (http://www.worldenergyoutlook.org/docs/weo2011/executive_summary.pdf).
8. IEA. **World Energy Outlook 2009**. Paris. 2009. (978 92 6406130-9).
9. IEA. **World Energy Outlook 2007 Edition: China and India Insights**. Paris. 2007. (ISBN: 978 92 64 02730-5).
10. IEA. **World Energy Outlook 2010: Executive Summary**. [S.l.]. 2012. (http://www.worldenergyoutlook.org/docs/weo2010/WEO2010_es_english.pdf).
11. DOE. **Strategic Plan**. [S.l.]. 2011. (http://energy.gov/sites/prod/files/2011_DOE_Strategic_Plan_.pdf).
12. FOY, K.; YANTOVSKI, E. History and State-of-the-Art of Fuel Fired Zero Emission Power Cycles. **International Journal of Thermodynamics**, v. 9, n.

- 2, p. 37-63, Junho 2006. ISSN 1301-9724.
13. MILLER, B. G.. **Clean Coal: Engineering Technology**. Oxford: Butterworth-Heinemann, 2011. ISBN ISBN: 978-1856177108.
 14. IEA. **Key World Energy World Statistics 2013**. IEA. [S.l.]. 2013.
 15. IEA. **Tracking Clean Energy Progress 2013**. IEA. [S.l.]. 2013.
 16. NOAA. **Trends in Atmospheric Carbon Dioxide**, 2014. Disponível em: <<http://www.esrl.noaa.gov/gmd/ccgg/trends/>>. Acesso em: 10 January 2014.
 17. COOK, J. et al. Quantifying the consensus on anthropogenic global warming in the scientific literature. **Environmental Research Letters**, v. 8, p. 1-7, 2013.
 18. LÜTHI, D. et al. High-resolution carbon dioxide concentration record 650,000–800,000 years before present. **Nature**, v. 435, p. 379-382, Maio 2008.
 19. ROBINSON, P. J.; HENSERSON-SELLERS, A. **Contemporary Climatology**. 2. ed. Essex: Pearson Education Limited, 1999. ISBN 0-582-27631-4.
 20. ZHANG, D. **Ultra-Supercritical Coal Power Plants: Materials, Technologies and Optimisation**. 1. ed. Cambridge: Woodhead Publishing, 2013. ISBN 0857091166.
 21. TOFTEGAARD, M. B. et al. Oxy-fuel combustion of solid fuels. **Progress in Energy and Combustion Science**, v. 36, p. 581-625, 2010.
 22. VINCE WHITE, V. et al. The Air Products Vattenfall Oxyfuel CO 2 Compression and Purification Pilot Plant at Schwarze Pumpe. **Energy EProcedia**, v. 37, p. 1490-1499, 2013.
 23. YAN, J. et al. Flue Gas Cleaning for CO 2 Capture from Coal-fired Oxyfuel Combustion Power Generation. **Energy Procedia**, v. 4, p. 900-914, 2011.
 24. WHITE, V. et al. Purification of oxyfuel-derived CO2. **International Journal of Greenhouse Gas Control**, v. 4, p. 137-142, 2010.
 25. KATHER, A.; KOWNATZKI, S. Assessment of the different parameters affecting the CO2 purity from coal fired oxyfuel process. **International Journal**

- of Greenhouse Gas Control**, v. 5S, 2001. ISSN S204–S209.
26. VATTENFALL. **Vattenfall & CCS - Carbon Capture and Storage Soon a Reality**. [S.l.]. 2008.
 27. ANHEDEN, M. et al. Overview of Operational Experience and Results from Test Activities in Vattenfall's 30 MW th Oxyfuel Pilot Plant in Schwarze Pumpe. **Energy Procedia**, v. 4, p. 941-940, 2011.
 28. STRÖMBERG, L. et al. Update on Vattenfall's 30 MWth Oxyfuel Pilot Plant in Schwarze Pumpe. **Energy Procedia**, p. 581-589, 2009.
 29. MASUYAMA, F. **Alloy Development and Material Issues with Increasing Steam Temperature**. Fourth International Conference on Advances in Materials Technology for Fossil Power Plants. Head Island: [s.n.]. 2004.
 30. VISWANATHAN, R.; BAKKER, W. Materials for Ultrasupercritical Coal Power Plants—Boiler Materials: Part 1. **Journal of Materials Engineering and Performance**, v. 10, n. 1, p. 81-95, Julho 2000.
 31. DIEULIN, A. et al. V&M's innovative contribution to the challenges of present and future conventional power plants. **VGB Powertech**, November 2011. 63-68.
 32. BÜRCEL, R. **Handbuch Hochtemperatur-Werkstofftechnik: Grundlagen, Werkstoffbeanspruchungen, Hochtemperaturlegierungen und -beschichtungen**. 3. ed. Wiesbaden: Vieweg, 2006. ISBN 978-3-528-23107-1.
 33. YOUNG, D. J. **High Temperature Oxidation and Corrosion of Metals**. 1. ed. Amsterdam: Elsevier, v. 1, 2008. ISBN 9780080445878.
 34. BIRKS, N.; MEIER, G. H.; PETTIT, F. S. **Introduction to the High Temperature Oxidation of Metals**. 2. ed. New York: Cambridge University Press. ISBN 9780521485173.
 35. MONCEAU, D.; PIERAGGI, B. Determination of Parabolic Rate Constants from a Local Analysis of Mass-Gain Curves. **Oxidation of Metals**, v. 50, n. 5/6, p. 477-493, 1998.

36. SAUNDERS, S. R. J.; MONTEIRO, M.; RIZZO, F. The oxidation behaviour of metals and alloys at high temperatures in atmospheres containing water vapour: A review, v. 53, p. 775–837, 2008.
37. GIBBS, G. B. A Model for Mild Steel Oxidation in CO₂. **Oxidation of Metals**, v. 7, n. 3, p. 173-184, 1973.
38. TAYLOR, M. R. et al. The Mechanism of Corrosion of Fe-9% Cr Alloys in Carbon Dioxide. **Oxidation of Metals**, v. 14, n. 6, p. 499-516, 1980.
39. FUJII, C. T.; MEUSSNER, R. A. Carburization of Fe-Cr Alloys During Oxidation in Dry Carbon Dioxide. **Journal of Electrochemical Society**, v. 114, n. 5, p. 435-422, 1967.
40. ROUILLARD, F. et al. Corrosion of 9Cr Steel in CO₂ at Intermediate Temperature II: Mechanism of Carburization. **Oxidation of Metals**, v. 77, p. 57–70, 2012.
41. ROUILLARD, F.; MOINE, G.; MARTINELLI, L. Corrosion of 9Cr Steel in CO₂ at Intermediate Temperature I: Mechanism of Void-Induced Duplex Oxide Formation. **Oxidation of Metals**, v. 77, p. 27–55, 2012.
42. ROUILLARD, F.; MARTINELLI, L. Corrosion of 9Cr Steel in CO₂ at Intermediate Temperature III: Modelling and Simulation of Void-induced Duplex Oxide Growth. **Oxidation of Metals**, v. 77, p. 71–83, 2012.
43. DOUGLASS, D. L. et al. International Workshop on High-Temperature Corrosion. **Oxidation of Metals**, v. 45, n. 5/6, p. 529-620, 1996.
44. RAHME, A.; TOBOLSKI, J. Einfluss von Wasserdampf und Kohlendioxyd auf die Oxydation von Eisen in Sauerstoff ibei hohen Temperaturen. **Oxidation of Metals**, v. 5, p. 333-346, 1965.
45. HÄNSEL, M.; QUADAKKERS, W. J.; YOUNG, D. J. Role of Water Vapor in Chromia-Scale Growth at Low Oxygen Partial Pressure. **Oxidation of Metals**, v. 59, p. 285-301, 2003.
46. YOUNG, D. J. et al. Temperature dependence of oxide scale formation on high-Cr ferritic steels in Ar–H₂–H₂O. **Corrosion Science**, v. 53, p. 2131–2141

Contents lists, 2011.

47. YOUNG, D. J.; YIN, H. Water Vapour Effects on FeO Scale Growth: Differences Between Iron and Steel. **Oxidation of Metals**, v. 79, p. 445–460, 2013.
48. JIANIAN, S.; LONGJIANG, Z.; TIEFAN, L. High-Temperature Oxidation of Fe-Cr Alloys in Wet Oxygen. **Oxidation of Metals**, v. 48, p. 347-358, 1997.
49. ASTEMAN, H. et al. Influence of Water Vapor and Flow Rate on the High-Temperature Oxidation of 304L; Effect of Chromium Oxide Hydroxide Evaporation. **Oxidation of Metals**, v. 54, p. 11-26, 2000.
50. ZUREK, J. et al. Corrosion Science. **Corrosion Science**, v. 46, p. 2301–2317, 2004.
51. OTHMAN, N. K.; ZHANG, J.; YOUNG, D. J. Water Vapour Effects on Fe–Cr Alloy Oxidation. **Oxidation of Metals**, v. 73, p. 337–352, 2012.
52. EHLERS, J. et al. Enhanced oxidation of the 9%Cr steel P91 in water vapour containing environments. **Corrosion Science**, v. 48, p. 3428–3454, 2006.
53. ENNIS, P. J.; QUADAKKERS, W. J. Mechanisms of steam oxidation in high strength martensitic steels. **International Journal of Pressure Vessels and Piping**, v. 84, p. 75–81, 2007.
54. FUJII, C. T.; MEUSSNER, R. A. The Mechanism of the High-Temperature Oxidation of Iron-Chromium Alloys in Water Vapor. **Journal of the Electrochemistry Society**, v. 111, n. 11, p. 1215-1221, 1964.
55. TUCK, C. W.; ODGERS, M.; SACHS, K. The oxidation of iron at 950°C in oxygen-water vapor mixtures - Tuck (1969), v. 9, p. 271-285, 1969.
56. MONTEIRO, M. J.; SAUNDERS, S. R. J.; RIZZO, F. C. The Effect of Water Vapour on the Oxidation of High Speed Steel, Kinetics and Scale Adhesion. **Oxidation of Metals**, Outubro 2010.
57. NAKAI, M. et al. Improvement in steam oxidation resistance of Fe–10%Cr–0.08%C steel by suppressing hydrogen dissolution, v. 48, p. 3869–3885, 2006.

58. NAKAI, M. et al. Correlation of High-temperature Steam Oxidation with Hydrogen Dissolution in Pure Iron and Ternary High-chromium Ferritic Steel. **ISIJ International**, v. 45, n. 7, p. 1066-1072, 2005.
59. PARVATHAVARTHINI, N.; SAROJA, S.; DAYAL, R. K. Influence of microstructure on the hydrogen permeability of 9%Cr±1%Mo ferritic steel. **Journal of Nuclear Materials**, v. 264, p. 35-47, 1999.
60. PARVATHAVARTHINI, N.; SAROJA, S.; DAYAL, R. K. Study on hydrogen permeability of 2.25% Cr - 1% Mo ferritic steel: correlation with microstructure. **Journal of Nuclear Materials**, v. 288, p. 187 - 196, 2001.
61. HUENERT, D.; SCHULTZ, W.; KRANZMANN, A. **Corrosion of steels in H₂O-CO₂ atmospheres at temperatures between 500°C and 700°C**. 15th International Conference on the Properties of Water and Steam. Berlin: [s.n.]. 2008.
62. HÜNERT, D. **Korrosionsprozesse und Aufkohlung von ferritisch-martensitischen Stählen in H₂O-CO₂ Atmosphären**. BAM. Berlin. 2010.
63. PIRÓN ABELLÁN, J. et al. Scale formation mechanisms of martensitic steels in high CO₂/H₂O-containing gases simulating oxyfuel environments. **Materials at High Temperatures**, v. 26, n. 1, p. 63-72, 2009.
64. MU, N. et al. Water Vapor Effects on the Oxidation Behavior of Fe–Cr and Ni–Cr Alloys in Atmospheres Relevant to Oxy-fuel Combustion. **Oxidation of Metals**, Maio 2012.
65. MEIER, G. H. et al. Effect of Alloy Composition and Exposure Conditions on the Selective Oxidation Behavior of Ferritic Fe–Cr and Fe–Cr–X Alloys. **Oxidation of Metals**, v. 74, p. 319–340, 2010.
66. GHENO, T.; MONCEAU, D.; YOUNG, D. J. Mechanism of breakaway oxidation of Fe–Cr and Fe–Cr–Ni alloys in dry and wet carbon dioxide. **Corrosion Science**, v. 64, p. 222–233, 2012.
67. NAKAGAWA, K.; MATSUNAGA, Y.; YANAGISAWA, T. Corrosion behavior of steels on the air side of boiler tubes in steam/air dual environment. **Materials at High Temperature**, v. 20, n. 1, p. 67-73, 2003.

68. YANG, Z. et al. Anomalous corrosion behavior of stainless steels under SOFC interconnect exposure conditions. **Electrochemical and SolidState Letters**, v. 6, n. 10, p. B35-B37, 2003.
69. YANG, Z. et al. Oxidation behavior of ferritic stainless steels under SOFC exposure conditions. **Jornal of the Electrochemical Society**, v. 151, n. 12, p. B669-B678, 2004.
70. YANG, Z. et al. High temperature oxidation/corrosion behavior of metals and alloys under hydrogen gradient. **International Journal of Hydrogen Energy**, v. 32, p. 3770-3777, 2007.
71. YANG, Z. et al. Effects of water vapor on oxidation behavior of ferritic stainless steels under solid oxide fuel cell interconnect exposure conditions. **Solid State Ionics**, v. 176, p. 1495-1503, 2005.
72. KUROKAWA, H.; KAWAMURA, K.; MARUYAMA, T. Oxidation behavior of Fe-16Cr alloy interconnect for SOFC under hydrogen potential gradient. **Solid State Ionics**, v. 168, p. 13-21, 2004.
73. TANAKA, M. et al. Hydrogen permeability throu n-type Cr₂O₃ scale at 1273K under the oxygen activities of 1.6×10^{-18} - 1.0×10^{-16} . **ISIJ International**, v. 51, n. 4, p. 638-644, 2011.
74. HORITA, T. et al. Oxide scale formation and stability of Fe-Cr alloy interconnects under dual atmospheres and current flow conditions for SOFCs. **Journal of The Electrochemical Society**, v. 153, n. 11, p. A2007-A2012, 2006.
75. HOLCOMB, G. R. et al. Dual-environment effects on the oxidation of metallic interconnects. **Journal of Materials Engineering and Performance**, v. 15, p. 404-409, 2006.
76. SKILBRED, A. W. B.; HAUGSRUD, R. The effect of dual atmosphere conditions on the corrosion of Sandvik Sanergy HT. **International Journal of Hydrogen Energy**, v. 37, p. 8095-8101, 2012.
77. RUFNER, J. et al. Oxidation behavior of stainless steel 430 and 441 at 800 1C in single (air/air) and dual atmosphere (air/hydrogen) exposures. **International**

Jornal of Hydrogen Energy, v. 33, p. 1392 – 1398, 2008.

78. HUENERT, D.; KRANZMANN, A. Impact of oxyfuel atmospheres H₂O/CO₂/O₂ and H₂O/CO₂ on the oxidation of ferritic–martensitic and austenitic steels. **Corrosion Science**, v. 53, p. 2306–2317, 2011.
79. HÜNERT, D.; KRANZMANN, A. **Influence of pressure and chromium content on corrosion reactions at 600°C in a CO₂-H₂ O atmosphere**. Corrosion 2008. New Orleans: [s.n.]. 2008.
80. VOSS, D. A.; BUTLER, E. P.; MITCHELL, T. E. The Growth of Hematite Blades during the High Temperature Oxidation of Iron. **Metallurgical Transaction A**, v. 13A, 1982.
81. YUAN, L. et al. The origin of hematite nanowire growth during the thermal oxidation of iron. **Materials Science and Engineering B**, v. 177, p. 327– 336, 2012.
82. YUAN, L. et al. Driving force and growth mechanism for spontaneous oxide nanowire formation during the thermal oxidation of metals. **Acta Materialia**, v. 59, p. 2491–2500, 2011.
83. SRIVASTAVA, H. et al. Effect of substrate texture on the growth of hematite nanowires. **Applied Surface Science**, v. 258, p. 497-500, 2011.
84. YUAN, L. et al. Morphological transformation of hematite nanostructures during oxidation of iron. **Nanoscale**, v. 5, p. 7581-7588, 2013.
85. HINDAM, H.; WHITTLE, D. P. Microstructure, Adhesion and Growth Kinetics of Protective Scales on Metals and Alloys. **Oxidation of Metals**, v. 18, p. 245-284, 1982.
86. DURHAM, R. N.; GLEESON, B.; YOUNG, D. J. Factors Affecting Chromium Carbide Precipitate Dissolution During Alloy Oxidation. **Oxidation of Metals**, v. 50, p. 139-165, 1998.
87. YOUNG, D. J.; GLEESON, B. Alloy phase transformation driven by high temperature corrosion processes. **Corrosion Science**, v. 44, p. 345-357, 2002.

88. SUSANTO, L. B.; YOUNG, D. J. Selective Oxidation and Sub-surface Phase Transformations in Chromium-bearing Austenitic Steels. **Oxidation of Metals**, v. 65, p. 277-302, 2005.
89. GESMUNDO, F.; GLEESON, B. Oxidation of Multicomponent Two-Phase Alloys. **Oxidation of Metals**, v. 44, 1995. ISSN 211-236.
90. WANG, G.; GLEESON, B.; DOUGLASS, D. L. Diffusional Analysis of the Oxidation of Binary Multiphase Alloys. **Oxidation of Metals**, v. 35, p. 333-348, 1991.
91. PURDY, G. R.; KIRKALDY, J. S. Kinetics of the Proeutectoid Ferrite Reaction at an Incoherent Interface, as Determined by a Diffusion Couple, v. 227, p. 1255, 1963.
92. AARONSON, H. I.; ENOMOTO, M.; LEE, J. K. **Mechanisms of Diffusional Phase Transformations in Metals and Alloys**. Boca Raton: CRC Press, 2010. ISBN 978-1-4200-6299-1.
93. HUTCHINSON, C. R.; ZUROB, H. S.; BRÉCHET, Y. The Growth of Ferrite in Fe-C-X Alloys: The Role of Thermodynamics, Diffusion, and Interfacial Conditions. **Metallurgical and Materials Transactions A**, v. 37A, p. 1771-1720, June 2006.